Establishing a Neural Progenitor Cell Model of Huntington's Disease

Smith, Edward John

Awarding institution:
King's College London

Establishing a Neural Progenitor Cell Model of Huntington's Disease

by

Edward John Smith

A thesis submitted for the degree of Doctor of Philosophy in Genetics

Department of Medical and Molecular Genetics

Division of Genetics and Molecular Medicine

Faculty of Life sciences and Medicine

King's College London

September 2016

Abstract

Huntington's disease (HD) is caused by the expansion of a CAG repeat in the huntingtin (*HTT*) gene The R6/2 transgenic mouse model exhibits a rapid onset of Huntington's disease-like phenotypes including neurodegeneration and aggregation of mutant huntingtin protein (mHTT). Neural progenitor cells (NPCs) are a pool of cells with stem cell-like properties and are responsible for self-renewal and differentiation into the cells of the central nervous system and mature brain.

In this thesis, NPC lines were established from cells extracted from foetal R6/2 and wildtype mouse embryos and cultured in optimised culture media. NPCs were successfully maintained in a mitotic state as monolayer cultures for multiple passages without effects to karyotype or CAG repeat length. Cultures were differentiated by removal of growth factors, into mixed neurons and glia populations that expressed proteins indicative of mature cell types; neurons showed evidence of synaptophysin expression at junctions between cell neurites, suggesting synaptic functionality and formation of rudimentary neural networks. After differentiation, mHTT aggregation was detectable using immunohistochemistry from 14 days of differentiation in 5% of R6/2 cell nuclei, rising to 20% by 28 days, recapitulating an HD-like phenotype found *in vivo*. Detection of detergent insoluble mHTT-aggregated protein was also validated via western blotting. Super high resolution cell imaging showed aggregation of mHTT is also present in the cytoplasm.

High-content imaging analysis system was performed using the Operetta system to explore morphological differences between WT and R6/2 cultures, as well as within the subset of cells with detectable aggregation. R6/2 nuclei were found to be larger than those of WT cells. Novel compounds known to affect protein aggregation were applied to the cell lines to assess their potential use in screening for approaches to modulation mHTT aggregation. The cells developed in this thesis are a novel and useful complement to the R6/2 mouse; phenotypes observed *in vivo* can be interrogated at the molecular level in terms of how mHTT protein misfolding and aggregation occur and how this affects cellular function.

Statement of Originality

All experiments presented within this this thesis were planned and performed by myself.

Mouse breeding was performed with the assistance of Sophie Franklin, Christa Benjamin, Hayley Lazell, Dan Goodwin and Dr Donna Smith. CAG repeat sizing was carried out with the assistance of Sophie Franklin. Western blots were performed with the assistance of Dr Christian Landles.

All animal procedures were carried out in accordance with the Institutional and UK Animals (Scientific procedures) Act (1986) guidelines.

This studentship was generously funded by the Medical Research Council granted to Professor Gill Bates at King's College London and Dr Omar Aziz at Biofocus Discovery limited.

Table of Contents

Table of Figures

Table of Tables

Acknowledgements

Firstly, I would like to express my sincere gratitude to my supervisor, Prof. Gill Bates for her continuous support during my PhD research, for all her patience, motivation, and the sharing of her enormous knowledge. Her guidance has helped me to accomplish this research and her time and effort in amending the writing of this thesis was indispensable. I would also like to extend appreciation to my other supervisors, Dr Omar Aziz and Prof. Fiona Watt for their input over the last four years. I would like to thank Prof. Erich Wanker for the kind gift of the compounds used in within this thesis.

This process has been made easier with the help of those I have worked with in the lab. I would like to thank all the members of the Bates lab and members of the medical and molecular genetics department who have come and gone over the last four years. In particular, my thanks to Dale, Ivan, Davina, Kirupa, Gina, Nadira, Andreas, Christian and Sophie for their input and assistance whilst in the lab.

A huge thank you to my friends for supporting me throughout writing this thesis and my life in general away from the lab. If I had a pound for every time one of you asked how the mice were, I wouldn't need to go on working.

I would like to thank my parents, Karen and Ian, for their support, not just over the last four years, but throughout my life. Having Dyslexia has always made the process of expressing things with the written word a challenge. To think I have achieved a piece of work in the scope of a doctoral thesis is beyond anything my younger self would have imagined. When I was young my parents were told I would never become anything special, "just don't expect him to be a rocket scientist" they were told. With their love, guidance and support I can now say that these people were partially correct, I am a Neuroscientist instead.

Lastly, and most importantly, I would like to thank Hels, my best friend and soulmate. Every day you encouraged me to go and achieve all I can, and when it goes wrong, I come home to your love and support. Without you I could not have done this. Thank you.

Abbreviations

Abbreviation	Full Term
General term	
Arpp-21	cAMP-regulated phosphoprotein-21
ATP	Adenosine triphosphate
BAC	Bacterial artificial chromosome
BDNF	Brain-derived neurotrophic factor
BLBP	Brain-lipid-binding protein
CNS	Central nervous system
CRISPR	Clustered regularly interspaced short palindromic repeats
DARPP-32	Dopamine- and cAMP-regulated neuronal phosphoprotein
Dc	D Cell line from the cortex
Dl	D Cell line from the lateral ganglionic eminence
DLX	Distal-Less Homeobox protein
Dm	D Cell line from the medial ganglionic eminence
DMSO	Dimethyl sulfoxide
dPBS	Dulbecco's Phosphate-Buffered Saline
EGF	Epidermal growth factor
ESC	Embryonic stem cell
FACS	Fluorescence-activated cell sorting
FBS	Foetal Bovine Serum
FGF	Fibroblast growth factor - 2
FOXP1/2	Forkhead box protein P1/p2
GAP-43	Growth Associated Protein 43
GLAST	Glutamate aspartate transporter
HD	Huntington’s disease
HEAT	Huntingtin, Elongator factor 3, the regulatory A subunit of protein phosphatase 2A, and TOR1
HTT	Huntingtin protein
ICC	Immunocytochemistry

Abbreviation	Full Term
IHC	Immunohistochemistry
ILS1	Insulin gene enhancer protein
iPSC	Induced pluripotent stem cell
mHTT	Mutated huntingtin protein
Meis	Meis Homeobox 2
NES	Nuclear export signal
NPC	Neural progenitor cell
PCR	Polymerase chain reaction
PFA	Paraformaldehyde
PRD	Proline-rich domain
PRN	Poly-dl-ornithine
RA	Retinoic acid
Rarβ	Retinoic Acid Receptor Beta
RG	Radial glia
SIM	Structured illumination microscopy
TALENS	Transcription activator-like effector nucleases
TPR	Translocated promotor region
TUNEL	Terminal deoxynucleotidyl transferase dUTP nick end labelling
UPS	Ubiquitin–proteasome system
VA	Valproic acid
WT	Wildtype
YAC	Yeast artificial chromosome

Anatomy

CA	Cornus ammonis
CC	Corpus callosum
CTX	Cortex
DG	Dentate gyrus

Abbreviation	Full Term
LGE	Lateral ganglionic eminence
LV	Lateral ventricle
MGE	Medial ganglionic eminence
STR	Striatum
SVZ	Sub-ventricular zone
Antibodies	
BLBP	Brain-lipid-binding protein
DAPI	4',6-diamidino-2-phenylindole DNA stain
DCX	Doublecortin
GABA	Gamma-aminobutyric acid
GAD67	Glutamic acid decarboxylase
GFAP	Glial fibrillary acidic protein
GLAST	Glutamate aspartate transporter
Ki67	Ki-67 protein encoded by the *MKI67* gene
MAP2	Microtubule-associated protein 2
Nestin	Neuroectodermal stem cell marker
NeuN	Neuronal nuclei, FOX-3
P62	SQSTM1
S100b	S100 calcium-binding protein B
S830	Polyclonal sheep antibody S830
TUJ1	Class III beta-tubulin
Ubiquitin	Ubiquitin
Measurements	
µg/ng	Microgram/nanogram
µl	Microliter
µm/nm	Micrometre/nanometre
µM/nM	Micromolar/nanomolar mass

Chapter 1 Introduction

1.1 Introduction to Huntington's disease

Huntington's disease (HD) is an autosomal dominant disease, caused by the expansion of a polyglutamine (CAG) repeat in the huntingtin gene (*HTT*) which in turn translates to alterations in the ubiquitous protein huntingtin (HTT) (HDCRG, 1993), resulting in a mutated pathogenic form that underlies the disease. HD typically clinically presents in middle-aged adults in the prime of their life with particular ferocity in the brain; the motor, cognitive and behavioural problems make it a devastating condition to both patients and their families.

The most common and well-documented type of motor problems seen in HD is chorea, which are rapid 'dance-like' movements involving all the muscles of the trunk, face and extremities. As well as chorea, patients can suffer from bradykinesia, a slowness to initiate voluntary movements; hypokinesia, the partial or complete loss of muscle movement; and dystonia, abnormal muscle tone resulting in muscular spasm. Cognitive problems often present as a slowness of thought, which progresses to difficulty to maintain attention and difficulties with memory (Lawrence et al., 1998). Sleep disturbances are often reported with a delayed onset to sleep and longer duration of time spent asleep (Morton, 2013). All these symptoms increase over time as the disease becomes more severe, slowly making reliance on care a necessity. Eventually, the final stages of the disease lead to a patient becoming completely bedridden, incontinent and mute. HD is the most common monogenetic neurological disorder in the developed world (Evans et al., 2013, Fisher and Hayden, 2014, Morrison et al., 2011), yet therapeutic interventions have been extremely hard to develop.

1.2 Genetics

HD was named after George Huntingtin who made the first thorough medical description of the symptoms of HD in 1872 (Huntington, 1872), although other less prominent descriptions can been found as early as 1841 (Bates et al., 2014). During the subsequent decades, reports of HD were made in medical texts around the world in almost all continents (Marsden, 1975). In terms of neuropathology, the experts of the time argued widely about how the disease manifested in the brain. Considering the modern day findings around the differences that can been seen between patients with the same CAG repeat lengths (Waldvogel et al., 2012), this disagreement is not surprising. In the 1920s, it was finally agreed upon that the brain changes were principally degenerative and atrophic, with the caudate nucleus most obviously affected, despite an overall generalised brain shrinkage. Because of the autosomal dominant aspect and age of onset of HD, patients have been found in concentrated locations as the result of a single ancestor with the disease who produced decedents over many generations who carry the mutant gene. One such population in Venezuela was crucial to the success of the work of the HD foundation and Huntington's disease collaborative research group to isolate and map the huntingtin gene (*HTT*), which was achieved in 1993. Mapping *HTT* was a major step in accurately diagnosing and describing HD. *HTT* is found on the short arm of chromosome 4 and contains 67 exons, which encode for a protein of around 350 kDa. The HD collaborative group of researchers observed that sufferers had an expansion in a CAG repeat within the first exon of *HTT*, in at least one allele (HDCRG, 1993). CAG codon repeat lengths in the range of between 9 and 35 are considered normal and not connected with HD. Repeat lengths over 35 are generally associated with development of HD; repeats in the range of up to 39 are rare and are estimated to make up only around 3% of sufferers (Huntington Study Group and Dorsey, 2012), while those over 39 are considered pathogenic. An inverse correlation exists between CAG repeat length and age of onset,

with patients with longer repeats generally presenting with symptoms at younger ages (Wexler et al., 2004, Langbehn et al., 2004, Langbehn et al., 2010). Indeed, those with extreme repeat lengths can present with a juvenile form of HD before the age of 20 years (Quarrell, 2009). In these cases, the pathological features of the disease can present differently to the adult form (Vonsattel et al., 2011). Due to the somatic instability of the CAG repeat in HD, the repeat can lengthen over time, particularly in the brain (Wheeler et al., 1999, Kennedy and Shelbourne, 2000, Kennedy et al., 2003). Evidence is varied to how this instability occurs and how it relates to the overall pathology; it is thought to mainly take place during DNA repair and replication (McMurray, 2010).

1.3 Normal HTT

In mammals, HTT is expressed ubiquitously throughout the body, with the highest levels found in central nervous system (CNS), neurons, and the testes (Strong et al., 1993, Landwehrmeyer et al., 1995, Sharp et al., 1995). HTT is a large protein of 3144 amino acid residues and is mainly found in the cytoplasm and dendritic processes, as well as at the axon terminals of neurons, although to a lesser extent (Trottier et al., 1995, Ferrante et al., 1997, Sharp et al., 1995). Within these cell compartments, HTT is associated with the Golgi apparatus and endoplasmic reticulum (DiFiglia et al., 1995, Hilditch-Maguire et al., 2000). In some cells, HTT is also found in the nucleus (Hoogeveen et al., 1993, Kegel et al., 2002). Within the cell the function of HTT is varied and changes depending on stage of mammalian life studied. HTT intereacts with a number of other proteins.

1.4 HTT in Development

In development, HTT is expressed early in the post-fertilisation stages (Dragatsis et al., 1998). A targeted disruption of the protein function at this stage in mice or production of nullizygous mice (*Htt*$^{-/-}$) halts development and is lethal between embryonic day 8.5 and 10.5 (Duyao et al., 1995, Nasir et al., 1995, Dragatsis et al., 1998, Zeitlin et al., 1995) indicating the importance of HTT at this developmental stage. This time point is roughly just after the start of neural tube development and CNS formation. At this stage, HTT is involved in control of neuroepithelial cell-cell interaction by regulation of cell adhesion pathways (Lo Sardo et al., 2012). Later in CNS development, HTT is known to control mitotic spindle orientation during cortical neurogenesis (Godin et al., 2010). Indeed, HTT is specifically needed for the development of cortical and striatal neurons (Reiner et al., 2001).

Evidence exists for HTT having an anti-apoptotic function. In striatal derived cells, overexpression of HTT is protective against lethal stresses such as deprivation of serum or introduction of 3-nitropropionic, a mitochondrial toxin (Rigamonti et al., 2000, Rigamonti et al., 2001). Postnatal inactivation of the *Htt* gene in mice resulted in apoptotic cells in the cortex, striatum, and hippocampus, and a reduction in axonal processes (Dragatsis et al., 2000). HTT blocks the creation and function of the apoptosome complex and activation of caspase-3 and caspase-9 (Rigamonti et al., 2000, Rigamonti et al., 2001), which could be the mechanism by which it moderates apoptotic cell death (Zhang et al., 2006).

Within neurons, HTT is partially important for normal function. HTT stimulates the production of brain-derived neurotrophic factor (BDNF), which is important to neuronal function and survival (Zuccato et al., 2001). BDNF levels are directly lowered in cortical neurons of mice heterozygous for *Htt* (Zuccato et al., 2003). HTT in the cytoplasm is

found enriched in compartments containing vesicle-associated proteins (Velier et al., 1998). In the axon, where HTT interacts with motor proteins such as HAP1 (Gunawardena 2005, 15642849), it is vital for the transport of mitochondria (Trushina et al., 2004) and BDNF (Gauthier et al., 2004). At the synapse, HTT interacts with vesicle proteins that are vital for exocytosis and endocytosis (Smith et al., 2005), linking HTT to the normal synaptic activity of neurons. In the presence of longer CAG repeats in HD, this transport function can become impaired (Smith et al., 2005).

1.5 Neuropathology

HD induces pathology throughout the body. Heart disease affects around a third of HD patients (Lanska et al., 1988), and muscle wasting (Farrer and Meaney, 1985) and bone loss (Goodman and Barker, 2011) are common HD phenotypes. However, it is within the brain that HD has most pronounced effects. The most striking pathology in the human brain occurs in the caudate nucleus and putamen, which compose the striatum (Figure 1-1). That said, other areas of the basal ganglia, particularly areas that receive striatal projections such as the global pallidus and substantia nigra, are also highly affected. The cortex is consistently substantially affected but few brain regions are spared in severely degenerated brains. Although the areas of the striatum and cortex are most classically associated with HD neurodegeneration, the speed and extent of cell loss can be variable, even in patients with the same CAG repeat length (Hadzi et al., 2012, Pillai et al., 2012). Indeed, the same pattern is true for the clinical manifestation of the disease. HD is a single gene disease with a measurable pathological CAG repeat expansion, yet symptoms can present as a mixture of deficits in mood, cognition, and motor ability. This variation is most eloquently displayed by twin studies where onset can differ by many years

(Georgiou et al., 1999, Friedman et al., 2005). This said, eventually a similar pattern of neurodegeneration eventually occurs in all patients.

Within the striatum, the most highly effected cell population are the medium spiny neurons that make up 90-95% of neurons in this region (Kemp and Powell, 1971, Holt et al., 1997). The loss of these GABAergic inhibitory neurons leads to the dysfunction in motor functions commonly observed in HD (Marshall et al., 1983). The particular vulnerability of medium spiny neurons is unclear because the exact mechanisms that cause cell death in Huntington's disease remain unclear. With the aggregation of mHTT being a concentration dependent process, it could be due to an endogenously higher steady state of the protein accelerating the process in this cell population. Particular processes within these cells might also altered by the presence of mHTT and could lead to damaging processes such as transcriptional dysregulation, excitotoxicity, oxidative stress and detrimental changes to neurotransmitters. Cells from other areas such as the cortex, which project to the medium spiny neurons, could be compromised and so have reduced delivery of pro-survival factors such as BDNF. A combination of these processes most probably causes the selective vulnerability of the medium spiny neuron population rather than a specific effect of mHTT on these cells.

The neurons making up the rest of the striatum are also affected but to a lesser extent, especially at the earlier stage (Ferrante et al., 1987, Hedreen et al., 1991). It is known that a population of large cholinergic neurons are consistently lost as the disease progresses (Cicchetti and Parent, 1996), while other populations are almost always spared (Ferrante et al., 1987, Cicchetti et al., 2000). Why certain neuronal populations have an increased vulnerability in HD is still not fully understood, however it might be related to their function and the neurotransmission-associated mechanisms they undergo.

Like the striatum, the cerebral cortex is a structure comprising many different regions and cell types affected in HD. Grossly, overall volume loss is seen in the cerebral cortex, with cortical thinning and increased cellular density as well as neuronal cell loss (de la Monte et al., 1988, Hedreen et al., 1991, Rajkowska et al., 1998). The earliest gross studies on the cortex found total cortical volume loss to be in line with total brain volume loss (around 19% reduction in total volume) and to correlate with both striatal atrophy and CAG repeat number (Halliday et al., 1998). Cortical thinning occurs early in the disease and is greatest in the sensorimotor cortex at all stages of the disease (Rosas et al., 2002), however other cortical areas also show varying degrees of thinning (Rosas et al., 2008). The degree of increased cell density and cell loss is different between each cortical layer. The cortical pyramidal projection found in layers III, V, and VI suffer the largest degeneration and happen to be those that primarily project to the striatum (Hedreen et al., 1991, Cudkowicz and Kowall, 1990). Despite the connection between the two structures, the degeneration that happens is thought to be a parallel rather than a downstream process (Hedreen et al., 1991, Cudkowicz and Kowall, 1990). Unlike in the striatum, the interneurons of the cortex are relatively less affected by cell death. Some loss of inhibition has been observed in the frontal cortex but little in other regions (Beal, 1994). This loss of inhibition could lead to excitotoxicity in other neurons as well as the regions they project to (Cepeda et al., 2007, Fusco et al., 1999).

The mechanism by which the mutated form of HTT (mHTT) leads to cell death is still not fully understood. The CAG repeat of HTT exon 1 is thought to interact with a number of other genes. Genome-wide expression studies using post-mortem tissue have found large numbers of altered RNAs (Hodges et al., 2006). This finding has been backed up with similar evidence using HD mouse models (Luthi-Carter et al., 2000). This evidence leads to a complex picture, which implicates a number of possible dysfunctions, including transcriptional dysregulation, excitotoxicity, alteration to neurotransmitters, and vesical

transport and disruption of morphogens such as BDNF (Cattaneo et al., 2001, Morton et al., 2001, Zuccato and Cattaneo, 2007, Rosas et al., 2008).

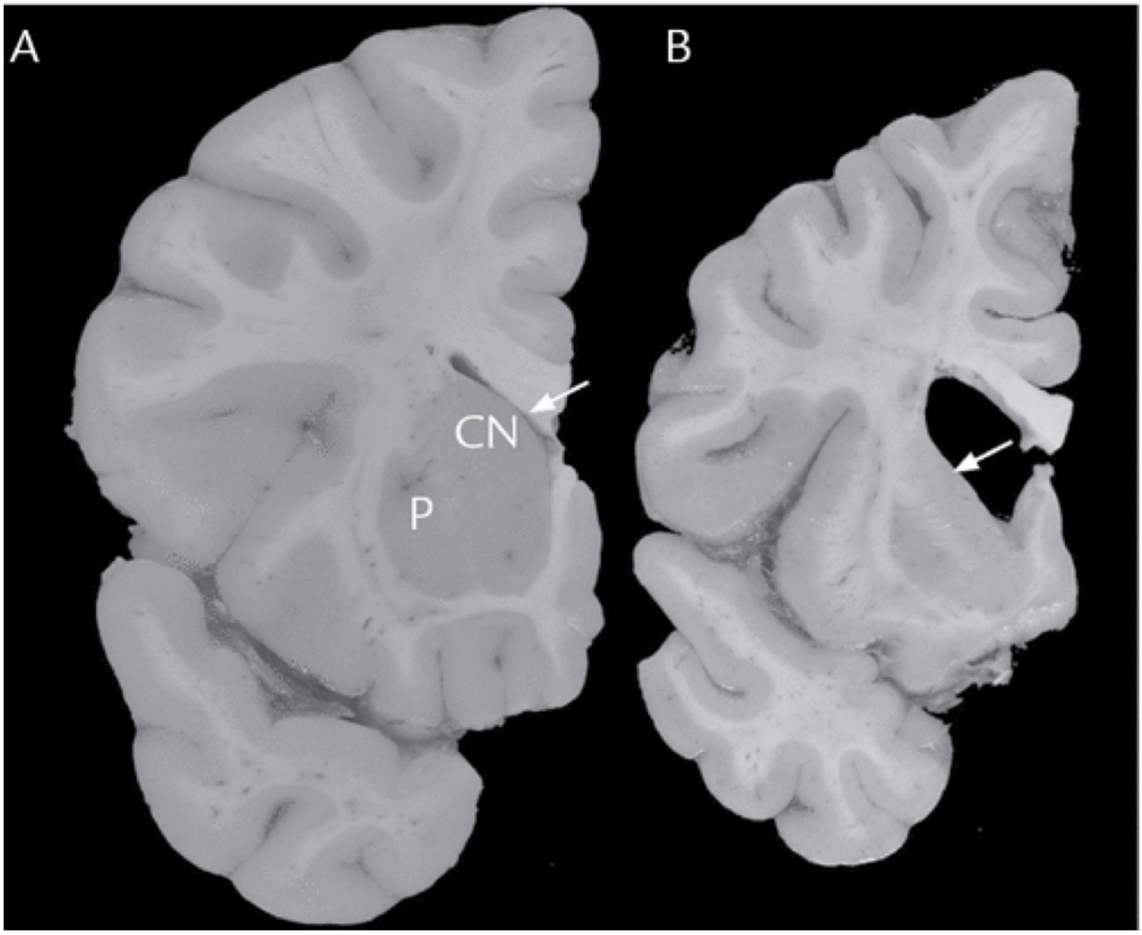

Figure 1-1. Pathological effects of HD on the brain. Coronal sections through the human brain of (A) a normal control left cerebral hemisphere of a 35-year-old male, and (B) an advanced HD case. Sections cut at the level of the striatum and the nucleus accumbens. Shrinkage of the caudate nucleus and putamen (arrows) is apparent in the HD case. Reduction of the cerebral cortex is also evident. HD=Huntington disease; CN=caudate nucleus; P=putamen. Adapted from Bates et al., 2014 with permission from Oxford University Press.

1.6 The HTT protein and its structure

The translated product of the *HTT* gene is the HTT protein, which is made up of several domains with distinct functions. At the N-terminus is a short 17 amino acid sequence termed N17, which is followed by the polyQ stretch that becomes elongated in HD. The protein contains multiple HEAT (Huntingtin, Elongator factor 3, the regulatory A subunit of protein phosphatase 2A, and TOR1) repeats (Andrade and Bork, 1995). These repeats produce a series of ordered domains interspersed with intrinsically disordered segments. HTT is thought to contain 16 HEAT repeats grouped into 3 clusters (Tartari et al., 2008) which interact with other proteins. Some HEAT sequences, known as karyopherins, are also involved in trafficking of other proteins through the nuclear pore complex (Conti et al., 2006). Between the clusters of HEAT repeats are disordered segments of unknown function, in which post-translational modifications have been identified

HTT is dynamically mobile across the nuclear membrane, a process enabled by its HEAT repeats (Truant et al., 2006, Truant et al., 2007). N17, the first 17 amino acids of exon 1 of HTT that precede the polyQ region, interacts with the nuclear pore protein translocated promotor region (TPR), which allows for protein export from the nucleus. Disruption of these amino acids can cause HTT to accumulate in the nucleus (Cornett et al., 2005). HTT can shuttle between the cytoplasm and nucleus (Truant et al., 2007), which is enabled by the presence of both nuclear localisation signal (Desmond et al., 2012) and nuclear export signals (Xia et al., 2003, Zheng et al., 2013).

1.6.1 Post-translational modifications

HTT is known to undergo many post-translational modifications, including phosphorylation, ubiquitination, acetylation, and SUMOylation, which can influence its cellular location and stability (Warby et al., 2008). Most of these post-translational modifications are found within four regions, described as the PEST domains, because of

their enrichment in proline (P), glutamate (E), serine (S), and threonine (T) (Warby et al., 2008). The first PEST domain of HTT contains the N17, the polyQ tract and is a site of phosphorylation, ubiquitination, and SUMOylation. In the presence of an expanded polyQ, the ubiquitination and SUMOylation processes, which normally act on the lysines within HTT, are impaired (Steffan et al., 2004). This modification has been linked to nuclear phenotypes such as to changes DNA repair, nuclear export, endocytosis and enzymatic activity, (Jackson and Durocher, 2013) as well as changes at the synapse (Haas and Broadie, 2008).

Phosphorylation also plays an important role in HD. HTT has multiple phosphorylation sites, including threonine 3, the levels of which are reduced to an increasing extent with longer polyQ repeats in striatal neurons (Aiken et al., 2009). Other sites at serine 13, and possibly serine 16, promote the ubiquitin–proteasome system (UPS) and autophagy pathways when phosphorylated (Thompson et al., 2009). This process is reduced in the presence of a longer polyQ and could inhibit the clearance of mHTT from cells (Thompson et al., 2009). Furthermore, phosphorylation of serine 421 of HTT has been implicated in a number of disease phenotypes (Warby et al., 2005). In the HD brain, the level of phosphorylation at serine 421 is lowest in areas with the highest levels of cell death suggesting a neuroprotective role (Warby et al., 2005), which could be related to excitotoxicity (Metzler 2010, 20980587). This same phosphorylation site is also important in the transport of BDNF (Colin et al., 2008, Zala et al., 2008).

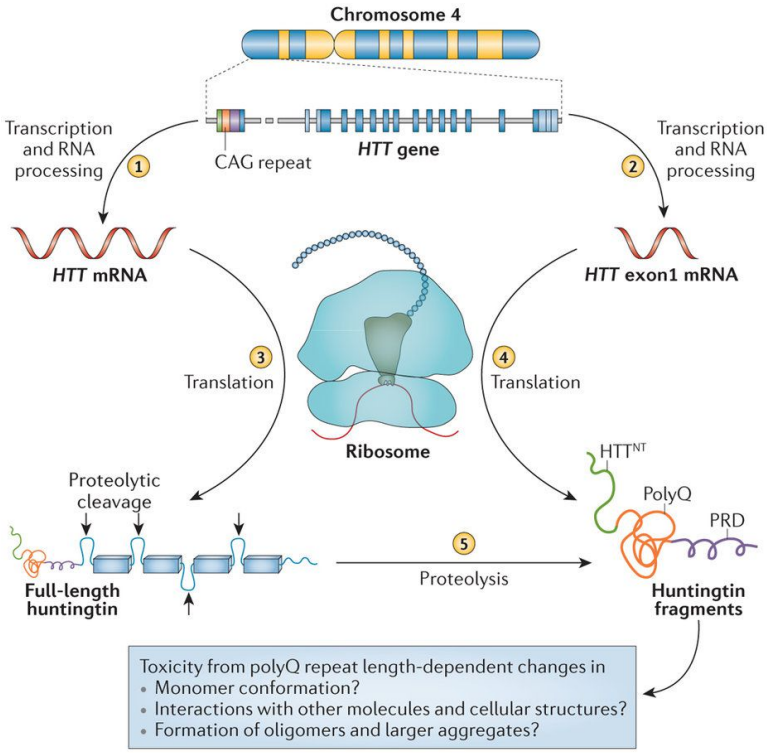

Figure 1-2. Processing of Huntingtin. The *HTT* gene is transcribed and processed to mRNA, which normally encodes the full length huntingtin protein (label 1), however, it can be aberrantly spliced into mRNA encoding only exon1 when the gene contains an expanded CAG repeat (label 2). Translation of full-length mRNAs generates the full-length huntingtin protein (label 3), whereas translation of aberrantly spliced mRNAs generates the HTT exon1 protein fragment N17 (label 4). Proteolytic cleavage sites (arrows) facilitated by recognition sequences in the disordered segments generate a group of products, including HTT exon1-like fragments (label 5). These fragments have important roles in triggering of Huntington disease when they contain expanded polyQ segments by mechanisms that are yet to be clarified. HTT=huntingtin. Figure adapted from Bates et al 2016 and reproduced under copyright agreement with Nature Publishing Group, License Number: 3925870186664.

1.6.2 HTT proteolysis.

Proteolytic cleavage of mHTT into smaller fragments could be a key step in the HD pathological mechanism (Goldberg et al., 1996, Graham et al., 2006). The HTT protein is cleaved by a number of different proteases. Caspases were the first enzymes shown to cleave HTT (Goldberg et al., 1996) before the observation that the protein is also cleaved by calpains (Kim et al., 2001) as well as aspartyle proteases (Kim et al., 2006).

Caspase cleavage of HTT is carried out by caspase-3 at amino acids 513 and 552, by caspase-6 at amino acid 586 as well as by caspase-2 at amino acid 552 (Wellington et al., 1998, Hermel et al., 2004). Evidence suggests that the caspases show no preference between cleavage of HTT and its mutated form, however the cleavage of mHTT results in fragments containing the longer polyQ. This observation combined with evidence that cellular toxicity increases in cells with huntingtin fragments (Martindale et al., 1998, Cooper et al., 1998) led to the toxic fragment hypothesis, in which the presence of the fragments promotes further caspase activity and cleavage resulting in a pathogenic feedforward cycle (Wellington and Hayden, 2000, Albrecht et al., 2007).

1.7 mHTT in HD brains and aggregation

Protein aggregation is a hallmark of several neurodegenerative diseases and in many of these the association between aggregation and cell death is still not understood. In HD mHTT misfolds, fragments at the N-terminus and accumulates in aggregated inclusions (DiFiglia et al., 1997). Aggregates can be found in a range of sizes with the largest thought to contain millions of protein molecules (DiFiglia et al., 1997, Sahl et al., 2012). Aggregates increase in size with disease progression and so have been suggested to be toxic, leading to the neurodegeneration seen in HD. The aggregating nature of mHTT might be related to its structure, and the larger polyQ region could promote a "poly-zipper"-like effect (Perutz et al., 1994). This hypothesis is based on anatomic models of the polyQ adopting β-sheets formed of β-strands held in place by hydrogen bonds. X-ray crystallography has shown that the HTT polyQ can also form other formations such as α-helix, extended loops, and random coils (Kim et al., 2009).

The aggregation process starts from HTT monomers which can self assemble into larger fibrils when their polyQ region is larger than 32 repeats (Scherzinger et al., 1999). The presence of these fribils is a catalyst for other mHTT monomers to aggregate. These fibrils together form beta-sheet formations.

It is widely agreed that the fragmentation of HTT is a key early step in HD pathology. HTT fragments have been discovered in HD post-mortem brains (DiFiglia et al., 1997, Lunkes et al., 2002) and mouse models before evidence of aggregation can be detected (Kim et al., 2006, Ratovitski et al., 2007, Landles et al., 2010). The fact that only antibodies raised against the N-terminus detect nuclear inclusions in human patient brains (DiFiglia et al., 1997, Schilling et al., 2007) and that N-terminal fragments aggregate more readily *in vitro* (Davies et al., 1997) implies that these fragments could underlie pathology. Many of the fragments found in HD mouse models can be mapped to various proteolysis cleavage sites along the protein (Landles et al., 2010).

The smallest of these fragments is an N-terminal fragment of around 100 amino acids. Because this N-terminal fragment is encoded by exon 1 of *HTT* it has thus been termed exon 1 HTT. This fragment contains the most N-terminal segment, N-17, the polyQ segment that is expanded when encoded by a larger CAG repeat, and a proline-rich domain (PRD). The exon 1 HTT fragments are formed in mouse models via the translation of aberrantly spliced mRNA transcript expressing *Htt* (Sathasivam et al., 2013) or *HTT* (Mangiarini et al., 1996). This transcript is also found in fibroblast lines from HD patients, along with HD post-mortem tissue (Gipson et al., 2013). The splicing process is regulated by SRSF6 splicing factor, which binds to the 5' end of the *Htt* gene with an expanded CAG repeat, and can facilitate translation of a partially spliced transcript (Sathasivam et al., 2013).

This exon 1 HTT fragment can be involved in the formation of a variety of aggregated structures, especially when elongated with a longer polyQ (Benn et al., 2005, Arrasate et al., 2004, Davies et al., 1997, DiFiglia et al., 1997) (Figure 1-3). Indeed, this aggregation could begin from small oligomers of between 4–15 HTT exon 1 monomers that are driven by the ability of the N-17 to self-associate and assemble into alpha–helical clusters (Jayaraman et al., 2012, Ossato et al., 2010). These oligomers can grow in size as non-β-oligomers and then become rearranged to β-sheet-rich polyQ amyloid fibrils in a process that increases in the presence of a longer polyQ (Scherzinger et al., Jayaraman et al., 2012, Bhattacharyya et al., 2005). In HD, the length of the polyQ is correlated with the onset of disease and severity (Bhattacharyya et al., 2005) once over the pathogenic threshold of 37Q. The process of amyloid fibrillation can still occur below the 37Q threshold (Sivanandam et al., 2011, Lee et al., 2012a, Ansaloni et al., 2014) but there is no evidence that this occurs in physiological concentrations. As the poly Q expands the HTT becomes more prone to aggregate. The length of the polyQ determines the stiffness of the HTT fibril. Increased polyQ length results in a stiffer and smoother structure which allows for more bonds with other HTT sheets and so are more readily able to aggregate (Ruggeri et al., 2016).

The kinetics of mHTT aggregation are proportional to its concentration. Higher concentrations make the correct orientation of the fibrils required for aggregation formation more likely (Thakur et al., 2009, Jayaraman et al., 2012). The concentration will depend on many factors including the quantity and length of fragments, somatic instability, PMTs, and proteolysis within each cell. Increases in these factors are thought to result in more aggregation events (Scherzinger et al., 1999, Bhattacharyya et al., 2005).

As such, the concentration factor could be behind why neurons are more readily affected in HD brains compared with glial cells; neurons express higher levels of HTT (Landwehrmeyer et al., 1995). Additionally, increasing evidence shows the potential of

non-cell autonomous HTT transmission from other cells (Frost and Diamond, 2010, Babcock and Ganetzky, 2015). It has long been known that mammalian cells can import amyloid polyQ fibrils (Yang et al., 2002) and that this process can recruit other polyQ proteins in the cells into aggregates and even result in cell death (Yang et al., 2002, Ren et al., 2009). Evidence suggests that this process can also take place in HD (Cicchetti et al., 2014, Pecho-Vrieseling et al., 2014).

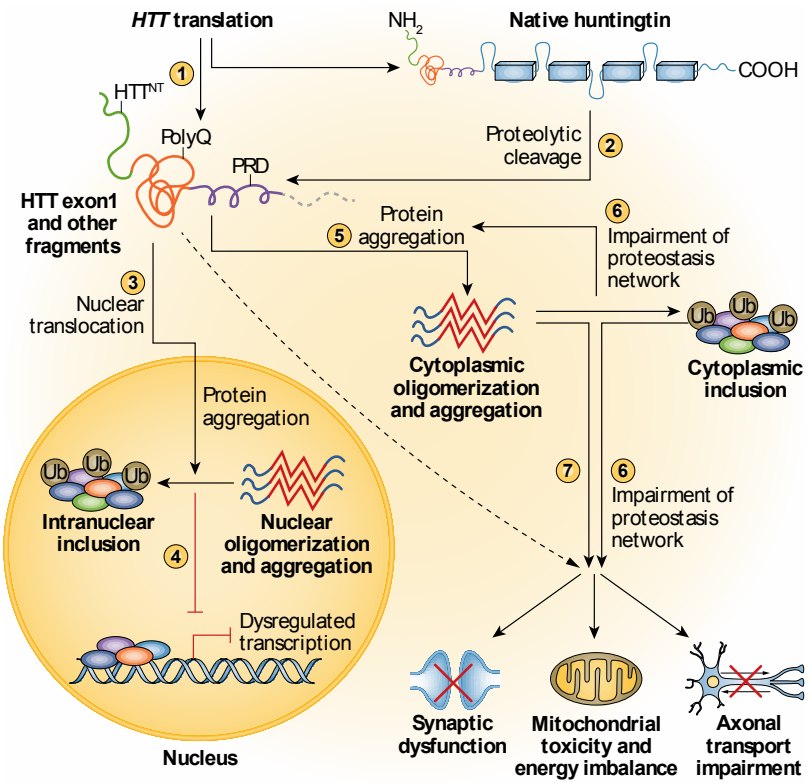

Figure 1-3. HTT pathology within the cell. The Huntintin gene is translated into the full length HTT protein, or HTT exon 1 fragments via spliced RNA when an expanded CAG repeat is present (label 1). The full length protein is cleaved via proteolysis to generate additional fragments (label 2). These fragments can enter the nucleus (label 3) and are retained inside through self-association, oligomerization and aggregation which in turn results in the formation of inclusions that cause transcriptional dysregulation through the sequestration of other proteins and by additional incompletely defined mechanisms (label 4). The fragments also oligomerise and aggregate in the cytoplasm (label 5). This aggregation is intensified through the disease-associated impairment of the proteostasis network, which in turn leads to global cellular impairments (label 6). All together, the presence of mHTT results in global cellular impairments, including synaptic dysfunction, mitochondrial toxicity, and a decreased rate of axonal transport (label 7). HTT=hungtingtin; PRD=proline rich domain; Ub=ubiquitin. Figure from Bates et al 2016 and reproduced under copyright agreement with Nature Publishing Group, License Number: 3925870186664.

The mechanisms driving the complex and numerous cellular pathologies of HD and the role that mHTT aggregation plays within the context of the disease are still not fully understood.

1.8 Animal models

Manipulation of the mouse genome to model HD has conventionally been achieved using two approaches: creation of transgenic animals (Mangiarini et al., 1996) or by manipulation of the *Htt* locus that encodes the murine HTT protein (Barnes et al., 1994, Lin et al., 1994).

The original transgenic models of HD were created by implantation of DNA containing fragments of the human *HTT* gene into a single cell mouse embryo (Mangiarini et al., 1996). Subsequently, other transgenic models were made using whole genomic sequences of the human *HTT* gene in the form of either a bacterial artificial chromosome (BAC) (Gray et al., 2008) or yeast artificial chromosome (YAC) (Hodgson et al., 1999, Slow et al., 2003).

The complementary method of editing the murine *Htt* can be used to alter gene sequences to produce knock-in models or to knock-out the gene, and so prevent its expression altogether. These knock-out models of HTT are embryonically lethal (Duyao et al., 1995, Nasir et al., 1995, Dragatsis et al., 1998, Zeitlin et al., 1995). Knock-in models replace the normal 7 glutamines in mouse *Htt* with an expanded tract on one or both alleles (Levine et al., 1999, Shelbourne et al., 1999). Expansion of the *Htt* repeat length to a pathogenic range more accurately reproduces the genetics of the human disease compared with those represented by transgenic models, However, such models also generally have a slower onset of pathology. In all HD mice, a longer CAG repeat length, beyond the

range observed in humans, is needed to produce a model with measurable phenotypes within a 2-year laboratory mouse life span (Levine et al., 1999, Shelbourne et al., 1999).

The R6 transgenic mouse models, created by our research group, develop an early disease phenotype followed by a rapid pathological disease advancement (Mangiarini et al., 1996). Of these mouse models, the R6/2 model has become the most commonly used in HD research. The R6/2 mouse was created with fragments of the human *HTT* gene containing exon 1 with around 150 CAG repeats. The R6 models are models of the missplicing that occurs in HD, which produces the exon 1 HTT (Sathasivam et al., 2013). Phenotypically, R6/2 mice rapidly develop many of the HD-like symptoms found within the human disease and die around 16 weeks of age. Impairments in cognition (Lione et al., 1999), motor ability (Carter et al., 1999), and a decrease in brain volume (Zhang et al., 2010a, Rattray et al., 2013) are observed. HD-like behavioural phenotypes can be detected from 4 weeks of age in some novel activity analyses (Hickey et al., 2005). Rotorod and grip strength tests show deficits by 8 weeks and increase progressively until death (Carter et al., 1999, Rattray et al., 2013). Alterations in the electrophysiology in the corticostriatal pathway (Cepeda et al., 2003) and deficits to hippocampal synaptic plasticity (Murphy et al., 2000) underlie some of these symptoms. HTT aggregates also appear early within the brain, before the onset of many other phenotypes (Davies et al., 1997). Many studies have shown the presence of inclusions in R6/2 mice between 3-4 weeks of age (Davies et al., 1997, Li et al., 1999a, Morton et al., 2000, Meade et al., 2002) while others have shown they can be detected even earlier, in p1 neonates (Stack et al., 2005) although at low concentrations. Similar to in the human HD brain, this aggregation is a useful phenotype to monitor the disease.

Data for whether the R6/2 mouse model replicates the neurodegeneration seen in the human HD are conflicting. A stereological analysis by Stack and colleagues in 2005 found a 25% reduction in striatal neurons in 12 week old R6/2 mice compared with their

WT littermates (Stack et al., 2005). However, analysis performed in our lab found little cell death in R6/2 mice compared with their WT littermates at 16 weeks of age in either the striatum or the cortex (Rattray et al., 2013). Lack of cell death was apparent, despite a widespread inclusion phenotype and dramatic progressive reduction of brain volume and of cortical thickness measured using MRI. Many other groups have also found low levels of cell death in the brains of R6/2 mice (Davies et al., 1997, Zhang et al., 2010a). The CAG repeat in the R6 lines is unstable (Mangiarini et al., 1996) and so independent colonies can have varied CAG repeat sizes. The length of CAG repeat influences disease onset, progression, and survival time with a longer repeat accelerating the disease (Menalled et al., 2009, Morton et al., 2009). However, when this repeat becomes very long, over 330 repeats, phenotypes become milder and onset is delayed (Morton et al., 2009), which is important to consider when using R6/2 mice.

Despite varied approached to modelling HD in mice, no single HD mouse model recapitulates all aspects of human HD disease progression—most likely due to the fundamental genetic differences between rodents and humans.

Other than mice, additional animal models of HD have been created. These include transgenic rats (von Horsten et al., 2003), as well as models using larger mammals such as sheep (Jacobsen et al., 2010), pigs (Yang et al., 2002), and the rhesus macaque nonhuman primate (Yang et al., 2008). These models have been useful to study effects of mHTT on larger brains more similar to the human CNS. Because these larger models have longer lifespans than the laboratory mouse, shorter CAG repeats closer to those commonly seen in human HD patients can be used. Even so these repeats are still artificially extreme so that it is possible to study the disease in a reasonable time frame. Cognitive and memory deficit phenotypes were seen in the rats with 53Q (Brooks et al., 2009), while the larger models have developmental abnormities (Jacobsen et al., 2010, Chiang et al., 2012) and many of the105Q pigs and 84Q monkeys die soon after birth

(Yang et al., 2010, Yang et al., 2008). The 73Q sheep model, under the human HTT promotor, shows reduction of striatal DARPP-32 (dopamine- and cAMP-regulated neuronal phosphoprotein) staining by 7 months (Jacobsen et al., 2010). These models will be useful to study the disease over longer lifespans than the laboratory mouse yet still do not fulfil all the needs required to understand the disease process.

Animals provide excellent models of how HD affects the brain and body as a system, dissecting molecular mechanisms in an animal model is a slow and challenging. An alternative is to transfer the underlying processes and tissue to study *in vitro*. To be able to study the process of HD pathology in a cell would be hugely beneficial to understand the disease mechanism and the ideal approach to do this would be to establish human HD cultures that exhibit measurable phenotypes within a reasonable time-frame for experimentation.

1.9 Human tissue research

The use of human HD post-mortem tissue has long been the most accurate way to distinguish HD neuropathology. However, in general, such tissue only really gives information on the late-stage processes of the disease and not those that underlie pathology (Sterneckert et al., 2014). Beyond this, studying HD *in vitro* had been limited to extractable cell pools such as blood or spinal fluid. Despite huge leaps being made during the last decades in stem-cell science, a reliable cell model of HD for therapeutic development remains elusive.

1.9.1 Immortalised human cell lines.

A traditional way to maintain neural cells *in vitro* was to artificially immortalise them. Immortalised neuronal cells lines, such as human SH-SY5Y, as well as murine mouse

N2a, rat PC-12m lines, can be transfected with different polyQ-expanded huntingtin constructs to model HD (Scotter et al., 2010, Cisbani and Cicchetti, 2012, Zemskov et al., 2003). One study using an immortalised line transfected with polyQ constructs of 150Q showed mHTT localisation in the nucleus, as well as changes to cell morphology, gene expression, and decreased viability (Li et al., 1999a). The process of immortalisation might impact the cells and introduce unpredictable variables, including genetic mutations and karyotype instability, and therefore such cell lines might not be ideal to model HD.

Besides neuronal cells, mHtt has also be transfected into non-neuronal cells (Cisbani and Cicchetti, 2012) including HeLa cells (Iwata et al., 2005, Majumder et al., 2006, Raychaudhuri et al., 2008) human embryonic kidney cell-line 293T (HEK293T) (Sancho et al., 2011, Iwata et al., 2005, Cooper et al., 1998) as well as monkey kidney cell lines (COS-7) (Ossato et al., 2010, Ho et al., 2001) with various phenotypes. Despite much potential, candidate compounds in drug screens using these models have yet to translate to larger HD models or in clinical trials (Bard et al., 2014). This failing could be down to the levels of HTT differing from physiological levels in such lines, as well as the potential effects of immortalisation.

1.9.2 Human stem cells.

Advances in cell culture knowledge and techniques have allowed non-immortalised cells to be used. Embryonic stem cell (ESC) technology has created a resource of human cells that can be isolated and cultured long-term (Thomson et al., 1998). Such advances led to the creation of several HD ESC lines capable of differentiation into mature adult cell types and tissues (Verlinsky et al., 2005, Niclis et al., 2009, Bradley et al., 2011, Lu and Palacino, 2013). These lines, once differentiated into neural cells, exhibited HD-like phenotype such as CAG repeat length instability, mitochondrial abnormalities, and abnormal neurotransmitter responses. However, use of such embryonic human tissue has always been hampered by ethical concerns raised by of the destruction of a human

blastocyst during the process of ESC creation rendering the availability of new lines limited.

Advancements in stem cell technology include the promising upheaval in the stem cell dogma by the possibility of new sources of stem cells using induced pluripotent stem cell (iPSC) technology (Takahashi et al., 2007, Takahashi and Yamanaka, 2006). This technology can allow for the production of stable progenitor cell lines derived from almost any adult human tissue (Zhou et al., 2012). This process bypasses the need for embryonic tissue by essentially converting adult cells back into ESC-like iPSCs using four transcription factors responsible for an embryonic phenotype (Takahashi et al., 2007). Stable lines formed in this way can be created from human HD patients. Researchers using this approach have produced HD iPSC lines that replicate certain HD phenotypes (An et al., 2012, Cheng et al., 2013, HD iPSC Consortium, 2012, Chae et al., 2012, Jeon et al., 2012, Camnasio et al., 2012).

The first iPSC line from an HD patient were created by Park et al (2008) who attempted to make lines from fibroblasts taken from patients with various diseases (Park et al., 2008). The patient from whom the fibroblasts were taken for the HD lines had an allele with 72 CAG repeats, suggesting a juvenile form of HD. Despite this highly extended CAG repeat, gene expression analysis of the iPSC lines by the researchers identified no pathological phenotypes (Park et al., 2008).

This juvenile HD iPSC line was subsequently used by other groups to investigate possible phenotypes that Park and colleagues did not investigate in their initial study. A range of phenotypes were exposed that differed from iPSCs derived from healthy people, including an increased caspase activity upon growth factor removal (Zhang et al., 2010b), and high susceptibility to oxidative stress followed by apoptotic cell death (Chae et al., 2012), when in a NSC state. The cells could be differentiated into GABAergic neurons

and survive transplantation into rat brains. An aggregation phenotype was not present within these neurons unless the cultures were treated with the proteasome inhibitor MG-132 (Jeon et al., 2012). The levels of this aggregation were reduced by treatment with an microRNA, miR-196a, which has similar effects in HD-mouse models (Cheng et al., 2013).

An and colleagues identified additional pathological phenotypes in the juvenile HD iPSC cell line, including increased apoptosis, decreased BDNF expression, and altered caspase activity (An et al., 2012). Subsequently, these authors used homologous recombination in the HD iPSCs to reduce the expanded allele of the *HTT* gene from 76 CAG repeats to 21 repeats. This reduction in CAG repeat length reversed the pathological phenotypes they had previously seen with these lines (An et al., 2012).

A collaboration of labs formed the HD iPSC consortium to generate 14 iPSC lines from seven individuals. These lines were created with CAG repeats of 21, 33, 60, 109, and 180, to represent the range from healthy controls through to CAG repeats that would cause severe pathology. Once differentiated to NSCs, gene expression was analysed by microarray and cluster-based analysis. This analysis revealed that the control lines with CAG repeats of 21 and 33 differed from those with pathogenic repeat lengths. The differentiated NSCs and derived neurons with longer repeats exhibited problems with cell adhesion and decreased adenosine triphosphate (ATP) production, increased caspase-3 activation, increased cell death after prolonged culture or BDNF withdrawal, and increased vulnerability to stress and toxicity. These HD-like phenotypes correlated with CAG repeat number and became more severe with longer CAG repeats (HD iPSC Consortium, 2012).

Ideal HD cell models for screening purposes would limit genetic background variance while also representing multiple CAG repeat lengths (An et al., 2012). This ideal has been

made more realistic with advances in genome engineering using zinc finger nucleases and transcription activator-like effector nucleases (TALENS) (Baker, 2012, Alberts, 2012). Subsequently, use of clustered regularly interspaced short palindromic repeats (CRISPR) has dramatically cut the time and cost of gene editing (Jinek et al., 2012, Segal and Meckler, 2013). CRISPR uses a bacterial nuclease to cut specific sites in DNA. The nuclease is directed to the site by a guide RNA, which recognises 18–21 base pairs in the DNA, allowing unique sites in the genome to be targeted (Bassett et al., 2013). CRISPR is therefore an ideal system for making a library of varying length CAG repeat models for HD.

Researchers modelling other neurodegenerative diseases have made gains in understanding using iPSCs. For example, in amyotrophic lateral sclerosis research, subtypes of motor neurons can now be created from patient iPSCs to model relevant pathologies in ways that were not possible with ESCs derived neurons (Sances et al., 2016, Richard and Maragakis, 2015). This suggests with time similar breakthroughs could be made within the HD research field.

A limitation of iPSC technology is the time needed to create and differentiate these patient-specific lines, which is currently extensive. Reliable methods of neuronal differentiation within reasonable turnaround times still need to be optimised. Artificial genetic alteration of these lines has also been problematic because of the difficulty of homologous recombination into endogenous alleles (Han et al., 2011), although the advances in editing with technologies like CRISPR could alleviate this. If and when these hurdles can be overcome, iPSC cells will be vital in the future of HD research.

Until the technologies using human tissue and cells can be improved further, the use of cells from non-human models remains an important approach for the study of certain HD phenotypes and to compliment and dissect findings made with *in vivo* models.

1.10 Mouse stem cell models

Use of mouse models of HD that exhibit measurable HD-like phenotypes is a useful approach for translational *in vitro* research. Isolation of cells from the R6/2 HD model would allow for the study of HD-like phenotypes that underlie the disease at a cellular level. The technique applied to obtain cells to culture and when during the mouse life span such techniques are applied are important considerations when assessing what aspect of HD is to be studied. With the emergence of iPSC technology, this pool of potential cells has been expanded greatly yet, as already discussed, this new technology has its limitations. Techniques that had fallen out of general use have been newly revitalised, mainly due to advancements in the understanding of the growth and maintenance conditions required to produce stable lines.

Mouse ESCs and NSCs both offer a source of cells with great promise to the HD research field, especially due to their intrinsic properties to produce a range of cell types. ESCs, in theory, permit the creation of all cell types; however, differentiation protocols can be complex, as is their required growth on feeder layers (Reubinoff et al., 2000, Thomson et al., 1998) or artificial substrates (Nakagawa et al., 2014, Xu et al., 2001).

NSCs on the other hand are a population of multipotent cells found in the developing brain and adult CNS. NSCs are mitotic and are capable of self-renewal (proliferation). They can exit the cell cycle to differentiate into the three neural linages of the CNS: neurons, astrocytes, and oligodendrocytes. During development, NSCs produce the cells that form the CNS, dividing many times to produce the daughter cells that create the eventual brain. In the adult brain, a pool of NSCs remain in the sub-ventricular zone (SVZ) and dentate gyrus (DG). They have a limited regenerative potential (Doetsch and Alvarez-Buylla, 1996, Lois and Alvarez-Buylla, 1994, Gage et al., 1998) as well as vital roles in processes such as memory formation (Deng et al., 2010).

NSCs divide and survive in specialised neurochemical niches, which help to regulate asymmetrical division giving rise to identical daughter cells that can divide themselves or migrate and further differentiate into mature cells (Temple, 1989). In the developing brain, a set programme of maturation gives rise to NSC populations with ever more regionally specific fates precise to the spatiotemporal area they develop (Temple, 2001). The mitogens and chemotactic factors each mitotic NSC is exposed to acts to decide the role and function that each cell comes to adopt within the CNS network. Understanding of how spatiotemporal fate is controlled and can be manipulated to artificially guide cells towards appropriate fates is a key process in the culturing of cells.

1.11 Neurogenesis

To comprehend the nature of cultured NPCs, endogenous *in vivo* neurogenesis in the developing mammalian embryo must first be understood. Neurogenesis is considered to begin when the neuroectoderm is induced into forming the neural plate, the most rudimental CNS structure. In mice, this process is considered to occur at about embryonic day 7.5 (E7.5). By E8.5, the neural plate folds into the neural tube. The neural cell progenitors present at this stage *in vivo* are thought to be the same populations that can be induced from embryonic stem cells (ESCs) during *in vitro* differentiation protocols (Conti et al., 2005, Pollard et al., 2008, Elkabetz et al., 2008). They are thought to divide and produce identical daughter cells to expand the progenitor pool along the then single layered ventricular zone (Gotz and Huttner, 2005).

At around E9.5 in the mouse, a population of neural progenitors termed radial glial (RG) cells develop. The RG cells are a transient population with specific morphological hallmarks which develop from neuroepithelial cells. These cells are characterised by their morphology with radial process reaching from their ventral niche, to the basal surface of

the brain (Hartfuss et al., 2001). RG cell division produces the majority of cells that eventually form the brain and their scaffolding properties help to move their progeny to the appropriate area (Hansen et al., 2010, Noctor et al., 2008).

RG cells in development are defined by lineage heterogeneity based on spatiotemporal variety (Hartfuss et al., 2001, Anthony and Heintz, 2008). Similarly, separate RG populations *in vitro* act differently depending on the area and the stage of the embryo that they represent (Pinto et al., 2008, Li et al., 2004). At around mouse E18 developmental neurogenesis is considered to end as the RG cells mostly migrate and differentiate (Edwards et al., 1990, Miyata et al., 2001, Shen et al., 2006, Noctor et al., 2008). However, some RG cells do remain, and fate mapping experiments using adult SVZ derived NSCs have shown this population of adult progenitors originate from a subpopulation of radial glia cells that become B type stem cells that survive and retain their pluripotency after development *in vivo* (Merkle et al., 2004).

RG cells obtained from within the neural developmental window can be expanded *in vitro* and provide a valuable source of stem cells (Johe et al., 1996, Hartfuss et al., 2001, Conti et al., 2005). This approach is used within this thesis to produce cell models using transgenic mouse foetal CNS tissue. The lines between the definition of a neural stem cell rather than a neural progenitor cell are somewhat blurred. True neural stem cells are the cells that become all those which make up the nervous system, and also retain the ability to become each and every type of cell found in neural tissue (Ramalho-Santos and Willenbring, 2007, Clayton et al., 2007). Neural progenitors on the other hand are presumed to be restricted in terms of having regional specification, a finite mitotic potential, or restricted differentiation fate (Seaberg and van der Kooy, 2003). However, the two terms are often used interchangeably in research literature, which can cause confusion.

Cells extracted from mouse foetal brain sources are potentially more accurately termed RG-like neural progenitor cells (NPCs) and are referred to as such in some publications. Because the stem abilities of the population of cells extracted and cultured in this thesis were not fully characterised, they will be referred to as NPCs throughout the results chapters.

1.12 Culturing neural stem cells

It has long been hoped that the potential of culturing and maturing NSCs *in vitro* could allow for long-term models of the mechanics of neural networks and disease. The scalable potential of cell models is an ideal platform to probe treatments for many diseases on a mass scale. The initial attempts to obtain, purify, and expand NSCs from developing embryos and areas of adult neurogenesis proved problematic. Original attempts during the 1990s to maintain a culture of NSCs *in vitro* was on a small scale and varied in success (Reynolds et al., 1992, Reynolds and Weiss, 1992), mainly because of a lack of understanding of the conditions required to maintain the stable NSC physiological state outside the brain.

These methods fell out of favour with more attention being diverted to the use of artificial immortalisation techniques to produce stable cultures. However, developments in growth factor-based protocols allowed cell maintenance and long term expansion as both free floating cell clusters termed neurospheres and adherent monolayer cell cultures. The breakthrough was achieved with the understanding that cells could be maintained as proliferative cultures in media supplemented with the morphogens epidermal growth factor (EGF) and basic fibroblast growth factor-2 (FGF2) (Conti et al., 2005). These factors allow for stable cultures extracted from the embryo to be maintained *in vitro* with relative ease.

1.13 From niche to dish

NSCs can be expanded as free-floating neurospheres or as a monolayer of cells adhering to the plastic of the dish (Conti and Cattaneo, 2010, Conti et al., 2005) (Figure 1-4).

1.13.1 Neurosphere system:

Neurospheres are free-floating masses of predominantly NSCs, which can potentially form from a single NSC (Laywell et al., 1999, Reynolds et al., 1992). NSCs can be harvested from the developing mouse neural tissue between E10.5 and E18.5 or from areas of adult neurogenesis such as the sub-ventricular zone (SVZ) (Louis and Reynolds, 2005, Chojnacki and Weiss, 2008). NSCs can also be created from ESCs or from iPSCs once neuralised (Chojnacki and Weiss, 2008). NSCs will form neurospheres when cultured without a surface they can adhere to and left to settle in serum-free media supplemented with EGF (10-20 ng/ml) and FGF-2 (10-20 ng/ml) (Singec et al., 2006). Under these conditions differentiated or differentiating cells do not survive, resulting in pure populations of mitotic NSCs. In response to media containing mitogens, the cells divide and produce the free-floating neurosphere masses. These clusters can then be expanded for long periods, dissociated and re-plated to expand the NSC population relatively quickly.

The characteristics of cells that form neurospheres have been investigated in relation to the age of the source and the location they are isolated from. Neurosphere-forming cells extracted from the adult SVZ are thought to be either glial fibrillary acidic protein (GFAP)+ 'B-Type' or the distal-less homeobox (DLX)2+ 'C–type' cells (Doetsch et al., 2002). Neurosphere-forming cells dissected from the embryo are less well characterised; the expression levels of NSC markers can differ from those observed *in vivo*. Many cultures only express the NSC marker nestin, although some also express NSC markers

such as SOX-2, prominin and RG markers such as RC2, the glutamate aspartate transporter (GLAST), and the brain-lipid-binding protein (BLBP) (Hartfuss et al., 2001).

Evidence suggests that, with human cells at least, cells comprising neurospheres are mostly RG cells, which might be because these are the cells most suited to survive in the culture conditions. Activation or signalling of the EGF receptor using high concentrations of EGF (Nelson et al., 2008) produces cells that are morphologically, antigenically, and functionally definable as RGs when allowed to adhere (Gregg and Weiss, 2003).

With neurospheres being a 3-dimensional bulbous of cells rather than a single monolayer, the cells at the centre experience a different neurochemical environment to those on the outside. As their size increases, this environment becomes more of a limiting factor and can result in cells beginning to differentiate because of the lack of contact with mitogens and increased notch signalling (Campos, 2004). As the neurosphere becomes larger still, cells towards the centre of the neurosphere can become necrotic due to lack of nutrients (Xiong et al., 2011, Moeller and Dimitrijevich, 2004)

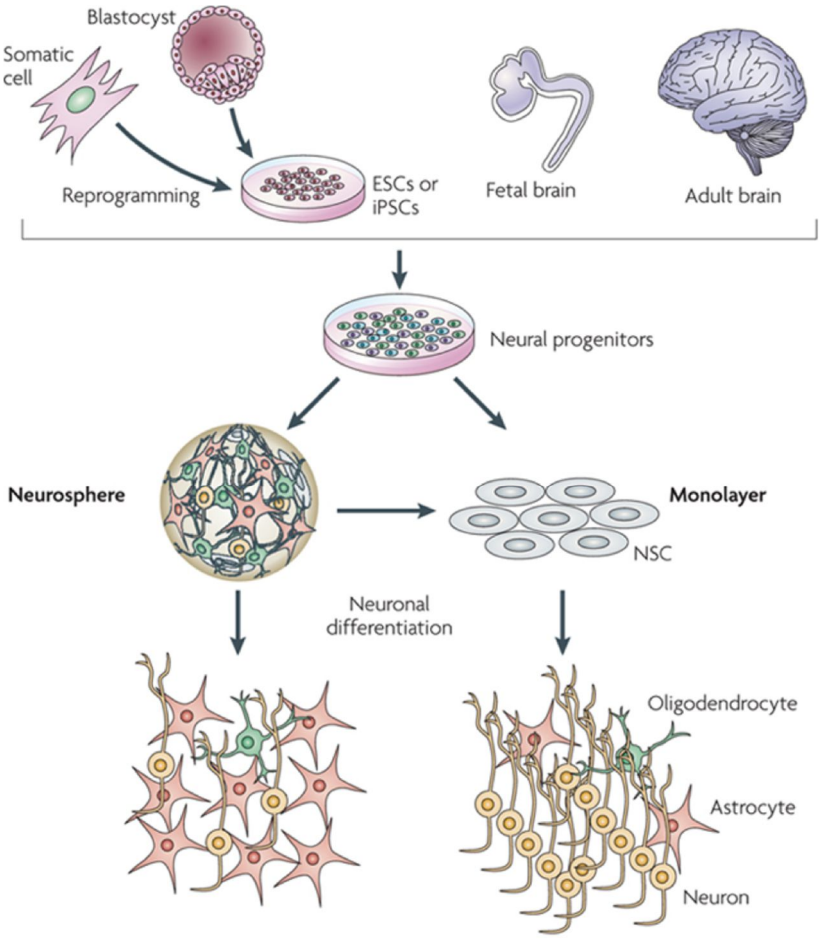

Figure 1-4. Sources for establishment of neural progenitor cell lines. ESCs derived from the inner cell mass of blastocysts, iPSCs derived from reprogrammed somatic cells, and the germinative areas of the foetal and adult brain can be used to harvest neural stem cells. Neurospheres and cells grown in monolayers are considered tripotent as they can give rise to neurons, astrocytes and oligodendrocytes. The distinctive cellular compositions of the neurosphere (mixed, with only a fraction of the cells exhibiting NSC properties) and NSC monolayer culture systems results in low and high neurogenic potential, respectively. ESC= embryonic stem cells; iPSCs=induced pluripotent stem cells; NSCs=neural stem cells. Reproduced from Conti and Cattaneo (2010) under copyright agreement with Nature Publishing Group, License Number: 3925970196918

NSCs grown as neurospheres retain their CNS tripotent differentiation potential. Over time and passages the potential to produce neurons decreases and a predilection to glial cells dominates (Bibel et al., 2007). Various differentiation protocols have been applied to neurospheres based on mitogen removal, exposure to bovine serum, and specific cytokines and substrates. However, none of these protocols produce a population of beta-III-tubulin positive cells totalling beyond a proportion of 20% (Weiss et al., 1996, Grandbarbe et al., 2003, Chojnacki and Weiss, 2008). With the relative speed and ease of expansion of neurospheres, cell-sorting techniques such as fluorescent activated cell sorting (FACS) could produce large numbers of individual neurons from an appropriate quantity of neurospheres.

A certain limitation of the neurosphere system could be its inability to preserve region-specific phenotypic profiles. Cells harvested from different developmental regions of the brain and cultured as neurospheres keep their region-specific molecular profiles for 1-2 passages (Hitoshi et al., 2004), however beyond this number of passages *in vitro,* region-specific patterns are altered in terms of expression of both rostral-caudal and dorsal-ventral markers (Zappone et al., 2000, Gabay et al., 2003, Hack et al., 2004).

The neurosphere system has been used to study HD. NSCs from the cortex and striatum have been isolated from WT and R6/2 mice between 1 and 4 days after birth (p1-p4) (Chu-LaGraff et al., 2001). Most of these cells died within 24 hours, suggesting they were post-mitotic thus unable to survive in proliferation media. The surviving cells were grown as neurospheres, and maintained over many months. The authors showed that NSCs could be differentiated into neurons and glia upon morphogen withdrawal, however the majority of cells became GFAP+ glia. Differentiated neurons were found to express mHTT in a manner that resembled neurons during the pathogenic stages of the R6/2 mouse model (Chu-LaGraff et al., 2001). These findings suggest that NSCs isolated from

the R6/2 mouse can be cultured *in vitro* and retain some HD-like phenotypes exhibited by mouse models.

1.13.2 Monolayer system

The initial efforts to produce homogenous monolayer NSC cultures systems were not very successful, with only a few examples producing stable cultures (Palmer et al., 1997, Alexson et al., 2006). This changed with the understanding that NSCs cultured with EGF and FGF-2 will remain stable and can be expanded as adherent clonal identical cell lines (Conti et al., 2005, Elkabetz et al., 2008, Koch et al., 2009). The presence of EGF and FGF-2 in this technique allows maintenance of the stable culture of adhered cells regardless of whether the cells are harvested from ESCs, foetal or adult tissue (Palmer et al., 1997). In the right conditions, monolayer NSCs have been cultured to 130 passages with no major differences in proliferation or differentiation patterns (Spiliotopoulos et al., 2009).

As a monolayer, cells divide symmetrically producing identical daughter progeny and retain their potential for differentiation into the three neural cell types (Conti et al., 2005). The cells will continue with mitotic expansion until their density reaches a point where contact inhibition through notch signalling triggers their differentiation. As such, differentiation needs to be prevented by passaging the cells into new plates when the cells become too confluent. Regular passaging allows monolayer cultures techniques to produce large NSC populations with negligible spontaneous differentiation. As with neurospheres, cells that form monolayer cultures display many similarities to forebrain neurogenic RG cells (Conti et al., 2005, Pollard et al., 2008). The monolayer environment probably allows for more uniform cell culture of RG-like NSCs compared with a neurosphere culture. Indeed, the cells enriched by the monolayer technique might be the RG-like NSC portion of the neurospheres. The neurogenic potential of NSCs grown as

monolayers appears to be maintained over several passages unlike with neurospheres (Goffredo et al., 2008).

The nature of a monolayer system as an artificial 2-dimentional culture seems to prevent lineage restriction as well as preventing spontaneous differentiation. As such, the relatively homogeneous self-renewing cell population is ideal for *in vitro* modelling of genetic alternations and resulting phenotypes. Evidence suggests monolayer cultures could be grown for many passages while retaining their radial glial NSC identity and characteristics (Sun et al., 2008). One concern remains over how representative *in vitro* cultures are of their *in vivo* counterparts. A subpopulation might be prone to survive *in vitro* that are forced to reprogram for the culture environment (Temple, 2001), especially with the preservation reliance on EGF and FGF2 (Reynolds and Rietze, 2005). However, analysis of gene expression in RG-like progenitors derived from various areas of the brain show that the expression of some region-specific genes is maintained (Onorati et al., 2011) suggesting any reprograming that takes place will not be total. When looking to investigate phenotypes of HD this uncertainty is worth noting.

The monolayer approach to culture NSCs has been used by several groups to study HD. A full length *Htt* knock-in mouse model with 111 repeats has been used as a source of NSCs from E14 foetal mice (Reis et al., 2011). These *HdhQ111* knock-in lines have been used by a few groups. The lines were immortalised to create clonal striatal cell lines from E14 *HdhQ111* mice, which were established with both homozygous and heterozygous full length HTT expression. Expression of mHTT is found in both the cytoplasm and nucleus with abnormalities in endoplasmic reticulum (ER) stress and metabolic problems established (Trettel et al., 2000). Other groups have used these *HdhQ111* knock-in lines to investigate the links between cellular ATP/ADP energy regulation, which is reduced in the *HdhQ111* mouse model, and N-cadherin, a protein known to be involved with cell adhesion, differentiation, and synaptic function (Reis et al., 2011).

Knock-in mice with CAG repeats of 20, 50, 9,1 and 111 were also used to create ESC lines expressing the varied polyQ (Jacobsen et al., 2011). These cells were used to investigate gene expression against lines with 7 repeats as well as *Htt* null lines. Problems with energy metabolism and ATP/ATD levels were found in these lines, confirming evidence seen in other models (Jacobsen et al., 2011). Using similar knock-in cells with a 150 CAG repeat, neurogenesis was found to be increased (Lorincz and Zawistowski, 2009). This model system proves ideal for the study of how the endogenous polyQ expansion on the mouse *Htt* can affect HTT-related proteins.

Snider et al (2003) used a similar approach for cells from E14–E16 *Hdh*Q111 along with R6/2 mice (Snider 2003, 12895502). The researchers created foetal cell lines on adherent poly-D-lysine and laminin-coated vessels, which were maintained with bovine and horse serum. Non-neural cell division was prevented with cytosine-arabinoside to purify the population. The authors observed ubiquitinated inclusions in cultured neurons from R6/2 animals as early as 14–16 days after plating, however no data were shown to support this. The researchers primarily investigated the cells' response to toxins, which had previously been observed to affect similar mouse models. No deleterious effects were observed in the HD cell lines and their WT counterparts in response to the toxin kainate, N-methyl-D-aspartate (NMDA) receptor antagonists, proteasome inhibitor-induced death, and oxidative injury (Snider et al., 2003).

Culturing of cells extracted from human foetal tissue, using the same approach as for mouse tissue, has also been attempted. Cells were extracted from 12–20-week old foetal striatal tissue and grown as adherent cultures. These human cultures could be differentiated into the three neural linages (Li et al., 2005). The use of such an approach from HD foetal tissue would be very interesting but is also extremely hard to source, and has ethical considerations that would limit the approach as a source of cells for research.

Therefore, foetal human cell lines to study HD are limited to artificial alteration of HTT levels in the NSC line by transduction with *HTT* with longer CAG repeats.

1.14 Differentiation

The simplest way to induce differentiation of NSC cultures is by the removal of the mitogenic growth factors from the cultures. ESC sourced NSCs differentiated in media with EGF and FGF2 removed and B27 added produces cells positive for the neuronal markers beta-III-tubulin (TUJ), gamma-aminobutyric acid (GABA) and glutamic acid decarboxylase (GAD67). By 7 days of culture in this differentiation media some neurons were found to be immunoreactive for synaptophysin (Conti et al., 2005), suggesting neurons with functional synapses could be produced. Further investigation with electrophysiology confirmed these findings. Subsequent adaption of original protocol by the same group allowed potential neuronal yield of around 80% after 21 days in differentiation media (Spiliotopoulos et al., 2009).

Other groups have concentrated on cells from foetal sources. E12 cells were obtained from a population of striatal precursor cells found by dissection from the ganglionic eminence, the niche pool which produces the striatum (Onorati et al., 2011). These cells were cultured and then differentiated using a previously optimized system developed on maturing adult SVZ cells. After 23 days, cells positive for TUJ, microtubule-associated protein (MAP)2, and GFAP, and GABAergic positive neurons were present. These observations are consistent with the typical characteristics of *in vivo* striatal neurons. Additionally, some neuronal cells expressing growth-associated protein (GAP)-43 were present, which is evidence of active neurite outgrowth and plasticity. No O4-positive oligodendrocytes were found with this method (Onorati et al., 2011).

To specifically investigate the neuronal and glial fates that differentiation of these cells produced, this same group subsequently examined lineage-specific regional gene expression. Foetal striatal cells were exposed to retinoic acid (RA), a morphogen that is important in the fate determination of the lateral ganglionic eminence (LGE) and for striatal neuron differentiation, as well as the effects of valproic acid (VA), which promotes differentiation into GABAergic neurons (Laeng et al., 2004, Onorati et al., 2011). The cells were exposed to these morphogens for 15 days. The researchers found that neither the early post-mitotic striatal precursor marker insulin gene enhancer protein (*Isl1*) nor *Dlx6* or *Dlx5* were expressed. Expression of these markers would be expected *in vivo* in striatal precursor cells (Stenman et al., 2003). Markers of striatal precursors and of the striatal medium spiny neurons, forkhead box protein (*Foxp*)*1*, *Foxp2*, meis homeobox (*Meis*)*2*, and *Rarβ1* were not found to be differentially expressed when cultured with or without RA or VA. The medium spiny neuron marker dopamine- and cAMP-regulated neuronal phosphoprotein (DARPP)-32 was not seen via immunostaining nor visible on blots. One gene that was constitutively expressed under both self-renewal and differentiation conditions was *cAMP-regulated phosphoprotein-21 (Arpp-21),* suggesting some striatal specificity does remain (Onorati et al., 2011). These results point towards NSCs harvested from the developing striatum expressing some striatum-specific genes during differentiation, however, the cell line they produced did not acquire a fully mature striatal neuron phenotype.

1.15 Functionality

NSCs cultured *in vitro* generate antigenically and electrophysiologically mature neurons when exposed to suitable differentiation conditions (Conti et al., 2005, Goffredo et al., 2008, Spiliotopoulos et al., 2009, Onorati et al., 2011). Differentiated NSCs produce

voltage gated Na^+ currents similar to those of *in vivo* neurons and can be blocked in the same way with tetrodotoxin (Onorati et al., 2011, Conti et al., 2005). Whole-cell patch clamp experiments in both current and voltage clamp modes showed about 30% of differentiated neurons could elicit a voltage gated fast Na+ current and the associated delayed K^+ current to rectify the action potential (Onorati et al., 2011). Voltage-gated Ca^{2+} channel conductance has also been detected (Conti et al., 2005). The traces the cells produced show distinct characteristics of both low-voltage activated (LVA) and high-voltage activated (HVA) channels. These results suggest that these cells expressed some of the Na^+ and Ca_2^+ channel complement found in typical maturing neurons.

Other groups have found similar electroactivity of NSC neurons cultured from adult neurogenic niches. RG-like cells established from 2-month-old mouse SVZ cultures and grown as neurospheres before monolayer conversion are electroactive (Goffredo et al., 2008). NSCs derived and differentiated into neurons showed a set of markers specific to GABAergic neurons, which has been suggested to be the default pathway that NPC differentiation produces (Sah et al., 1997, Jain et al., 2003). With these neurons, GABA can actively be released from active synapses of NSC derived neurons.

The ability of these electroactive foetal NSC derived neurons to form networks was probed by looking for the presence of ligand-gated receptors and channels that could be activated by excitatory and inhibitory neurotransmitters. RT-PCR confirmed the presence of GABA-B receptors with large percentages of cells responding to GABAergic agonists (Onorati et al., 2011). When GABA was applied locally to clamped cells, a GABAergic response occurred in 70% of striatal-derived cells from a holding potential of -80mV, demonstrating the ability of differentiated foetal NSC-derived neurons to form functional networks *in vitro*. RT-PCR experiments showed the consistent expression of D2 dopaminergic receptors on these striatal cells. When a range of neurotransmitters for receptors found on striatal cells *in vivo* (glutamate, glycine, acetylcholine, nicotine,

carbachol, and dopamine) were applied to the neurons, no effect on membrane currents occurred, suggesting they lacked functional receptors for them. However, the presence of dopamine decreased the inward current produced by GABAergic activation, suggesting the dopaminergic receptors present have only developed a neuromodulator effect in this cell line (Onorati et al., 2011).

With all this evidence, it is hypothesised that the harvest of NSCs from foetal R6/2 tissue that differentiate into mature neurons is possible and that similar phenotypes to that detected in the mouse models could be present in a reasonable timeframe to study *in vitro*. Because our lab can produce transgenic mouse models, an abundant source of tissue to create and culture NSC lines is available. NSCs from the R6/2 mouse can be used to complement *in vivo* work, mechanistically dissecting approaches found to modulate HD phenotypes *in vivo*. From there, the ability to perform high-throughput analysis of phenotypes will allow a thorough characterisation of alterations to be studied in detail.

As such the aims of this thesis are to:

- Establish HD relevant cell lines from the R6/2 mouse model.
- Investigate phonotypes in these lines
- Establish the potential for high-throughput screening to be applied to these lines and for disease modifying compounds to be tested.

Chapter 2 Materials and Methods

2.1 Materials

Reagents and media	Supplier	Cat number
Accutase	Sigma	A6964
Amersham ECLTM Western Blotting Kit	GE Lifesciences	RPN2109
Amersham Hyperfilm ECLTM	GE Lifesciences	28906837
Ammonium persulfate	Fisher	A/p470/46
B27 supplement	Gibco	17504044
BDNF	Source Bioscience	ABE3214
Bovine serum albumin	Sigma	A9418
Cell culture water	Sigma	W3500
ColorPlus Prestained Protein Marker, Broad Range, 7-175 kDa	New England Biolabs	P7709S
DMSO	Sigma	D2438
DNA loading dye	Promega	G1881
DNA loading dye		
DPBS -Ca/Mg	Gibco	14190-169
DPX mounting media	Sigma	6522
Dulbecco's Modified Eagle Medium: Nutrient Mixture F-12 (DMEM/F12)	Gibco	31331-028
EDTA	Sigma	3620

Reagents and media	Supplier	Cat number
Foetal Bovine Serum (FBS)	Thermo Scientific	10270106
Gelatine	Sigma	G1890
Giemsa stain modified solution	Sigma	48900
Glacial acetic acid	BDH	10001CU
Heparin	Sigma	H3149
Hoechst dye	Invitrogen	H3570
Lambda Hind III / phiX Hae III Marker	BIO-RAD	161-0375
Laminin	Life Technologies	23017-015
Methanol	Fisher	M/4000/25
N-methyl-N-deacetyl-colchicine "Colcemid"	Roche	10295892001
N2 supplement	Gibco	17502048
Neurobasal media	Gibco	10888-022
NeuroCult™ NSC Basal Medium	STEMCELL Technologies	5700
NeuroCult™ NSC differentiation Kit	STEMCELL Technologies	5704
NeuroCult™ NSC differentiation Supplement	STEMCELL Technologies	5703
NeuroCult™ NSC Proliferation Kit	STEMCELL Technologies	5702
NeuroCult™ NSC Proliferation Supplement	STEMCELL Technologies	5701
Normal donkey serum	Sigma	D9663
Normal goat serum	Sigma	G9023

Reagents and media	Supplier	Cat number
paraformaldehyde (PFA)	PCR	R/38
Penicillin-streptomycin	Sigma	P4333
Pierce® BCA protein assay kit	Thermo Scientific	23225
Poly-DL-ornithine hydrobromide	Sigma	P8638
Proteinase K	Thermo Scientific	EO0491
Protogel®	Thermo Scientific	EC- 890
Protogel® Resolving Buffer	Thermo Scientific	EC- 892
Protogel® Stacking Buffer	Thermo Scientific	EC- 894
Recombinant mouse epidermal growth factor (EGF)	Peprotech Inc	315-09
Recombinant mouse fibroblast growth factor 2 (FGF2)	Peprotech Inc	450-33
Sodium pentobarbital	J.M.L	103-9130
Sucrose	Fisher Scientific	744771
TAE	Thermo Scientific	B49
TEMED	Sigma	T-8133
Thermo-Start master mix	Thermo Scientific	AB0908B
Thermo-Start master mix	Thermo Scientific	
Tissue-Tek optimum cutting Temperature (O.C.T.) compound	VWR	25608-930
Tris	Sigma	T1503
Triton X-100	Sigma	X100

Reagents and media	Supplier	Cat number
Trypan blue solution	Sigma	Sigma
TUNEL*: In situ* cell death detection kits, fluorescein	Roche	11-684-795-910
Vectorshield mounting solution	Vector	H1000

Equipment	Supplier	Cat number
24 well plate	Falcon	353047
96 well opaque walled plates	Falcon	10281092
CFX96 with C1000 Thermal cycler	BIO-RAD	-
Consort power pack	Consort	E802
Coverslips	VWR	23801-202
Cryostat	Bright-	OTF
Cuvettes	Fisher Scientific	FB55147
Gel-Doc UV trans-illuminator	BIO-RAD	-
Glass slides	VWR	631-0446
Hydrophobic Wax pen	DAKO	S2002
Mr. Frosty™	Thermo Scientific	5100-0001
Nanodrop	Thermo Scientific	1000
Neubauer cell counting chamber	VWR	HIRS8100103
Nitrocellulose membrane	BIO-RAD	162-0115
Photometer (Bio-Photometer)	Eppendorf	-
SIM µ-Dish	Ibidi	81158
SuperFrost slides	VWR	631-0446
T175 culture flask	Falcon	353112
T25 culture flask	Falcon	353109
T75 culture flask	Falcon	353135

2.2 Media

2.2.1 Culture media

In this section the compositions of cell culture media used in this thesis are described. Adaptations that have been made to cell culture media compositions are stated in text where appropriate. Working solutions were made up in 50 ml stock solutions and the formulation for each media is outlined for this quantity (Table 2-1).

2.2.2 Proliferation medium

The proliferation medium was based on a commercially available stem cell maintenance kit from STEMCELL Technologies that was specifically formulated to culture mouse neural stem cells. The NeuroCult™ NSC Proliferation Kit (mouse; STEMCELL Technologies, Cat#05702) consists of NeuroCult™ NSC Basal Medium (mouse; STEMCELL Technologies, Cat#05700) to which NeuroCult™ NSC Proliferation Supplement (mouse; STEMCELL Technologies, Cat#05701) must be added before use. Standard growth factors, recombinant mouse epidermal growth factor (EGF, 20 ng/ml; Peprotech Inc, Cat#315-09) and recombinant mouse fibroblast growth factor (FGF2, 10 ng/ml; Peprotech Inc, Cat#450-33) along with heparin (2 μg/ml; Sigma, Cat#H3149), were added to the media to maintain cells in a proliferative state.

2.2.3 Dissection medium

Dissection of embryos and cells was performed in a modified proliferation medium containing penicillin/streptomycin (pen/strep; 10 ml/l; Sigma, Cat#P4333) and without growth factors or heparin.

		Media						
	50ml Aliquots	Dissection	Proliferation	Differentiaion	Modified differentiation			
					D1	A	Bs	Bw
Component	Neurocult base media	45ml	45ml	45ml	22.5ml	22.5ml	22.5ml	22.5ml
	Neurocult proliferation suppliment	5ml	5ml	-	2.5ml	2.5ml	2.5ml	2.5ml
	Neurocult differentiaion suppliment	-	-	5ml	-	-	-	-
	DMEM/F12	-	-	-	6.25ml	6.25ml	6.25ml	6.25ml
	Neurobasal	-	-	-	18.75ml	18.75ml	18.75ml	18.75ml
	FGF2		50µl	-	25µl	20µl	12.5µl	5µl
	EGF		50µl	-	-	-	-	-
	Heparin		50µl	-	25µl	20µl	12.5µl	5µl
	N2	-	-	-	250µl	250µl	250µl	250µl
	B27	-	-	-	1ml	1ml	1ml	1ml
	BDNF	-	-	-	-	100µl	150µl	150µl
	Pen/Strep	100µl	(50µl)*	(50µl)*	(50µl)*	(50µl)*	(50µl)*	(50µl)*

*Optional

Table 2-1. Summary of media compositions.

2.2.4 Differentiation medium

The basic differentiation medium is a commercially available product and an adaption of the NSC Proliferation Kit the NeuroCult™ NSC differentiation Kit (mouse; STEMCELL Technologies, Cat#05704). It is made up of NeuroCult™ NSC Basal Medium (mouse; STEMCELL Technologies, Cat#05700) to which NeuroCult™ NSC Differentiation Supplement (mouse; (STEMCELL Technologies, Cat#05703) must be added before use.

2.2.5 Modified differentiation media

Based on the modifications of Spiliotopoulos and colleagues (2009) to their differentiation protocol, adaptions were made to the medium used for differentiation. This contained the Neurocult proliferation kit, mixed with Dulbecco's Modified Eagle

Medium/ Nutrient Mixture F-12 (DMEM/F12; Gibco, Cat#31331-028) and Neurobasal media (Gibco, Cat#10888-022) in a ratio of 4:1:3. All media included 10 µl/ml pen/strep when required.

The differentiation medium mixture was supplemented with 1% B27 (Gibco, Cat#17504044) and 0.5% N2 (Gibco, Cat#17502048). FGF, heparin and BDNF (Source Bioscience, Cat#ABE3214) were added at varying concentrations depending on the differentiation protocol step

2.3 Culturing surface and substrates

2.3.1 Plastics

Cell were grown in flasks (Falcon: T25, Cat#353109, T75, Cat#353135, T175, Cat#353112) of varying sizes for proliferation. For smaller culture experiments, cells were grown in 24-well (Falcon, Cat#353047) or 96-well opaque walled plates (Fisher Cat#10281092). Specialised glass bottomed 'µ-Dish' plates were used to grow cultures for SIM (Ibidi, Cat# 81158)

2.3.2 Gelatine

Gelatine-coated plates were prepared by applying a 0.1% gelatine (Sigma, Cat#G1890) in Dulbecco's Phosphate-Buffered Saline (dPBS) with no calcium, no magnesium (–Ca/Mg; Life technologies, Cat#14190-169) for at least 2 hours before use at 37°C. Coated plastic can be stored for up to 48 hours at 37°C in a 5% CO_2 incubator.

2.3.3 Poly-DL-ornithine

Poly-DL-ornithine hydrobromide (PRN; Sigma, Cat#P8638) was prepared at 0.1 mg/ml in sterilized cell culture water (Sigma, Cat#W3500). Aliquots were stored at -20°C until required. Culture surfaces were covered with the solution for at least 4 hours at 37°C but

for no longer than 24 hours. The excess solution was washed off with sterilized PBS for three washes before use. When laminin was used with PRN, 5 μg/ml natural mouse laminin protein (Life Technologies, Cat#23017-015) in dPBS was applied for a further 2 hours. Prior to use, the coating liquid was removed before culture medium was applied.

2.3.4 Laminin

3ug/ml natural mouse laminin protein (Life Technologies, Cat#23017-015) in DPBS was applied for at least 2 hours but no longer than 24 hours. Prior to use, the coating liquid was removed before culture medium was applied.

2.4 Cell culture procedures

2.4.1 Dissection of radial glial niches

Neural stem cell/progenitor lines were established from isolated foetal brain tissue at embryonic gestation day 14 (E14.5). CBA×C57BL/6 F1 female mice (B6CBAF1/OlaHsd, Harlan Olac, Bicester, UK) were mated with R6/2 males. Resulting pregnant females were euthanized by cervical dislocation before the uterus was dissected and placed into a petri dish of warm dissection medium (45 ml Neurocult Basal media, 5 ml proliferation supplements: EGF 10 ng/ml, FGF 10 ng/ml, heparin 2 μl/ml and pen/strep 20 μl/ml). Individual embryos were removed from the uterine membrane and transferred to a petri dish containing dissection medium. Under a stereomicroscope, the embryo head was isolated, and the rudimental skull and meninges were carefully peeled away to expose developing brain tissue, which was eased away from the head (Azari et al., 2011). Using micro-scissors, the dorsal part of the developing cortex was cut away to reveal the ganglionic eminences through the rudimental ventricles. The medial side of the cortical tissue and the ganglionic eminences both lateral (LGE) and medial (MGE) were carefully removed using curved forceps and transferred to tubes containing fresh dissection medium.

Tissue solids were manually homogenised using repetitive pipetting before centrifugation at 100 x g for 7 minutes at room temperature. All subsequent centrifugation was performed at these settings. The supernatant was discarded and the cell or tissue pellet was resuspended in 6 ml Neurocult proliferation medium (as dissection medium above without pen/strep) and transferred to uncoated T25 flasks to proliferate for 5-7 days, depending on growth rates and a visual assessment of neurosphere size, in a 37°C incubator with 5% CO_2. Incubators remained at these settings for all subsequent culture.

2.4.2 Liquid nitrogen storage and revival.

Cells banked for storage in the liquid nitrogen cell bank were removed from culture plates and centrifuged at 100 x g for 7 minutes at room temperature to form a pellet. Cells were resuspended in 1 ml of a 10% DMSO (Sigma, Cat# D2438) Neurocult proliferation medium mix and frozen in a Mr. Frosty™ cryopreservation chamber (Thermo Scientific, Cat# 5100-0001) overnight at -80°C. The vials were transferred into liquid nitrogen storage vessels for long-term storage. For revival, vials were removed from liquid nitrogen and immediately brought back to 37°C. Cells were washed in 10 ml PBS before centrifugation at 100 x g for 7 minutes at room temperature to form a pellet. Cells were then counted and used as required.

2.4.3 Harvest, fixation, cryoprotection and cryosectioning of whole embryo brains

Embryo brain tissue for immunohistochemistry (IHC) was dissected from the uterine membrane and the rudimental skull, before being transferred directly into 15-ml falcon tubes containing 4% paraformaldehyde (PFA, PCR, Cat#R/38). After one-week fixation, embryo brains were transferred to a 30% sucrose solution (Fisher Scientific, Cat#0744771) for cryoprotection. The point at which the brains had sunk to the bottom of the solution was when they were judged to be ready for sectioning but it is possible to store the brains for at least a month before sectioning. For sectioning, embryo brains were rinsed in PBS (Gibco, Cat#14190) before being snap-frozen onto a specimen stage that

was cooled on dry ice. The embryo brain was then covered in Tissue-Tek optimum cutting temperature compound (O.C.T.; VWR, Cat#25608-930), which solidifies when below -10°C. Using a cryostat (Bright-OTF), 25-µm frozen coronal sections were collected directly onto SuperFrost slides (VWR, Cat#631-0446) and stored at -20°C.

2.5 Passage of lines

2.5.1 Neurospheres

Tissue from embryo brains that was dissected as described above was placed in uncoated plastic plates in proliferation medium and placed in a 37°C incubator with 5% CO_2, to allow NPCs to proliferate and form neurospheres. Fresh proliferation medium was added if the medium containing the neurospheres began to discolour. After 5-7 days, when the neurospheres had reached a suitable size and opaqueness for harvesting, roughly 100 µm in diameter, all medium was transferred from the culture flask into tubes and centrifuged at 100 x g for 7 minutes at room temperature. The supernatant was removed and the cell pellet was resuspended in 1 ml accutase (Sigma, Cat#A6964) for 5-7 minutes to dissociate the neurospheres. The cell suspension was washed by adding 10 ml basal neurocult medium without supplements to the accutase cell solution and centrifuged. The supernatant was removed and the cell pellet was resuspended in 1 ml neurocult proliferation medium before cell counting. Cells were then either placed into fresh uncoated plastic plates in proliferation medium, at a ratio of around 1:10, to continue growth as neurospheres or converted into monolayers.

2.5.2 Monolayer culture

Cells that have been enzymatically dissociated from neurospheres or from other monolayer cultures can be plated onto substrate-coated plastic to encourage adherence and the formation of monolayer cultures. Those cells that adhere to the substrate will stay

attached and divide until they reach confluence and cell division is prevented by contact inhibition. When confluence reached 80-90%, the cells were dissociated from the plastic. The proliferation medium was removed and 100 µl/cm^2 accutase was added to cover the plate for 5-7 minutes. 10 ml fresh proliferation medium was added to dilute the accutase before the total liquid cell suspension was removed and centrifuged at 100 x g for 7 minutes at room temperature. Cell pellets were resuspended in 1 ml fresh media for quantification and replated at the required densities.

2.5.3 Quantification of cells and amplification

To quantify the number of cells within a culture during passaging, cell pellets were resuspended in 1 ml fresh medium and a 10 µl sample was taken and mixed with 90 µl 0.4% trypan blue solution (Sigma, Cat# Sigma). 10 µl of this 100 µl counting solution was placed in a glass Neubauer cell counting chamber (VWR, Cat#HIRS8100103) to quantify the concentration of cells. The average number of cells in each of the four counting squares was used to estimate the total cells in the counting solution. This total was then scaled up by 1×10^5 to estimate the total cells in the cell pellet. The desired quantity of cells was then calculated and the required volume was diluted into new plates containing medium.

2.6 Differentiation

2.6.1 Neurocult differentiation kit

To induce differentiation, cells were grown with the NeuroCult™ NSC differentiation Kit. This was either applied upon passage when cells were replated into differentiation medium or when the cells reached the desired confluence, when the medium was replaced with differentiation medium. The medium was replaced every 48-72 hours as required and cells were maintained in differentiation medium until the required time point.

2.6.2 Spiliotopoulos and colleagues protocol

Spiliotopoulos and colleagues (2009) published an adapted version of the differentiation procedure, which was tried initially in this thesis to differentiate NPCs. In their protocol, Spiliotopoulos and colleagues adapted the medium in 3 steps to gradually lower mitogen levels and introduce BDNF (Source Bioscience, Cat#ABE3214; Table 2-1). Here, cultures were dissociated using accutase and replated at a density of $1\times10^5/cm^2$ onto uncoated plastic plates in D1 medium (Table 2-1). Cells were left in the plates for 3 days with fresh medium added after 2 days. Secondly, cells that had adhered to the uncoated plastic during the 3 days were dissociated with accutase and collected. These cells were then counted, resuspended, and plated onto laminin-coated plastic at a density of $5\times104/cm^2$ into medium A (Table 2-1). Cultures were maintained in this media for 3 days and half of the medium was replaced after 48 hours. Lastly, the medium was changed to medium B (Table 2-1) and cultures were differentiated for the indicated time. Day 1 of differentiation was counted from when the differentiation medium was first applied.

2.6.3 Adapted Spiliotopoulos and colleagues protocol

Within this thesis, the Spiliotopoulos and colleagues protocol was adapted to meet the needs of NPCs created here. The first step above was altered so that cultures were dissociated using accutase and replated at a density of $1\times10^5/cm^2$ onto laminin-coated plastic plates (3μg/ml) in D1 medium (Table 2-1). Cells were left in the plates for 3 days with fresh medium added after 2 days. The rest of the protocol was continued as above.

2.6.4 Compound containing media

For compound differentiation experiments, stock compound solutions were diluted 1:10 in distilled water to a working solution, before mixing to appropriate experimental concentration using the adapted Spiliotopoulos and colleagues protocol and medium.

2.7 Fixation and Harvest

To fix cells for histological purposes, cultures were washed with PBS (–Ca/Mg) before fixation in 4% PFA for 15 minutes. Cultures were then washed twice in PBS (–Ca/Mg) before storage in PBS at 4°C until processed. To harvest cells for analysis (genotype analyses, western blot), cultures were washed in PBS (–Ca/Mg) before lysis. To lyse cells, cultures were either removed from plates. 100µl/cm^2 accutase was applied to cover the plate for 5-7 minutes. 10 ml fresh proliferation medium was added to dilute the accutase before the total liquid cell suspension was removed and centrifuged at 100 x g for 7 minutes at room temperature. Cell pellets were washed in PBS (–Ca/Mg) before lysis buffer was added. The alternative approach saw cells lysed directly in the plate with lysis buffer after one wash with PBS (–Ca/Mg). All lysates were kept on ice until used for analysis.

To harvest brain tissue, 16-week WT and R6/2 mice were anesthetised with an injection of 100 µl sodium pentobarbital (J.M.L, Cat#103-9130) and failure to respond to a toe and tail pinch was ensured. Once unresponsive, mice were transcardially perfused with PBS followed by perfusion with 4% PFA solution (PRC, Cat#PRC/R/38) until *riga mortis* had taken place. Whole heads were removed and stored in PFA until processed. 4-week-old WT and R6/2 mice were euthanised by 100 µl sodium pentobarbital. Death was confirmed with decapitation. Mouse heads were stored in 4% PFA at 4°C for at least 48 hours prior to being processed.

2.8 DNA extraction

To extract DNA from mouse tissue or cell pellets, samples were incubated in 100–300 µl lysis buffer (50 nM Tris-HCL, 100 mM EDTA, 0.5% SDS, 0.5 mg/ml Proteinase K) at 50°C. Tissue was lysed overnight and cells were lysed for a minimum of 2 hours. Once lysed, 300 µl saturated NaCl solution was added to the samples and mixed thoroughly

before centrifugation at 1.7 x 10^4 x g for 30 minutes. The resulting supernatant was transferred into twice the volume of 100% ethanol, mixed and centrifuged at 1.7 x 10^4 x g for 15 minutes. The resulting pellet was washed in 300 µl 70% ethanol and allowed to dry at room temperature. The DNA pellet was then resuspended in 300 µl 0.1 x TAE and dissolved overnight. DNA concentration was measured using a NanoDrop (Thermo Scientific, Cat#1000)

2.9 Gentotyping PCR

After DNA extraction, R6/2 cell lines were identified by amplifying the *HTT* exon 1 transgene DNA using PCR. The 10-µl reaction mixture consisted of 100 ng DNA, 1 × Thermo-Start master mix (Thermo Scientific, Cat#AB0908B), 1 µl DMSO, 10 ng/µl forward primer 33727 [5′-CGCAGGCTAGGGCTGTCAATCATGCT-3′] and 10 ng/µl reverse primer 32252 [5′-TCATCAGCTTTTCCAGGGTCGCCAT-3′] and DNA was amplified using cycling conditions of 15 min at 95°C, 35 × (30 s at 94°C; 30 s at 60°C, 60 s at 72°C) and a final extension at 10 min at 72°C (BIO-RAD CFX96 with C1000 Thermal cycler). The amplified R6/2 transgene product was 272 bp.

Once amplified, the PCR products were mixed with 2 µl 6x DNA loading dye (Promega, Cat#G1881) and separated by electrophoresis at 125 V/cm^2 for 30 min in a 1% agarose gel in a 1x TAE buffer (Thermo Scientific, Cat#B49). The products were visualised using Gel-Doc UV trans-illuminator and their size was determined against a Lambda Hind III / phiX Hae III Marker (BIO-RAD, Cat#161-0375)

2.10 Protein extraction

Cells were lysed either as washed pellets or directly in plates in ice cold RIPA buffer (150 nM NaCl, 1% NP-40, 0.5% sodium deoxycholete, 0.1% SDS, 50 mM Tris-HCl pH8, 1 nM 2-mercaptoethanol, 10 nM DTT, 1 mM PMSF, proteinase inhibitors [1 tablet per 50

ml]). Lysates were kept on ice through all subsequent processes unless stated. Lysates were collected and protein concentration was measured using Pierce® BCA protein assay kit (Thermo Scientific, Cat#23225). Serially diluted bovine serum albumin (Sigma, Cat#A9418) was used as a concentration standard. Samples were placed in cuvettes (Fisher Scientific, Cat#FB55147) and analysed with a photometer (Bio-Photometer, Eppendorf). Protein lysates were stored at -80°C and used within 48 hours.

2.10.1 Quantification and loading buffers

To analyse protein by western blotting, a 7.5-mm thick 10% resolving gel (for 2 gels: 3.33ml Protogel® [Thermo Scientific, Cat#EC-890], 2.6 ml 4x Protogel® Resolving Buffer [Thermo Scientific, Cat#EC- 892], 3.96 ml distilled water, 100 μL 10% ammonium persulfate [Fisher, Cat#A/p470/46], 10 μL TEMED [Sigma, Cat#T-8133]) was poured and topped with butanol to level the surface and remove any bubbles. After the gel had set, the butanol was washed away and the surface was dried before a stacking gel (for 2 gels: 0.65 ml Protogel® [Thermo Scientific, Cat#EC-890], 1.25 ml 4x Protogel® Stacking Buffer [Thermo Scientific, Cat#EC- 894], 3.05 ml distilled water, 50 μL 10% ammonium persulfate [Fisher, Cat#A/p470/46], 10 μL TEMED [Sigma, Cat#T-8133]) was poured on top and a loading comb placed inside to structure the loading wells.

The cast gels were placed inside an electrophoresis tank filled with 1X electrophoresis running buffer (25 mM Tris, 129 mM glycine and 0.1% SDS.). The appropriate protein quantity required was diluted in distilled water and 2X laemmli buffer (125 mM Tris-HCl pH8.8, 20% glycerol, 4% SDS, 0.01% [w/v] bromophenol blue) and denatured at 85°C for 10 minutes. These protein solutions were then loaded into individual running lanes alongside a ColorPlus Prestained Protein Marker, Broad Range, 7-175 kDa (New England Biolabs, Cat#P7709S) for size reference. The gel was then electrophoresed for the appropriate time at 150 V/cm^2 (Consort E802).

The resolved proteins were transferred from the gels to 0.45 μm nitrocellulose membrane (BIO-RAD, Cat#162-0115) using wet transfer. The transfer was carried out in transfer buffer (15.4 g/L glycine, 3 g/L Tris, 20% methanol in dH_2O) for 90 minutes. On completion the membranes were treated with 3% milk (non-fat dry milk powder, Marvel) in PBS for 60 minutes. After five washes in PBST (0.02% Tween PBS), the membranes were incubated in 1% milk-PBST solution containing the primary antibody at 4°C overnight.

The following day, the membranes were treated with five PBST washes before a 1-hour incubation in the appropriate secondary antibody. After the membranes were treated with five more PBS washes they were ready to be developed. The membranes were developed using an Amersham ECL™ Western Blotting Kit (GE Lifesciences, Cat#RPN2109) and Amersham Hyperfilm ECL™ (GE Lifesciences, Cat#28906837).

2.11 Immunohistochemistry and immunocytochemistry

Cells for immunocytochemistry (ICC) were grown in black-walled 96-well plates with optical bottoms specialised for microscopy (Fisher Scientific, #10281092). Cells were fixed with 100 μl of 4% PFA for 15 minutes. Cells were then washed three times with 100 μl PBS. Cell plates were stored in PBS until processed for staining. Slides of cut embryo brains were removed from frozen storage and allowed to thaw to room temperature. Before staining, a hydrophobic band was drawn round tissue sections using a wax pen (Dako, Cat#S2002).

Cells and embryo slices were washed in 100 μl PBS before a 2 hour incubation step in 100 μl blocking solution of 0.1% Triton X-100 (Sigma, Cat#X100) PBS for cells and 0.3% Triton X-100 PBS for embryo tissue, both with 10% normal goat serum (Sigma,

Cat#G9023) or normal donkey serum (Sigma, Cat#D9663). Primary antibodies were applied at the appropriate concentration (Table 2-2) in 100 μl fresh blocking solution overnight at +4°C. Appropriate goat or donkey secondary antibodies, matched to primary antibody host species and desired emittance spectrum were applied for 2 hours at room temperature. Secondary antibody solution was removed and Hoechst dye (Invitrogen, Cat#H3570) was applied in 100 μl PBS for 15 mins to label cell nuclei. Cells and embryo slices were washed three times in 200 μl PBS between all of the above steps. Cell plates were stored in PBS and tissue and embryo slides were coverslipped (VWR, Cat#23801-202) using Vectorshield mounting solution (Vector, Cat#H1000).

TUNEL staining was performed using '*in situ* cell death detection kits, fluorescein' (Roche, Cat#11-684-795-910). This procedure was carried out according to the manufacturer's instructions. Pre-fixed cells were permeabilized with 0.1% Triton X-100 PBS prior to application of the TUNEL reaction mixture for 1 hour at 37°C. Samples were then washed three times with 100 μl PBS prior to analysis with ICC. Negative controls were performed without terminal transferase in the TUNEL reaction mixture. Positive controls were performed on cells pre-treated with recombinant DNase 1 to induce DNA strand breakage.

Antibody	Species	Dilution	Supplier	Catalog #	Usage
Actin	Mouse	1:500	SantaCruz	sc-71210	ICC
Atp5b	Mouse	1:30000	Abcam	ab14730	WB
Doublecortin (DCX)	Rabbit	1:400	Cell Signalling	4604S	ICC
GFAP	Rabbit	1:2000	Dako	Z0334	IHC/ICC
Glutamine Synthase (GS)	Mouse	1:400	Millipore	MAB302a	ICC
Ki67	Rabbit	1:200	Abcam	ab15580	IHC/ICC
MAP2	Rabbit	1:500	Millipore	AB5622	IHC/ICC
Nestin	Mouse	1:200	Abcam	ab81755	ICC
NeuN	Rabbit	1:500	Abcam	ab177487	IHC/ICC
SQSTM1 (p62)	Mouse	1:500	MBL Int'l	PM045	IHC/ICC
S100b	Rabbit	1:100	Sigma	S6677	ICC
S830 -Huntingtin (ex1/PolyQ)	Sheep	1:2000	GB Lab	S830	IHC/ICC/WB
Synaptophysin	Rabbit	1:200	Abcam	ab8049	ICC
Tubulin - Alpha	Mouse	1:10000	Sigma	T6074	WB
Tubulin - Beta III (TUJ1)	Rabbit	1:400	Millpore	MAB5564	IHC/ICC
Ubiquatin	Rabbit	1:500	DAKO	z0458	ICC
Vimentin	Rabbit	1:1000	Abcam	ab92547	ICC

ICC - Immunohistochemistry, IHC - Immunocytochemistry, WB - Western blot

Table 2-2. Antibodies and concentrations used.

2.12 Karyotype analysis

When cells reached 80% confluence, mitotic activity was arrested using fresh medium including 75 ng/ml of N-methyl-N-deacetyl-colchicine "Colcemid" (Roche, Cat#10295892001) for 2 hours. The cells were then washed twice with 5 ml PBS and removed from culture plates by incubating with accutase for 3 minutes. Detached cells were collected in a hypotonic solution of 3 ml of 5% fetal bovine serum (FBS, Thermo Scientific, Cat#10270106) in dH_2O in 15 ml tubes and incubated for 20 minutes at 37°C. Karyotype fixative was 75% methanol (Fisher scientific, Cat# M/4000/25) and 25% glacial acetic acid (BDH, Cat#10001CU). The fixative was made immediately prior to use and 300 µl was added to the cell solution. The cells were pelleted from the hypotonic solution at 250 x g for 5 minutes. The supernatant was removed and the cell pellet was

twice resuspended and pelleted using 3 ml fixative. The final cell pellet was resuspended in 500 µl of fixative and incubated at -20°C for at least 3 hours.

The cell suspension was mixed by vortexing and 100 µl was dropped onto a glass slide (VWR, Cat# 631-0446) from a height of 1 m to ensure well separated metaphase spreads. Once the slides were dry they were submerged in 10% giemsa stain modified solution (Sigma, Cat#48900) in PBS for 5 minutes followed by five washes in 50 ml PBS. The slides were left to dry in air before cover-slipping with DPX (Sigma, Cat# 06522) and glass coverslips (VWR, Cat# 631-1575). Images of chromosomes were 15 individual geimsa-stained metaphase spreads captured by light microscopy and exported into TIFF files. The chromosomes were manually counted offline using ImageJ (Fiji) cell counting tool (ImageJ: http://imagej.nih.gov/ij/index.html).

2.13 LD_{50} toxicity calculation

The toxicity of compounds was calculated by estimating the concentration of each compound at which it reduced cell number by 50% (LD_{50}). Brightfield images were captured at days 1, 3 and 7 of differentiation in the presence of compounds. Manual cell counts were carried out and compared with the no compound control in each plate. Total surviving cells were graphed to estimate the LD_{50}.

2.14 Imaging

Geimsa-stained metaphase spreads for chromosome counting were captured using a Ziess Axioscope 2 plus with an AxioCam HRc camera. Images were saved as ZVI files using Ziess Axiovision software and exported as TIFF files. Bright field images of live cell cultures were captured using a Nikon eclipse TS100 with DS-Fi1 cameral and Nikon

Digital sight display. Images were saved in TIFF format and exported. Non-confocal widefield fluorescent images were captured using a Nikon Eclipse Ti-E Inverted Live Cell Imaging System and Cool SNAP HQ 2. Images were saved as ND2 files and processed using Nikon NIS Elements AR software. Final images were exported as TIFF files. Confocal microscopy was captured using a Nikon Eclipse Ni-E Upright A1 confocal system with DS-U3 Digital Sight Colour Camera. Images were saved as ND2 files and processed using Nikon NIS Elements C software. Final images were exported as TIFF files. Super resolution fluorescent images were captured using a Nikon Eclipse Ni-E N-SIM Super Resolution system and Andor Ixon camera. Images were saved as ND2 files and processed using NIS Elements AR software with n-SIM module. Final images were exported as TIFF files images and AVI videos.

2.15 Image analysis

Individual images were captured and converted to TIFF and were analysed by counting by eye using image-J software offshoot Fiji (Schindelin et al., 2012). Cells whose nucleus touched the bottom or left hand sides of the image were excluded, while those that touched the top or right sides remained included. The number of cells were recorded using the DAPI stained nuclei before the identity of each cell was counted using the appropriate antibody. Each well was considered a technical replicate and each line considered a biological replicate. Within these replicates any outliers were identified using Grubbs test and excluded. These values were subsequently used to calculate a mean ± standard deviation for each condition from the corresponding number of experiments performed. The PerkinElmer Operetta High-Content Imaging System was combined with the Harmony Imaging and Analysis Software to capture and process images for high content screening.

2.16 Statistics

Statistical analysis was performed using SPSS (IBM) software, version 22, with Student *t*-test set to 95% confidence when analysing two groups and performed as a one-way analysis od variance (ANOVA) test with bonferroni post-hoc test when analysing groups of three or more.

Chapter 3 Results 1: Creation of neural progenitor lines from the R6/2 mouse model of Huntington's disease

3.1 Introduction

Creation of models of HD *in vitro* that mimic phenotypes of the human disease is an important research target to develop potential treatments. Understanding of the disease at a cellular level is vital to dissect disease mechanisms, and to then enable a platform for disease modifying interventions to be tested.

The R6/2 mouse model is one of the most widely used models of HD. R6/2 mice exhibit a rapid aggregation phenotype in neurons throughout their brains until their death at around 16 weeks of age. In theory, NPCs can be extracted from any viable mouse model that survives the first 2 weeks of gestation. On this basis, the work in this chapter attempted to create NPC lines from the R6/2 mouse model and WT litter mates. These populations would allow for investigation of *in vivo* findings using the R6/2 mouse and for phenotypes to be probed at a cellular level. Once established these cells needed to be examined for their ability to retain stable genetic characteristics and to differentiate into the neurons and glia, which make up the brain.

3.2 Chapter aims:

The aims of the experiments performed in this chapter were to:

1. Establish novel NPC lines with and without the presence of mHTT, which are viable long term, with the potential to be differentiated from a progenitor state into mature functional adult cells, as found in the mature brain.

2. Assess how the stability of the NPC lines changes with increasing passage numbers with a view to investigate how mHTT affects this.

3. Induce NPCs to exit the cell cycle by the removal of growth factors and allow them to differentiate into mature cells found in the adult CNS and characterise how these populations are affected by mHTT expression.

3.3 Establishing neural progenitor cell lines.

Maintenance of cells in the cell cycle allows them to remain in a proliferative self-renewing state, as long as space and nutrients allow. This approach was using by Conti and colleagues who sustained proliferative cultures of NPCs using the mitogens, EGF and FGF2 (Conti et al., 2005). Despite a variety of approaches to establish NPC *in vitro* cultures, from embryo, foetal and adult sources, many lines produced showed various similar characteristics (Conti et al., 2005, Pollard et al., 2006, Chojnacki and Weiss, 2008). Foetal-derived NPCs express identical histological markers of RG and neurogenic cells compared to those seen in NPCs derived from ESCs (Conti et al., 2005). Consistent profiles were also seen with mRNA using RT-PCR and by gene-chip analysis. Foetal-derived NPCs also differentiate into glial and neuronal lineages when they exit the cell cycle. Therefore, they are considered to share the same properties of neural cell lines created from ESCs, which are widely used as *in vitro* models (Conti et al., 2005, Han et al., 2011).

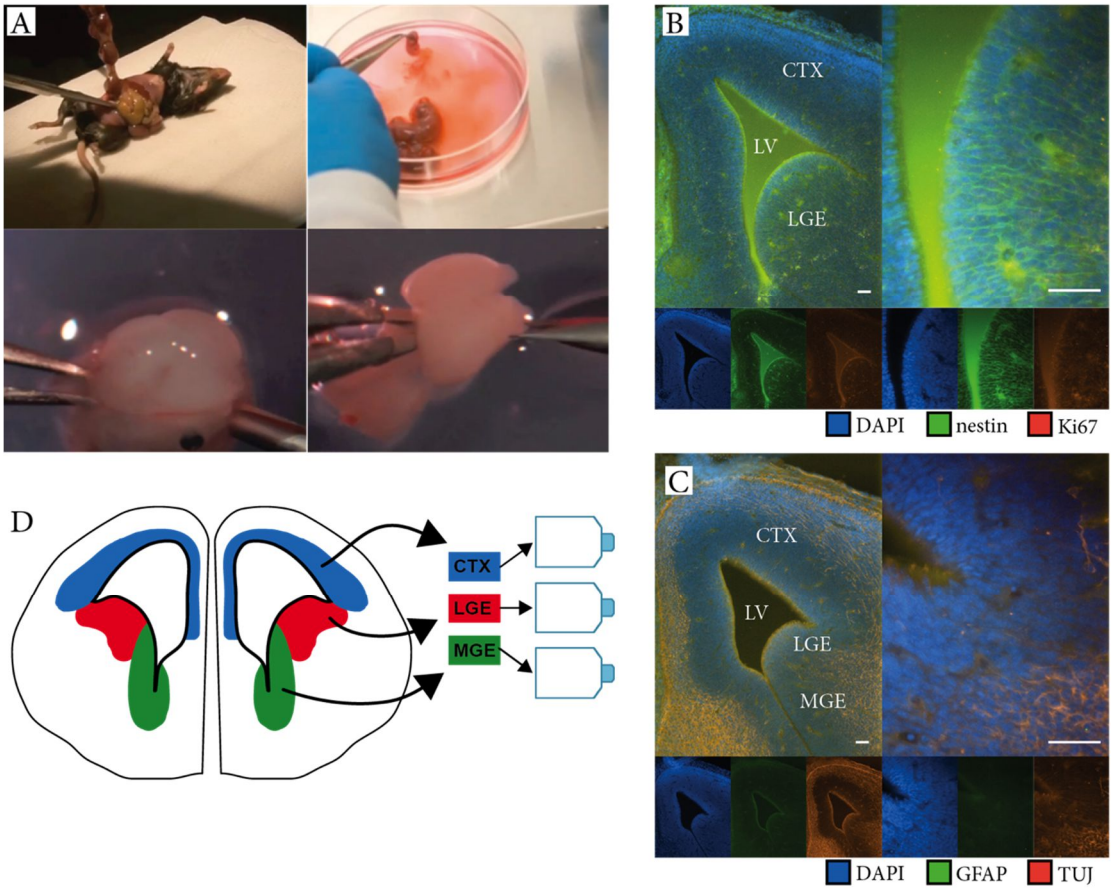

Figure 3-1 Harvesting of NPCs from E14.5 mouse embryos. (A) Pregnant dam was euthanized by cervical dislocation, 14.5 days after mating. An incision was made from ribcage along the medial line to allow access to uterine system. The uterus was removed and placed in a dish containing dissection media. Each individual embryo was removed from uterine sack and the head isolated for dissection. Under the microscope, the rudimental skull and meninges are cut and peeled away from the brain to leave the developing cortices. (B) Coronal cross sections of E14.5 embryos were cut on a cryostat into 15 μm sections, immunohistochemically stained for the marker of neural progenitors, nestin (green) and for the cell cycle maker Ki67 (Red). (C) Adjacent E14.5 cross sections stained for the differentiation makers for neurons (TUJ1, red) and for glia (GFAP, green). Both panels are stained for the nuclear marker DAPI (blue). (D) This technique allows for distinct and specific areas of the developing brain to be accessed and cells lines created from each region. These lines can be expanded and banked *in vitro*. NPCs=neural progenitor cells, CTX=cortex, LGE=lateral ganglionic eminence, LV=lateral ventricle, MGE=medial ganglionic eminence, TUJ1= beta-III-tubulin, GFAP=glial fibrillary acidic protein. Scale bars 50 μm.

3.4 Generation of neural progenitor cell lines from E14.5 foetal brains

Wildtype embryos were used to initially establish the technique to isolate foetal NPCs. C57BL/6TxCBA/Ca female F1 mice were bred with males and on embryonic day 14.5 (E14.5) uteri were dissected from pregnant female mice and each embryo was isolated from the uterine sack (Figure 3-1A). Each embryo was dissected to reveal and isolate the neural tissue from the rudimental meninges and the RG-like niches were isolated (Figure 3-1A). Reynolds and Weiss pioneered this process in 1992 (Reynolds et al., 1992) by using the extracted niche tissue to establish primary cell cultures.

The areas of the developing brain containing progenitor cell populations exist as niches around the ventricles towards the centre of the rudimental brain (Hartfuss et al., 2001). In mice, the earliest time point at which the brain starts to develop distinct lineages of NPCs is around embryonic day 7.5 (E7.5) (Gotz and Huttner, 2005). By E14.5 the brain has established itself with a structure reminiscent of the adult brain with lateral ventricles, cortices, and a rudimental striatum (Edwards et al., 1990) (Figure 3-1B). To visualise these areas E14.5 embryos were harvested, sectioned, and processed for immunohistochemistry (Figure 3-1B).

The niche from which cells are extracted can determine the gene expression pattern when these cells differentiate (Hartfuss et al., 2001, Anthony and Heintz, 2008). These separate niches were dissected individually to create distinct lines (Figure 3-1C). When cultured and matured *in vitro,* similar expression patterns to that seen in the corresponding adult brain areas could affect the fate of cells in that culture (Hartfuss et al., 2001, Anthony and Heintz, 2008).

This method of directly creating NPC lines from their *in vivo* niche has some distinct advantages over other methods, such as differentiating them from ESC. Firstly, the NPCs have been grown *in situ* to the point of dissection and so avoid the extra artificial steps

needed to proliferate and differentiate ESCs, which can introduce unwanted variety and separate populations (Conti et al., 2005, Pollard et al., 2006, Conti and Cattaneo, 2010). Secondly, lines can be created from any available genetic cross that can survive gestation until E14.5. This gives the decisive advantage of producing genetically distinct lines from transgenic and knock-in mouse models. However, this does mean the genetic model must be available, and viable, to establish the cell lines in the first place. In short, allowing neural progenitor niche populations to be created naturally *in vivo* creates the best source of these cells we can currently access (Conti et al., 2005).

NPCs cultured from neural progenitor niches are not necessarily a homogenous population. The lines are created from a pool of cells which may have already began to differentiate along specific linages resulting in cells that are different from their neighbours. This could generate variation in cultures and may mean that any cells with a selective advantage, such as proliferating at a higher rate, could come to dominate cultures at later passages. Different areas of the brain are established by distinct pools of RG cells, which migrate and differentiate into the mature cells of the brain (Hartfuss et al., 2001). After dividing, RG daughter cells migrate along the processes of their parent cells (Figure 3-1B) to travel to the areas where they will eventually become integrated into the mature brain (Figure 3-1C).

3.5 Culture of cells as free-floating neurospheres or adherent monolayers

Once cells are extracted from their niche (Figure 3-2A) they can be grown as free-floating neurospheres (Figure 3-2B) or adherent monolayers (Figure 3-2C). Both growth states can be maintained using mitogens but need to be passaged. For neurospheres, this point

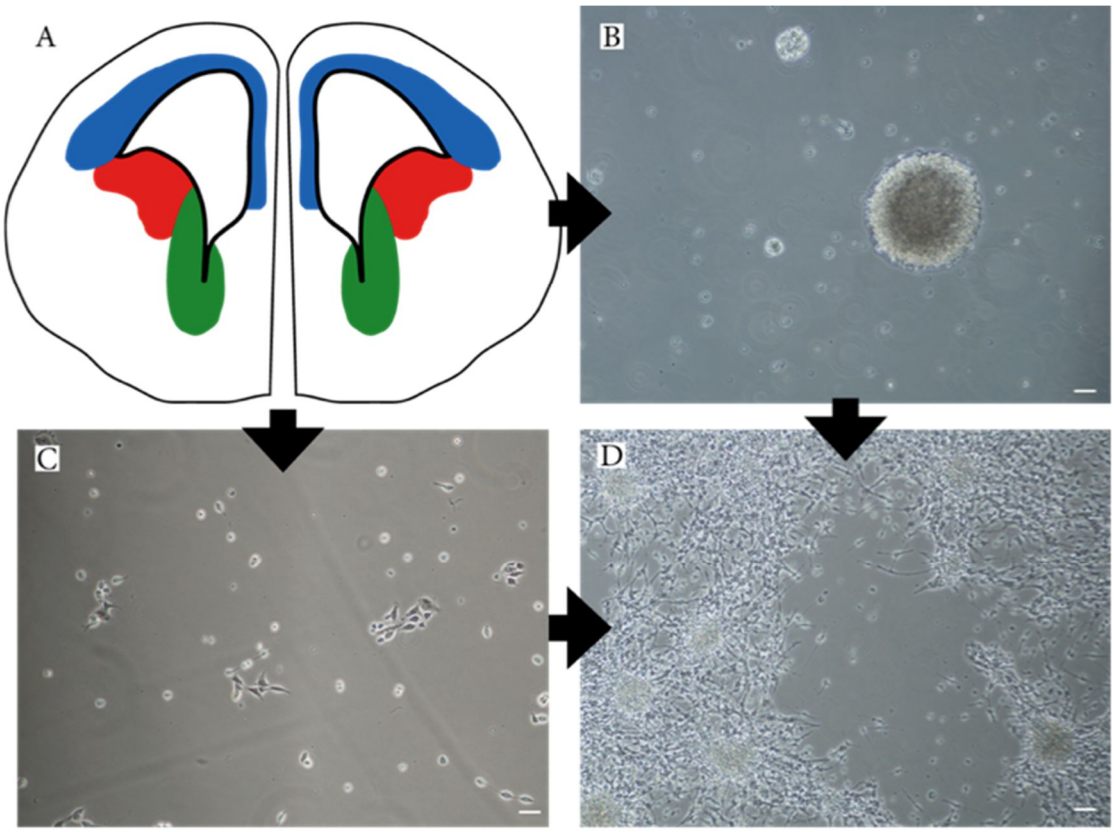

Figure 3-2. Establishment of cell lines from embryo dissections. (A) Tissue was removed from the desired area of the brain, mechanically broken up with pipetting before plating straight into uncoated flasks. These cells can then grow as (B) neurospheres or onto substrate coated plastic to grow as (C) monolayers. Representative images here are from LGE dissections. Scale bars 50 μm. LGE=lateral ganglionic eminence.

is when the sphere becomes too large and cells inside cease to proliferate due to lack of contact with mitogens and increased notch signalling (Campos, 2004). Cells towards the centre of the neurosphere can also become necrotic due to lack of nutrients (Xiong et al., 2011, Moeller and Dimitrijevich, 2004). As such, larger neurospheres need to be broken apart; either chemically with accutase or trypsin, or mechanically, using repeated pipetting to produce smaller neurospheres or singular cells. Monolayer cells will keep dividing until they become confluent and run out of space to adhere to in the dish. Similar to neurospheres, this lack of space results in increased notch signalling and cells will begin to differentiate (Liu et al., 2010, Borghese et al., 2010).

To optimise the methods to establish NPC cultures, a comparison of the two approaches was performed. Cells from WT embryos were grown as both neurospheres (Figure 3-2B) and as primary monolayers (Figure 3-2C) directly from the dissected tissue. The rate of expansion of lines was quicker for neurospheres, potentially because of their ability to grow in 3-dimensional space rather than under the 2-dimensional constraints of monolayer cells. As such, the lines were initially grown as neurospheres for 5 days after dissection for a rapid expansion of cell number before plating down into monolayers (Figure 3-2D). Cell lines from this point, passage 1 (p1), were maintained as monolayers for ease of proliferation and differentiation.

Uncoated cell culture plastics alone can allow for adhesion of cells but this method is unreliable. The degree of adherence differs between brands and culture vessel sizes and it is likely that cells will lift off with changes of media. A number of substrates are available to help cells adhere to the plastic surface such as gelatine, laminin, and poly-dl-ornithine (PRN).

NPC lines created from mouse foetal tissue were plated onto both PRN and laminin coated plastic to investigate which substrate produced the best growth conditions. Both substrates supported substantial adherence of monolayer cultures (Figure 3-3A,B). Laminin was chosen as the most suitable as the monolayer cultures grew more evenly (Figure 3-3A), while coating plates with PRN resulted in increased clumping of cells in patches (Figure 3-3B). Gelatine coated plastic generally resulted in cells growing in mounted clumps before detaching from the surface and floating away as neurosphere-like bodies within a few days. These gelatine bodies were indistinguishable from neurospheres. Similar effects with gelatine detachment have been reported (Sun et al., 2008).

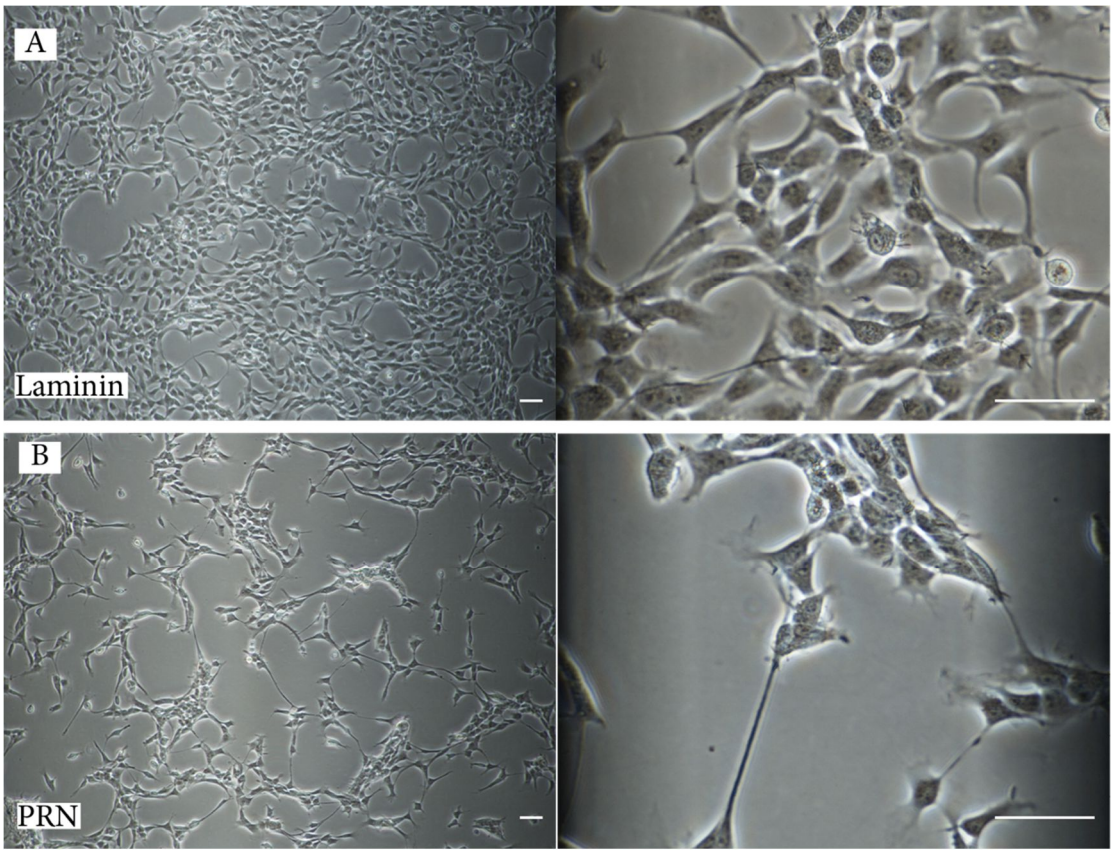

Figure 3-3. Establishment of cell lines from embryo dissections. Neurospheres can be broken up and plated onto substrate coated plastic to produce monolayer lines. Various substrates can be used. (A) Laminin produces the better growth conditions for monolayer cell lines, here compared to (B) PRN. PRN=poly-dl-ornithine. Scale bars 50 μm.

3.6 Initial establishment of A and B lines, from the LGE of WT and R6/2 mice

To establish the first HD cell lines in this thesis, R6/2 male mice were bred with C57BL/6TxCBA/Ca female F1 mice. 14.5 days after the detection of a plug, the embryos were removed from the pregnant mother and dissected. The first attempts to dissect lines of both genotypes focused on the LGE cell population located laterally to the lateral ventricle (LV, Figure 3-4A). These progenitors differentiate into the cells that later become the neurons of the striatum (Nat and Dechant, 2011, Rubenstein et al., 1994, Fishell, 1995).

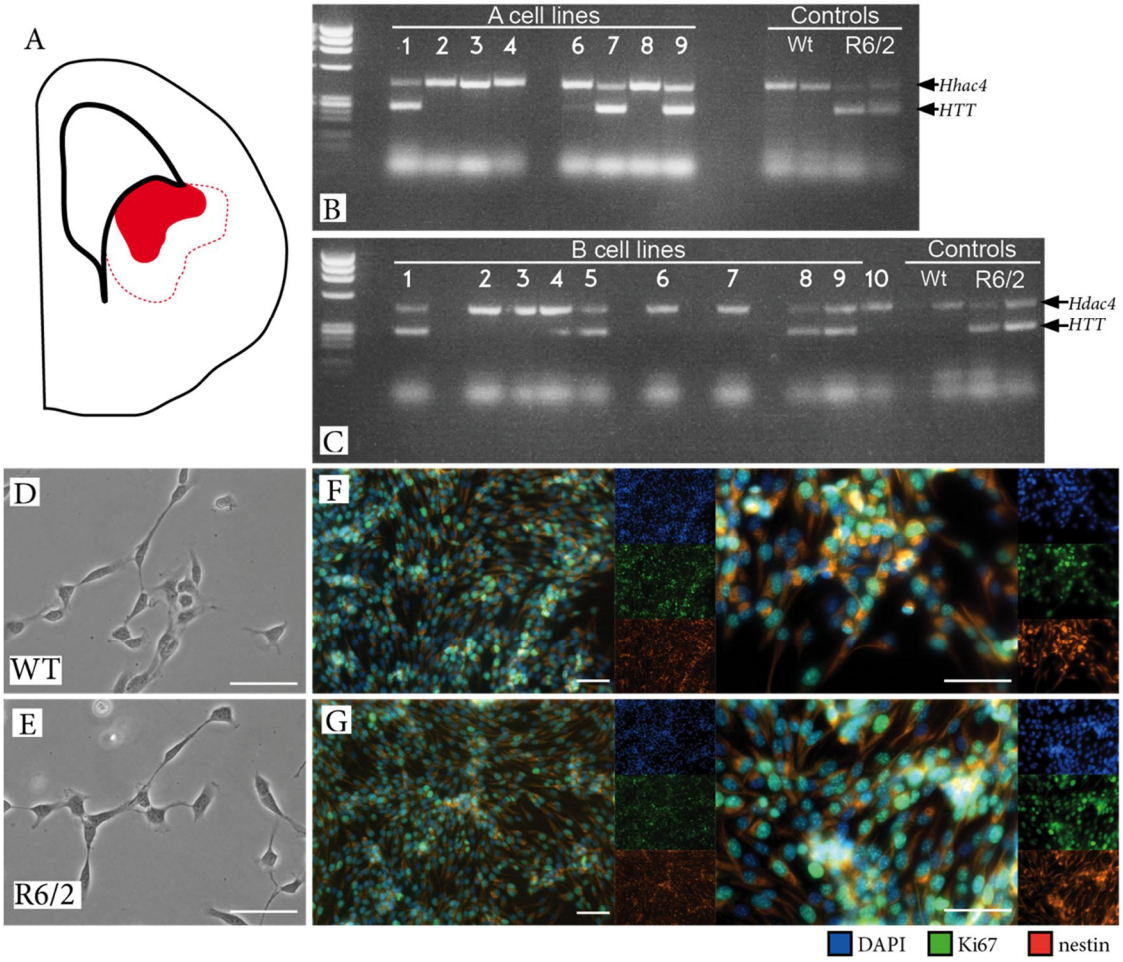

Figure 3-4. Creation of the initial cell lines from the LGE region. (A) LGE is depicted in red. The larger area dissected for the A lines is represented by the dotted red line. Genotyping of (B) 'A' lines and (C) 'B' lines. Lines with lower PCR band express the exon 1 *HTT* transgene. (D) WT monolayer lines were indistinguishable by eye from (E) R6/2 lines, in terms of morphology and organisation. (F) WT and (G) R6/2 genotypes remain in proliferative states *in vitro* expressing markers of neural progenitors (nestin) and the cell cycle (Ki67). LGE=lateral ganglionic eminence area, HTT=huntingtin, WT=wildtype. Scale bars 50 μm.

In the experiments performed here, the A lines were generated from dissections that captured more tissue than just the niche (Figure 3-4, red dotted area). The technique was optimised after the establishment of Line A, and a more accurate niche area was dissected to establish line B. Tissue from each individual embryo was used to determine the genotype of that embryo and the resulting cell lines using PCR for *HTT* exon 1. Approximately half the embryos would be expected to have inherited the R6/2 transgene and the other half WT. Of the embryos used for dissections, 3/9 of A lines (Figure 3-4B) and 5/10 of B lines (Figure 3-4C) expressed the R6/2 transgene. Expression of the HDAC 4 gene was used as a PCR positive as a control. The resulting cell lines were grown as neurospheres and converted to monolayers on laminin. These lines were passaged at least 4 times before banked as frozen stocks, prepared for long-term storage in liquid nitrogen.

No distinguishable differences were observed between the morphology of the WT (Figure 3-4D) and R6/2 lines (Figure 3-4E). At p10, cells were fixed and immunoprobed with nestin to assess the presence of neural progenitors and Ki-67 to mark proliferative cells. Nuclei were also stained with DAPI. While maintained in Neurocult proliferative media with mitogens, most cells remained in proliferative cells and were positive for Ki67 and nestin (Figure 3-4F,G). Higher-powered magnification showed the Ki67 staining in the nucleus, where it is involved in mitosis (Scholzen and Gerdes, 2000), while nestin, an intermediate filament protein thought to be involved in the disassembly of vimentin to allow splitting during mitosis (Park et al., 2010, Chou et al., 2003), was mainly expressed in the cytoplasm and highlights the morphology of the cell body (Figure 3-4F,G).

3.7 Establishment of the D lines from the cortex, LGE, and MGE of WT and R6/2 mice

After NPC lines were successfully established from foetal brains, a better understanding of the E14.5 brain was developed and the surgical technique in the process had become familiar, sub-regions of the brain were dissected from similar embryos and cultured in separate flasks to create matched lines of distinct progenitor populations (Figure 3-5A). Genotype analysis of rudimental tail tissue revealed that 4/9 embryos expressed the exon 1 transgene and were R6/2 while the others were WT (Figure 3-5B). These 'D lines' were identified as D1-11 and subdivided as Dc (cortex), Dl (LGE) and Dm (MGE) dependent on the brain region from which they were derived. The D lines were banked at p4 once there were sufficient quantities of cells. Lines D6c, D6l, and D6m grew the most slowly and were excluded from later experiments leaving the D4, D5, and D7 sets of R6/2 lines. Three WT lines were chosen as controls. 'C' lines were not produced as these embryos were used for histological sectioning (Figure 3-1A,B).

To test for markers of proliferation, Dl, Dl, and Dm cultures were revived from liquid nitrogen storage and plated on laminin, as adherent monolayer cultures. Cells were grown for 48 hours before being fixed and stained by ICC (Figure 3-6A). Each of the D lines showed markers of proliferation with nestin (green) and Ki67 (red) staining easily detectable in the majority of cells (Figure 3-6A).

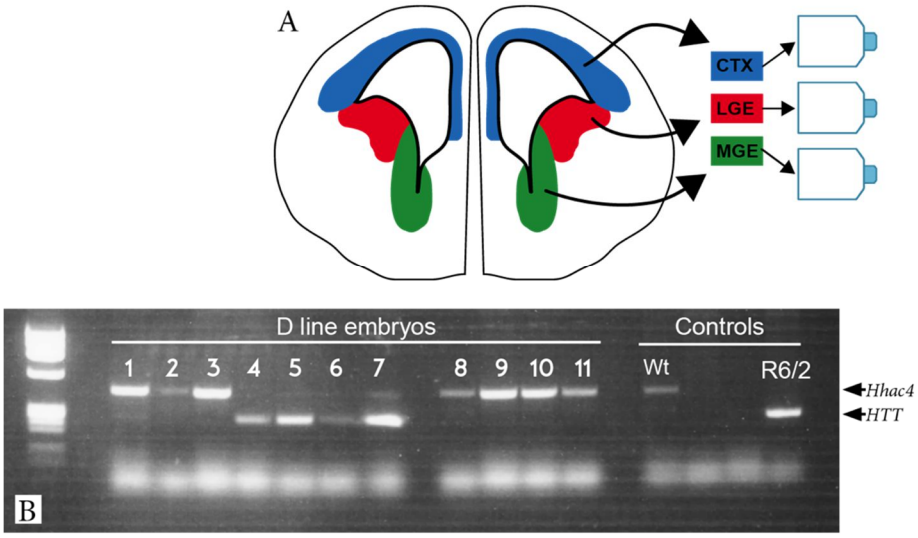

Figure 3-5. Creation of cell lines from multiple progenitor regions. (A) Cells were dissected from the CTX, LGE, and MGE. (B) Genotype analysis identified 7 WT and 4 R6/2 embryos from one pregnant female. CTX=cortex, LGE= lateral ganglionic eminence, MGE= medial ganglionic eminence.

3.8 Expansion of lines and longitudinal characterisation at specific passages

The number of times a cell line is passaged while *in vitro* could have a dramatic effect on the cells in the dish. For instance, there is a gradual loss of neurogenic potential in neurospheres over passages (Conti and Cattaneo, 2010). However, even though this has not been seen on monolayer cultures (Gregg and Weiss, 2003), each time cells are removed, and a subset are either banked or used for the next passage, could affect the remaining cells. To investigate the effect of passaging on these neural progenitor cell lines, Dc lines were banked in liquid nitrogen at p15, p30, and p40.

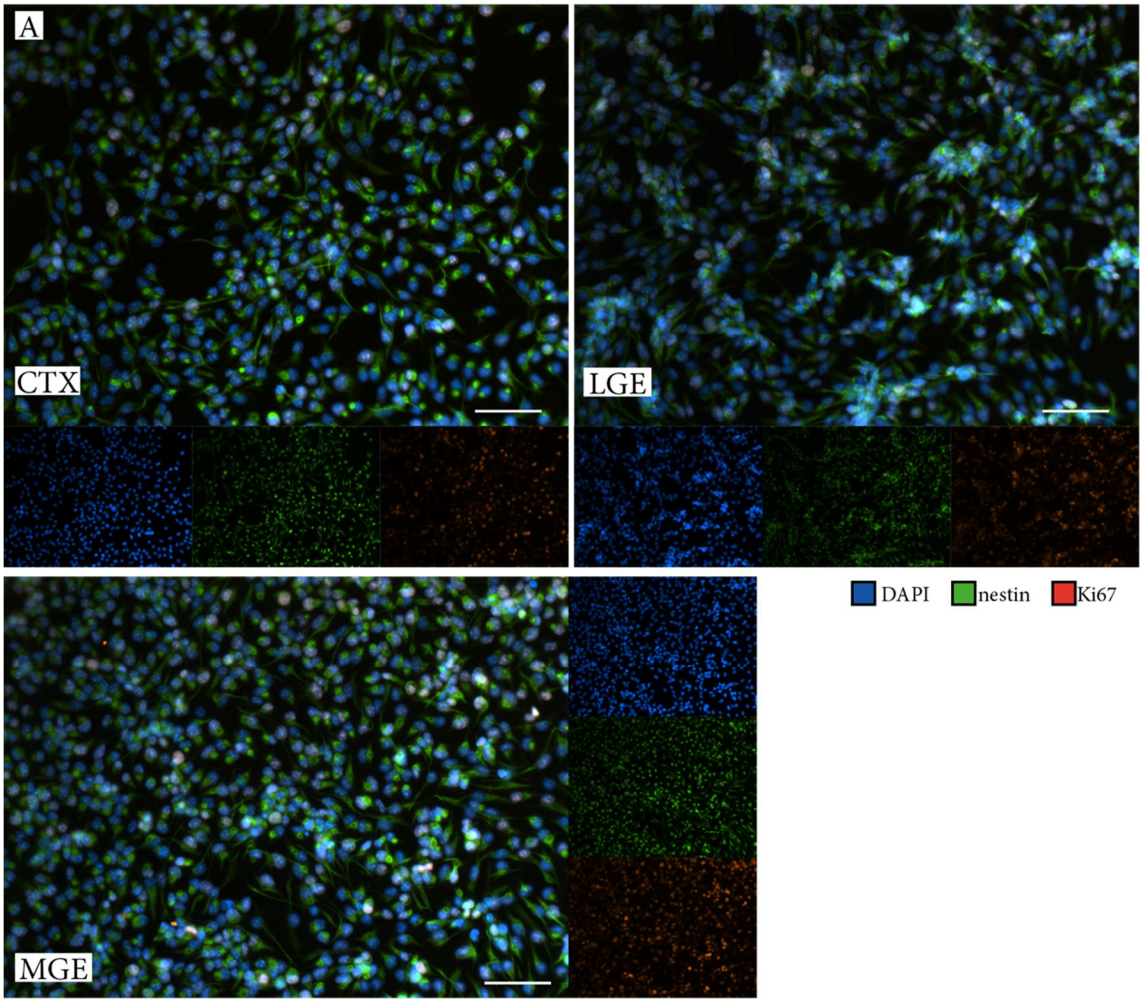

Figure 3-6. Proliferation status of multiple progenitor regions. (A) Cells were grown as adherent from progenitor areas for Dc, Dl, and Dm lines. All D-lines were grown as monolayers after an initial expansion period as neurospheres. All lines showed markers of proliferative neural progenitor cells with most of the cultured cells expressing nestin (green) and Ki67 (red). CTX=cortex, LGE= lateral ganglionic eminence, MGE= medial ganglionic eminence, Dc=D line from cortex, Dl= D line from LGE, Dm= D line from MGE. Scale bars 50 μm.

Two WT and two R6/2 Dc cell lines at p15, p30, and p40 were recovered from liquid nitrogen and grown for 4 days as proliferative monolayer cultures in parallel under the same conditions to investigate the effects of longer passage numbers. Each of the lines tested maintained their respective genotypes as expected (Figure 3-7A). To check whether a normal karyotype had been maintained, metaphase spreads were prepared and stained with giemsa (Figure 3-7B). The normal diploid mouse karyotype has 40 chromosomes. The number of chromosomes in 15 cells was counted for each passage

number of each line. The vast majority of karyotype images (around 80%) showed a normal 40 chromosome count with comparable variability in all lines at all 3 passage numbers (Figure 3-7C). This variance was most likely due to chromosome movement or loss induced by the technique. Care was taken to minimize this but some chromosome spreads might have lost or gained a chromosome from neighbouring spreads. There was no evidence of chromosome instability or that chromosome instability increased with passage number.

The R6/2 mouse model exhibits gametic instability, which results in an increase in the CAG repeat when inherited through the male line and a decrease through the female line (Mangiarini et al., 1996). Somatic instability also occurs in a tissue-specific and cell-specific manner (Gonitel et al., 2008). The CAG repeat length was therefore also monitored in the p15, p30, and p40 R6/2 cortical cell lines. These lines were created from an R6/2 male mouse with 219 CAGs. The CAG repeat number of the embryos from which the cells were harvested was not recorded in an oversite.

Both lines analysed showed a small increase in repeat length, which could have occurred through gametic instability in the sperm of the R6/2 male, with peaks of equivalent sizes (Figure 3-7D). Readings from the summits of the peaks showed one line decreasing from 230 to 222 CAG while the other slightly increased from 228 to 235 and then down to 232 (Figure 3-7E). These findings suggest that the CAG repeat lengths in these cells lines are relatively stable.

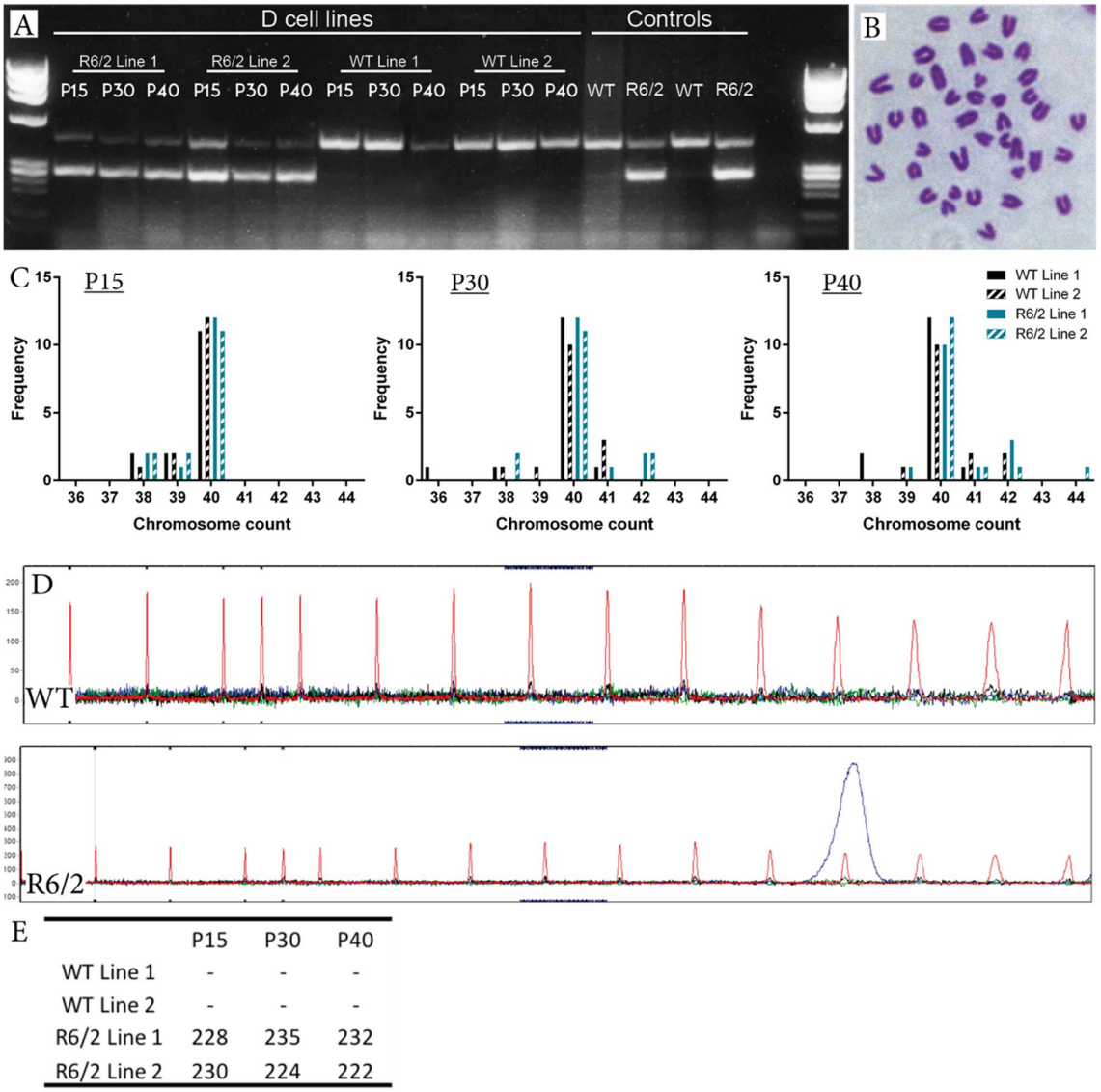

Figure 3-7. Genetic characteristics of cells lines at increasing passage number. Two WT and two R6/2 cell lines derived from the cortex and banked at p15, p30, and p40 were revived from storage and grown as monolayers. (A) The genotype of each line was tested throughout passage expansion and expression of the appropriate transgene was maintained in the R6/2 lines. (B) Representative geimsa stained metaphase spreads used for karyotype analysis. (C) Number of chromosomes per metaphase was consistent with most cells maintaining the appropriate number of chromosomes (murine, 40). (D) Size of the CAG repeat analysed by PCR with fluorescent-tagged primers and sized using an ABI3730 DNA analyser to produce traces of PCR products. The WT spread above shows only the red peaks from the size marker ladder while the bottom trace also shows a blue CAG peak against the red markers. Note: the software used for analysis automatically rescales the Y-axis, to the top peak so scales are equivalent. (F) Top of the peak was used to calculate CAG repeat length. The CAG repeat length remained fairly stable with a slight expansion in one line and a retraction in the other.

3.9 Assessment of proliferation rates in cell lines of increasing passage number

To assess proliferation rates, p15, p30, and p40 cells from WT and R6/2 cortical cell lines were plated in equivalent densities of $1x10^4$ cells/cm^2 in multiple plates. Every 24 hours the cells in a plate for each line were dissociated and an estimation of the number of cells in that plate performed. There was a dramatic increase in proliferation rate as the passage number was increased particularly between p15 and p30, where there was an almost 3-fold increase in the final cell numbers in all lines apart from WT line 1 (Figure 3-8). WT line 1 showed the same proliferation rate at p30 as that seen at p15.

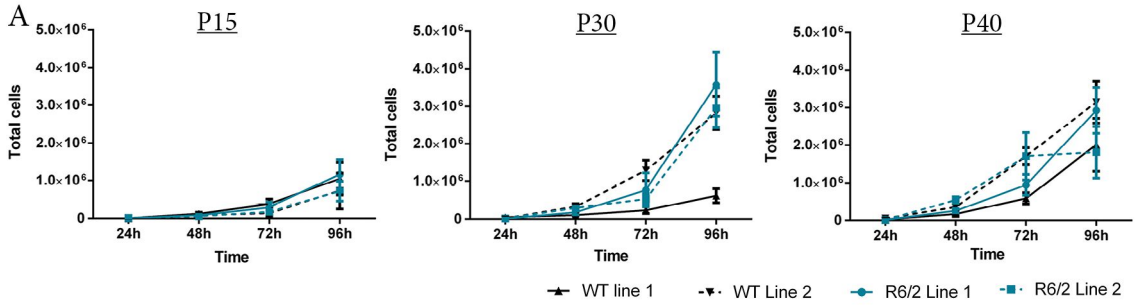

Figure 3-8. Growth rates of cells lines at increasing passage number. WT and R6/2 lines from the cortex with increasing passage numbers were grown in cohorts and harvested every 24 hours for cell number estimation. (A) Cell number expansion rate increased in all lines as passage number increased. No noticeable difference in rate was observed between lines with the exception of the slower growing WT line 1 at P30. WT line 1 had an equivalent proliferation rate to the others again by P40.

The increase in proliferative rate levelled off after p30; at p40 all lines were similar to that of the increased rates seen at p30 with the proliferation rate of WT line 1 also having increased with respect to p15.

These cultures are not homogenous cell populations and the initial cells dissected would have varied in their proliferation rates. Longer passage times will tend to favour selection and amplification of those cells with an increased proliferation rate as there will simply be more of them due to the speed with which they create daughter cells. As such this result is to be expected and must be taken into account when comparing results from lines grown from different passage numbers.

3.10 Differentiation of the neural progenitor cells using Neurocult differentiation media

HD is a late onset neurodegenerative disease, which affects the mature adult cells across the brain. Mitotic cells appear unaffected possibility due to mHTT not reaching a concentration threshold to affect them (Bates et al., 2015, Colby et al., 2006). As such, NPCs were differentiated into neurons and glia to gather meaningful insights into HD at a cellular level. To induce cells to exit the cell cycle and differentiate, the media culture was changed. To study cell differentiation, WT and R6/2 lines from the cortex were plated on laminin at a density of $2x10^4/cm^2$ in the commercially available Neurocult differentiation media without growth factors.

The cells adhered as monolayers upon plating as they did when passaged. By 7 days of differentiation, noticeable differences in the cell morphology were observed by light microscopy. The cells looked less 3-dimensional and displayed less of the uniform shape typical of NPCs. Some cells had a star like shape while others were longer with processes

stretching out of each image (Figure 3-9). Differentiation was continued for 21 days at which stage the morphology of different cells was hard to distinguish using just light microscopy. Cells appeared to have an increased soma size and to have flattened out considerably (Figure 3-9). Little difference was detected between the WT and R6/2 lines.

ICC antibody markers GFAP and TUJ1 are markers of astrocytes and neurons, respectively. GFAP is an intermediate filament protein expressed by CNS astrocytes in mammals (Eng and Ghirnikar, 1994, Sofroniew and Vinters, 2010). GFAP is thought to be a structural protein and therefore, antibodies against GFAP stain the soma and cytoskeleton of astrocytes. GFAP is also expressed in non-CNS cells such as in cells of rat kidneys (Apte et al., 1998) but it is widely used for the purposes of glial cell identification (Eng and Ghirnikar, 1994). Beta-III-tubulin or 'TUJ1' is a microtubule protein found exclusively in neurons (Lee et al., 1990, Menezes and Luskin, 1994). ICC for these markers was used to show that neither of these proteins were present in either WT or R6/2 cells while they were still proliferative. After induction of differentiation, a very high proportion of WT and R6/2 cells stained positively for GFAP indicating that they had differentiated toward the astrocyte lineage (Figure 3-10A). ICC also revealed that some TUJ1+ neurons were present in WT and R6/2 cultures but these were few and far between (Figure 3-10B). These TUJ1+ cells displayed the traditional neuronal shape and differed in morphology from the GFAP+ glia.

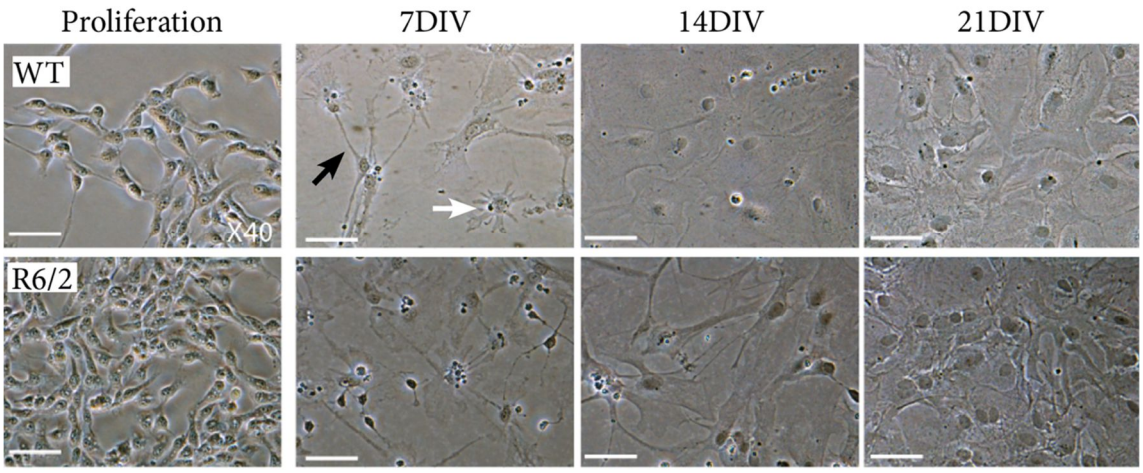

Figure 3-9. Differentiation of NPCs using Neurocult differentiation media. The NPCs remained in the cell cycle as proliferative lines with growth factors in the medium. Removal of these growth factors and application of Neurocult differentiation media induced differentiation into mature neural cells. (A) Cell morphology was noticeably changed from that in the proliferative cultures after 7 days of differentiation (7DIV) with cells having a flatter, less 3-dimensional morphology and longer, thinner processes (black arrow). These changes continued as cells mature further (14DIV and 21DIV) with larger astrocyte-like cells becoming more prominent (white arrow). Plates of cells were fixed every 7 days up to 21 days post differentiation. NPCs=neural progenitor cells. Scale bars 50 μm

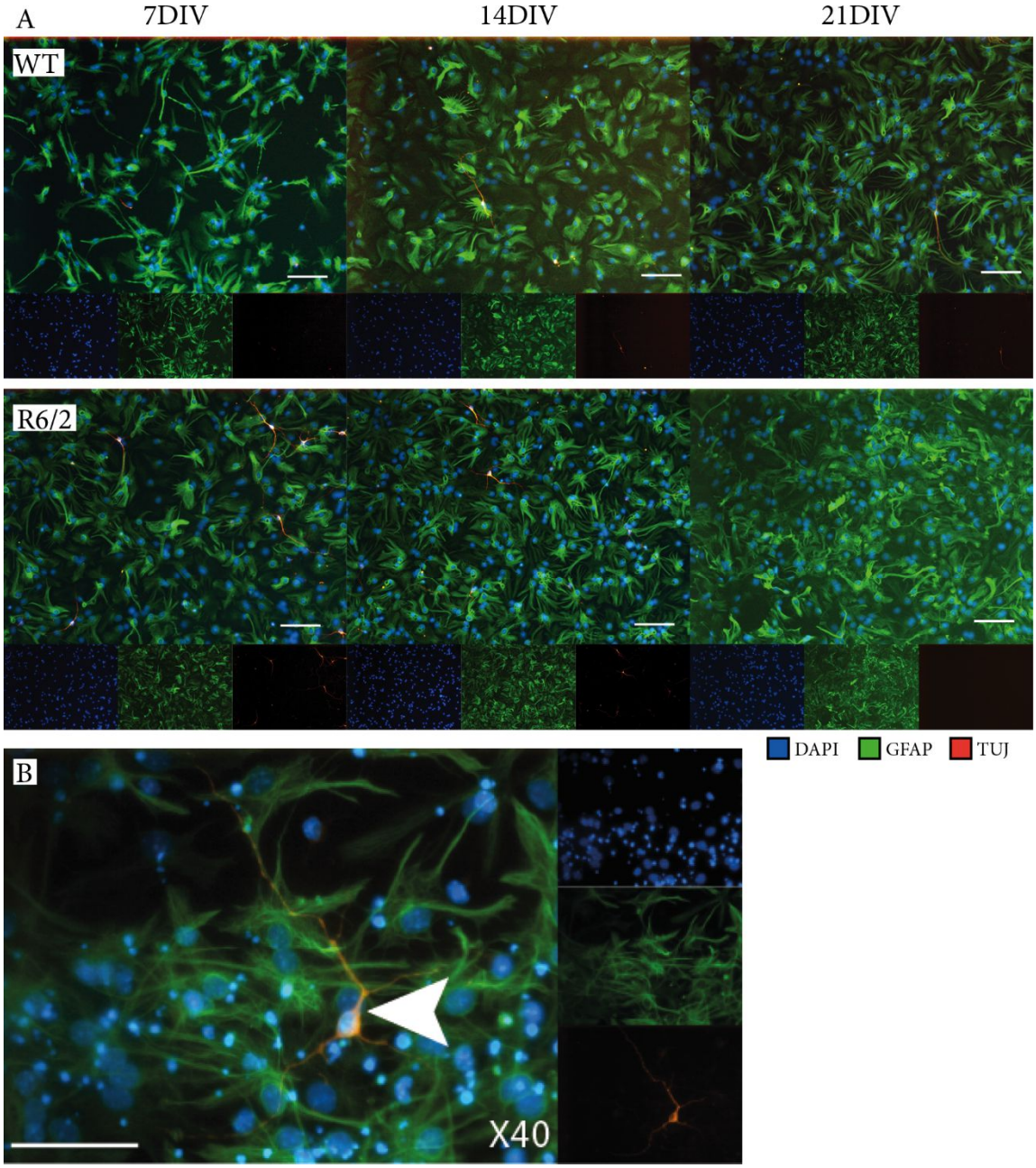

Figure 3-10. Analysis of differentiated neural progenitor cells using ICC. Differentiated cells were fixed every 7 days up to 21 days. (A) ICC staining was applied to determine the differentiation fate of cells at the fixed time points using GFAP+ (green) glia, and TUJ1+ (red) neurons. GFAP staining was very prominent while fewer examples of (B) TUJ1+ neurons were seen (white arrowhead). ICC=immunocytochemistry, GFAP=glial fibrillary protein, TUJ1=beta-III-tubulin. Scale bars 50 μm.

To assess the number of cells that differentiate in to neurones and glia, cell counts were performed on cells from the rudimental cortex from three different WT and R6/2 lines. Four wells were analysed for each line and 15 individual images were captured at x20 magnification at the same co-ordinates for each well using a non-biased grid system. Each well was considered a technical replicate and each line considered a biological replicate. Within these replicates any outliers were identified using Grubbs test and excluded. These data were pooled for the three biological replicates for each genotype. Statistical analysis was performed using SPSS (IBM) with Student's *t*-test set to 95% confidence for genotype. Analysis was performed by counting by eye using image-J software offshoot Fiji (Schindelin et al., 2012). DAPI+ cells were counted and then identified as glial or neuronal based on their cytoplasmic staining. Overall, the number of R6/2 cells per image was higher than the number of WT cells, which was seen at all three time points investigated (Figure 3-11A). This effect is likely to be due to the R6/2 cells surviving the process of seeding in larger numbers. The levels of cells also stay constant throughout the differentiation time points suggesting little cell death had occurred over this period. A pruning process might occur during the first few days of differentiation, which could also account for the lower number of WT cells than R6/2 cells that survived the first 7 days of differentiation. The loss of NPCs upon differentiation is well documented (Conti et al., 2005, Biella et al., 2007).

Of the cells analysed, 80% were GFAP+ glia by day 7 (Figure 3-11B), which increased to 90% by day 21. The same effect was observed for both genotypes. The highest level of TUJ1+ cells was seen at 7 days, when 2% of WT cells were stained as neurons (Figure 3-11C). Few neurons were seen throughout the continuing differentiation period. Some DAPI+ cells were not accounted for with either GFAP+ or TUJ1+ staining. Such cells were also negative for the oligodendrocyte marker, O4.

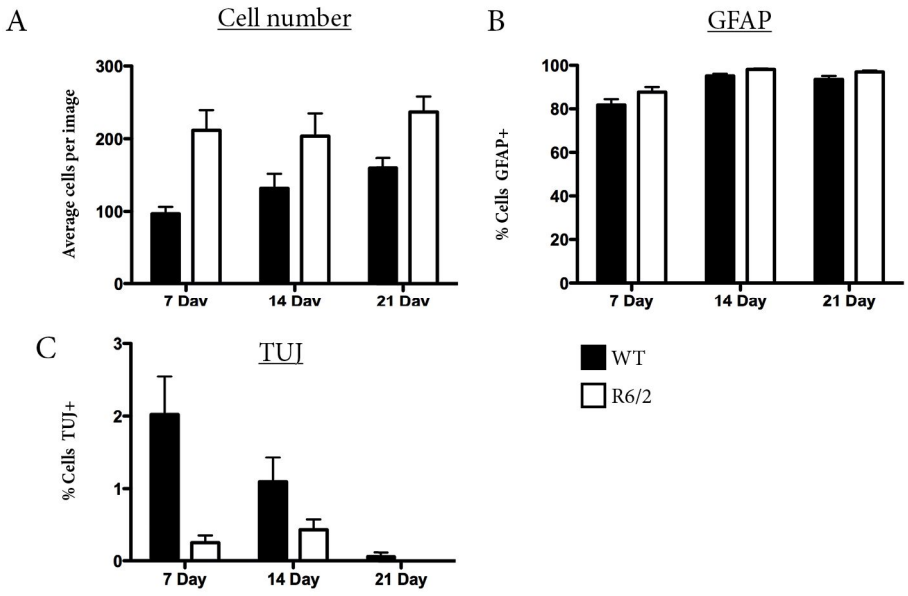

Figure 3-11. Cell types of differentiated cells. (A) Cell counts carried out at three time points up to day 28 on two WT and two R6/2 cortical lines. Both WT (black) and R6/2 (white) survived in large cell numbers throughout the time-points analysed. The vast majority of cells were positive for (B) GFAP staining while few were positive for (C) TUJ1, with those cells that were TUJ1+ decreasing over the longer differentiation period. ICC=immunocytochemistry, GFAP=glial fibrillary protein, TUJ1=beta-III-tubulin.

3.11 Differentiation of neural progenitor cells using an alternative adapted differentiation media

Spiliotopoulos and colleagues (2009) used an adapted protocol based on that of Conti and colleagues. (2005) in an attempt to improve cell viability upon differentiation and increase the number of cells showing a neuronal cell fate (Spiliotopoulos et al., 2009). This protocol involved a gradual reduction of FGF2 concentration while brain-derived neurotrophic factor (BDNF) was introduced and then gradually increased in concentration. This protocol was applied to the HD NPC lines developed in this thesis. The initial step of the process is to plate the cells onto uncoated plastic before detaching them after 3 days and re-plating the cells onto a substrate as previously described. This additional process was termed the neuralisation step (Table 2-1).

Two WT and R6/2 cell lines from the cortex were used to test this adapted protocol. All lines had previously been grown to p15 and banked in liquid N2 and allowed one complete passage after being recovered. In response to this uncoated plastic neutralisation step the cells initially attached but soon gathered in clumps that resembled neurospheres (Figure 3-12A). After 48 hours, some of the larger clumps began to detach and become free-floating bodies. These detached clumps were lost in the media change that was done at this stage. The cells that remained attached, both as single cells and as the clumps, were dissociated and reseeded in A-media with no EFG and a lower level of FGF-2 (Figure 3-12B). From here, the cells remained attached as a monolayer as the media was adapted further to become the B media (Table 2-1, Figure 3-12B). Cells remained in the dish and were differentiated for up to 28 days with cohorts being fixed for ICC every 7 days (Figure 3-12C). As with the previous differentiation protocol using neurocult differentiation media, little noticeable difference was evident between WT and R6/2 cells using light microscopy. Both lines underwent noticeable changes to morphology as the cells differentiated. A large amount of debris formed over small clumps of cells (black arrows), a phenomenon that did not occur with the commercial differentiation kit (Figure 3-12C).

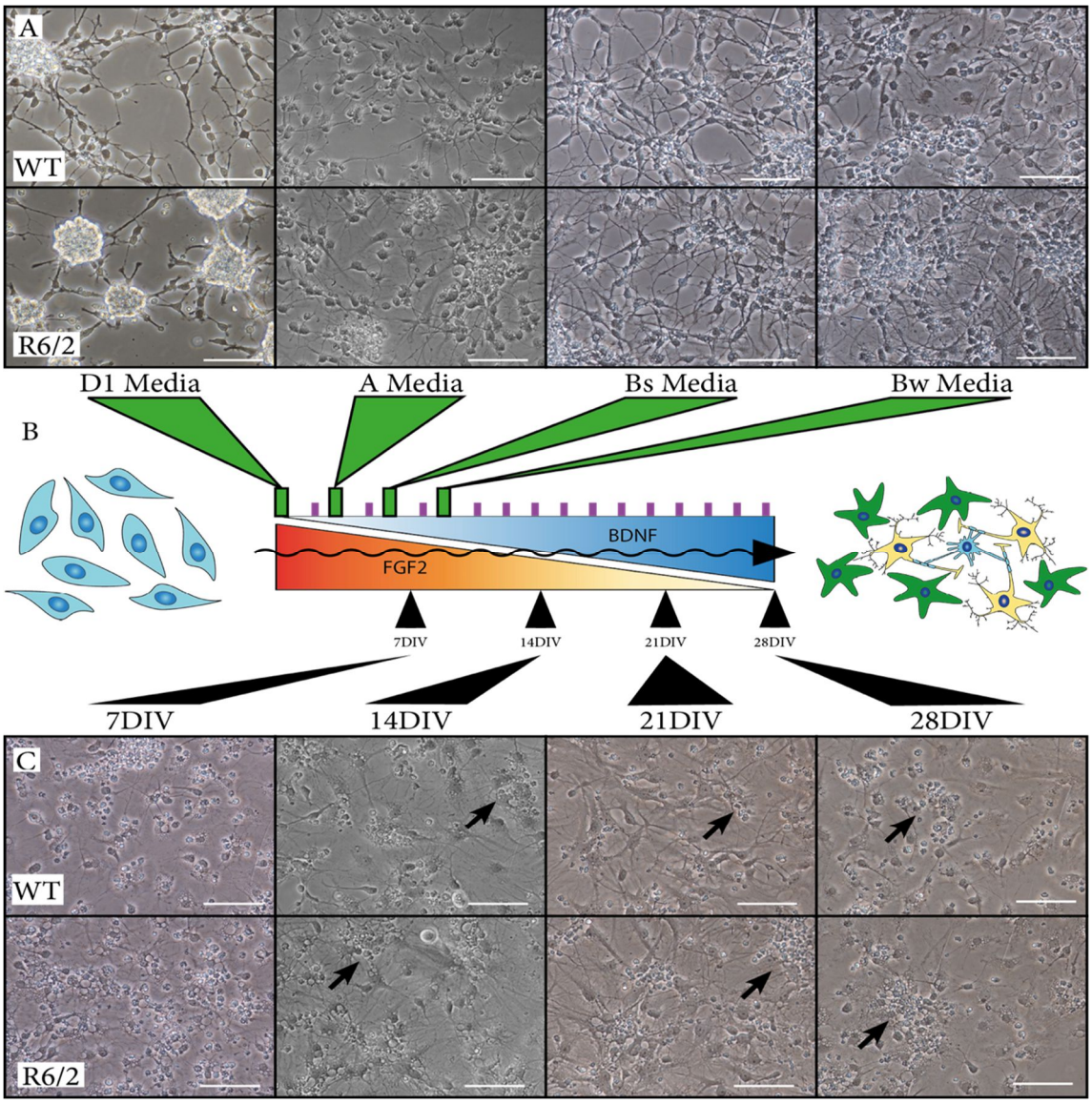

Figure 3-12. Differentiation of the neural progenitor cells using an alternative adapted differentiation media. The differentiation protocol was adapted from that of Spiliopoulos and collegues (2009), who used the concept of a graduated transition from media containing growth factors FGF2 (and EGF) to one containing increasing amounts of BDNF. (A) Cells were passaged and plated onto uncoated plastic in D1 media as an initial 'neutralisation step' for 3 days. During this time, cells adhere to the plastic and begin to gather in clumps similar to neurospheres. After 3 days, the cells were removed again and re-plated onto laminin-coated plastic with A media. The media used was then altered every 3 days from A-media followed by B media containing lower (Bs) and then the lowest (Bw) levels of growth factors. The cultures were then maintained in Bw media for the duration of the culture and media was half changed every 48 hours (purple bars). (B) The gradual reduction in growth supplement FGF2 while increasing levels of BDNF through 4 different media compositions takes the cells from a proliferative state to differentiated and mature state. Green bars represent media composition changes with purple bars representing half media changes with the media composition appropriate for that point of the experiment. (C) At 7 days a cohort of cells was usually fixed or removed for analysis with subsequent cohorts taken every 7 days. EGF=epidermal growth factor, FGF=fibroblast growth factor, BDNF=brain derived neurotrophic factor. Scale bars 50 μm.

3.12 Differentiation counts using the adapted protocol

Two WT and R6/2 cell Dc lines were differentiated for 28 days in the adapted protocol and cohorts fixed and stained for ICC at 7-day time-points using antibodies against GFAP and TUJ1. In all cell lines, there was an evident increase in the level of TUJ1+ cells compared with the previous differentiation attempts using the Neurocult commercial differentiation media protocol (Figure 3-13A). After 7 days, less TUJ1 staining was seen compared with the later time points which might be because a proportion of cells remained in an immature state, in which mature proteins for neurons remain at low levels. As such, analysis of cell fate was only undertaken at the time points later than 7 days. Analysis was performed by taking a series of images using a non-biased grid system and counting by eye using image-J. DAPI+ cells were counted and then identified as glial or neuronal on the basis of their cytoplasmic staining. In these differentiation experiments, cells were grown in both 24-well and 96-well plates.

The number of cells per image was not significantly different between the WT and R6/2 lines, nor between the 24-well and 96-well plates (Figure 3-13B,E). The total number of cells in the 21-day cohort was slightly reduced in all lines from 14 days but this could be due to random variation in the plate seeding rather than cell loss (Figure 3-13B). The percentage of GFAP+ cells remained around 80% in the 24-well plates throughout the time points studied, while it was consistently around 60% in the 96-well plates (Figure 3-13C,F). This finding suggests that less cells differentiated to a glial fate in the smaller wells. Indeed, this effect was echoed in a larger percentage of cells being TUJ1+ in the 96-well plates compared with the 24-well plates. Around 10% of cells were TUJ1+ by 14 days in the 24-well plates, which reduced to around 5% by 28 days (Figure 3-13D). In the 96-well plates around 20% of cells stained positive for TUJ1 at 14 days, decreasing

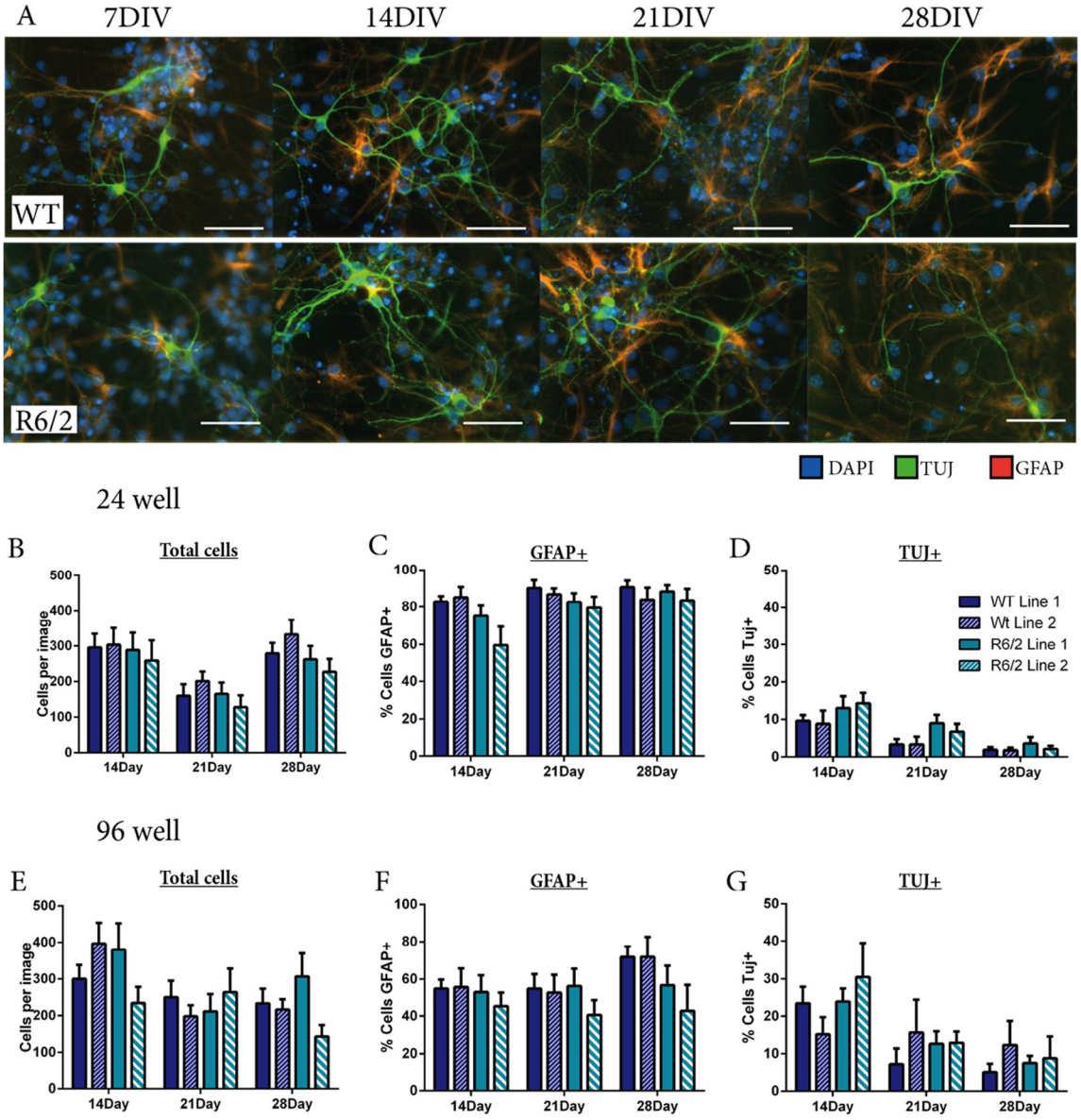

Figure 3-13. NPC differentiation cell type counts using the Spiliopoulos and colleagues protocol. The differentiation fate of NPCs using the adapted protocol was analysed using ICC. (A) When staining using the neuronal marker, TUJ1 (green), and astrocytic marker, GFAP (red), the increase in number of neurons was easily noticeable by eye. To compare the effect of different size growth environments, cells were grown in 24-well and 96-well plates. 24-well plates: (B) total cells, (C) percentage of cells positive for GFAP and for (D) TUJ1. 96-well plates: (E) total cells, (F) percentage of cells positive for GFAP and for (G) TUJ1. Cell numbers were counted from images captured using an automated grid and total cells, as well as the numbers of GFAP+ astrocytes and TUJ1+ neurons captured. NPCs=neural progenitor cells, ICC=immunocytochemistry, GFAP=glial fibrillary protein, TUJ1=beta-III-tubulin. Scale bars 50 μm.

to ~10% of cells at 28 days (Figure 3-13G). Again, no difference in TUJ+ cell numbers were observed between the genotypes of the cells.

3.13 Differentiation of neural progenitor cells into mature cell types

As neurons mature, the pattern of protein expression alters and can be used to identify the maturity of neurons and give an indication of their potential of becoming electrophysiologically active. Doublecortin (DCX) and microtubule-associated protein-2 (MAP2) are both markers of neurons from the microtubule-associated protein family (Sanchez et al., 2000, Francis et al., 1999). Although DCX and MAP2 are members of the same family, their expression in neurons changes as they differentiate from NPCs. DCX is expressed early upon neuronal differentiation and has been suggested as an alternative marker of neurogenesis in areas of the brain where the process still takes place (Francis et al., 1999, Brown et al., 2003). The levels of DCX decrease as neurons mature and as other markers, such as TUJ1 and MAP2, begin to increase (Brown et al., 2003). This expression pattern, seen during neurogenesis in the developing and mature brain, was echoed in the neurons *in vitro*. To examine the maturity of cells differentiated into neurons in this thesis, R6/2 and WT NPCs were differentiated into neurons and stained for DCX and MAP2 by ICC. By 7 days, R6/2 neurons expressed DCX while only the odd neuron had begun to also express MAP2 (Figure 3-14A). From 14 days, fewer neurons expressed DCX and more neurons co-expressed DCX with MAP2 (Figure 3-14B). By 21 days the vast majority of remaining DCX-positive cells also expressed MAP2. Some MAP2+ cells were present that expressed only very low levels of DCX, suggesting these cells had matured further (Figure 3-14C). By 28 days, the few DCX+ cells left co-expressed MAP2 (Figure 3-14D).

Figure 3-14. Mature R6/2 NPCs. Differentiated NPCs express different markers as they mature. R6/2 NPCs were differentiated into neurons for varying lengths of time and stained by ICC for DCX, MAP2, and synaptophysin. (A) At 7-days multiple cells expressed the early immature marker of neurons, DCX, (green), while only a few expressed the marker MAP2 (red) considered to be expressed in more mature neurons. (B) As cells were cultured for a longer period more cells expressed MAP2 while numbers of DCX alone cells begun to decrease, which continued to (C) 21 days. (D) By 28 days, almost all DCX signal was co-localised with that of MAP2 and remaining neurons exhibited a mature neuron shape with processes that resemble classical dendrites and axons. (E) Synapse formation, visualised with the synaptophysin antibody, represents evidence of neurotransmission potential between neurite branches. Synaptophysin (green) is present where TUJ1 positive neuronal branches meet and interact. (F) Orthogonal views through the Z stack shows synapse formation taking place on both sides of the neuronal process. WT cells showed similar phenotypes. NPC=neural progenitor cells, DCX=doublecortin, MAP2=microtubule-associated protein. Scale bars 50 μm.

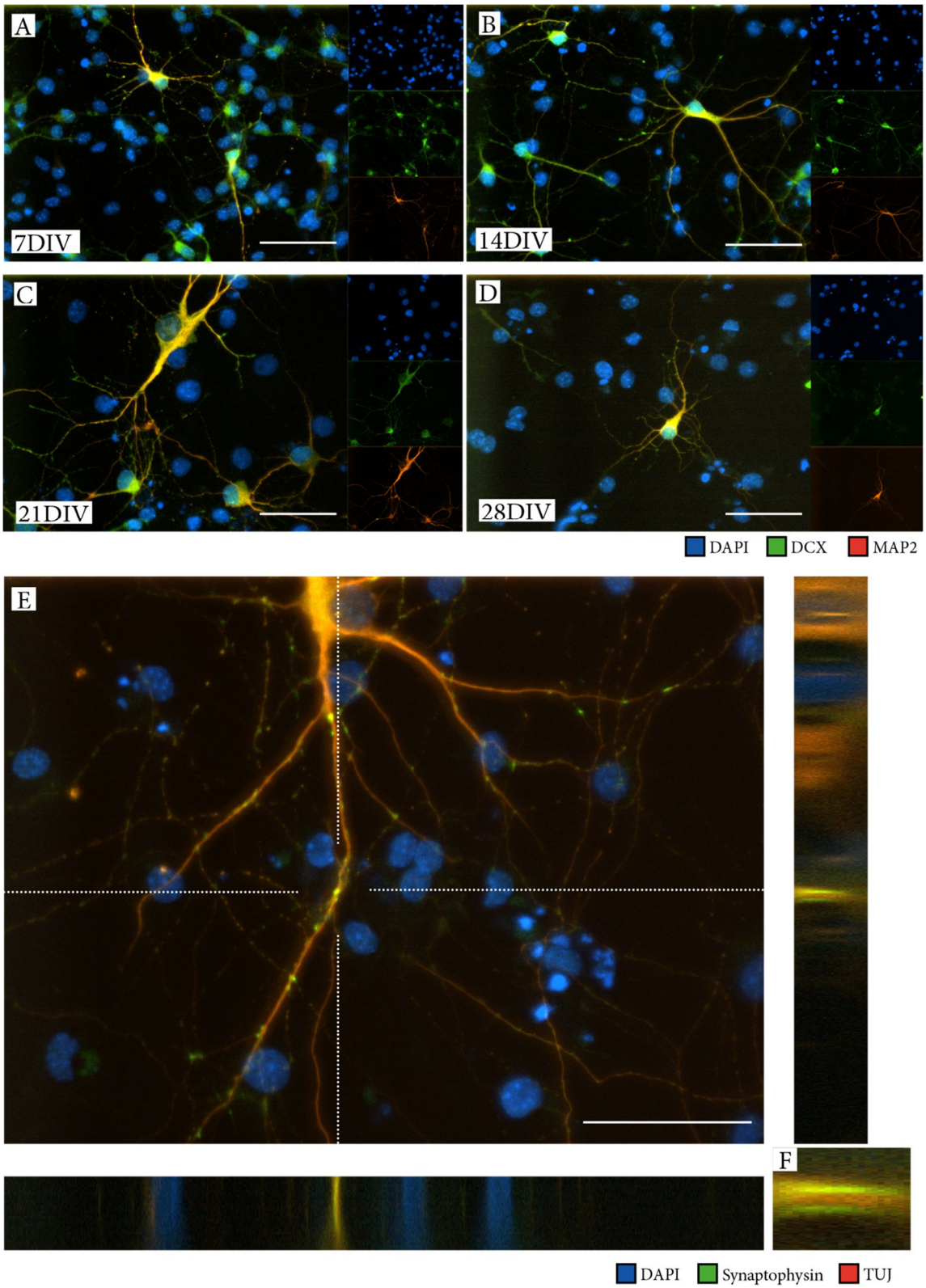
A
7DIV
B
14DIV
C
21DIV
D
28DIV
DAPI
DCX
MAP2
E
F
DAPI
Synaptophysin
TUJ

Although cells might have the morphology and express neuronal-associated proteins, the true measure of a mature neuron is its ability to communicate with the other neurons and to form neural networks. This communication takes place at synapses, which are located along the dendrites of neurons and on dendritic spines (Gray, 1959, Ballesteros-Yanez et al., 2006). Synaptophysin is a protein found at the synapse and involved in the mechanism vesicles use in neurotransmitter storage and release (Wiedenmann et al., 1986). To assess the neurons found in the cultures differentiated for up to 28 days, cells were stained using ICC with antibodies against MAP2 and synaptophysin. In both 24-well and 96 wells plates the presence of synaptophysin was abundant on the mature MAP2 and TUJ1+ neurons (Figure 3-14E). Punctate intensities of synaptophysin staining were present along the dendritic processes, suggesting synaptic expression (Calakos and Scheller, 1994, Kwon and Chapman, 2011). These intensities of staining are junctions where other large dendritic branches from neighbouring neurons cross. Using stacked images though the Z-plane, an orthogonal view of these synaptic interaction zones was visualised (Figure 3-14F). At these junctions the synaptophysin staining is present between the two dendritic processes as a marker of where neurotransmission takes place (Figure 3-14F). These data suggest the neurons identified in the differentiated cultures have the potential for neurotransmitter release and that rudimental neural networks have the potential to form.

3.14 Chapter discussion

3.14.1 Existing HD cell models

Despite concerted efforts to model HD *in vitro*, few reliable cell models exist that replicate measurable HD-like phenotypes. HD cell lines have long been rather limited to immortalised artificial lines but with the advent of iPSCs and gene editing technology there are new possibilities in the application of cell lines to advance HD research. These

lines have the potential to replace many existing cell lines used to model HD; however, they are unlikely to replace the need for animal models which have been vital for the identification of HD-like phenotypes and study of the onset and development. However, some of these system-wide findings have been hard to interrogate further at the cellular level without time-consuming techniques, such as breeding new lines and dissecting the underlying disease mechanisms. Creation of cell lines from foetal HD mouse models complements the work done *in vivo* using animal models and allows measurable, and relatable phenotypes to be translated *in vitro* for dissection in more user manageable settings.

Groups who have created cell lines from R6/2 mice have not observed the same results in aggregation pattern expression as observed in this thesis. Chu-LaGraff and colleagues used neonatal p1–p4 R6/2 mice to establish primary cell cultures that they grew and passaged as neurospheres before differentiating for 2 weeks (Chu-LaGraff et al., 2001). The authors presented examples of cells stained with an HTT amino-terminal specific antibody, which had speckled nuclear staining throughout the cytoplasm and nucleus. This aggregation phenotype observed by Chu-LaGraff and colleagues were less robust than those seen in the cells developed in this thesis. The staining pattern is they observed was more reminiscent of the diffuse stain that was initially seen in this thesis, before the protocol was adapted to facilitate the detection of the aggregation phenotype. The range and reliability of HTT antibodies used to observe aggregation have improved since this work was published in 2001, and so it is hard to compare the aggregation profile detected. Chu-LaGraff and colleagues only differentiated cells for 14 days, which was the lower time limit needed for aggregation to become visible in the cells described in this thesis. Other groups have produced cell lines which exhibit an aggregation phenotype but these have been produced via transfection of polyQ constructs into immortalised cells rather than from mouse models. Aggregation is present in HD mouse models and can be

synthetically created in the test tube (Ehrnhoefer et al., 2006, Heiser et al., 2002), or with primary cells from HD mouse models (Hackam et al., 1998) but creating cell lines to replicate these phenotypes without immortalisation has been less successful.

The NPCs in this thesis were differentiated into neurons and glia from radial glia cells that were extracted from the foetal brain, which have been allowed to develop *in situ* for the first 14 days of development. This extra time *in vivo* might allow the cells to develop the potential for phenotypes, such as aggregation, observed in the adult mouse, that are not observed in neurons created from embryonic stem cells *in vitro* (Verlinsky et al., 2005, Conforti et al., 2013, Trettel et al., 2000). The results presented here suggest the R6/2 NPCs lines which exhibit aggregation could be one of the most useful *in vitro* models to study the aggregation of HTT.

3.14.2 Regional specific dissection of lines

To develop the cell lines in this thesis, cells were extracted from distinct regions of the developing mouse brain that would go on to produce different cell populations in the adult brain. Only two of these cell populations were examined in detail: the lines from the cortex and LGE. Both of these lines produced cell populations that were affected in the R6/2 mouse model and would translate to cell populations that degenerate in human HD patients. The cells from the MGE that were established as lines but not investigated beyond ascertaining they were Nestin/Ki-67+ progenitor cells. These cells would produce an interneuron population in the brain. Although these cells were not further characterised they could be a valuable resource to examine in the future to investigate the effect of the HD mutation in the interneuron population. No analysis of regional specification was carried out on these lines to assess whether region-specific traits were retained. It was not considered to be initially important to investigate this unless differences between cells from different progenitor regions were found.

Groups who have taken a similar foetal cell approach to establish HD lines have extracted whole brain populations for culture with cells from all regions cultured together. Ritch and colleagues (2012) created NPC lines using foetal knock-in *Hdh*Q140 mice in a manner very similar to the approach used in this thesis, maintaining the cells as mitotic using growth factors EGF/FGF2 and differentiating them in the presence of an increasing BDNF gradient (Ritch et al., 2012). Using these lines, the authors found reduced BDNF expression pathways and cholesterol levels within the cells after differentiation. They also found that the foetal NPCs has a much lower neuronal differentiation potential compared to the work of Spiliotopoulos and colleagues (2009), much like that observed in this thesis. Although these cell lines are similar to the cultures analysed here, in that regional traits are probably unimportant for most of the questions we might want to answer, an advantage of the cell lines developed in this thesis is that the source of the cells in the dish is known and was carefully controlled. This regional source information will allow potential future experiments that involve regional-specific traits to be investigated, if required.

To further characterise the cultures from different dissected areas the expression of markers from these regions could be analysed. This could be achieved by either assessing these markers at the RNA or protein level using PCR or ICC. The use of transcriptome analysis to assess when and where genes are expressed is of crucial importance to understanding and predicting the physiological role of genes and proteins (Diez-Roux et al., 2011). Applying findings of these analyses to maps of the embryo help relate them to regional development. Using such atlases and applying the relevent genes and proteins to analysis on *in vitro* cell culture can help assess how much regions specific genetic expression is maintained in the dish. Examples in this thesis would be to assess if levels of protein and RNA are expressed in LGE and CTX lines and retained over multiple passages and differentiaton.

3.14.3 Monolayer cultures over neurospheres

The cultures established here were initially grown as primary free-floating neurospheres before dissociation and expansion as adherent monolayers. Maintenance of cultures as a monolayer provided distinct advantages over further expansions of the population as neurospheres. Neurospheres have a reduced neurogenic potential after longer culture periods, whereas in monolayer cultures neurogenic potential is maintained (Bibel et al., 2007, Conti and Cattaneo, 2010). There is evidence to suggest that although population expansion is quicker when growing cultures as neurospheres, the cells produced from monolayers cultures are less prone to spontaneous differentiation and cell death (Conti and Cattaneo, 2010). Monolayer cultures have the distinct advantage of being applicable to high content screening, which uses automated microscopy and requires a single layer of cells at a relatively consistence depth to maintain and limit variability in the focus plane (Danovi et al., 2012). The use of monolayer cultures in this thesis enabled the use of the Operetta and a platform to screen the effects of novel compounds on the R6/2 HD phenotypes.

3.14.4 Differentiating neural progenitor cells into mature neurons and glia.

HD-like phenotypes, such as inclusion formation and CAG repeat instability, observed in the human disease and mouse models are mainly found in post-mitotic neurons (Gonitel et al., 2008). It is not known if this is because the concentration of mHTT fails to reach the threshold needed to trigger pathological events, because the pool of mHTT is reduced with each mitotic event, or if it is because of another protective mechanism (Bates et al., 2015). As such, to study these phenotypes in culture it was necessary to arrest mitosis and induce the cultures to differentiate. The protocol used to differentiate cells was adapted throughout the thesis and eventually was based on the removal of growth factors and alteration of base medium to produced cultures of mixed glia and neurons. The resulting

cultures were mostly compromised of GFAP+ astrocytes with roughly 10% of cells being neurons. The neural percentage was much lower than previously reported in the papers that the protocols were adapted from, in which cultures contained up to 80% neurons (Spiliotopoulos et al., 2009). The cells used in the Spiliotopoulos and colleagues protocol were NSCs that had been derived and differentiated from ESCs, so differ from those used in this thesis. This could explain the difference in the percentage of neuronal cells observed here and with those obtained by other labs using foetal derived NPCs (Ritch et al., 2012). The lower neuronal number was not a problem within this thesis, however it could be a limiting factor for techniques that might be applied in the future. Techniques such as electrophysiology require a large number of neurons in culture, as patch-clamping has to be performed by eye and without fluorescent markers for selection, therefore the neuronal density determines how easy it is to establish connections and gather data.

A population of cells also were negative for markers of neuronal and glial fate. The identify of these cells remains a mystery although they seem to correlate with those cells discussed in the following chapters which contain aggregation. It is possible these cells maybe other cell types such as Neuroepithelial cells, which would be the precursor cells to the presumed radial glial population maintained as NSCs. These cells have the potential to differentiate into other non-neural cell types which could be present in cultures. A further characterisation of the cells that are present before and after differentiation of NPCs would help to identify these cells.

Although the use of immunofluorescence has revealed the presence of synaptic markers, observation of electrophysiological parameters would be required to assess neuronal functionality. For example, iPSC neurons that show a similar expression profile for neural ICC markers have shown high states of functional immaturity (Belinsky et al., 2011). Groups using similar techniques to culture NSCs have shown that differentiated neurons can be electrophysiologically active in the dish (Hogg et al., 2004, Song et al., 2002,

Spiliotopoulos et al., 2009). Electrophysiological properties of neurons are central to their function yet the development of these properties in the cultures used here remains unknown.

The differentiation protocol used in this thesis, adapted from that of Spiliotopoulos and colleagues (2009) used the gradual addition of BDNF to cultures. BDNF was introduced and gradually increased over the differentiation period to help improve neuronal survival. Disruption of BDNF transcription, trafficking and signalling has been observed in HD (Zuccato and Cattaneo, 2007) and overexpression of the *Bdnf* transgene in the R6/1 mouse model can reverse some phenotypes such as weight loss and the mice exhibit an improved motor function (Gharami et al., 2008).

Whether BDNF was also disrupted in the R6/2 NPC cells was not investigated but would be of interest to follow up. To achieve this, BDNF supplementation in the medium would need to be controlled to check for the BDNF baseline levels in the cells. However, removal of BDNF from culture medium could challenge cell survival and those cells with reduced BDNF expression could be lost before a quantitative analysis could be performed. The experiment could therefore be performed at the early differentiation phase, after removal of EGF and with low levels FGF before and after BDNF is first introduced into the media. The BDNF pathway involves BDNF binding to the TrkB (Tropomyosin receptor kinase B) receptor and activation of first PI (Phosphoinositide) 3-kinase and then PDK1 (3-phosphoinositide dependent protein kinase-1), which phosphorylates the pro-survival effector molecule AKT (Zuccato and Cattaneo, 2007). As well as levels of BDNF, the downstream pro-survival effector molecule AKT could be analysed to assess whether survival factors are affected within these cultures.

In the mouse brain neither BDNF mRNA nor BDNF protein are present in neuronal cell bodies of the striatum, but rather as in puncta in the neuropil. Conversely, the cortex, of

BDNF mRNA is easily detected in neurons of cortical layers responsible for projecting to the striatum (Altar et al., 1997). It is from these neurons which the punctate BDNF found in the striatum is supplied. On the basis of these observations one would expect variation in how NPC cultures, derived from different areas of the brain, would express BDNF and its downstream molecules. These regional differences would be interesting to explore.

3.15 Summary

Establishment of a new NPC line to investigate HD is of high importance. The aim of this chapter was to create stable NPC lines from three district regions of the brains of WT and R6/2 foetal mice, which can be maintained *in vitro* and manipulated to differentiate into mature neural cells. Cell lines were established from E14.5 foetal mouse brains and cultured *in vitro* to remain in the cell cycle. These cells retained a stable karyotype throughout a series of passages and extended time in cultures. R6/2 lines showed little variation in their CAG repeat length over time. Cultures were induced to exit mitosis by removal of growth factors. Cells differentiated into neuronal and glial cells after adaption of the differentiation protocol with gradual addition of BDNF. Markers of synaptic activity were detected on the dendritic branches of neurons suggesting the potential for neurotransmission and the formation of rudimental neural networks. These cell lines are an ideal culture system to probe for HD-like phenotypes and to complement findings in the R6/2 mouse.

Chapter 4 Results 2: Characterising phenotypes present in cell lines created from the R6/2 mouse model of Huntington's disease

4.1 Introduction

The clinical effects of mutations in the *HTT* gene manifest in a series of complex changes to behaviour, cognition, and personality. How these changes relate back to the lengthening of the polyQ within the gene is not well understood. At a cellular level, mHTT results in cellular aggregates. These aggregates gather as inclusions within the cell. Inclusion formation of aggregates is a hallmark of HD at the cellular level. The R6/2 mouse model exhibits a detectable aggregation phenotype in neural cells soon after birth. This aggregation increases progressively in both the number of affected cells and quantity of aggregated protein throughout the 16-week R6/2 mouse lifespan. The link between cell dysfunction and the progressive aggregation of mHTT is still not fully understood and difficult to study *in vivo*. The R6/2 NPC cultures established in the previous chapter are potentially a usual model to examine the disease mechanism as they are essentially the cells which would eventually form the R6/2 mouse brain. On that basis, the WT and R6/2 NPC cultures established in the last chapter were differentiated and probed for HD-like phenotypes using immunohistochemical analysis of mHTT expression and microscopic techniques to visualise the aggregation.

4.2 Chapter aims:

The aims of the experiments performed in this chapter were to:

1. Establish whether differentiated R6/2 NPCs develop HD-related phenotypes representative of those found in the brains of HD patients and HD mouse models.

2. Investigate how these phenotypes appear to develop in the R6/2 NPC model.

4.3 Huntingtin aggregation in the brains of adult R6/2 mice.

The development of HD mouse models with HD-related phenotypes has been vital in the study of disease progression and mechanisms. The R6/2 mouse exhibits a rapid onset of HD-like symptoms. HD is a late-onset neurodegenerative disease, yet the R6/2 mouse typically reaches its equivalent human endpoint around 16 weeks of age. At this point, the mouse exhibits profound behavioural (Carter et al., 1999) and cognitive (Lione et al., 1999) problems, as well as severe atrophy to muscles, and weight loss (Mangiarini et al., 1996, Davies et al., 1997, Rattray et al., 2013). HTT aggregates also appear early within the R6/2 mouse brain, before the onset of many other phenotypes (Davies et al., 1997). To visualise deposition of the aggregated form of the mutated huntingtin protein (mHTT), 16-week-old R6/2 mouse brain sections were examined by immunohistochemistry (IHC) using the polyclonal sheep antibody 'S830'. The S830 antibody was raised against exon 1 of HTT with 53 glutamines (Sathasivam et al., 2013) and was developed in this lab. The antibody is now used throughout the field to label the polyQ expansion of the mHTT (Refs). Multiple antibodies have been developed both commercially as well as within individual laboratories. Each antibody corresponds to different epitopes along the mHTT protein and can be selected based on the structural conformer of mHTT being investigated. Within the R6/2 mouse, the highly expanded PolyQ is thought to allow for robust staining using the S830 antibody. The sections were also stained with an antibody against MAP2 to identify neurons. S830+ mHTT (green) inclusions were mostly but not exclusively found in neurons, as shown by co-localisation with MAP2 (Figure 4-1). S830+ mHTT inclusions were abundant in the cortex (CTX) and striatum (STR), but were mostly absent from the corpus callosum (CC; Figure 4-1A,B).

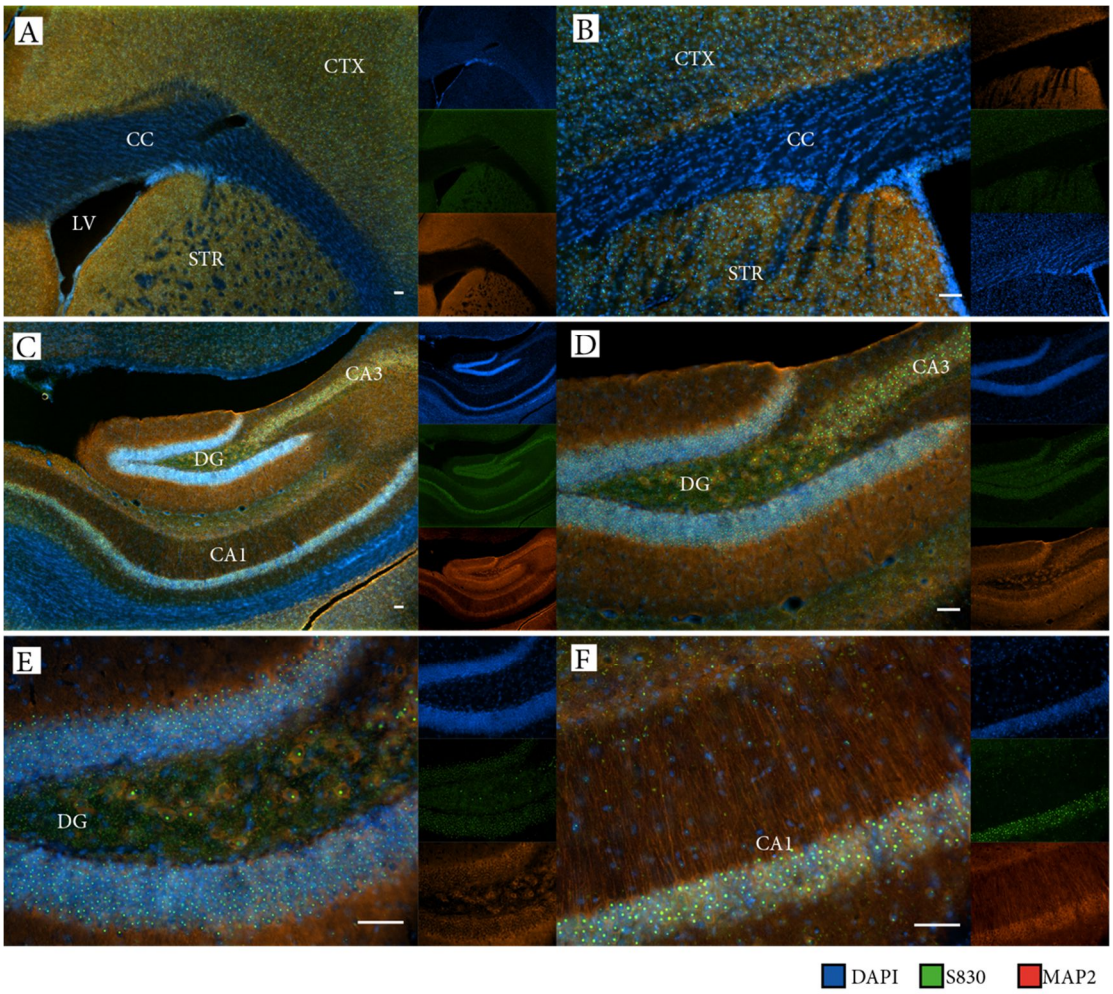

Figure 4-1 Huntingtin aggregation in the brains of R6/2 mice. mHTT inclusions in the R6/2 mouse brain can be visualised using the S830 antibody (green) and visualised in neurons using MAP2 (red). (A) Macroscopic and (B) further higher powered microscopic views of a slice taken around bregma 1.10mm containing both cortex and striatum, which have widespread S830 staining, separated by the CC which contains little to none S830+ nuclei. (C) Similarly macroscopic and (D) more microscopic views of the more caudal hippocampal region around bregma -2.30mm. (E) The neuronal nuclei rich DG and (F) CA1 structures show intense S830 staining with particular large intensities in the neurons projecting from the CA1. mHTT=mutant huntingtin, CTX=cortex, STR=striatum, LV=lateral ventricle, CC=corpus callosum, DG=dentate gyrus, CA1,CA3=cornus ammonis regions 1 and 3. Scale bars 50 μm

Because of the apparent predilection for mHTT inclusions in neurons, the hippocampus, which contains highly dense neurons, is a useful region of the brain to monitor aggregation. The dentate gyrus (DG) and cornus ammonis (CA) hippocampal regions are neural dense structures where adult neurogenesis has been shown to take place (Eriksson et al., 1998). Similarly to the striatum and cortex, show high levels of S830+ mHTT

aggregates present in the DG (Figure 4-1C) and CA (Figure 4-1D) at the end stage of the disease. At high power magnification, it was evident that S830+ inclusions were present in the nuclei of neurons in the DG (Figure 4-1E). These inclusions were also seen in the CA regions, where the MAP2+ neurons were evident projecting out from the nuclear layer, each with an S830+ inclusion in the nucleus (Figure 4-1F). These data were collected to guide the use of the S830 antibody to identify aggregated inclusions in affected R6/2 cells. Understanding the potential expression of the mHTT protein is important to identify similar expression *in vitro*.

4.4 Huntingtin aggregation in the brains of 4-week-old R6/2 mice

The use of traditional wide-field optical microscopy has been useful when combined with the ability to label proteins through antibodies tagged with fluorescence, however this type of microscopy does have certain limitations. Secondary or X-ray fluorescence can be emitted from samples, which limits the resolution of the features of interest. Out of focus light is also a problem, especially when sections are thicker than about 2 μm. These problems can be nullified by the use of 'laser scanning confocal microscopy' (hereon just referred to as confocal microscopy). With this technique, a spatial pinhole eliminates out of focus light to produce optical slices within a thick object and increases both resolution and contrast. The sample is also not bathed in light as with wide-field microscopy, rather lasers scan across the specimen at the point of focus, which lowers the level of fluorescence bleaching at the same time as only exciting fluorescence within that optical slice.

The quantity and size of detectable mHTT inclusions increases with age in R6/2 mice. Many studies have shown the presence of inclusions in R6/2 mice between 3-4 weeks of age (Davies et al., 1997, Morton et al., 2000, Li et al., 1999b, Meade et al., 2002) while

others have shown they can be detected even earlier, in p1 neonates (Stack et al., 2005) although at low concentrations. The presentation and onset of HD-like phenotypes in R6/2 mice can vary depending on the length of the expanded CAG repeat (Morton et al., 2009). The R6/2 mice used here have repeats lengths of around 220, and so have a comparable repeat length consistent with many previous studies from this lab. To investigate whether younger mice have detectable levels of mHTT inclusions, 4-week-old R6/2 mouse brains were fixed and sectioned while frozen into 25-µm coronal sections using a cryostat. Confocal microscopy was used to assess the presence of mHTT inclusions stained using the S830 antibody alongside an antibody against TUJ1 to identify neurons. The age of the cells within these sections would represent those in the 28-day-old differentiated cultures described in Chapter 3. As positive and negative controls for the staining of mHTT+ inclusions, 16-week-old R6/2 end-stage mice and WT mice sections were also used.

The optical sectioning and resolution of the confocal microscope allows for identification of individual cells within dense areas of neurons, which is particularly useful for studying the neuronal nuclei of the hippocampus, and in particular the dense neuronal cell bodies of the DG. This density makes it an ideal region to investigate the presence of detectable mHTT inclusions. In R6/2 end-stage mice, S830+ neurons are detectable in the DG of the hippocampus (Figure 4-2A) while these were absent from sections from WT littermates (Figure 4-2B).

In the 4-week-old R6/2 mouse sections both nuclear and extra-nuclear S830+ inclusions were detected using IHC (Figure 4-2C). At the resolution and magnification used, inclusions were detected at a relatively low frequency (arrows). The inclusions appeared smaller than those detected in the end stage R6/2 mouse sections. The S830+ stained nuclei often appeared to contain multiple individual inclusions, although multiple optical slices through the Z-plane would be needed to confirm this. Because inclusions were

successfully identified in the 4-week R6/2 mouse brain using IHC, if the same process takes place *in vitro,* it would be expected that inclusions should be detectable in differentiated NPCs.

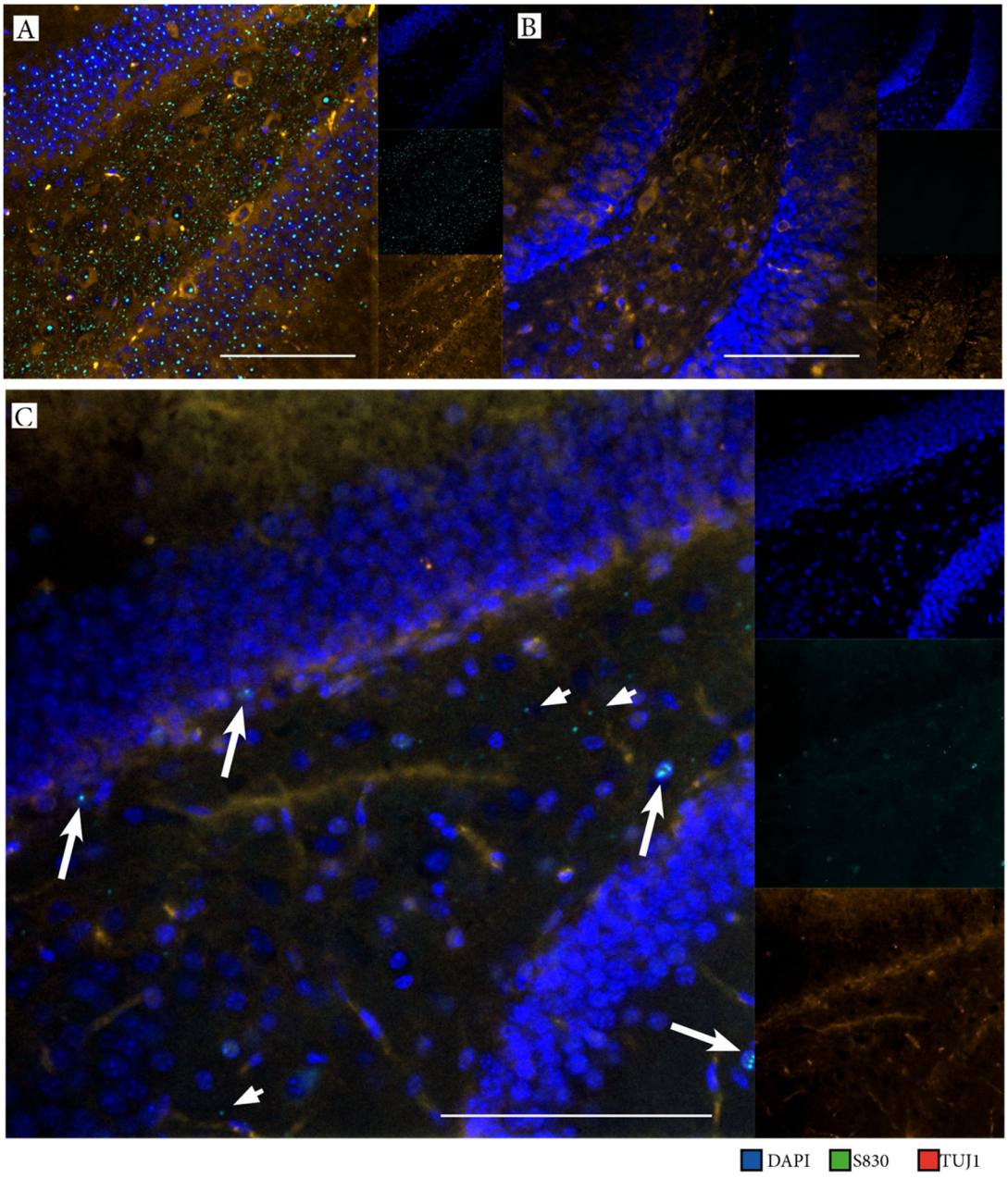

Figure 4-2. Huntingtin inclusions in the brains of 4-week-old R6/2 mice. The R6/2 mouse exhibits a detectable aggregation phenotype from an early age. (A) S830+ positive mHTT inclusions are evident in end-stage R6/2 tissue hippocampal sections but absent in (B) their WT littermates. (C) Presence of S830 staining in 4-week-old R6/2 mouse sections showed mHTT aggregation as inclusions by this time-point. Both cytoplasmic (short arrows) and nuclear inclusions (longer arrows) were observed. mHTT=mutant huntingtin, WT=wildtype, TUJ1=beta-III-tubulin. Scale bars 50 μm

4.5 Assessment of aggregation in differentiated neural progenitor cells

To assess whether aggregation of HTT was taking place *in vitro*, R6/2 and WT Dc lines were differentiated using the modified Spiliotopoulos and colleagues (2009) method developed in Chapter 3. p15 Dc cells were differentiated for 28 days with cohorts harvested and fixed every 7 days. Differentiated cells were immunostained using ICC with the anti-exon1 mHTT antibody S830 and neuronal marker MAP2 (Figure 4-3). A diffuse cytoplasmic staining was apparent throughout most cells in both WT and R6/2 lines. The most pronounced S830 staining was observed at the earliest time point studied (Figure 4-3A) at 7 days. This diffuse cytoplasmic staining remained throughout the differentiation period but was less evident as the cells matured from 14 days (Figure 4-3B).

The strongest staining was presumed to be in non-neuronal cells as it mostly appeared in cells that did not stain with the neuronal marker MAP2. However, some MAP2+ neurons did co-localise with S830 staining. Little change to the staining profile was observed at the later time points. S830 staining was still mostly cytoplasmic in both WT and R6/2 cell lines. However, in one R6/2 line at 21 days, the intensity of S830 staining had increased in the nucleus of a R6/2 mature MAP2+ neuron (Figure 4-3C). This finding was not replicated in other R6/2 lines or after 28 days (Figure 4-3D).

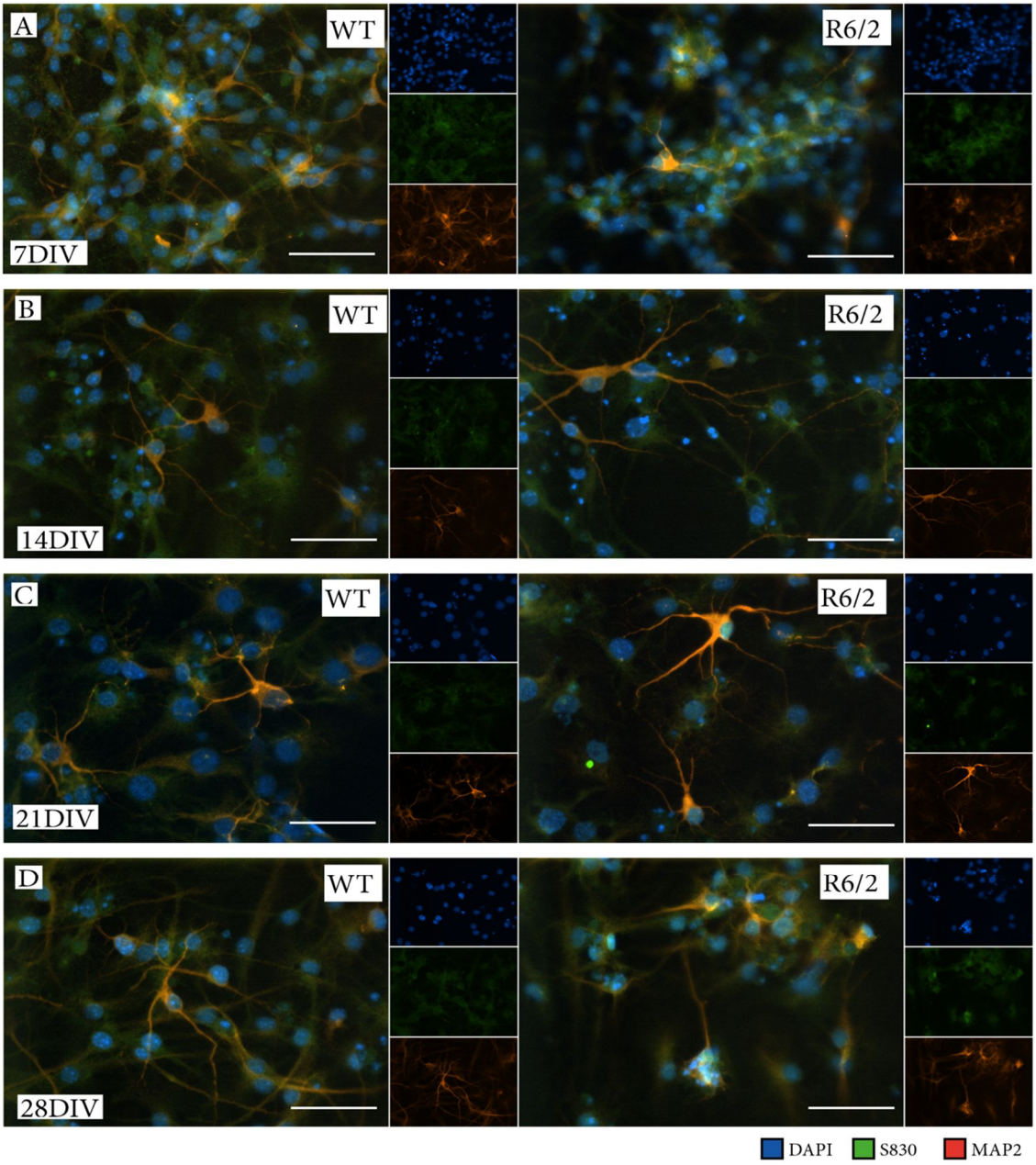

Figure 4-3. Assessment of aggregation in differentiated NPCs. Aggregation of mHTT in cells of the CNS is a hallmark of HD and is present in many models of the disease. ICC staining using S830 in differentiated cells can determine whether this neuropathological phenotype occurred *in vitro*. (A) NPCs were grown in differentiation media on uncoated plates for 3 days and then switched to laminin-coated plates for further differentiation. At 7 days, cells were stained for MAP2 to identify neurons, (red) and for S830 to identify mHTT (green). (B) After 14 days and (C) 21 days of differentiation, a distinct haziness around cell nuclei in both WT and R6/2 cell lines was present, with a higher degree of staining around MAP2- cells. (D) At 28 days, the hazy S830 staining was still present and mostly in the cytoplasm with little staining co-localised with DAPI+ nuclei. A marked difference was not observed between the WT and R6/2 lines. NPCs=neural progenitor cells, CNS=central nervous system, HD=Huntington's disease, ICC=immunocytochemistry, MAP2=microtubule-associated protein 2, WT=wildtype. Scale bars 50 μm.

Classically, aggregation is detected in inclusions, as shown previously here *in vivo* (Figure 4-1, Figure 4-2). The staining profile exhibited in these cells does not represent what would be expected from mHTT aggregation and indeed is present in equal quantities in both WT and R6/2 cell lines. It is unlikely that this staining is the endogenous WT mouse HTT because S830 does not recognise endogenous mouse HTT (Landles et al., 2010). These data suggest that S830 cross reacts with a cytoplasmic protein other than HTT. S830 is a polyclonal antibody for which the epitopes have not been mapped and any proteins with which it cross reacts are unknown.

4.6 Adjustment of the differentiation media and the effect on aggregation

The neuralisation step that Spiliotopoulos and colleagues developed was designed to increase the neuronal content of their cultures (Spiliotopoulos et al., 2009). The Spiliotopoulos method converts ESCs to NPCs to neurons; in their method, proliferative cells were plated without a substrate, and the differentiation protocol that followed also did not use substrates for the first differentiation step (Table 4-1 – Spiliotopoulos original). By contrast, in the protocol developed in this thesis, proliferative cells were grown on a substrate of laminin. The neuralisation step in the improved differentiation protocol that was presented in Chapter 3 involved a switch from laminin-coated plates to uncoated plates and then back to laminin-coated plates (Table 4-1 - NPCs). To investigate whether this switching step was a necessary adaption to the protocol, the differentiation experiment was repeated as previously performed, but without the switch to uncoated plates (Table 4-1 – adapted protocol). This adaptation allowed cells to be directly switched between proliferative and differentiation protocols without the extra disruption of removal from the plates during the neuralisation step. It also allowed a higher number

of cells to be used for differentiation because cells are lost during neuralisation if they do not remain adhered to the uncoated plastic.

		Self-renewal	D1	A	B
Coating	Spiliotopoulos et al - Original	–	–	Laminin (3 ∝g/mL)	Laminin (3 ∝g/mL)
	Spiliotopoulos et al - NPCs	Laminin (3 ∝g/mL)	–	Laminin (3 ∝g/mL)	Laminin (3 ∝g/mL)
	Adapted proticol	Laminin (3 ∝g/mL)	Laminin (3 ∝g/mL)	Laminin (3 ∝g/mL)	Laminin (3 ∝g/mL)

Table 4-1 Substrates used for adherence in the Spiliotopoulos and colleagues protocol adaption in this thesis.

This adapted method without the switch to uncoated plates was followed and the same differentiation and ICC staining was performed as described above to identify S830+ mHTT aggregation and MAP2+ neurons.

At day 7 and day 14 of differentiation, diffuse cytoplasmic staining was observed in cells differentiated on laminin similar to with those that were switched to uncoated plates. This staining pattern was observed for both WT and R6/2 lines (Figure 4-4A, B). At 21 days, a distinct change in the S830 staining prolife was observed. In the WT lines, the diffuse cytoplasmic staining pattern remained; by contrast, in R6/2 lines, intense S830+ inclusions appeared in the nuclei of some cells (Figure 4-4C arrows). These inclusions appeared similar to those seen in the brain of the R6/2 mouse (Figure 4-2C). The inclusions were seen at both 21 days and later at 28 days in the R6/2 lines (Figure 4-4C,D arrows) in a small number of cells per region of interest. The cells that contained nuclei with inclusions did not appear to co-localise with MAP2+ staining. On the basis of these results, all subsequent experiments were performed using laminin-coated plates throughout the differentiation process.

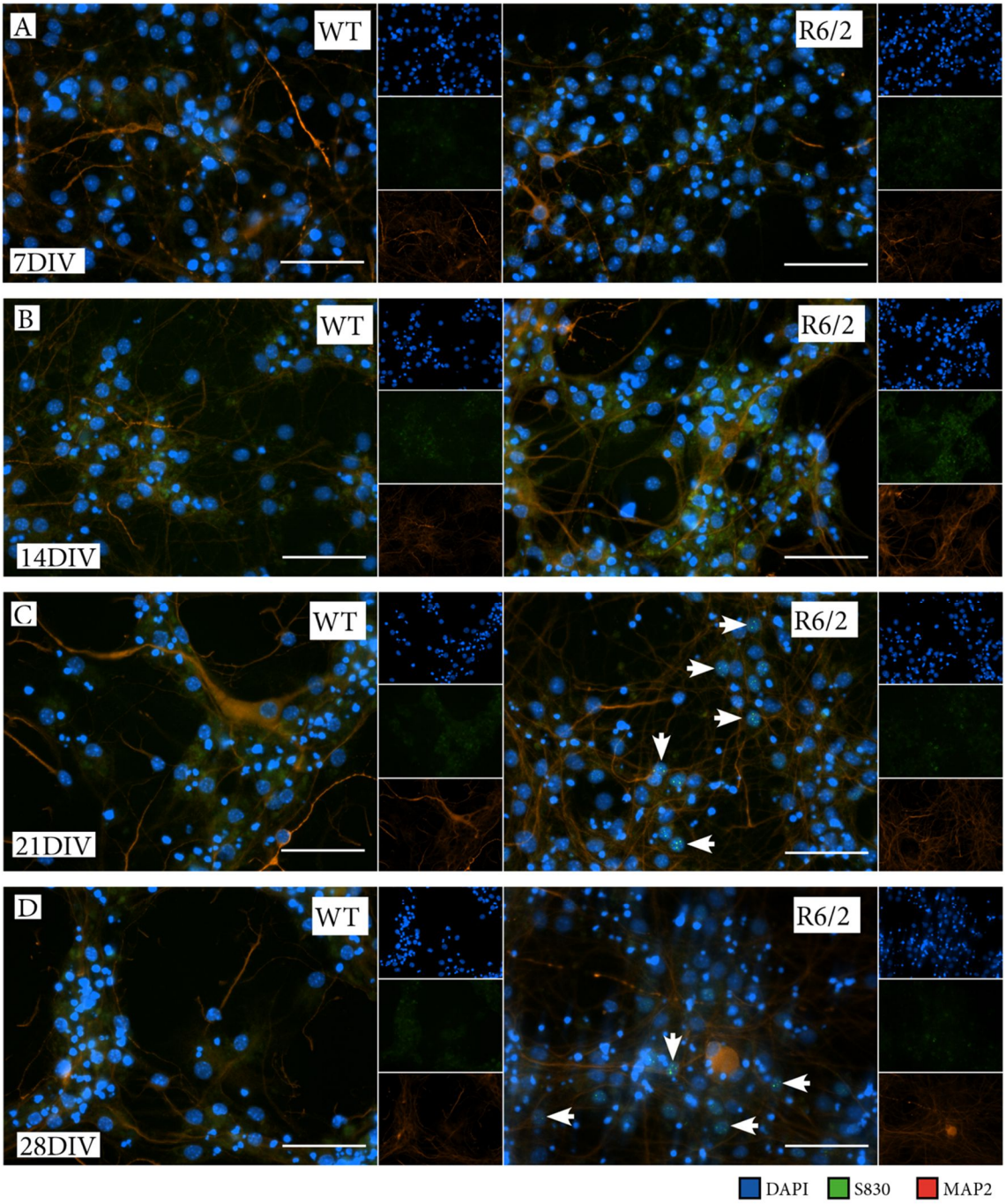

Figure 4-4. Adjustment of substrate coating and the effect on S830 staining. Adaption of the Spiliotopoulos and collegues protocol with removal of the uncoated plastic step to the use of a consistent laminin monolayer. (A) NPCs were grown for 7 days and (B) 14 days in differentiation media on laminin-coated plates and stained with S830 to identify mHTT (green) and MAP2 to identify neurons (red). (C) After 21 days of differentiation, S830+ inclusions were present in the nuclei of some cells (arrows). No inclusions were present in the WT cells. (D) At 28 days, S830 inclusions were present in the nuclei of some R6/2 cells (arrows) and absent from WT cells. NPCs=neural progenitor cells, mHTT=mutant huntingtin, MAP2=microtubule-associated protein 2, WT=wildtype. Scale bars 50 μm.

4.7 Identification of the location of the aggregation signal.

The mechanism by which mHTT aggregates and forms inclusions in specific locations is important for the assessment of their role as part of the HD disease mechanism. mHTT inclusions exist both in the nucleus and cytoplasm of cells in the brains of HD patient and mouse models (DiFiglia et al., 1997, Davies et al., 1997). Inclusions present in the cytoplasm can be cleared by autophagy (Martin et al., 2015), a process that does not occur in the nucleus (Martin et al., 2015, Kaushik et al., 2010).

Images taken of inclusions found in R6/2 cell lines (Figure 4-4) suggest that inclusions were mainly nuclear. To confirm this hypothesis, confocal microscopy can be used. Thus, to investigate whether the inclusions were intra-nuclear, a stack of images from R6/2 cells was taken through the Z plane to produce a 3-dimensional image (Figure 4-5A). An orthogonal view shows the profile of a cell though the dotted lines below (Figure 4-5B) and to the side of the image (Figure 4-5C). The large bright S830 inclusions were located inside the nucleus. Such inclusions account for 4% of the nucleus by volume and appear as single continuous objects at the resolution used. Two large inclusions could be seen inside one nucleus, which seemed independent of each other (Figure 4-5A).

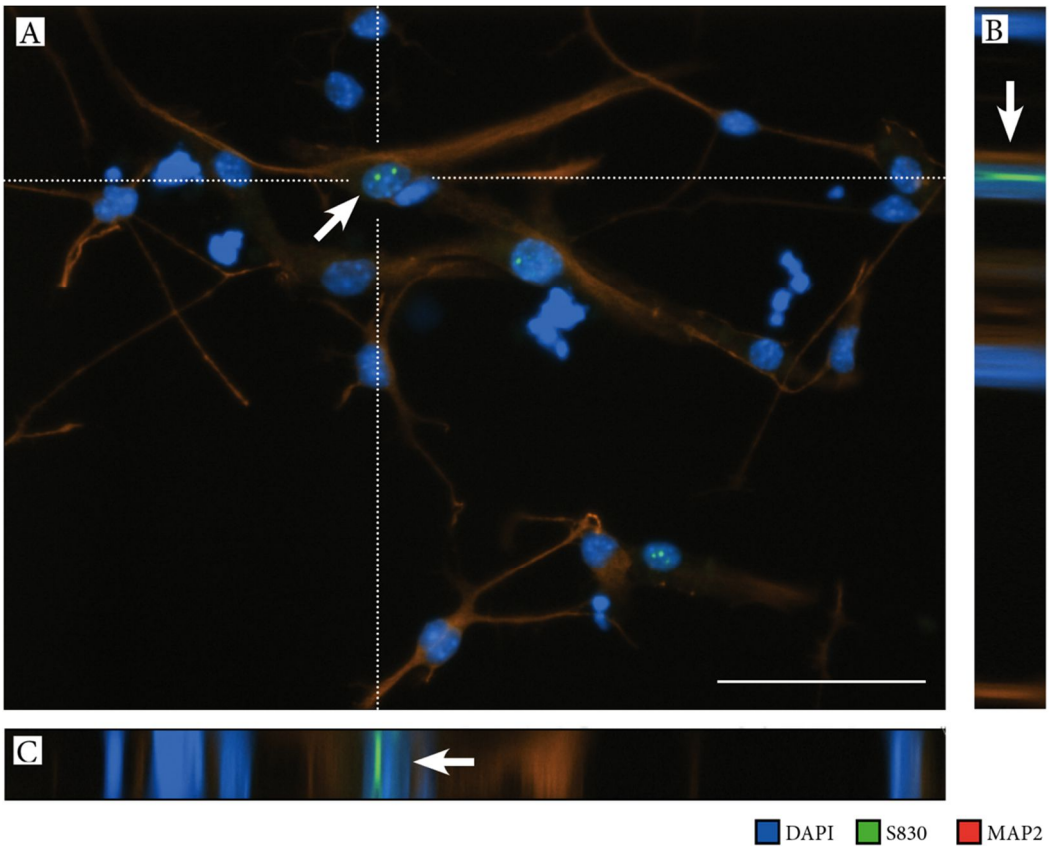

Figure 4-5. Identification of the location of the aggregation signal within an R6/2 cell. A series of images were taken through the Z-plane to form a stack and allowed a 3-dimentional representation to be constructed. (A) A single DAPI stained (blue) nucleus with inclusions stained with S830 (green). Dashed white lines represent intersection of orthogonal slices though the stack of images with the nucleus of interest marked with a white arrow. (B) Panel represents profile of staining marked by vertical dashed line and (C) through the horizontal dashed line. Nucleus with inclusions marked with white arrow. Green S830+ inclusion evident throughout the nucleus and contained within the nuclear envelope. MAP2=microtubule-associated protein 2. Scale bar 50 μm.

4.8 Assessment of mHTT using western blot analysis

Western blotting can be used to quantify protein levels and as an alternative approach to detect detergent insoluble protein aggregation. To assess whether a mHTT aggregation signal could be detected using western blot analysis, whole cultures from 75cm^2 plates were lysed for protein extraction. Lysates from R6/2 and WT Dc cells after 28 days of differentiation were produced and proteins separated by SDS-PAGE and immunoprobed using the S830 antibody (Figure 4-6A). While WT cells showed no evidence of S830+ mHTT, in the R6/2 lines, prominent bands were present at around 90 kDa, indicative of the soluble R6/2 transprotein. A signal was also present within the stacking gel, which is likely to have been insoluble mHTT that does not enter the resolving gel. The WT lines were free from any mHTT S830 bands at around 90 kDa, confirming the ICC results previously seen (Figure 4-4). Non-specific bands between 83 and 62 kDa were present in lanes of both genotypes and might represent the other proteins that the S830 antibody detected by ICC. The loading control was alpha tubulin, which has a molecular weight of around 50 kDa (Figure 4-6B).

An identical cohort of cells was differentiated for 28 days and processed for ICC in parallel to those cultures used for protein lysates. These cells were stained for S830 and the neuronal marker MAP2 (Figure 4-6C). As previously observed, a subset of cells had inclusions of S830+ mHTT within the nucleus. A persistent feature of the nuclei with mHTT inclusions was that they rarely stained for markers of neurons or glia. Indeed, these nuclei were located in cells that were more often separated from clumps of cells and appeared relatively isolated. The cells located in clumps appeared less likely to contain inclusions. These data from western blot analysis and ICC provide strong evidence to confirm that mHTT was expressed and that the aggregation process occurs in R6/2 NPC cultures, appearing as inclusions within the nuclei of some cells.

Figure 4-6. Assessment of mHTT using western blot analysis and ICC. WT and R6/2 cells lines differentiated for 28 days were harvested to examine mHTT expression. Whole cell lysates were examined by western blotting and were immunoprobed with (A) S830 antibody and (B) alpha-tubulin antibody as a loading control. Two protein concentrations of 50 μg and 100 μg were assessed. Bands around 90 kDa represent the soluble mHTT transprotein. Bands above the interphase are detergent insoluble mHTT aggregates, which do not enter the resolving gel. Other bands between 62 and 83 kDa are most likely to be non-specific protein. (C) R6/2 cells grown in parallel to those used in the lysates were stained by ICC to visualise protein *in situ*. ICC staining for S830 (green) shows mHTT colocalised with DAPI stained (blue) nuclei (white arrows). No MAP2+ cells (red) in these cultures appeared to have mHTT co-expression. (D) WT cells grown and stained in parallel with those above. (E) Control images for R6/2 clls with no secondary antibody included to rule out autofluorescence. ICC=immunocytochemistry, WT=wildtype, mHTT=mutant huntingtin, MAP2=microtubule-associated protein 2. Scale bar 50 μm.

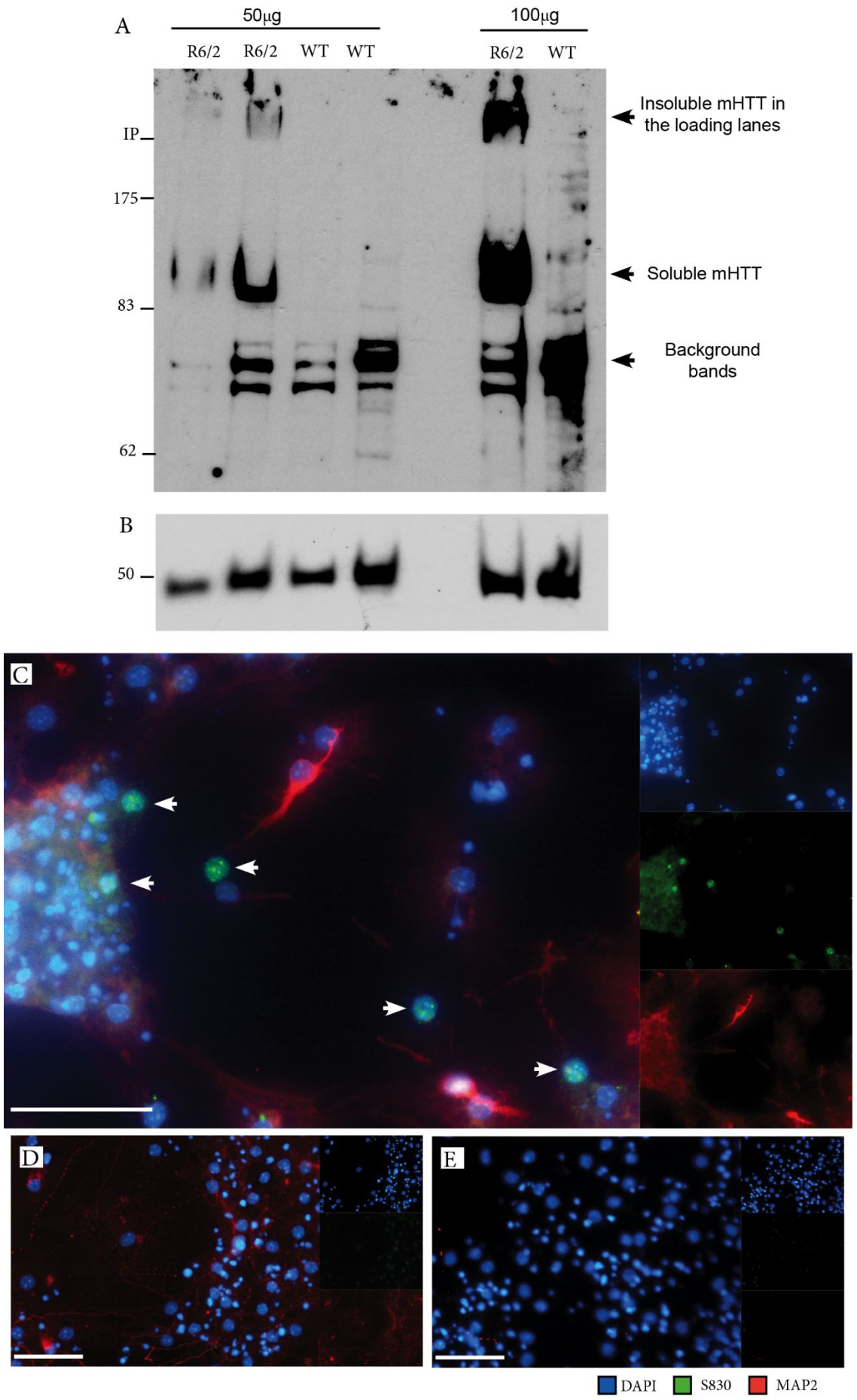
A
50µg
100µg
R6/2
R6/2
WT
WT
R6/2
WT
IP
175
83
62
Insoluble mHTT in the loading lanes
Soluble mHTT
Background bands
B
50
C
D
E
DAPI
S830
MAP2

4.9 Use of confocal microscopy to examine aggregation in differentiated neural progenitor cells

Confocal microscopy was used to clarify the identity of the R6/2 cells with mHTT inclusions. As discussed previously, confocal microscopy has advantages over widefield microscopy, with increased resolution and reduction of noise; it also allowed for the addition of the far-red channel to visualise three different proteins at once in addition to DAPI.

R6/2 Dl cell cultures were used to assess whether aggregation occurred in lines from the LGE and the cortex. Cells were differentiated for 28 days to reveal inclusions. In these Dl cultures, a distinct dual population of cells with nuclei containing inclusions (white arrows) and those without was apparent (Figure 4-7). Those cells that contained inclusions tended to be separate from clumps of cells, although not exclusively.

The mature cell type, that these inclusion containing nuclei belonged to, was difficult to identify. Neurons in the differentiated R6/2 (and WT) cultures did not express FOX3 and so could not be identified using the antibody NeuN; as such, no nuclear-based markers could be used to identify them (Figure 4-8). Instead, cytoplasmic or cell surface markers had to be used. However, use of cytoplasmic markers made it difficult to identify individual cells containing inclusions within clumps because of the dense intertwined nature of the cells.

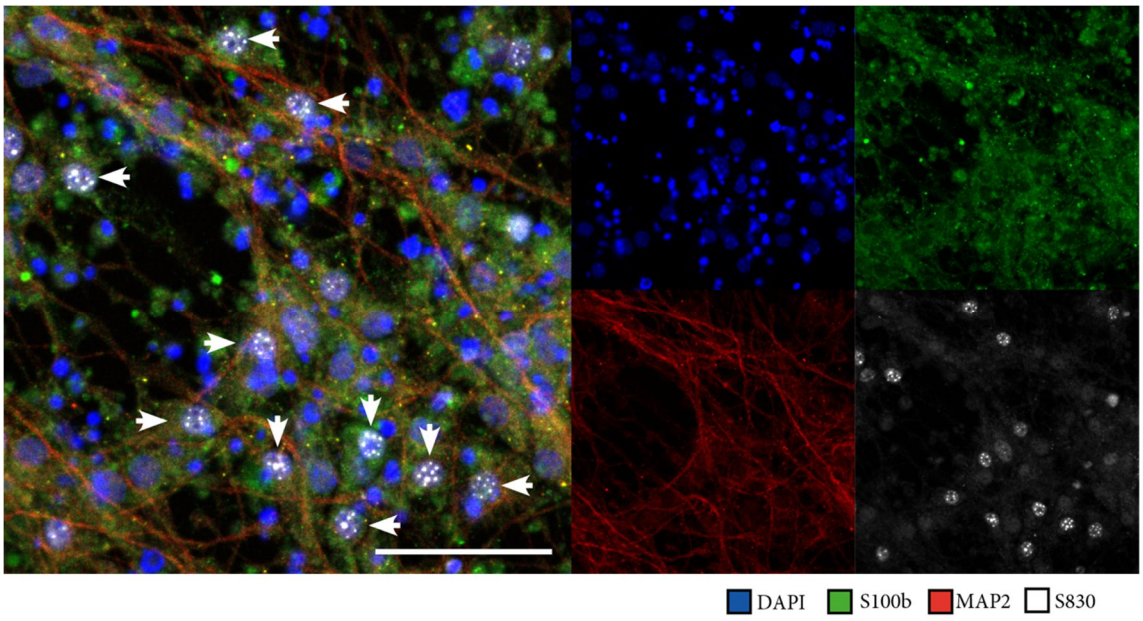

Figure 4-7. Use of confocal microscopy to identify inclusions in differentiated R6/2 NPCs. Confocal images of differentiated R6/2 cultures after 28 days with staining for DAPI (blue), astrocyte marker S100b (green), neuronal marker MAP2 (red) and mHTT marker S830 (white). Numerous S830+ nuclei were present (white arrows). NPCs=neural progenitor cells, MAP2=microtubule-associated protein 2. Scale bar 50 μm

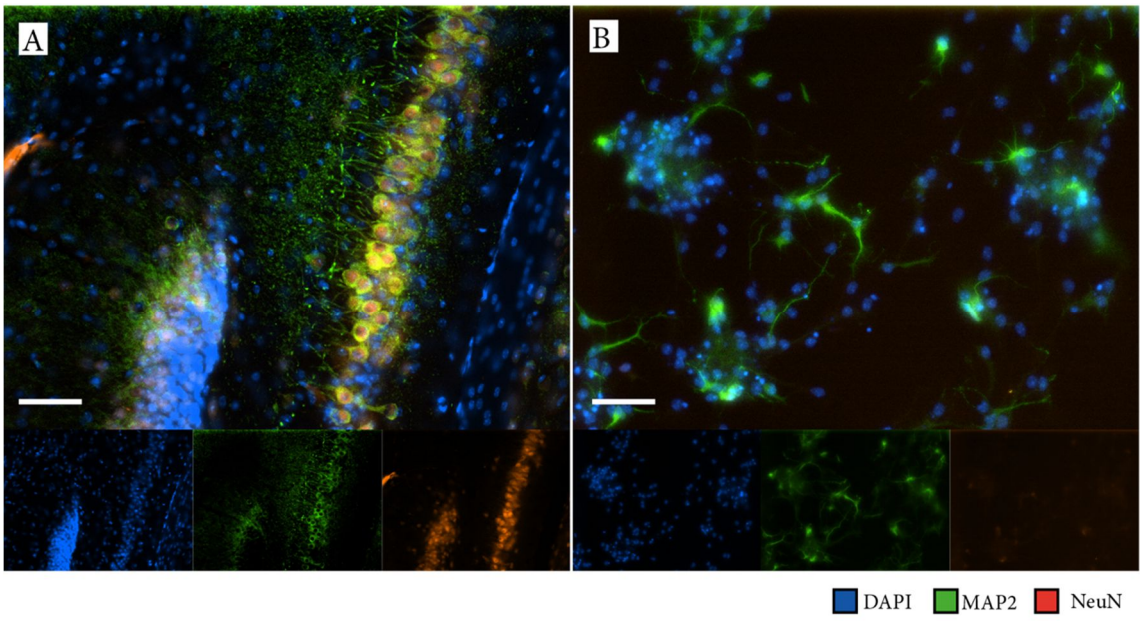

Figure 4-8. Assessment of neuronal marker expression in NPCs. (A) Adult R6/2 mouse hippocampal sections stained with the cytoplasmic neuronal marker MAP2 and the nuclear marker NeuN. (B) 21 day differentiated R6/2 NPCs expressed a staining for MAP2 neurons but no signal for NeuN was observed. NPCs=neural progenitor cells, MAP2=microtubule-associated protein 2. Scale bar 50 μm

4.10 Counting of S830+ cells in R6/2 cultures

The age of cells, as measured by the number passages a cell line has experienced, could affect the number of cells within the culture which exhibit aggregation. The levels of mHTT in these cells when mitotic may increase over multiple passages although no aggregation is detectable while they remain proliferative. As the aggregation of mHTT is thought to be a concentration dependent event an increased baseline in cells when they shift to post-mitotic differentiated cells might alter the appearance and levels of aggregation in these mature cells. To study any effect of time spent in culture and passage number on the quantity of cells containing S830 inclusions, lines previously grown and banked for 15 (p15), 30 (p30) and 40 (p40) passages were used. R6/2 cells from two Dc and two Dl lines were used for each of these three passage numbered lines. Cells were removed from liquid nitrogen storage and allowed one passage to recover, before being plated in differentiation media, fixed and then stained in cohorts after 21 and 28 days. Images were captured from 15 regions of interest from each well using an established set of coordinates. Thus the user did not influence the contents of the captured images. These images were used to manually count the number of nuclei with an S830+ inclusion signal. These data are summarised in Table 4-2. S830+ nuclei were detected in R6/2 Dc and Dl cell lines differentiated from NPCs at three passage numbers. Within the Dc lines, significantly more cells per image had a nuclear S830 signal in cultures started at p40 compared with the lines with started at lower passages at both time points (Figure 4-9A). However, this finding was not reflected in the percentage of the total nuclei containing nuclear inclusions within the culture at either

Cell line	Timepoint	Passage number	Percentage cells S830+		
			Mean	Std.D	Sig.
R6/2 Dc	21 day	p15	7.3	5.2	-
		p30	6.9	4.7	
		p40	5.9	3.6	
	28 day	p15	15.9	9.6	-
		p30	18.0	13.0	
		p40	9.4	5.9	
R6/2 Dl	21 day	p15	9.9	5.6	***
		p30	22.1	9.4	**
		p40	13.8	4.4	
	28 day	p15	8.8	2.4	**
		p30	23.4	11.8	**
		p40	24.2	11.8	

Table 4-2. Summary of S830+ cell counts in R6/2 Dc and Dl lines of different passage numbers and duration of differentiation. Statistical analysis performed as one way ANOVAs with bonferroni post-hoc test: *p≤0.05, **p≤0.01, ***p≤0.001. Dc=D line from the cortex, Dl=D line from the lateral ganglionic eminence, Std.D=standard deviation, Sig=statistical significance of p-value.

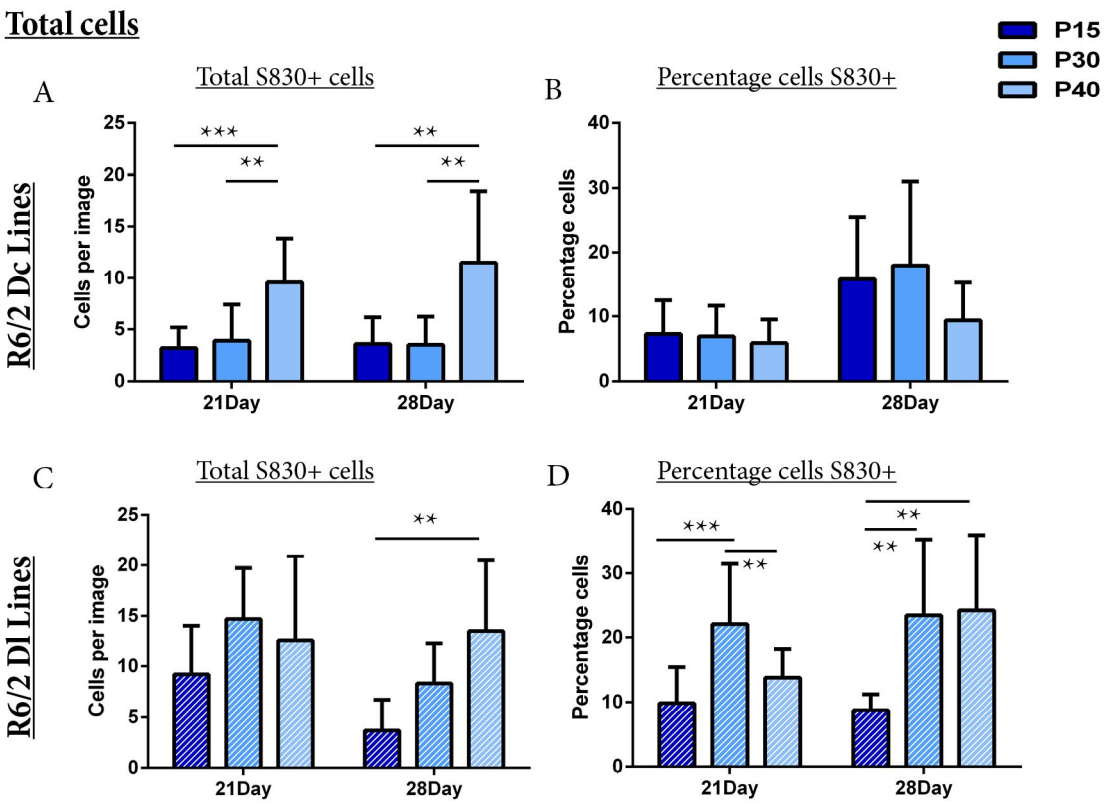

Figure 4-9. Proportion of R6/2 cells containing nuclear S830 inclusions. (A) R6/2 Dc cultures from three lines were stained for S830 and DAPI. The total number of DAPI nuclei that contained an S830+ inclusion were counted for lines differentiated for 21 and 28 days. (B) Percentage of Dc DAPI nuclei co-localised with S830. (C) The same analysis was carried out on three R6/2 Dl lines for total number of S830+ DAPI nuclei and (D) a percentage of the cultures that these consisted of. Error bars are standard deviation. Dc=D line from the cortex, Dl=D line from the lateral ganglionic eminence. Statistical analysis performed as one way ANOVAs with bonferroni post-hoc test: *p≤0.05, **p≤0.01, ***p≤0.001.

time point (Figure 4-9B). Within the Dl lines, significantly more cells per image had a nuclear S830 signal when started at p40 compared with the lines initiated with lower passage numbers after 28 days of differentiation, but not at 21 days (Figure 4-9C). When viewed as a percentage of the total nuclei within the culture those lines started at p30 had a significantly higher percentage of cells with S830+ inclusions after 21 days compared with those initiated at the other passages. This significant increase compared with lines started at p15 was retained at 28 days, however the percentage of cells with S830+ inclusions in p40 initiated lines had increased to a similar percentage as the p30 started lines at this time point and were also significantly higher than those started at p15. (Figure 4-9D).

4.11 Assessment of cell death in differentiated cultures

HD causes neurodegeneration in the human brain. Data for whether the R6/2 mouse model replicates this neurodegeneration phenotype are conflicting. A stereological analysis by Stack and colleagues in 2005 found a 25% reduction in striatal neurons in R6/2 mice compared with their WT littermates at 12 weeks of age (Stack et al., 2005). However, analysis performed in our lab found little cell death in R6/2 mice compared with their WT littermates at 16 weeks of age in either the striatum or the cortex (Rattray et al., 2013). Lack of cell death was apparent, despite a widespread inclusion phenotype and dramatic progressive reduction of brain volume and of cortical thickness measured using MRI. Many other groups have also found low levels of cell death in the brains of R6/2 mice (Davies et al., 1997, Zhang et al., 2010a). The reasons behind this finding could be technical variation but also due to variables such as CAG repeat length, which can impact how the disease manifests (Morton et al., 2009).

Apoptosis is the process of preprogramed cell death. During development, apoptosis is a common process to allow for tissue populations of the correct size and to select for those

cells that are best suited to thrive (Glucksmann, 1951, Kerr et al., 1972, Deckwerth and Johnson, 1993). Within brains affected by neurodegenerative disease or following traumatic brain injury and stroke, apoptosis can be a major process behind cell death (Dragunow et al., 1995, Mochizuki et al., 1996, Broughton et al., 2009, Smith et al., 2012). Evidence exists for HTT having an anti-apoptotic function. Overexpression of HTT in conditionally immortalised human striatal cells *in vitro* is protective against lethal stresses such as deprivation of serum or introduction of 3-nitropropionic, a mitochondria toxin (Rigamonti et al., 2000, Rigamonti et al., 2001).

As a cell becomes apoptotic it morphologically shrinks, retracting processes, and begins karyopyknosis; the condensation and fragmentation of nuclear chromatin (Kerr et al., 1972). This DNA fragmentation can be detected using 'Terminal deoxynucleotidyl transferase dUTP nick end labelling' (TUNEL) (Gavrieli et al., 1992). TUNEL staining allows cells with DNA damage to be labelled and therefore will identify those cells in apoptosis. The R6/2 NPCs with inclusions have an altered morphology and limited mature protein expression compared to those without inclusions, when analysed by ICC. This altered expression could be related to apoptotic processes such as karyopyknosis.

Mouse models with postnatal inactivation of the *Htt* gene resulted in apoptotic cells in the cortex, striatum, and hippocampus, and a reduction in axonal processes (Dragatsis et al., 2000). However, there is no evidence of apoptosis within the R6/2 mouse model brain (Turmaine et al., 2000), apart from within the olfactory zone, where TUNEL staining was slightly increased from normal cell death here (Kohl et al., 2010). Potentially this could be due to the R6/2 mouse retaining two copies of normal *Htt* with limited evidence of loss of endogenous HTT function with the presence of the mutant form. One mechanism by which HTT could help moderate apoptotic cell death is blocking of the creation and function of the apoptosome complex and activation of caspase-3 and caspase-9 (Rigamonti et al., 2000, Rigamonti et al., 2001, Zhang et al., 2006).

To study the extent of cell death in differentiating cultures, R6/2 and WT Dc cells were grown in differentiation media and fixed and stained in 7-day cohorts up to 28 days. The cells were then stained with a commercial '*In Situ* Cell Death Detection Kit, Fluorescein'. Proliferative cultures, which have minimal cell death, were used as negative controls. As positive controls, hydrogen peroxide was applied to induce DNA damage in all cells in the culture which could be detected with the green fluorescent TUNEL stain (Figure 4-10A). The proliferative negative control cells that were not treated with hydrogen peroxide displayed little if any green TUNEL staining (Figure 4-10B). 28-day-old R6/2 cultures that contained mHTT aggregation showed some TUNEL+ cell death but TUNEL+ cells did not correlate with the cells containing S830+ inclusions (short white arrows, Figure 4-10C). The TUNEL staining occurred mainly in cells present in clumps with only a few outside the clumps being labelled. Due to the nature of the culture, there is cellular debris that gathered between cells. This debris often labelled as TUNEL+ and so maybe cells which have died during the culture process. These data suggest the R6/2 cells with mHTT inclusions are not apoptotic. WT cells had similar levels of TUNEL staining, suggesting the cell death was caused by the *in vitro* environment rather than an HD-related phenotype. Some areas of intense S830 signal were detected outside and away from nuclei (long white arrows, Figure 4-10C). The size and location of these objects is unlikely to be from cytoplasmic inclusions and is more likely to be from autofluorescent debris.

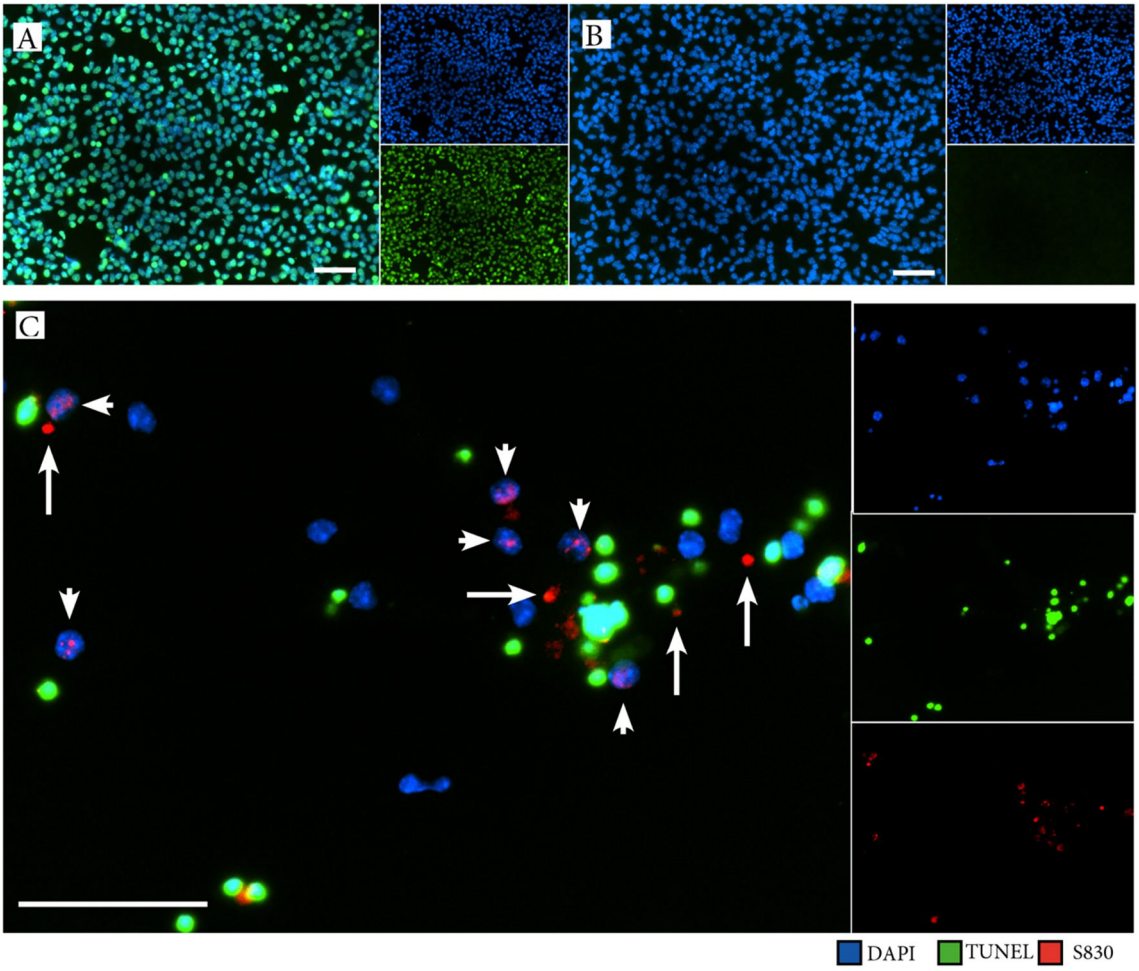

Figure 4-10. Assessment of the levels of cell death in differentiated cultures. TUNEL staining was used to assess whether mHTT cells were apoptotic and the level of cell death in the culture (A) Proliferative R6/2 cells were treated with hydrogen peroxide to damage DNA as a positive control. (B) Proliferative R6/2 cells without treatment. (C) S830+ mHTT inclusions (red) were apparent in cells without TUNEL staining (green, short white arrows) in R6/2 cells after 28 days of differentiation. Some S830+ staining apparent outside of the nucleus (long white arrows), which is most likely to be autofluorescent debris. TUNEL=terminal deoxynucleotidyl transferase dUTP nick end labelling, mHTT=mutant huntingtin. Scale bars 50 μm.

To study the extent of cell death in cultures and how this is related to cells with S830+ inclusions, lines previously grown and banked at p15, p30 and p40 passages were used. R6/2 cells from two Dc and two Dl lines were used for each of these three passage numbered lines. Cells were removed from liquid nitrogen storage and passaged once to recover, before being plated in differentiation media, fixed, and then stained in cohorts after 21 and 28 days. These cells were stained with a commercial '*In Situ* Cell Death Detection Kit, Fluorescein' kit for TUNEL alongside S830.

Images were captured from 15 regions of interest from each well using an established set of co-ordinates. Thus, the user did not influence the contents of the captured images. These images were used to manually count the number of nuclei with an S830+ inclusion signal, while excluding any cells with TUNEL staining. These data are summarised in Table 4-3

Cell line	Timepoint	Passage number	Percentage cells S830+		
			Mean	Std.D	Sig.
R6/2 Dc	21 day	p15	4.7	2.8	-
		p30	4.4	2.1	
		p40	3.9	1.4	
	28 day	p15	10.1	7.9	-
		p30	14.7	9.2	
		p40	4.6	2.2	
R6/2 Dl	21 day	p15	3.7	1.6	-
		p30	8.1	5.3	
		p40	6.6	3.1	
	28 day	p15	9.9	2.0	**
		p30	24.1	6.5	
		p40	11.4	6.2	

Table 4-3. Summary of S830+ cell counts in R6/2 Dc and Dl lines of different passage numbers and duration of differentiation, after TUNEL+ cells were excluded. Statistical analysis performed as one way ANOVAs with bonferroni post-hoc test: *p≤0.05, **p≤0.01, ***p≤0.001. Dc=D line from the cortex, Dl=D line from the lateral ganglionic eminence, Std.D=standard deviation, Sig=statistical significance of p-value, TUNEL= terminal deoxynucleotidyl transferase dUTP nick end labelling.

S830+ nuclei were detected in R6/2 Dc and Dl cell lines at all passage numbers despite the exclusion of cells displaying TUNEL staining. Within the Dc lines, significantly more TUNEL negative cells per image with a nuclear S830 signal were identified at the 21 day time point in the lines started at p40 compared with the cultures initiated at lower passages (Figure 4-11A). By 28 days, the number of TUNEL negative cells per image with a nuclear S830 signal in the lines started at p40 was only significantly higher than those started at p15 and not in those initiated p30. Once again this finding was not reflected as a percentage of the total TUNEL negative nuclei within the cultures at either time point, (Figure 4-11B).

Within the Dl lines, significantly more TUNEL negative cells per image with a nuclear S830 signal were identified in the lines started at p30 compared with those started at p15 at both time points (Figure 4-11C). After 28 days the percentage of the total TUNEL negative nuclei within the culture which contained S830+ inclusions was significantly higher in the p30 initiated lines compared with those started at p15, but not in those initiated at p40. (Figure 4-11D). These data show that the S830+ population of cells are not selectively dying within these cultures.

These data suggest that there is a variation in the aggregation profile of R6/2 lines with different passage numbers. The percentage of cells with inclusions increases at later passages but this effect is not consistent between lines derived from different progenitor pools. Regardless of the passage number or area the lines were derived from an S830+ inclusion phenotype was present in all R6/2 lines analysed.

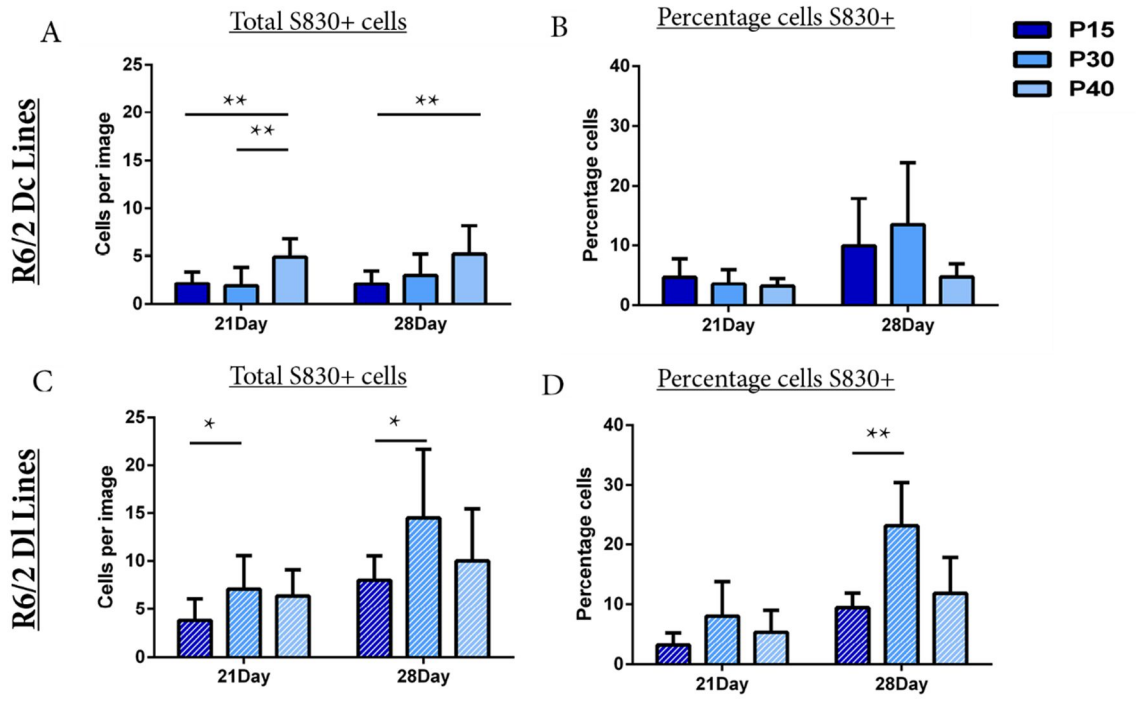

Figure 4-11. Proportion of TUNEL negative cells containing a nuclear S830+ inclusion. Manual cell counts were carried out on cells which were negative for TUNEL. (A) R6/2 Dc cultures from three lines where differentiation was initiated at increasing passage numbers were stained for S830 and DAPI while a TUNEL stain was applied to exclude nuclei showing signs of cell death. The total number of TUNEL negative DAPI nuclei that contained an S830+ inclusion were counted for lines differentiated for 21 and 28 days. (B) Percentage of Dc TUNEL negative DAPI nuclei co-localised with S830. (C) The same analysis was carried out on three R6/2 Dl lines for total number of TUNEL negative S830+ DAPI nuclei and (D) a percentage of the cultures that these consisted of. Error bars are standard deviation. Dc=D line from the cortex, Dl=D line from the lateral ganglionic eminence, TUNEL=terminal deoxynucleotidyl transferase dUTP nick end labelling, mHTT=mutant huntingtin. Statistical analysis performed as one way ANOVAs with bonferroni post hoc test: *p≤0.05, **p≤0.01, ***p≤0.001.

4.12 High throughput automated fluorescence analysis – Operetta

Quantification of cell parameters by eye is time consuming and can be biased even when the user is blinded to experimental groups. The Operetta® High-Content Imaging System (PerkinElmer, here-on just called Operetta) is specifically designed to analyse cultures in multi-welled plates using four channels of fluorescence. The automated stage and pre-programmed knowledge of plate design gives control over which wells are imaged and where in the well to focus. The captured images can be analysed using the built-in software, which has an intuitive sequence of algorithms that are pre-programmed to identity cells with specific stains as well as morphological aspects to the culture such as size and shape.

To test the effectiveness of the Operetta to analyse NPC cultures, three R6/2 and three WT Dl lines were grown in 96-well optical plates. These cells were differentiated up to day 28 and fixed for ICC and analysed using the Operetta. Using a x40 lens, the system was instructed to take 15 images per well in 4 wells per cell line (Figure 4-12A). The DAPI signal from these images was then used to identify individual cell nuclei (Figure 4-12B) and to count the number of nuclei in each image. The size and shape of each nucleus was also recorded. The level of S830 staining was then analysed in the area covered by the DAPI nuclei to assess whether the nucleus contained mHTT nuclear inclusions (Figure 4-12C). The nuclei were labelled as S830+ or S830-, as shown in the green and red examples (Figure 4-12C). The S830 signal within the S830+ nuclei were then further analysed. Individual inclusions, with a higher S830 signal than the background for the nuclei, were highlighted as individual intensities (Figure 4-12D). The number of these inclusions per nuclei was then calculated. These analyses were combined in an automated sequence of algorithms and applied to each image as it was taken, or retrospectively if required.

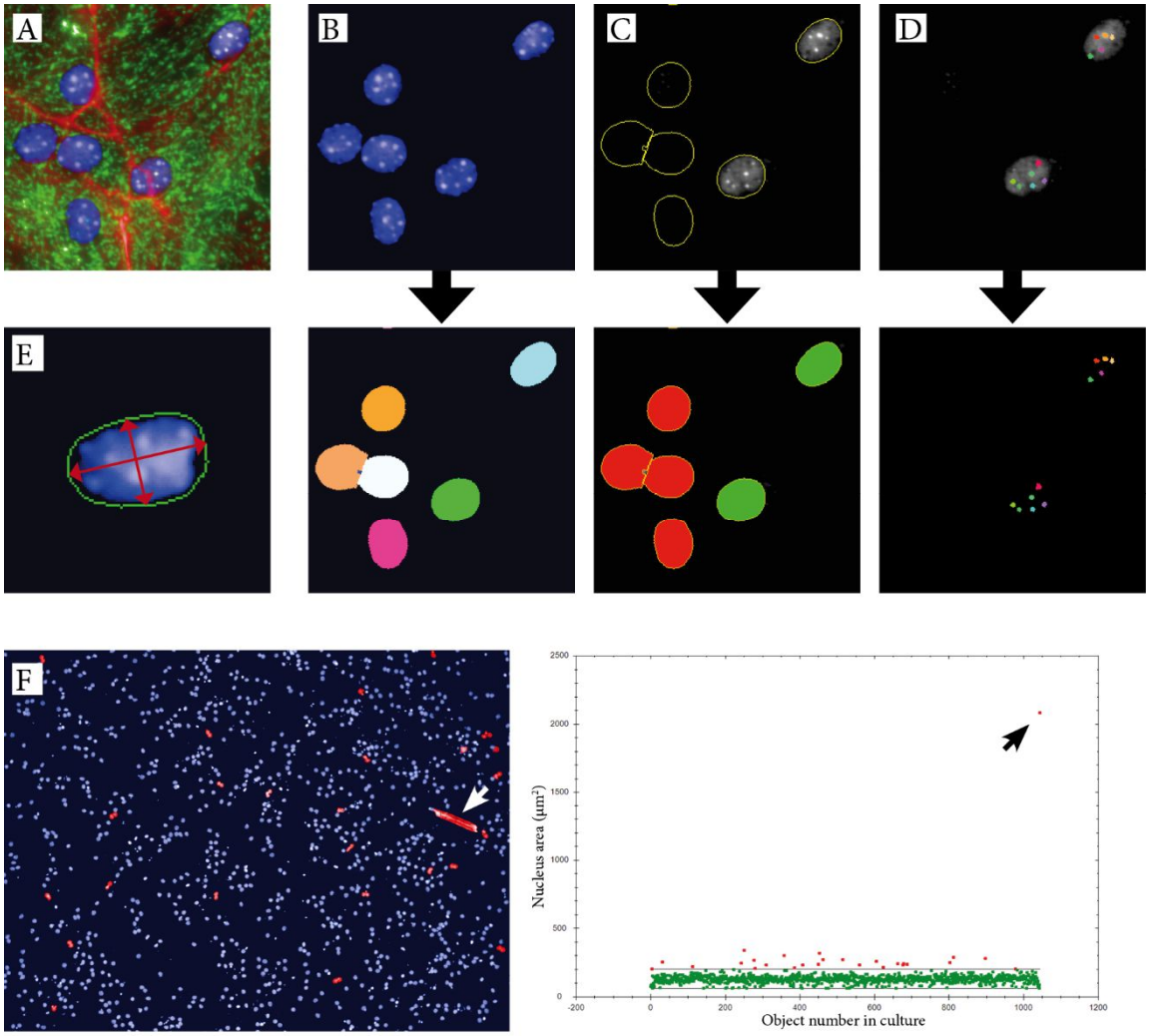

Figure 4-12. High throughput automated fluorescence analysis: Operetta. Automated image acquisition and analysis using the Operetta. (A) Images were obtained in 4 fluorescent channels from R6/2 and WT Dl lines grown in 96-well optical plates. (B) DAPI+ nuclei were identified using built-in locator modules, which allowed each individual cell nucleus to be identified and counted. (C) Within the boundaries of each nucleus, the level of S830 signal was assessed and a threshold was set to allow each nucleus to be labelled as S830+ (green) or S830- (red). (D) Within the S830 population, brighter intensities of S830 signal were identified and labelled with random colours for clarity. The number of these intense signals was counted per nucleus. (E) Examples of width and length measurements of a nuclei. (F) The software analysis was set to ignore oversized objects, above a set threshold, to avoid non-cellular objects and un-segmented nuclei. These are labelled in red. Extreme example of 2000 μm^2 object excluded as seen in the image and resulting graph (arrow)

The automated nature of any system needs optimisation and the Operetta was no different. The maximum area of each nucleus was manually set to only record nuclei less than 200 μm2 (Figure 4-12F). This setting safeguarded against larger pieces of debris being excluded, such as the 2000-μm^2 object detected in Figure 4-12F (arrows), ensuring that the system did not identify this as a single nucleus. The minimum size of nuclei was set to 60 μm^2.

Most DAPI+ nuclei will have some background level of signal in the other fluorescent channels by the nature of how fluorophores fluoresce. As such, a cut-off criteria were applied to the S830 signal colocalised with a DAPI+ nucleus to detect true S830 immunofluorescence. A level of 175 was set on the arbitrary scale within the relevant algorithm related to mean signal intensity to identify the S830+ cells.

Nuclei with inclusions can be selected by the mean intensity (Figure 4-13A). As well as total S830 signal (Figure 4-13B). These two measures did not differ in their ability to select S830+ nuclei to a huge degree and indeed the cells they identified correlated strongly (Figure 4-13C). However, the mean intensity was slightly more reliable at selecting those nuclei that were positively counted by eye, and therefore was the measure chosen for future analysis. This 175 level was chosen based on capturing the population with a signal above that of the S830- noise (red points, Figure 4-13D) and used to segregate the subpopulation with S830+ inclusions from those without. When the threshold was applied to the WT cells almost the entire population of DAPI+ nuclei fell below the S830+ threshold. The few WT cells that were labelled as S830+ by these criteria did so because of pieces of debris that bound the antibody or were autofluorescent (Figure 4-13E).

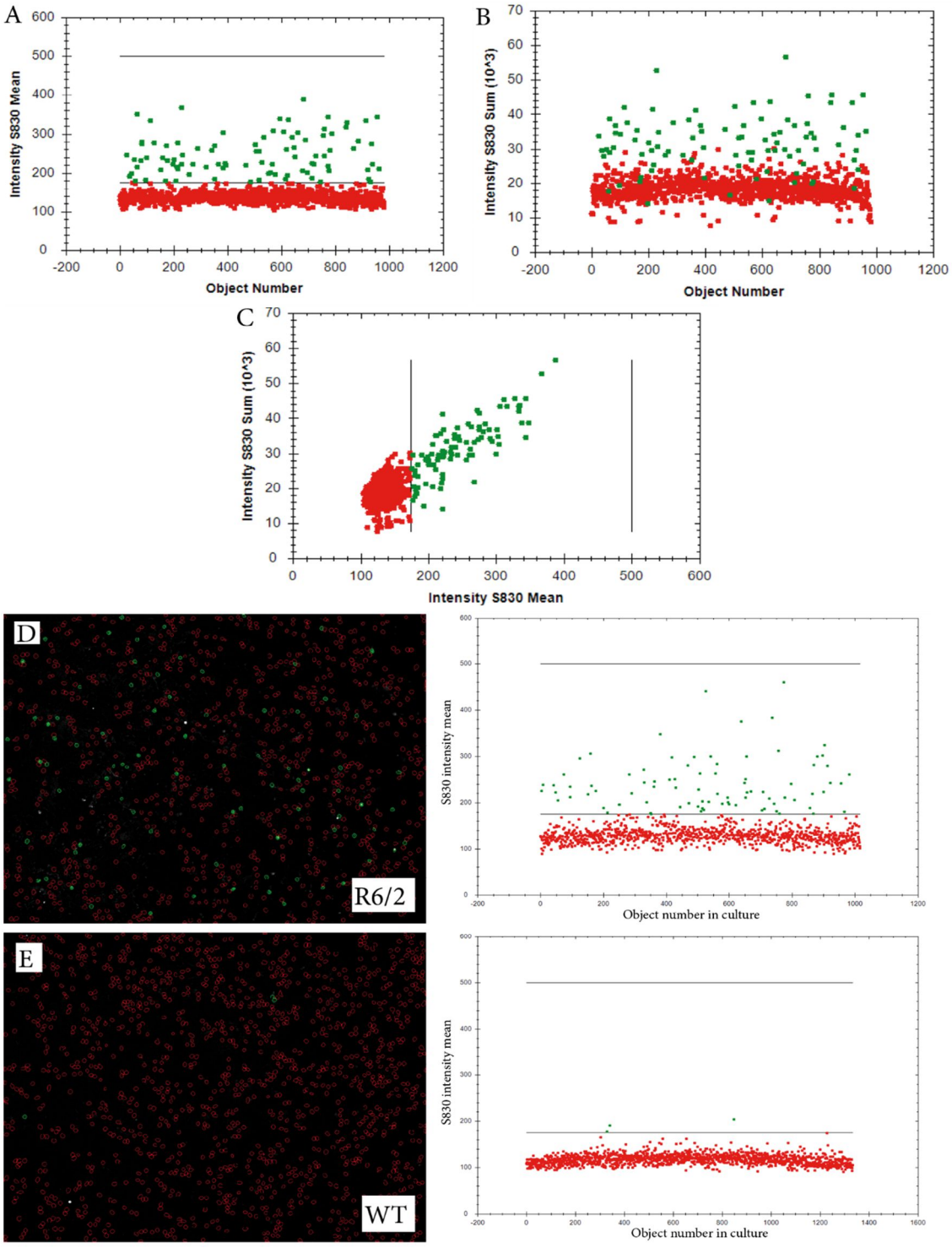

Figure 4-13. Establishing Operetta analysis thresholds. Automated image acquisition and analysis using Operetta® High Content Imaging System. (A) The mean intensity of S830 signal used as the selection criteria for S830+ nuclei. A value of 175 was set on the arbitrary scale. (B) The total S830 signal (sum) could be used as a selection but was less reliable at identifying the population that would be counted by eye. (C) The mean and sum intensity of S830 signal correlated. (D) The mean S830 signal within each nucleus was used to separate the R6/2 population into those S830+ (green) and S830- (red). (E) When the threshold was applied the majority of cells in WT cultures fall under the cut off and are labelled red. Some outliers were still registered as S830+ but were removed from later analysis. WT=wildtype.

4.13 High content analysis of WT and R6/2 cells using the Operetta

To quantify differences in the morphology and size of nuclei between WT and R6/2 lines, three WT and three R6/2 Dl cell lines, which had previously been passaged at least 15 times prior to differentiation, were differentiated in 96-well plates and stained for DAPI. Cohorts of cells were fixed every 7 days from day 14 of differentiation. Four wells were analysed for each line and 15 individual images were captured at a x40 magnification at the same co-ordinates for each well. Each well was considered a technical replicate and each line considered a biological replicate. Within these replicates any outliers were identified using Grubbs test and excluded These data were pooled for the three biological replicates for each genotype. Statistical analysis was performed using SPSS (IBM) with Student t-test set to 95% confidence for genotype.

Within each genotype, the total number of cells per replicate did not significantly change between the various post differentiation time points (Figure 4-14A). At 21 days, significantly more cells were present in the WT cultures compared with R6/2 cultures, a trend which continued after 28 days but that was not statistically significant (Figure 4-14A). The mean area of each nuclei was recorded. The R6/2 nuclei were significantly larger than WT nuclei at all time points (Figure 4-14B). This increased area remained constant between the time points within each genotype.

The Operetta can measure the roundness of each nucleus. This reading was given on a scale between 0 and 1, with 1 being perfectly round. No difference in the roundness of the nuclei was observed between the genotypes or at any of the time points analysed (Figure 4-14C). The width and length of each nucleus was also recorded. These measurements were taken by considering the longest part of the nuclei from side to side through the centre point as the length, and the perpendicular measurement to this as the width. For both length and width, a significant difference was observed between the WT

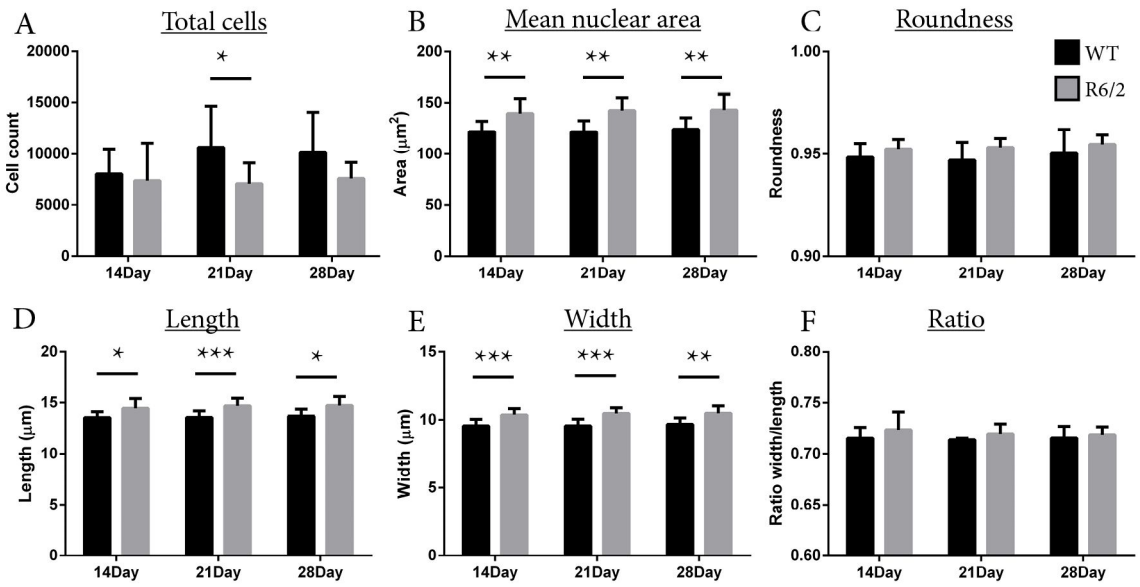

Figure 4-14. High content analysis of WT and R6/2 cells using the Operetta. The automated sequence of algorithms of the Operetta was applied to differentiated cultures at 3 time points up to day 28. (A) Total cells were counted based on DAPI nuclear staining. A selection criterion that excluded nuclei <60 μm^2 and >200 μm^2 was applied. Nuclear morphology was analyses for (B) mean size, (C) roundness, (D) length, (E) width, and (F) length:width. Error bars are standard deviation. Statistical analysis performed as Students t-test *p≤0.05, **p≤0.01, ***p≤0.001.

and R6/2 nuclei at each time point. (Figure 4-14D,E) with R6/2 nuclei being longer and wider. A product of these data was a ratio of the length against the width. This ratio measure is different to the roundness measure generated by the Operetta and differences in this would signify a change in the overall shape of the nucleus. No significant difference was observed in the ratio of length:width between R6/2 and WT cell lines at any time points. A trend for a higher length:width ratio was observed at 14 days (p=0.159), however this trend was no longer present by day 21 and 28 (Figure 4-14F). These data suggest that the nuclei driving the trend for the longer lengths are potentially the same nuclei driving the trend for a wider width.

Timepoint	Genotype	Total Cells			Nuclear area			Roundness			Length			Width			Ratio		
		Mean	Std.Dev	Sig.	Mean	Std.Dev	Sig.	Mean	Std.Dev	Sig.	Mean	Std.Dev	Sig.	Mean	Std.Dev	Sig.	Mean	Std.Dev	Sig.
14 Day	WT	8044	2558	-	121.36	9.42	**	0.948	0.007	-	13.56	0.52	*	9.57	0.44	***	0.715	0.012	-
	R6/2	7381	3324		139.16	13.59		0.952	0.005		14.46	0.85		10.36	0.42		0.724	0.017	
21 Day	WT	10612	4330	*	121.20	11.23	**	0.947	0.009	-	13.58	0.64	***	9.57	0.51	***	0.714	0.010	-
	R6/2	7071	2124		142.57	11.75		0.953	0.004		14.70	0.72		10.47	0.38		0.719	0.013	
28 Day	WT	10134	3947	-	123.83	11.42	**	0.950	0.011	-	13.70	0.69	*	9.69	0.49	**	0.715	0.015	-
	R6/2	7587	1841		143.05	14.14		0.955	0.005		14.72	0.85		10.48	0.49		0.718	0.011	

Table 4-4. Summary of data from high content analysis of WT and R6/2 cells using the Operetta. Statistical analysis performed as Students t-test: *p≤0.05, **p≤0.01, ***p≤0.001. Std.Dev=standard deviation, Sig=statistical significance of p-value.

The mean intensity of the S830 signal was used to separate two populations within each genotype, in which those above the threshold were considered to be S830+. The number of nuclei that reached this S830+ threshold was minimal for the WT cell lines as expected (Figure 4-15A).

In the R6/2 cell cultures, the number of S830+ cells increased over the three time points (Figure 4-15A). This finding was reflected in the percentage of cells reaching the threshold (Figure 4-15B). This analysis of the number of S830+ cells did not necessarily include all nuclei with inclusions but instead was a reproducible system of identifying those cells that had the highest levels of S830 immunoreactivity. This approach accounts for the fact that manual cell counts recorded a larger percentage of cells with an S830 signal compared with the Operetta: cells with weaker S830+ signals were included in manual counts as the user can more robustly identify true staining and, by eye, the issue of debris and clumping was not so limiting.

Aggregation within the R6/2 nuclei appeared as inclusions that stained with bright intensities (Figure 4-12D). These intensities were recorded as ‘S830+ spots’ These spots could be segmented within the nuclei and the number of individual spots per nuclei was counted. The mean number of spots per nuclei increased with the length of time in culture in all three R6/2 lines (Figure 4-15C).

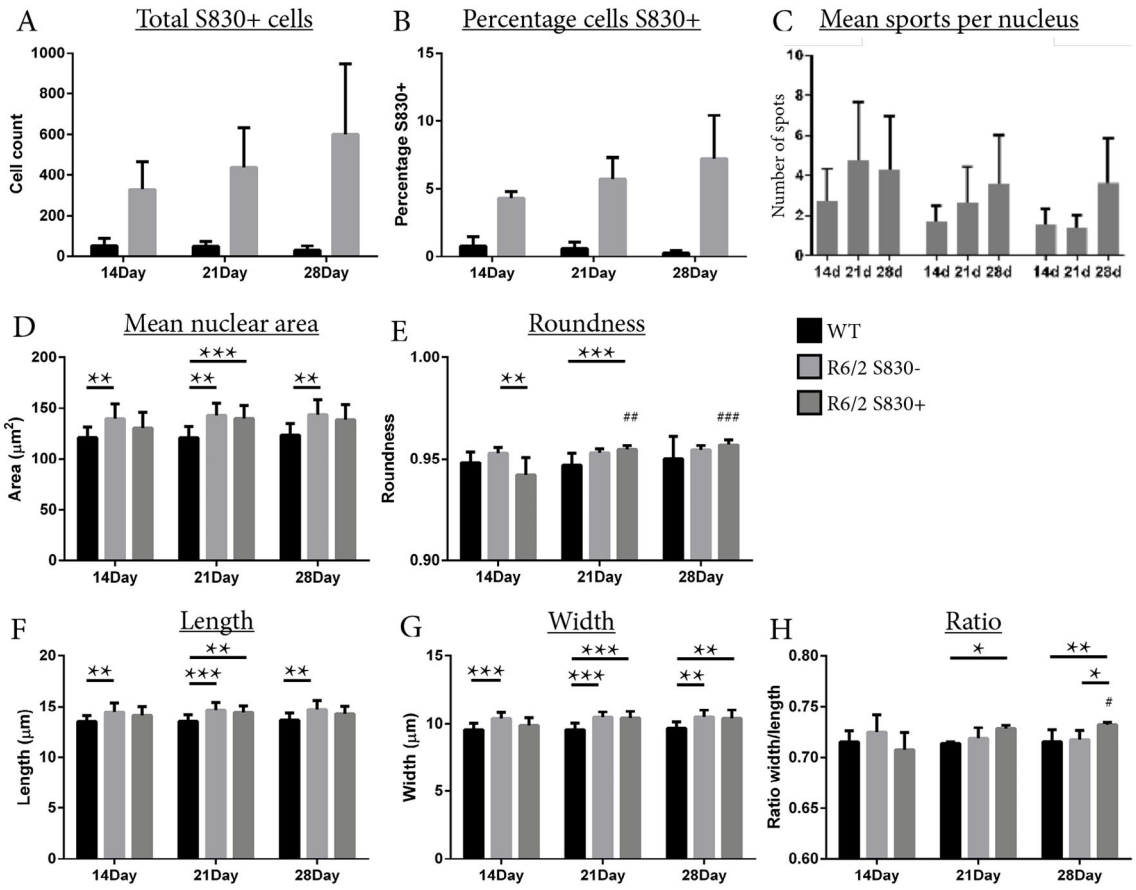

Figure 4-15. High content analysis of S830 signal in WT and R6/2 cells using the Operetta. The automated sequence of algorithms of the Operetta were applied to differentiated cultures at 3 time points up to day 28. (A) The number of nuclei with a S830 mean intensity above the threshold were counted and (B) displayed as a percentage of the total cells analysed. (C) The number of individual intensity spots was calculated and displayed at each time point for the three R6/2 lines. The population of S830- and S830+ R6/2 nuclei were compared with WT cells for (D) mean size, (E) roundness, (F) length, (G) width, and (H) length:width. Error bars are standard deviation. Statistical analysis performed as one-way ANOVA with bonferroni post-hoc test. Difference between genotype/subpopulation: *p≤0.05, **p≤0.01, ***p≤0.001. Difference within genotype/subpopulation between time points: #p≤0.05, ##p≤0.01, ###p≤0.001.

Timepoint	Genotype	Total S830+ Cells			Percentage S830+ Cells			S830+ Spots					
		Mean	Std.D	Sig.	Mean	Std.D	Sig.	Line 1		Line 2		Line 3	
								Mean	Std.D	Mean	Std.D	Mean	Std.D
14 Day	WT	54	50	***	0.78	0.76	***	-	-	-	-	-	-
	R6/2	329	218		4.28	2.68		2.7	1.6	1.8	0.7	1.7	0.6
21 Day	WT	51	45	***	0.60	0.62	***	-	-	-	-	-	-
	R6/2	439	215		5.70	1.91		4.8	2.8	2.6	1.7	1.4	0.6
28 Day	WT	30	29	***	0.29	0.25	***	-	-	-	-	-	-
	R6/2	600	333		7.22	3.35		4.3	2.6	3.6	2.4	3.6	2.2

Table 4-5. Summary of data from the high content analysis of nuclei with S830+ signal in WT and R6/2 cells using the Operetta. Statistical analysis performed as Students t-test: *p≤0.05, **p≤0.01, ***p≤0.001. Std.D=standard deviation, Sig=statistical significance of p-value.

To determine whether differences in nuclear morphology exist between S830+ and S830- R6/2 cells, the R6/2 cells were separated into S830+ and S830- subpopulations and the same analysis was run as above. WT cells were also re-analysed with any cells having reached a threshold for the S830 signal excluded. Statistical analysis was performed using SPSS (IBM) for one-way ANOVA with bonferroni post-hoc test.

Analysis of the mean nuclear area showed that S830- R6/2 cells had significantly larger nuclei compared with WT at all three time points (Figure 4-15D). This observation reflected the data from the R6/2 cells as a whole. The nuclei in the S830+ R6/2 cell population were only significantly larger than the WT nuclei at the 21-day time point although there remained a trend for larger nuclei at the other time points (p=0.080 at 14 days and 0.079 at 28 days). No difference in the size of nuclei was observed between the S830+ and S830- R6/2 cell subpopulations (Figure 4-15D).

Analysis of the roundness of the nuclei on the Operetta scale revealed significantly decreased roundness between the S830+ and S830- R6/2 cell subpopulations at 14 days (Figure 4-15E). This difference in the subpopulation was not seen at the later time points. The only significant change in roundness observed in the WT population was in the S830+ population being rounder at 21 days, although there was also a trend for rounder nuclei in the S830- population (p=0.067, Figure 4-15E). Within the S830+ R6/2

population, the nuclei became significantly more round over time from 14 days to both the later time points (Figure 4-15E). Analysis of nuclear length and width revealed no significant difference between the S830+ and S830- R6/2 cell subpopulations (Figure 4-15F,G). The nuclei in the S830- R6/2 cell population were significantly longer and wider than the WT nuclei at all time points as was seen with the R6/2 combined population (Figure 4-15F,G). The nuclei in the S830+ population of cells were only significantly longer at day 21 (Figure 4-15F) and wider from day 21 onwards (Figure 4-15G).

The ratio of the length to width showed a similar result to the roundness in that the length:width ratio of S830+ nuclei increased over time and after 21 days the ratio was significantly increased compared with the WT lines (Figure 4-15H). At 28 days this increase remained and was also significant between the S830- and S830+ subpopulations (Figure 4-15H).

Timepoint	Genotype	Nuclear area			Roundness			Length			Width			Ratio		
		Mean	Std.D	Sig.	Mean	Std.D	Sig.	Mean	Std.D	Sig.	Mean	Std.D	Sig.	Mean	Std.D	Sig.
14 Day	WT	121.36	9.42	**	0.948	0.007		13.56	0.52	**	9.57	0.44	***	0.715	0.012	
	R6/2 S830-	139.54	13.63		0.953	0.004	***	14.47	0.85		10.38	0.42		0.725	0.017	
	R6/2 S830+	130.65	14.68		0.942	0.012		14.15	0.88		9.88	0.57		0.707	0.023	
21 Day	WT	121.20	11.23	**	0.947	0.009		13.58	0.64	***	9.57	0.51	***	0.714	0.010	
	R6/2 S830-	142.77	11.69	***	0.953	0.004	***	14.72	0.72	**	10.48	0.38	***	0.719	0.013	*
	R6/2 S830+	139.67	12.23		0.955	0.004	§§	14.42	0.66		10.42	0.47		0.728	0.009	
28 Day	WT	123.83	11.42	**	0.950	0.011		13.70	0.69	**	9.69	0.49	**	0.715	0.015	
	R6/2 S830-	143.40	13.96		0.955	0.005		14.75	0.84		10.49	0.48	**	0.717	0.012	*
	R6/2 S830+	138.51	15.46		0.957	0.005	§§§	14.29	0.84		10.40	0.61		0.732	0.009	§ **

Table 4-6. Summary of data from the Operetta with R6/2 lines split based on S830 signal. Statistical analysis performed as one-way ANOVA with bonferroni post-hoc test. Difference between genotype/subpopulation: *p≤0.05, **p≤0.01, ***p≤0.001. Difference within genotype/subpopulation between time points: §p≤0.05, §§p≤0.01, §§§p≤0.001.

The Operetta is a high-throughput system that provides non-biased data based on replicable sequences of algorithms. The data reveal significant differences between WT and R6/2 nuclei, most notably in size. Further analysis of the R6/2 cultures based on the presence of inclusions revealed this difference is predominately driven by the S830- population.

4.14 Super resolution microscopy and R6/2 mouse brain aggregation

The resolution of light microscopy is limited due to the physics of the diffraction limits of light (Neice, 2010). As such it had traditionally been impossible to reach an image resolution of beyond around 250 nm (Gustafsson, 1999). This resolution limit makes it difficult to precisely view ICC staining in enough detail to visualise anything smaller than the largest cellular inclusion. Novel systems have now been developed to capture images beyond the diffraction limit with higher resolutions (Gustafsson, 2000, Galbraith and Galbraith, 2011). These super-resolution systems allow for greatly increased detail to be obtained using ICC. One such system is structured illumination microscopy (SIM). SIM applies the theory of structured light, a process of using a known pattern or grid, which is projected over and slightly moved between multiple images (Gustafsson, 2000, Galbraith and Galbraith, 2011). This produces the Moiré pattern, a phenomenon where the light at the fringes of each pattern is slightly deformed (Gustafsson, 1999, Gustafsson, 2000). The computational reconstruction of the multiple images, using this deformation to its advantage, allows for the superior resolution achieved in the final composite image.

To test the resolution of the SIM, end-stage R6/2 mouse tissue was processed for IHC onto glass slides. 50-µm sections were stained for the autophagy related protein SQSTM1 (P62), ubiquitin and S830. These sections were then visualised using a Nikon N-SIM microscope with x100 lens. Using this system, a resolution of 31.19 nm/pixel was achieved. Multiple images were obtained in the z-plane to allow a 3-dimensional

reconstruction. In the end-stage R6/2 cortex, large inclusions were found inside the nuclei of a large proportion of neurons. These inclusions were present as large single bodies, with co-localised staining for S830, P62 and ubiquitin (Figure 4-16A). Using an orthogonal view, the location of the large inclusion was clearly contained within the nuclear envelope of the cell (Figure 4-16B,C). The Nikon 'Elements' microscope's imaging software can be used to create 3-dimensional projections of the reconstructed images while retaining the resolution. The structure of the large inclusion can be made out to be a hollow 'doughnut' shape (Figure 4-16D). These images are an example of the potential of the SIM system to visualise structures beyond standard traditional fluorescence microscopy. Not all inclusions in the R6/2 mouse brain have this doughnut shape.

4.15 Super resolution microscopy and aggregation in R6/2 neural progenitor cells

The resolution afforded by SIM allows for smaller inclusions to be visualised, which would have been indistinguishable using conventional microscopy. To use SIM to analyse NPCs, R6/2 Dl cells were grown and differentiated in specialised glass-bottomed plates with an optical refractive index suitable for SIM. Cohorts of WT and R6/2 Dl cells were differentiated and fixed at 7-day time points up to day 21. The cells were processed for ICC using antibodies against P62 (green), S830 (red) and ubiquitin (far red, pink) (Figure 4-17A). Strong co-localised staining for all three antibodies was observed in large inclusions in the nuclei of some R6/2 cells, similar to those seen in the R6/2 mouse brain at end-stage (Figure 4-16). In the mouse brain, many cells had just one large inclusion while in the NPCs multiple inclusions were apparent. Rotation of the projected image allowed these inclusions to be visualised and showed that the R6/2 cells that contained

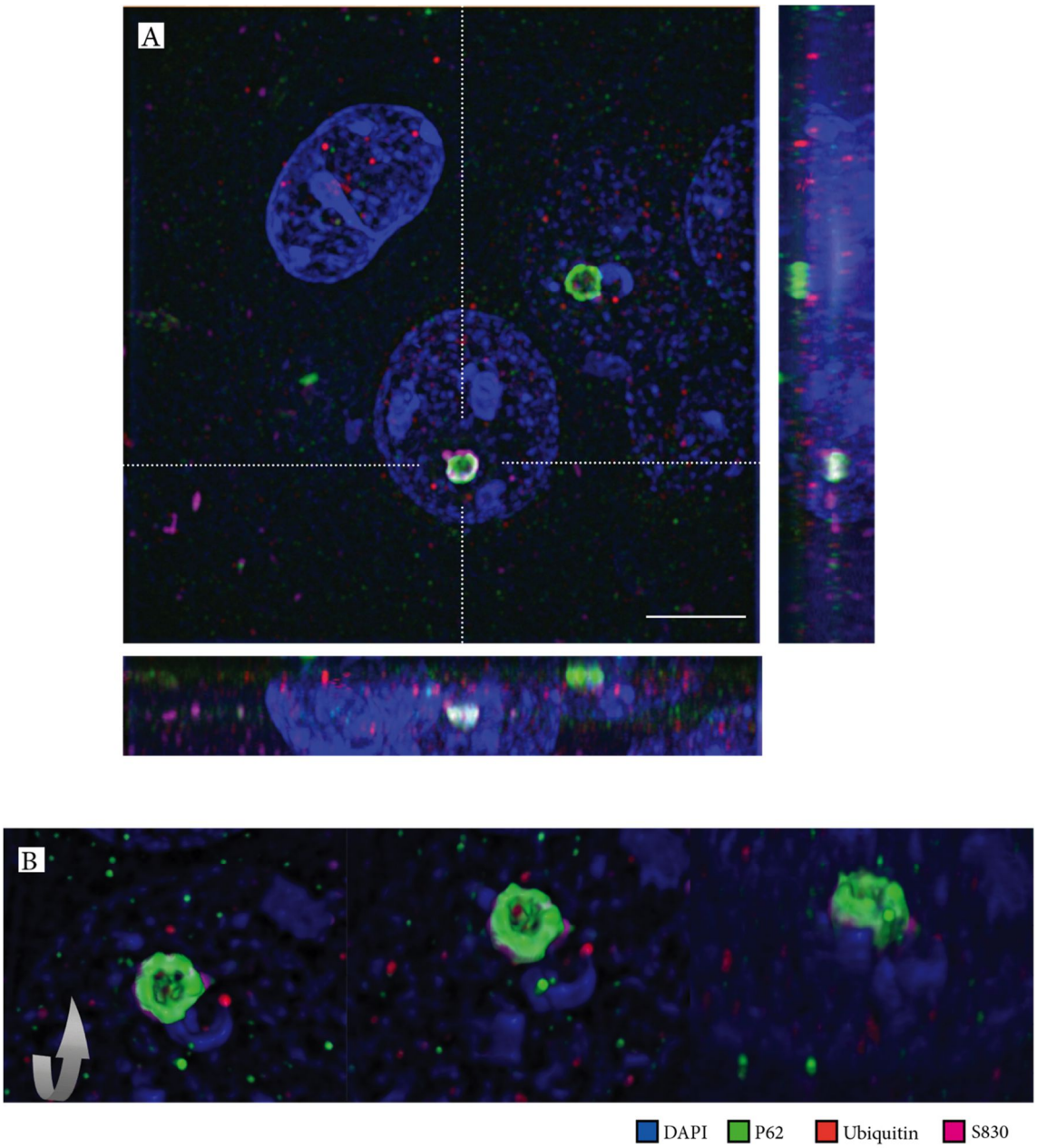

Figure 4-16. Super resolution microscopy and R6/2 mouse brain aggregation. The SIM microscope was used to visualise aggregation in cells of the adult R6/2 mouse cortex. Multiple images were obtained in the Z plane to provide a 3-dimensional image of the cells. (A) ICC staining for P62 (green), ubiquitin (red) and S830 (far red, pink) was used to identify inclusions within the DAPI stained nuclei. The orthogonal view allows the location of a large inclusion to be identified within the nuclear envelope (B) With the multiple z plane images and the higher resolution a 3-dimensional computational representation of the inclusion could be projected. Rotation of the image revealed detail to the stained inclusion not normally possible. SIM=structured illumination microscopy, ICC=immunocytochemistry. Scale bar 5 µm.

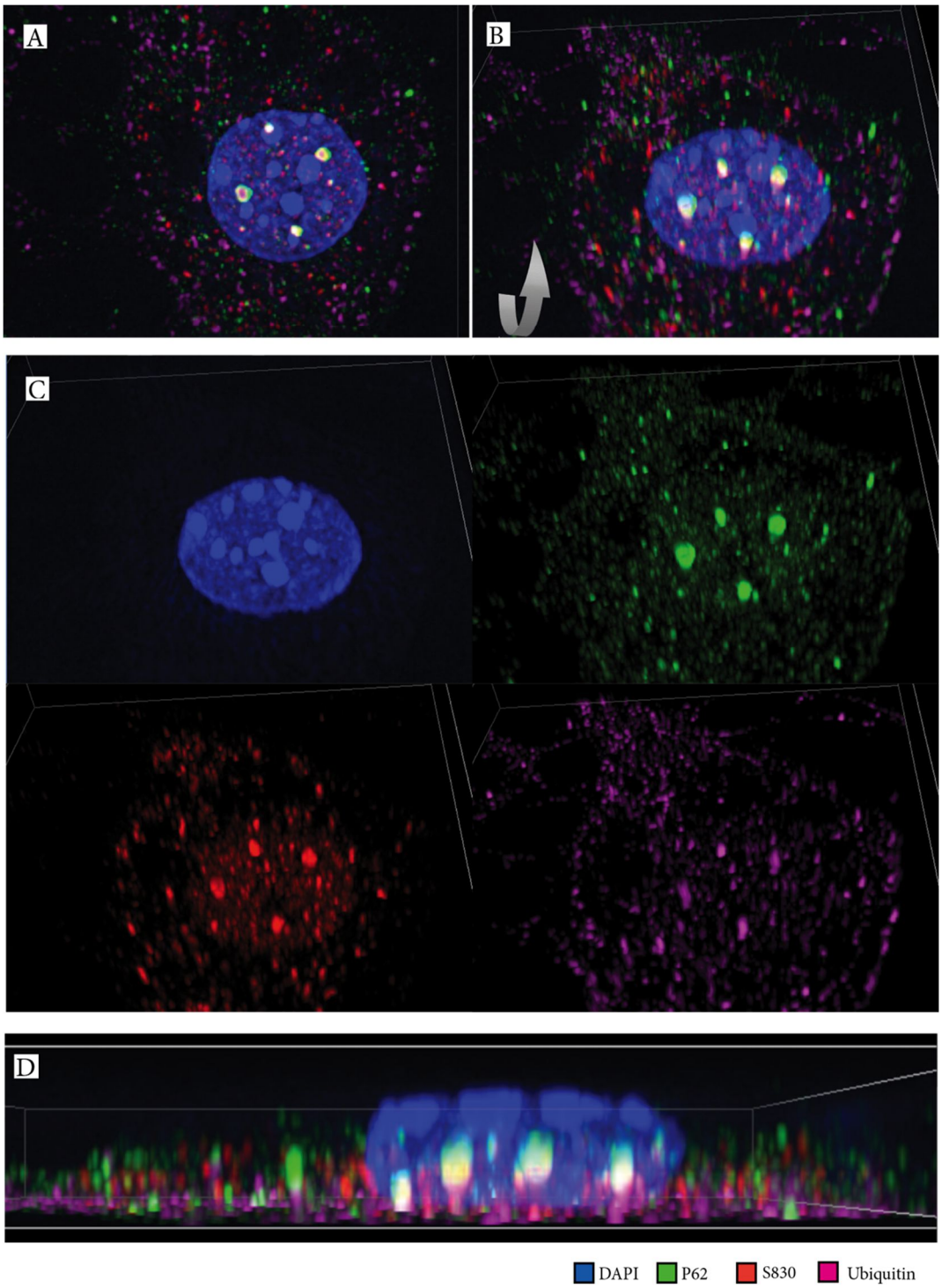

Figure 4-17. Super resolution microscopy and aggregation in R6/2 NPCs. R6/2 cell after 21 days in differentiation media with inclusions viewed using SIM. (A) A single R6/2 DAPI nucleus (blue) stained using ICC for antibodies P62 (green), S830 (red) and ubiquitin (far red, pink). (B) Rotation of the projected image helps reveal the location of the inclusions inside the nuclear envelope and the co-localisation with (C) the staining for the other proteins of interest. Outside the nucleus, S830 aggregation was clearly visible in the cytoplasm that did not co-localise with P62 or ubiquitin. A side view of the image confirms the co-localisation of the proteins inside the nucleus. NPCs=neural progenitor cells, ICC=immunocytochemistry.

inclusions were relatively round in shape and that the inclusions were located throughout the centre of the nucleus (Figure 4-17B).

Immunostaining with antibodies against P62, S830 and ubiquitin produced signals throughout the cytoplasm thereby highlighting the morphology of the cell (Figure 4-17C). Little co-localisation was observed between the signals obtained with the three antibodies outside the nucleus in the R6/2 cells. The staining pattern was further visualised using a side view of the image (Figure 4-17D). The co-localisation of P62, S830, and ubiquitin was clearly visible and the proteins were located relatively centrally in the nuclei. As from other angles, little co-localised staining could be seen outside the nucleus. The nuclear envelope of this cell appears to be grooved with potential invagination. This observation is reminiscent of work by Davies et al in 1997, where similar invagination of the nuclear membrane was seen in R6/2 mouse striatal neurons using electron microscopy (Davies et al., 1997).

4.16 Using super resolution microscopy to assess the R6/2 neural progenitor cells without aggregation

The previous sections established that only a subset of cells in R6/2 cultures contain mHTT aggregates at levels detectable by confocal microscopy and the Operetta. To determine whether aggregation can be assessed using SIM, R6/2 Dl cultures were differentiated for 21 days and analysed by capturing images of more than one nucleus present in the same field of view. A marked difference was apparent between a cell that contained S830+ mHTT aggregation and one that did not (Figure 4-18A). The cell to the bottom right in figure 18A had S830 staining (red) throughout the cytoplasm and nucleus.

Figure 4-18. Super resolution microscopy and aggregation differences between R6/2 NPCs. R6/2 cells after 21 days in differentiation media with S830 positive punctate staining viewed using SIM to identify one cell with and one cell without S830+ aggregation. (A) A 3-dimensional projection of the SIM image as viewed from above through the Z-plane. ICC for antibodies P62 (green), S830 (red) and ubiquitin (far red, pink) were used to visualise mHTT and the proteins with which it co-localises. Side panels for individual fluorescent channels show DAPI, P62, and S830 staining equivalent to the larger image. (B) A rotated view of the projection allows depth of staining to be visualised. (C) Combined P62 and S830 images to visualise co-localised staining and an indication of its size and depth into the nucleus. NPCs=neural progenitor cells, mHTT=mutant huntingtin, SIM=structured illumination microscopy.

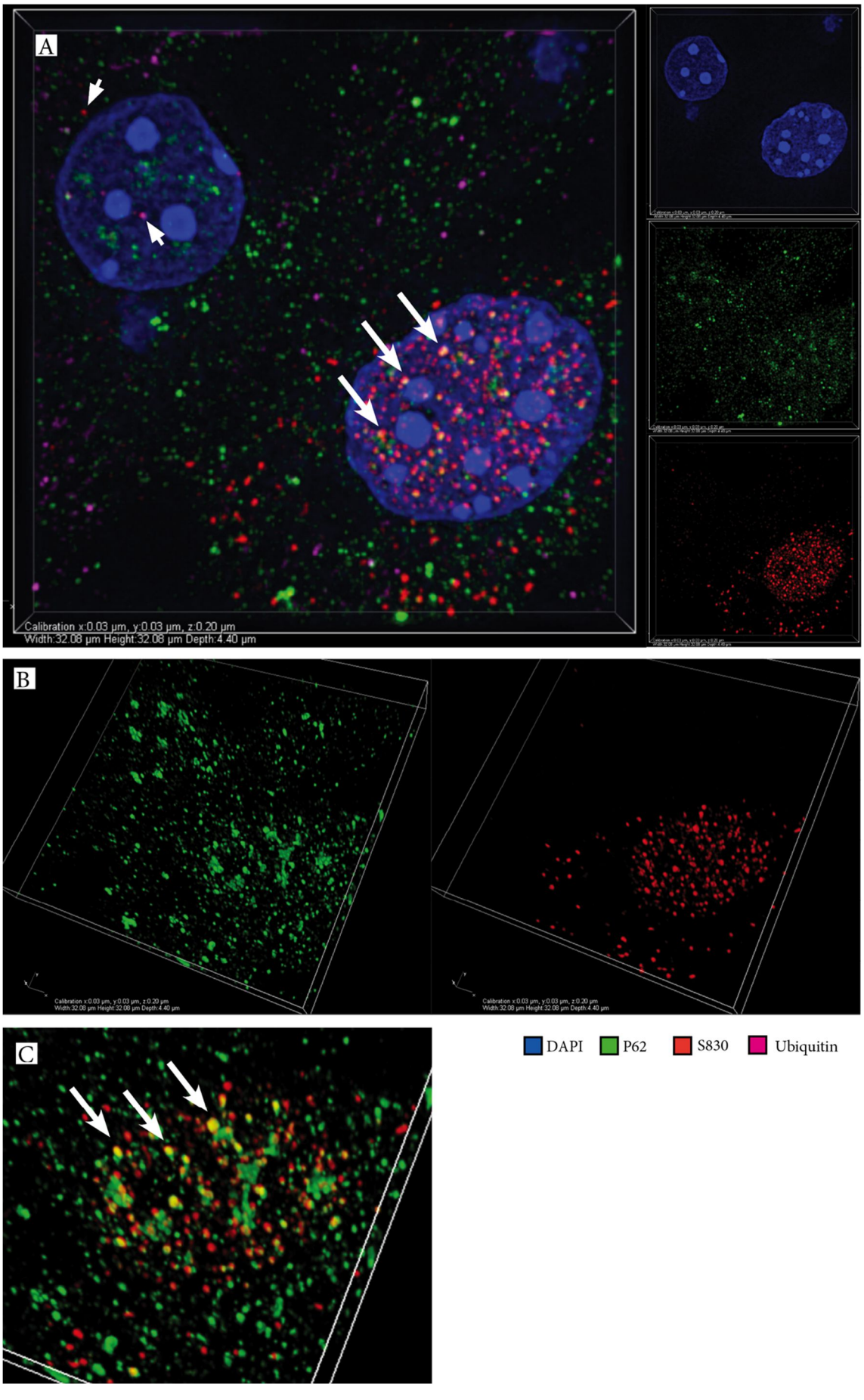
A
Calibration x:0.03 µm, y:0.03 µm, z:0.20 µm
Width:32.08 µm Height:32.08 µm Depth:4.40 µm
B
C
DAPI
P62
S830
Ubiquitin

This aggregation did not seem to be localised in the large inclusions seen in previous examples of R6/2 cells and in the R6/2 mouse brain. The other nucleus in this image did not appear to have any S830 signal apart from two small specks, one located in the nucleus and the other slightly outside the nucleus in the cytoplasm (Figure 4-18A, arrow heads). These specks of staining could be non-specific immunoreactivity or could be the initial stages of inclusion formation.

P62 staining was present in large, and by eye, equal amounts in both the cell with an inclusion and that without (Figure 4-18A). Using a slightly rotated view of the cells (Figure 4-18B), P62 staining did not appear to co-localise with the S830 staining in the cytoplasm (Figure 4-18C) However, P62 co-localisation was detected for some of the marginally larger S830 nuclear inclusions (long arrows). Whether the other cell pictured here without aggregation would eventually start to accumulate aggregates is not easy to answer. To find this out would require long-term live imaging of the cells that could use a method of marking the aggregation process.

Notably, because the S830 staining present in the S830+ cell has more diffuse punctate staining, this cell might not have been recorded as S830+ by the Operetta exclusion criteria.

4.17 Use of super resolution microscopy to assess R6/2 neural progenitor cells earlier in the differentiation process

In the previous sections, manual cell counts and the Operetta were used to show that the number of cells with inclusions increases over time throughout the differentiation process. Aggregation was detected as early as 14 days by the Operetta after the start of differentiation in R6/2 cells. To assess this earlier aggregation, R6/2 Dl cultures were

differentiated for 14 days and analysed using SIM. These cultures were stained with ICC with antibodies against S830, the cytoskeletal protein vimentin and P62. As before, an image with two separate nuclei was captured with one cell that appeared to have S830+ aggregation throughout the nucleus and cytoplasm and the other with a much lower S830 signal (Figure 4-19A).

The cell to the left side of the image has S830+ signal present throughout the nucleus when viewed from above (Figure 4-19A). The orthogonal view of the nucleus allows the location of the S830 signal to be displayed through the dashed line. This signal was represented as several smaller inclusions. The orthogonal view cutting the image horizontally, displayed underneath, also showed the cell on the right in which the nucleus did not appear to have S830+ inclusions: no aggregation was visible in this view. However, aggregation was apparent in the cytoplasm of both cells (Figure 4-19A).

Use of an alternate view of the captured Z stack made the image seem translucent and displayed the total staining throughout the cells. With this view, more aggregation could be detected and the cell on the right appeared to have some S830+ signal in the nucleus (Figure 4-19B, Arrows). However, rotating the projected image showed that this aggregation was located outside the nuclear envelope (Figure 4-19C). This rotated view indicated that only cytoplasmic aggregation was present in this cell. The cell with nuclear inclusions had a vast amount of aggregation in its nucleus. Both cells have relatively similar levels of aggregation in the cytoplasm; however, the boundary between each cell is only estimated and without a marker of the plasma membrane it was not possible to definitively say where one cell ends and the other begins.

Figure 4-19. Super resolution microscopy and differences in aggregation in R6/2 NPCs. R6/2 cells after 14 days in differentiation media with inclusions viewed using SIM to identify one cell with and one cell without S830+ nuclear inclusions. (A) A projected view of the cells from above the z-stack with orthogonal views through the dashed line to reveal S830 stained inclusions throughout the nucleus of one cell with no S830 signal in the other nucleus. (B) An average blended view though the z-stack from above showing average levels of staining and giving the cell a transparent quality. The left nucleus had a lot of individual S830 inclusions throughout. The cell on the right side appears to have staining in the nucleus, but (C) when the image was rotated, the staining could be seen to be outside the nuclear envelope and was cytoplasmic. NPCs=neural progenitor cells, SIM=structured illumination microscopy.

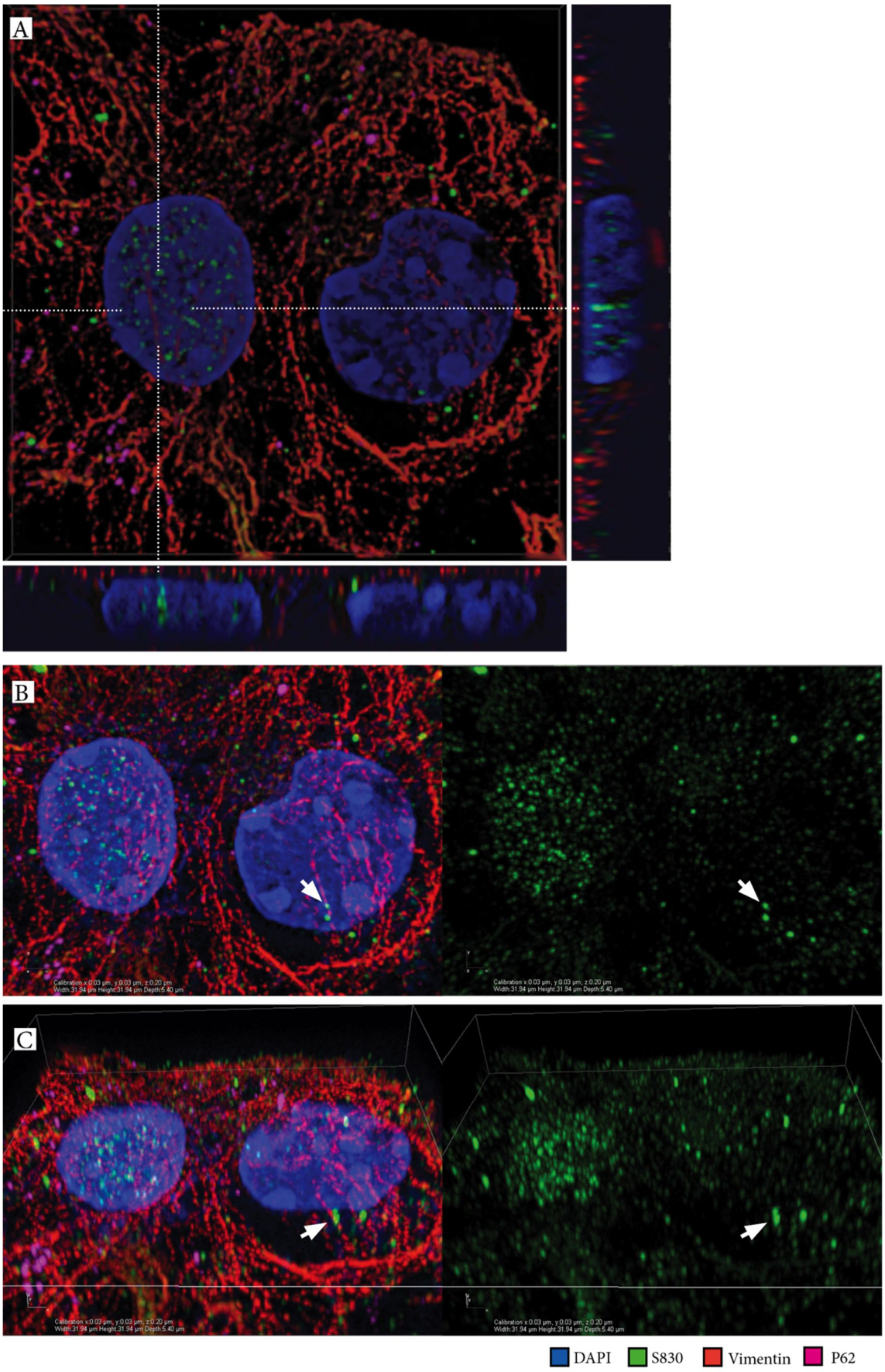
A
B
C
DAPI
S830
Vimentin
P62

4.18 Use of super resolution microscopy to assess aggregation in R6/2 neural progenitor cells at earlier time points

So far in this thesis, the earliest time point studied after induction of differentiation was 7 days, and at this time point evidence of mHTT aggregation had not been detected. To assess whether aggregation could be detected with the more sensitive SIM technique, R6/2 Dl cultures were differentiated for 7 days and stained using ICC with antibodies for S830, vimentin, and P62 (Figure 4-20A). A projected image from above shows very little S830 staining anywhere within the R6/2 cell. Orthogonal views show a nucleus free from staining, sitting on top of a base layer of vimentin-stained cytoskeleton. A rotated view of this projected image shows that some S830 signal might have been present, which could potentially be the first stage of aggregate formation. There was a P62 signal throughout the cytoplasm in the form small sparse entities that did not correlate with the other fluorescent signals.

4.19 Use of super resolution microscopy to assess wildtype neural progenitor cells

As a comparison to R6/2 cells, WT Dl cells were grown alongside R6/2 cells for 21 days and ICC stained for antibodies against P62, S830, and ubiquitin (Figure 4-21A). An S830 signal could not be detected in these cells beyond a few specks at the outer limits of the image (Figure 4-21A, Arrow). The ubiquitin signal was reduced compared with the R6/2 cells at 21 days (Figure 4-17). P62 staining was abundant throughout the cytoplasm and present the nucleus. In this thesis, previous observations of P62 in the nucleus have come in tandem with an S830 inclusion signal. P62 is most commonly identified for its role in the autophagy system contained within the cytoplasm as well as its presence in the

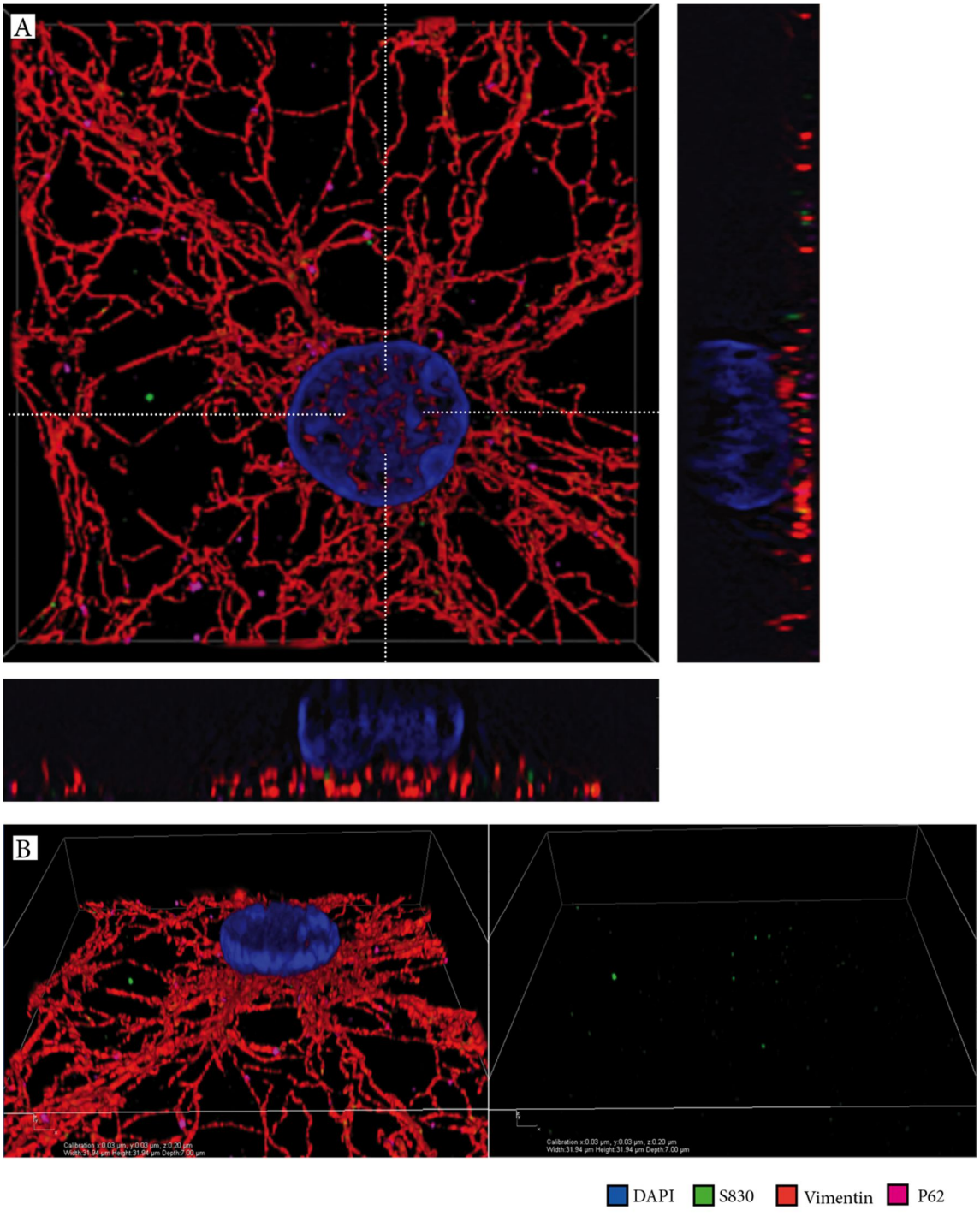

Figure 4-20. Super resolution microscopy to detect aggregation in 7 day R6/2 neural progenitor cells. (A) A projected image of the combined Z stack throughout the 7-day differentiated cell stained for S830 (green), vimentin (red), and P62 (pink). Orthogonal views display a DAPI nucleus sitting above a vimentin-stained cytoskeleton that did not contain S830 signal. Some evidence of S830 and P62 signals were present in the cytoplasm. (B) A rotated projection again displayed the nucleus on top of a cytoplasm cytoskeleton. Some S830 signals appeared to be forming in the cytoplasm.

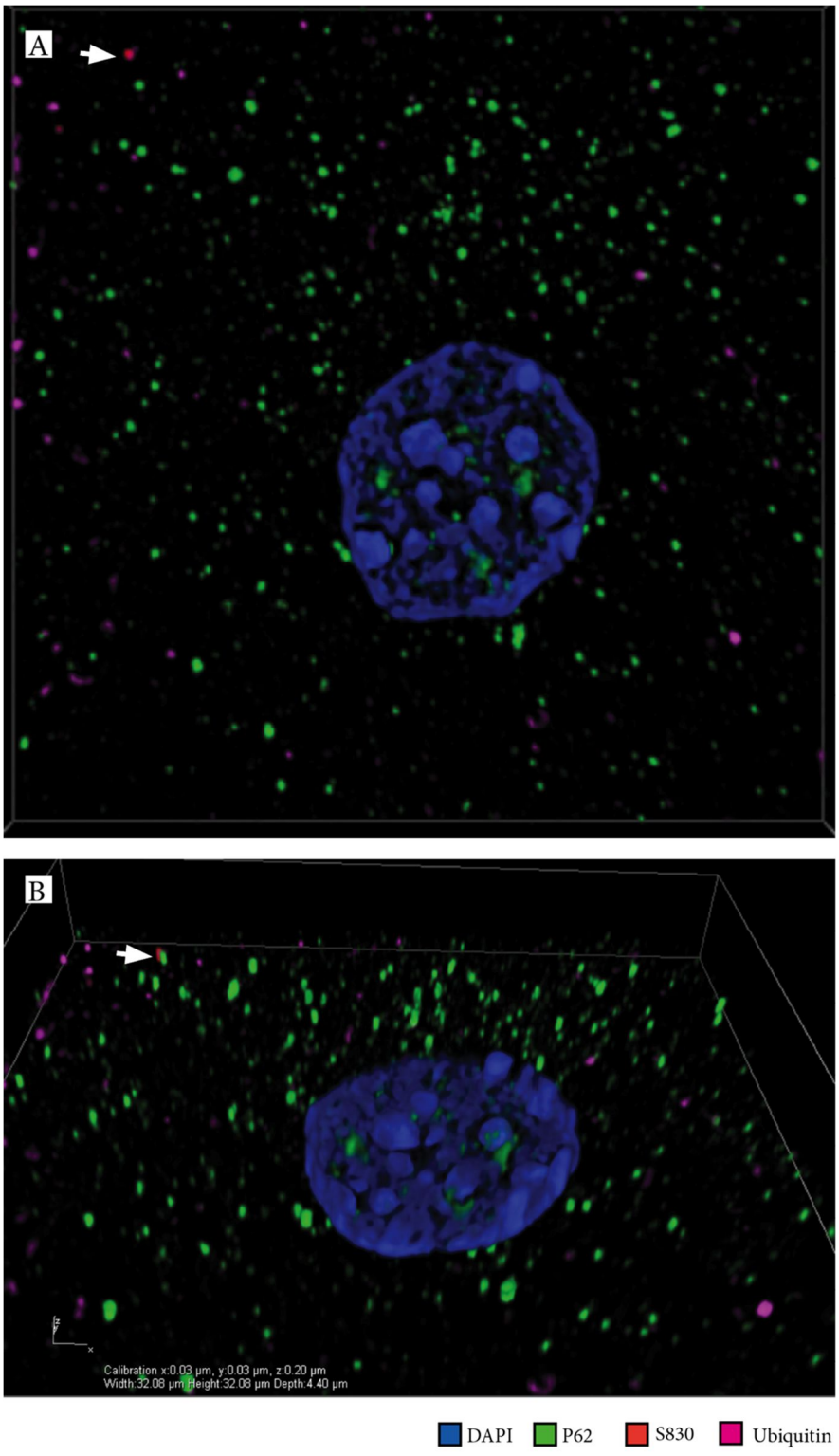

Figure 4-21. Super resolution microscopy and aggregation in 21 day WT NPCs. (A) WT cells after 21 days in differentiation media stained for ICC using P62 (green), S830 (red) and ubiquitin (pink) viewed using SIM. A single S830 stained element in the presumed cytoplasm highlighted by arrow. (B) A rotated projection of the WT cells shows no S830+ aggregation and weak ubiquitin staining. WT=wildtype, NPCs=neural progenitor cells, SIM=structured illumination microscopy.

nucleus in aggregated proteins of many neurodegenerative diseases (Ravikumar et al., 2002, Liebl and Hoppe, 2016). However, P62 has many roles within the cell beyond the autophagy system; it is known to be important in regulation of cell growth, survival and proliferation (Sanchez et al., 1998). Within this function in healthy cells P62 is shuttled in and out of the nucleus via its nuclear localization signal (NLS) and nuclear export signal (NES) sequences (Pankiv et al., 2010, Zhang et al., 2016). During times of oxidative stress, inflammation, or starvation, P62 can be found located in the nucleus as well as the cytoplasm (Zhang et al., 2016), however its role in these situations is still not fully understood. A rotated view of the WT cell image projection showed these P62 stained units have some depth and are large objects within the cells (Figure 4-21B). S830+ cytoplasmic signal did not co-localise with P62 signal in the cytoplasm of WT cells unlike the staining that was observed in the time matched R6/2 cells.

4.20 Chapter discussion

4.20.1 Modelling aggregation

The aggregation of mHTT and the appearance of cellular inclusions is one of the hallmarks of HD observed in the human disease and mouse models. These inclusions are a useful phenotype to study the disease because they can be visualised and used as a readout of aggregation. The mechanisms driving the complex and numerous cellular pathologies of HD and the role that mHTT aggregation plays within the context of the disease are still not fully understood. Aggregation of mutant or modified protein is observed in a variety of neurodegenerative diseases including Alzheimer's disease, Parkinson's disease, and amyotrophic lateral sclerosis, as well as many others. Whether this process is correlative or causative in each case has been vigorously investigated and debated, but not definitively answered.

Some studies of aggregated HTT have suggested these aggregates could be a protective mechanism against the disease (Arrasate et al., 2004, Saudou et al., 1998, Nucifora et al., 2012). However, correlations between detectable inclusions and cell death are hard to measure because much of the early underlying aggregation and its precursors are too subtle to detect with current microscopy techniques. The aggregation process probably contributes to the pathogenesis of HD disease. However, the presence of larger microscopically detectable inclusions might not be vital for all HD pathology.

In the R6/2 mouse, inclusions progressively increase throughout the brain and their number correlated with the severity of behavioural and cognitive phenotypes, although the appearance of inclusions proceeds the onset of these phenotypes. Although limited cell death is observed within the 16-week R6/2 mouse lifespan, neuronal density increases with brain shrinkage (Rattray et al., 2013) and neural dysfunction is widespread (Cepeda et al., 2003, Davies et al., 1997), thus replicating some HD-like phenotypes. HTT inclusions are ubiquitinated, suggesting that they are targeted for degradation. The ubiquitin-proteasome system (UPS), however, is impaired in R6/2 mice (Maynard et al., 2009). This impairment might be caused by saturation of the UPS by mHTT, either by providing excessive substrate or by directly inhibiting the proteasome (Ciechanover and Brundin, 2003, Bence et al., 2001, Cummings et al., 1998). This theory suggests, regardless of HTT's overall pathology, the presence of mHTT inclusions will affect the cells ability to function efficiently.

Aggregated mHTT inclusions can be visualised using ICC and quantified using western blot analysis with antibodies raised against different epitopes along the protein. In this thesis, the S830 sheep polyclonal antibody was used to identify aggregation. S830 recognises the N-terminus of the protein with an elongated polyQ and so will detect even the smallest mHTT fragments including the exon1 HTT found in the R6/2 mouse model

(Sathasivam et al., 2013, Sathasivam et al., 2001, Mangiarini et al., 1996, Landles et al., 2010).

4.20.2 Aggregation in R6/2 cell cultures

Aggregated mHTT inclusions were visualised in a population of R6/2 cells using ICC confocal and super resolution microscopy from day 14 of differentiation. The presence of mHTT aggregation was confirmed using western blot analysis to separate soluble HTT by size within the resolving gel and detergent insoluble mHTT. A sizable amount of detergent insoluble mHTT protein was present in the stacking gel, indicative of mHTT aggregated complexes. Within the cells, inclusions could be seen using confocal microscopy, and the S830 polyclonal antibody, in a subset of R6/2 nuclei. By 28 days of culture, around 10-20% of cells in the R6/2 cultures from striatal and cortical progenitors had aggregated inclusions in their nuclei. In the R6/2 mouse, the vast majority of neurons in the striatum and cortex have inclusions by 15 weeks of age (Meade et al., 2002). Whether similar proportions of cells with aggregates would eventually be present in R6/2 cultures, if they could be maintained for longer, remains to be determined. Preliminary experiments suggest that the number of surviving cells greatly decreases beyond 28 days of culture, in both WT and R6/2 cell lines, which could hamper such experiments.

Super resolution microscopy was successfully used to visualise aggregation in the cytoplasm of the R6/2 cell lines, which had not been distinguishable using confocal microscopy. Staining was more abundant in the cytoplasm at later time points, and seen alongside nuclear aggregation. Cytoplasmic aggregates appeared small and diffuse, which explains why they were not detected using brightfield or confocal techniques with lower resolution. Super resolution microscopy appeared to show that the larger inclusions in the nuclear colocalised with markers of autophagy and were ubiquitinated. These observations were similar to the co-localisation pattern seen in the R6/2 mouse brain. In cultured cells differentiated for 21 days, the nuclear aggregates appeared smaller but more

numerous than the aggregates seen in end stage R6/2 mice brains; these small inclusions did not colocalise with ubiquitin to the same extent as the inclusions *in vivo*. Because the aggregation process is progressive, the cultured cells might not have reached the extent of aggregation observed *in vivo* yet. This could also suggest that the quantity of smaller aggregates has overwhelmed the UPS or that they are not yet prioritised for degradation. The smaller inclusions also did not appear to colocalise with p62, which suggests they might not be targeted for autophagy like the larger inclusion bodies. It is known that P62 function is neuroprotective in some neurodegenerative conditions (Kuusisto et al., 2001) and colocalises with inclusions throughout the neurons in the R6/2 model (Nagaoka et al., 2004). However, it is also known that P62 is dysregulated in the presence of mHTT in the R6/1 mouse brain (Rue et al., 2013). This suggests that the function of P62 can become compromised in the presence of mHTT. However, P62's role in the cell is not limited to autophagy (Sanchez et al., 1998), and indeed, autophagy is carried out by other protein families or pathways (Lu et al., 2014, Komatsu et al., 2007) suggesting that further study is needed before conclusions can be drawn.

Using the super resolution microscopy, it was observed that the cells with larger inclusions appear to have some invagination of their nuclear envelope. This observation is reminiscent of work by Davies and colleagues in 1997, where similar invagination of the nuclear membrane was seen in R6/2 mouse striatal neurons using electron microscopy (Davies et al., 1997). The mechanism underlying this phenomenon is not known. It is possible the nuclear export signal at the terminus of HTT might draw the envelope and inclusion together and so in turn misshape the nucleus into the invaginated shape. This physical misshaping of the nuclear envelope could affect the function of other nuclear processes.

The use of super resolution imaging within this chapter has allowed the visualisation of smaller cytoplasmic inclusions. It is known that this aggregation type exists within HD

in the human brain and may be the toxic component within the disease which results in the vast cell death observed. Because of its more disuse and smaller nature the cytoplasmic aggregation can be easily missed when focus to paid to the nuclear aggregated HTT. Using super resolution this cytoplasmic aggregation can be detected and could be used as an indication of how the disease is affecting cell function.

4.20.3 Aggregated R6/2 cell fates

The R6/2 cells exhibiting nuclear inclusions rarely showed cell fate signals using ICC and antibodies for classical makers of neurons and glia. The reason for this remains unclear. The cells with inclusions do not have long processes but have a cytoplasmic structure that can be identified with cytoskeletal markers such as actin. At first it was thought that these cells could have retracted their processes to an extent that they had little remaining cytoplasm with which to distinguish markers, however this was not the case. The volume of the cytoplasm of the cells with aggregation, but no fate markers, was not measured in detail here. However, in cells of the R6/2 striatum, cells are known to shrink up to 20% of their total size without cell death (Klapstein et al., 2001), which could be similar to what was observed in the NPCs. It could be that the cells with inclusions remain undifferentiated, however the change in morphology and lack of expression of NSC makers nestin and Ki67 suggest this was not the case. The presence of inclusions and the lack of differentiated markers suggests that if these cells have differentiated, then the proteins recognised by common antibodies as markers might be downregulated in the presence of aggregating mHTT. Alternatively, it could be that these cells initially do start to differentiate but that this process terminates before the cell can mature to the point at which they express the specific markers of neurons or glia that were probed.

An alternative possibility is that these cells are quiescent stem cells, which do not express nestin or Ki-67 when in their quiescent G0 state (Maslov et al., 2004, Codega et al., 2014).

It would be unlikely that the inclusion-forming population, which can make up to 20% of the total R6/2 culture, could be quiescent stem cells—however, this was not investigated.

An alternative explanation could be that the inclusion-containing cells have become apoptotic. As a cell undergoes programmed cell death, proteins are downregulated and processes are retracted—similar to the inclusion-containing cells observed in R6/2 cultures. However, there was no evidence that the presence of inclusions increased cell death in the R6/2 cultures or that the inclusion-containing cell population was specifically apoptotic. These findings are in line with most evidence from the R6/2 mouse brain, in which cell death is minimal despite the widespread aggregation phenotype and apoptotic markers are not present (Rattray et al., 2013, Turmaine et al., 2000). This is not to say those cells in the mouse model with inclusions are not compromised in other ways. Gene expression changes have been detected in the striatum and cortex of R6/2 mice as early as at 6 weeks and become more pronounced with age (Luthi-Carter et al., 2000). These could be related to the lack of mature cell markers observed in the R6/2 inclusion-containing cells.

Apoptotic cell death was observed throughout both WT and R6/2 cultures from day 21 of differentiation with TUNEL+ cells being present in most regions of interest studied. This suggests that something about the *in vitro* culture system induces cell death once cells are post-mitotic and have differentiated. In development, apoptosis is not necessarily a negative process because it is required to remove cells that have become surplus to requirement during neurogenesis (Yeo and Gautier, 2004, de la Rosa and de Pablo, 2000, Meier et al., 2000). In culture, a similar effect might be observed with cells not receiving the required signals for their maintenance. If it could be determined why this apoptotic cell death was taking place across cultures of both genotypes, then longer culture durations could become feasible.

4.20.4 High content analysis of cultures

Because monolayer cultures were used, high-throughput imaging and analysis using the Operetta was possible to assess the presence of S830 inclusions in cell nuclei. Using this system, it was possible to count and analyse tens of thousands of cells across single 96-well plates for morphological changes and to separate data from the subpopulation of inclusion-containing cells. This analysis showed that R6/2 cells have larger nuclei compared with WT cells. It is not known why R6/2 nuclei would be larger than those in WT cells but this could be linked to the aggregation of the HTT protein. Nuclear aggregates could result in an increased size to accommodate the aggregation of mHTT protein. However, when the R6/2 cells were separated into inclusion-containing and inclusion-free cells it appeared that this size increase was mostly driven by those cells below the inclusion threshold. This opposes the theory of aggregation expanding the nuclei. It is possible that cells that were not above the required S830+ threshold contained inclusions that were too diffuse to detect but that they had more numerous inclusions, as seen previously with super resolution microscopy. These diffuse but numerous aggregates could increase nuclear size and, once the inclusions become very large in the nucleus, the nucleus might retract. Those cells captured with the larger inclusions retained the diffuse staining in the nucleus but too few were captured to probe if this was always the case or if the change in volume was related to their quantity.

The biological processes that govern the morphology of nuclei are complex and not fully understood. Indeed, little is known about how the nucleus is formed, what determines its shape and what defines its size (Webster et al., 2009, Edens et al., 2013). It is known that nuclear shape can change during aging or in diseases such as cancer (Zink et al., 2004, Webster et al., 2009) in which enlarged nuclei almost always represent more aggressive metastatic disease. The nuclear envelopes ability to change size and shape is a key part of the process of mitosis. It is not surprising that it would be able to perform similar

adaptations in response to abnormal protein folding and aggregate formation. Why this size of the nucleus does change is not known.

4.20.5 Aggregation in the R6/2 cultures only after adapted differentiation protocol.

When the differentiation protocol was changed to maintain cultures on laminin, the aggregation phenotype was observed in the R6/2 lines. Why this change resulted in the emergence of the aggregation phenotype is not known. One theory would be that this subset of R6/2 cells are predisposed to aggregation and are liable to other phenotypes such as an inability to attach to uncoated plastic without a substrate to bind to, and so were lost in the media when it was changed. Evidence exists that levels of neural cell adhesion molecule (PSA-NCAM) are reduced in the hippocampus and piriform cortex of the R6/1 and R6/2 mouse models (van der Borght and Brundin, 2007). In other HD knock-in mouse models, irregular synaptic and structural plasticity is observed in different brain areas, including the hippocampus and the cortex (Usdin et al., 1999, Cummings et al., 2006, Spires et al., 2004, Gil et al., 2005), both of which can be regulated by NCAM. Potentially, cells that will be prone to aggregation might struggle to adhere to uncoated plastic and therefore be the most readily lost over that period of culture. Unattached cells were present in the media; however, because a large number of cells were still attached this was not thought a problem. Whether these cells are those that would eventually show aggregation could be studied by collecting the media and plating it onto laminin which should allow for the previously floating cells to adhere. These cells could then be differentiated to examine their potential for aggregation.

The substrate used to coat plastic and encourage monolayer growth and attachment was laminin, which cells interact with via integrin signalling. Integrins are often found on the end of cellular filopodia, cellular membrane protrusions which act as sensors, probing

their microenvironment and regulating cell protrusion and cell migration in response to extracellular cues (Galbraith et al., 2007, Vasioukhin et al., 2000). Gene expression data from post-mortem HD brain highlighted the role of Rho family of GTPase signalling proteins in HD pathology (Tourette et al., 2014). Members of this Rho GTPase family, in particular ROCK1 and RAC1, are known HTT interactors (Bauer et al., 2009). They are also involved in BAIAP2-induced filopodia formation which is known to be interfered by the expression of mHTT in cell models (Shao et al., 2008). A reduced interaction of cellular adhesion components using the integrin signalling could result in decreased attachment of cells with mHTT expression.

Another explanation could be that the process of removing cells from their adhesion to the plastic once they had been induced to start differentiating could be lethal to the subset of cells that would differentiate with inclusions. In the original Spiliotopoulos and colleagues (2009) protocol, this replating took place at day 3 of the protocol. This once again would suggest that cells that are post-mitotic are more sensitive to the stress of being passaged. Some groups have reported an increase in vulnerability to apoptotic stimuli, in cell lines transiently transfected with expanded polyglutamine-containing proteins (Hackam et al., 1998, Cooper et al., 1998). This theory could be tested by inducing a stress to the culture to measure whether those cells with aggregates were more prone to being affected.

Another observation about the R6/2 cells that had nuclear aggregates was that they were more prone to be isolated and away from the clumps of cells that formed throughout the cultures. This is not to say all aggregating cell were isolated but that those that were made up the majority. NCAM has been implicated as having a role in cell–cell adhesion (Rutishauser et al., 1988) and levels have been shown to be reduced in HD mouse models. NCAM is strongly associated with brain plasticity and also interacts with BDNF (Kiss et al., 2001), which is known to also be reduced in HD. If the levels of NCAM were also

reduced in the cells cultured here that contained aggregates, then this could also contribute to why cells with aggregation were less prone to appear in the clumps with other cells in the culture. If this was the case it would suggest a very early phenotype in these cells, which would proceed the detected aggregation observed so far.

4.20.6 Subpopulation differences in the R6/2 cultures

The presence of a sub-population of R6/2 cells with inclusions is intriguing and suggests that those cells that develop detectable aggregation within the first 28 days might have been predisposed to do so before they were extracted from the foetal brain. In the brains of patients with HD and HD mouse models, the number of cells with inclusions increase over time suggesting that certain populations are prone to aggregation more than others. Why this is the case is not known and could be due to many different factors. In this thesis, little difference was observed with the different microscopy techniques, between those R6/2 cells with and without detectable aggregation. Use of the Operetta highlighted little difference in nuclear morphology between the cells with and without inclusions. Use of super resolution microscopy allowed a nucleus from cells of each population to be captured within one region of interest. Only a couple of these images were captured, due to the long time taken to capture and process the super resolution images and the rarity of cells of each subpopulation being close enough to capture in a single frame. Therefore, definitive differences cannot be draw from these data. However, the cells without the levels of aggregation that would separate them into the non-aggregated subgroups did appear to have some speckles of S830 staining. This finding suggests that the mHTT aggregation process could be just beginning to be detectable within those cells, and that this process would eventually produce more inclusions with enough time in culture.

It would be interesting if cells from each R6/2 subgroup population could be isolated and differences between cells of each subgroup, with and without detectable inclusions, analysed. RNA-Seq would be a valuable tool to look at levels of gene expression between

these populations. This analysis would require the isolation of cells into their sub-populations based on aggregation. Cell sorting methods such as fluorescence-activated cell sorting (FACS) are ideal to sort cells based on cell surface protein expression. However, the issue with the application of this method is that the only marker that distinguishes the sub-populations of R6/2 cells for ICC is the antibody S830, which targets the inclusions within the cells. The detectable inclusions appear to be mostly nuclear and so, for the antibody to penetrate through to the aggregations, the ICC techniques require lysis of cell and nuclear membranes. This lysis is not an issue with fixed cells while assessing protein levels using ICC but this could affect the quality and quantity of any RNA obtained after FACS. It would also destroy each cell and so prevent the ability to culture the isolated populations further. If cell surface markers were identified it would be possible to use FACS, however no such markers are known at present that could successfully identify these populations.

One potential way to tackle this problem this would be to exploit the fact that the sub-population with detectable inclusions does not show markers of differentiation. Those cells that do show neuronal and astrocytic markers could be sorted from the population sequentially (Feldmann et al., 2014). However, the resulting sorted population would not be only those cells with aggregates because not all cells without these makers have the aggregation phenotypes.

4.21 Summary

The establishment of cell lines with HD-like phenotypes to allow researchers to examine the disease mechanism are greatly needed. The R6/2 NPCs established here exhibited a

detectable nuclear aggregation, visualised using immunohistochemistry from 14 days of differentiation in 5% of R6/2 cell nuclei, rising to 20% by 28 days, recapitulating an HD-like phenotype found *in vivo*. Detection of detergent insoluble mHTT-aggregated protein was also validated via western blotting. Super high resolution cell imaging showed aggregation of mHTT also occurs in the cytoplasm. High-content imaging analysis system was performed using the Operetta system to explore morphological differences between WT and R6/2 cultures, as well as within the subset of cells with detectable aggregation. R6/2 nuclei were found to be larger than those of WT cells. The aggregation detected in these NPCs in combination with the ability to monitor the formation across cultures with high content analysis make this a useful platform to probe disease mechanisms.

Chapter 5 Results 3: Application of novel compounds to cells while assessing phenotypic changes

5.1 Introduction

The NPCs created and probed in the previous chapters can be used with high content analysis systems to monitor the aggregation phenotype exhibited by the R6/2 cultures in addition to assessment of nuclear morphology. The application of potential disease modifying treatments to these cells monitored on this platform would allow in-depth assessment of how these treatments affect the R6/2 and WT cultures.

Six compounds were supplied to us from professor Erich Wanker's laboratory (Berlin, Germany). These particular compounds were provided because they have shown promise in affecting aggregation of misfolded proteins in models of neurodegeneration. As such, these six compounds were applied to the R6/2 and WT NPC lines developed in this thesis to determine whether they had similar effects on HTT aggregation in these cells.

5.2 Chapter aim:

The aim of the experiments performed in this chapter was to:

- examine the toxicity and then test the effects of novel compounds supplied from our collaborators on the R6/2 neural progenitor cell lines developed and documented over the previous results chapters of this thesis.

5.3 Compounds

A description of each compound follows:

5.3.1 O4

O4 is an orcein-related small molecule which has been shown to help promote the fibrillarisation of amyloid-β (Aβ) polypeptides (Bieschke et al., 2012). The non-fibrillar forms of Aβ can form as soluble oligomers or protofibrils that instigate the neuronal dysfunction and memory impairments of Alzheimer's disease. This process of Aβ formation as β-sheets is similar to that observed in the aggregated polyQ sequences in HD (Takahashi et al., 2008, Perutz, 1996, Bieschke et al., 2012). Potentially O4 could have similar effects on mHTT aggregates as it does on amyloid aggregation in AD that form with similar β-sheet–rich oligomers and protofibrils.

5.3.2 B-lapachone

β-lapachone is as a naturally occurring quinone that has been shown to help reduce polyQ toxicity by stimulating autophagy clearance of Exon 1 aggregation (Shin et al., 2013). This effect is mediated through increase in activity of SIRT-1, a mammalian orthologue of the yeast Sir2 protein (Hwang et al., 2009, Lee et al., 2012b). SIRT-1 is reduced in the brains of R6/2 and *Hdh*Q150 mice (Tulino et al., 2016) and increasing expression of SIRT-1 diminished neurodegeneration and improved motor function in N171-82Q and BACHD mice (Jiang et al., 2012) and reduced brain atrophy and mutant HTT aggregation in R6/2 mice without lengthening lifespan (Jeong et al., 2012). β-lapachone has also shown some inhibitory effects in a FRET-based HTT exon 1 aggregation assay (personal correspondence, Wanker lab). β-lapachone inhibits indoleamine-pyrrole 2,3-dioxygenase in human immune pathways at an IC_{50} of 0.44 μM and is useful in cancer research where it helps prevent tumour cells to avoid immune responses (Uyttenhove et al., 2003).

5.3.3 Quinidine

Quinidine has long been used as an antiarrhythmic pharmaceutical agent in the heart, which acts by blocking the fast inward sodium current (Noujaim et al., 2011). It is also currently used as a combination treatment with dextromethorphan hydrobromide to treat the pseudobulbar affect in amyotrophic lateral sclerosis (Brooks et al., 2004) In HTT aggregate clearance assays quinidine has a substantially reduces the number of HTT Exon 1 aggregates in SH-EP (human neuroblastoma cell line) (Reddy et al., 1991) cells as counted by automated microscopy (personal correspondence, Wanker lab). In further analysis, using a HD fly model, quinidine reduced HTT aggregates in treated fly brains (Personal correspondence, Wanker lab). When used for its sodium channel blocking qualities the IC_{50} of Quinidine has be calculated to around 1.37 μM (Ballestero et al., 2005).

5.3.4 Hydrazone #6 and #9

Hydrazones are a group of organic compounds related to aldehydes and ketones. They have been shown to function as uncoupling agents in ATP synthesis (Heytler and Prichard, 1962). In a study of the effects of 120 hydrazones on HTTEx1Q49 using a filter retardation assay, two were identified to be effective in inhibiting aggregation. These two were labelled as hydrazones #6 and #9. Their anti-aggregation effect was confirmed using atomic force microscopy, kinetic analysis of HTT Exon 1-Q49 aggregation via filter retardation assay, AGERA (agarose gel electrophoresis for resolving aggregates), native dot blot assays (using the antibody MW8) and native PAGE (personal correspondence, Wanker lab). The IC_{50} of Hydrozone #6 has been calculated to around 218 μM with Hydrozone #9 being slightly less potent.

5.3.5 Guanabenz

Guanabenz has been identified as an inhibitor of protein stress in the endoplasmic reticulum by helping protect against the build-up of toxic misfolded proteins (Tsaytler et al., 2011). In HTT aggregate clearance assays guanabenz reduces the amount of HTT Exon 1 aggregates in SH-EP cells, as counted by automated microscopy (personal correspondence, Wanker lab). In further analysis, using a HD fly model, quinidine reduced HTT aggregates in treated fly brain, which was confirmed using native dot-blot assays (personal correspondence, Wanker lab). Guanabenz is an agonist of the alpha-2 adrenergic receptor and prescribed as an antihypertensive drug (Holmes et al., 1983). Evidence also suggests guanabenz has potential anti-prion activity (Tribouillard-Tanvier et al., 2008). The IC50 is around 8.6 μM as alpha 2-adrenoceptor agonists (Vago et al., 1985).

5.4 Toxicity

The potential toxicity of these compounds in differentiated NPCs had not previously been assessed. To determine the lethal dose to 50% of cells (LD_{50}) for each compound, one R6/2 and one WT Dl neural progenitor cell line previously passaged to p15 were differentiated on laminin in 96-well plates for 7 days in the presence of 4 concentrations of each compound (Table 5-1), and the proportion of surviving cells was visually assessed. Culture media was half-refreshed at least every 48 hours and fresh media was additionally applied as required by the differentiation protocol. Brightfield images were captured after 1, 3, and 7 days of differentiation to visually monitor the cultures (Figure 5-1&2). The compounds' effects were measured by comparison of cell number with cells differentiated in media containing no compound (NC), as had been optimised in chapters 3 and 4 of this thesis. Five brightfield images were captured per condition and the number

of cells present were counted. LD_{50} values were then calculated for each compound that showed toxicity.

Compound	Colour	Storage	Molecular weight g/mol	Weight of compound	Compound diluted in DMSO	Volume DMSO for 10mM Stock	Concentrations µM
O4- (TimTec)	Black	4℃	429,38	4.29mg	10mM	1ml	2, 5, 10, 20
βLapachone	Orange	RT	242,27	2.42mg	10mM	1ml	0.5, 1, 2, 5
Quinidine	White	RT	324,42	3.24mg	10mM	1ml	2, 5, 10, 20
Hydrazon #6	Brown	4℃	370,14	3.70mg	10mM	1ml	2, 5, 10, 20
Hydrazon #9	Dark Brown	4℃	289,24	2.89mg	10mM	1ml	2, 5, 10, 20
Guanabenz Acetat	White	RT	291,13	2.91mg	10mM	1ml	2, 5, 10, 20

Table 5-1. Properties of the novel compounds supplied from collaborators.

The compounds were stored as stock solutions at 10mM in DMSO. After dilution with water, the final percentage of DMSO in the compound solutions is shown in Table 5-2. To control for any effect caused by the residual DMSO, differentiation media was applied with DMSO at a concentration equal to what would be present at the highest compound concentration (Table 5-2).

Compound concentration	DMSO concentration
20 µM	0.2%
10 µM	0.1%
5 µM	0.05%
2 µM	0.02%
1 µM	0.01%
0.5 µM	0.005%
0.2 µM	0.002%

Table 5-2. DMSO concentration in media depending on the compound concentration used. A DMSO only control was used at the concentration present in the highest compound concentration used.

O4 is an example of a compound that did not affect cell survival (Figure 5-1). With the application of differentiation media containing O4, the WT and R6/2 cultures were transformed from the proliferative to a differentiated state with elongated morphology and process extension. The resulting morphology was similar to that previously observed within the adapted differentiation protocol, indicating these cells differentiated in the presence of O4. Little change in cell density was observed between normal culture conditions compared with those containing all concentrations of O4, suggesting little cell death and limited toxicity was associated with its application.

Hydrazon #9 is an example of a compound that did show some toxicity (Figure 5-2). The WT and R6/2 cultures showed visual signs of differentiation at day one. At higher concentrations of hydrazon #9 the number of surviving cells was significantly reduced. Treatment with 10 μM and 20 μM hydrazon #9 resulted in a decrease in the number of surviving cells observed in both WT and R6/2 lines after 7 days. Within the time frame studied here, the 10 μM and 20 μM concentrations were considered toxic to differentiating NPC lines and were not used in the subsequent compound studies (Table 5-4).

The LD_{50} for each compound was calculated based on the number of cells surviving the compound treatments. The estimated concentration which would cause 50% cell death was calculated (Table 5-3). The number of cells lost between day 0 and day 7 in the presence of the increasing concentration of each compound. Cell death was plotted on a graph against concentration and the linear line of best fit was applied. This equation allowed for an estimation of the concentration which would be toxic to 50% of cells and is called the LD50.

Compound	O4	B-lapachone	Quinidine	Hydrazone #6	Hydrazone #9	Guanabenz
Day 0	599	660	519	606	542	660
NC	534	581	497	554	521	612
0.5 µM	-	564	-	-	-	-
1 µM	-	622	-	-	-	-
2 µM	550	523	497	356	368	583
5 µM	529		522	306	344	531
10µM	525	-	493	56	175	320
20 µM	529	-	450	26	115	220
Linear LD50 toxicity equation	NA	NA	NA	y = 19.063x + 243.67	y = 14.793x + 154.67	y = 20.768x + 54.392
Estimated LD50	>20 µM	>5 µM	>20 µM	3.1 µM	7.9 µM	13.3 µM

Table 5-3. Summary of compound toxicity after 7 days via LD50 estimations. Cell counts were carried out on images take at day0 and after 7 days in differentiation media containing compounds at increasing concentration. From the number of cells lost between these cell counts the linear equation for toxicity was calculated and an estimation of the concentration for toxicity to 50% of the cells was estimated (LD50).

On the basis of these toxicity data, the compound concentrations were modified to avoid cell death in cells cultured for a longer duration.

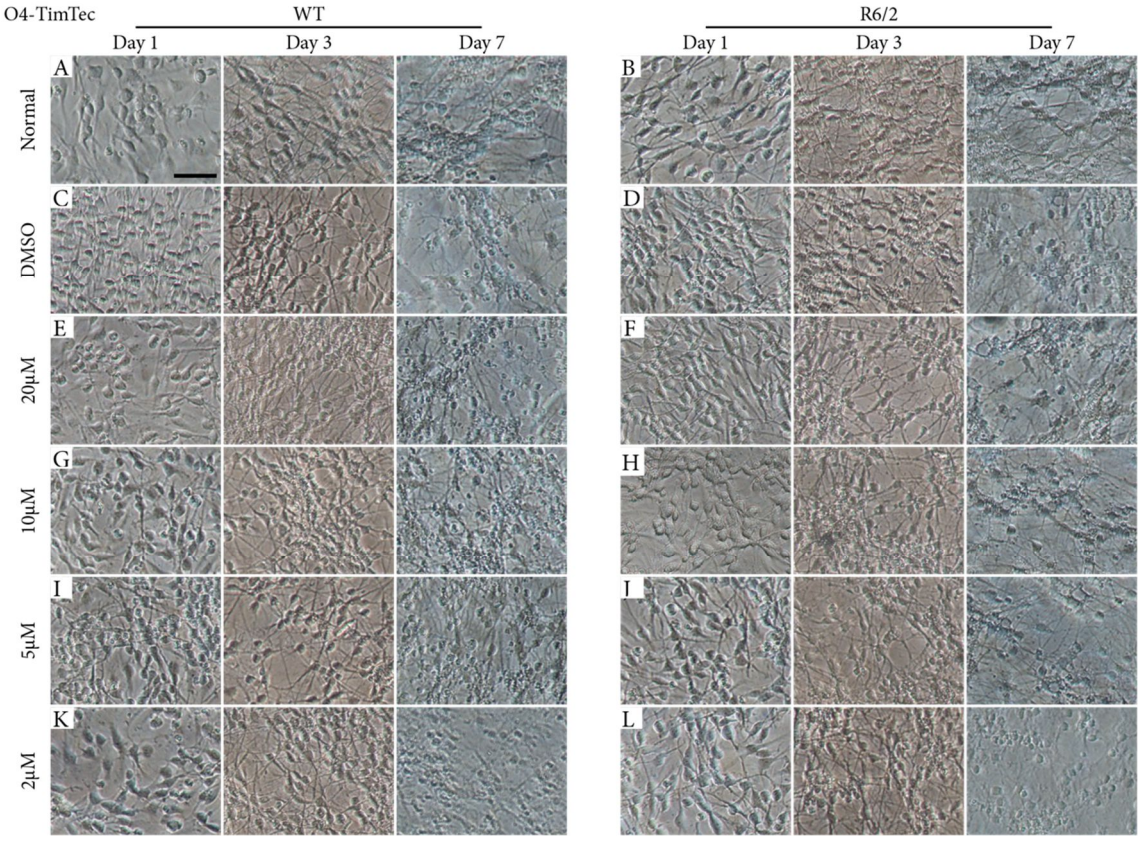

Figure 5-1. Effects of addition of compound O4 to growth media for R6/2 and WT cells. R6/2 and WT Dl lines were differentiated in standardised differentiation media containing O4 for 7 days to assess the survival of cells. (A,B) Normal differentiation media with the protocol optimised in previous chapters with (A) WT cells and (B) R6/2 cells. Normal differentiation media with DMSO (0.2%) added to the same concentration as the highest O4 concentration for (C) WT and (D) R6/2 cultures. Addition of O4 to differentiation media at a concentration of 20 μM for (E) WT cells and (F) R6/2 cells; 10 μM O4 (G) WT cells and (H) R6/2 cells; 5 μM O4 (I) WT cells and (J) R6/2 cells; and 2 μM O4 (K) WT cells and (L) R6/2 cells. WT=wildtype. Scale bar 50 μm.

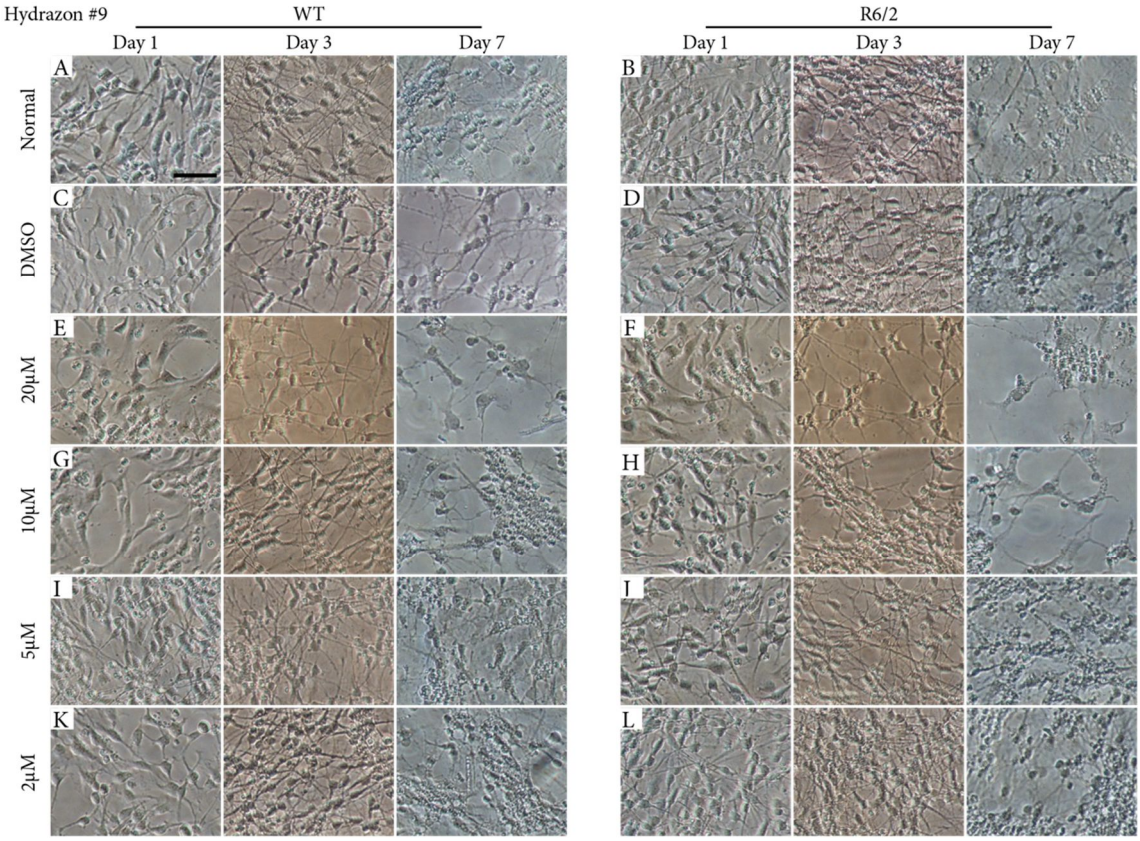

Figure 5-2 Effects of addition of Hydrazon #9 to growth media for R6/2 and WT cells. R6/2 and WT Dl lines were differentiated in standardised differentiation media containing compound Hydrazon #9 for 7 days to assess the toxicity to cells. Normal differentiation media with the protocol optimised in previous chapters with (A) WT cells (B) and applied to R6/2 cultures. Normal differentiation media with DMSO (0.2%) added to the same concentration as the highest Hydrazon #9 concentration for (C) WT and (D) R6/2 cultures. Addition of Hydrazon #9 to differentiation media at a concentration of 20 μM for (E) WT cells and (F) R6/2 cells; 10 μM O4 (G) WT cells and (H) R6/2 cells; 5 μM O4 (I) WT cells and (J) R6/2 cells; and 2 μM O4 (K) WT cells and (L) R6/2 cells.WT=wildtype. Scale bar 50 μm.

5.5 Assessment of the effect of compounds on nuclear morphology and HTT aggregation in differentiated neural progenitor cells

The concentrations of each compound were modified to avoid toxicity in longer term cultures (Table 5-4). This adapted concentration range for each compound was applied to three R6/2 lines and one WT Dl line, for which the differentiation protocol was initiated at p15. The effects on nuclear morphology and aggregation were assessed. The differentiation media used was as optimised in Chapter 4, with either no compound (NC), DMSO control (Table 5-2), or containing the appropriate compound concentration. Cells were grown for 21 days with half the media refreshed ever 48 hours before fixation in PFA and staining by ICC. To perform a non-biased and high throughput analysis of the effect of each compound, the Operetta system was used. Cultures were grown on laminin coated 96-well plates as indicated in Figure 5-3. A design flaw of the Operetta is that at x40 magnification the outside wells of a 96-well plate cannot be captured. As such, the experiments were designed without using the outside wells (Figure 5-3). The data were pooled for the three biological replicates for the three R6/2 lines. Statistical analysis was performed using SPSS (IBM) with Student t-tests set to 95% confidence.

Compound	Colour	Storage	Molecular weight g/mol	Weight of compound	Compound diluted in DMSO	Volume DMSO for 10mM Stock	Concentrations µM
O4- (TimTec)	Black	4℃	429,38	4.29 mg	10 mM	1 ml	2, 5, 10, 20
βLapachone	Orange	RT	242,27	2.42 mg	10 mM	1 ml	0.5, 1, 2, 5
Quinidine	White	RT	324,42	3.24 mg	10 mM	1 ml	2, 5, 10, 20
Hydrazon #6	Brown	4℃	370,14	3.70 mg	10 mM	1 ml	0.2, 0.5, 1, 2
Hydrazon #9	Dark Brown	4℃	289,24	2.89 mg	10 mM	1 ml	0.5, 1, 2, 5
Guanabenz Acetat	White	RT	291,13	2.91 mg	10 mM	1 ml	1, 2, 5, 10

Table 5-4. Adapted concentrations of compounds applied to cultures long term.

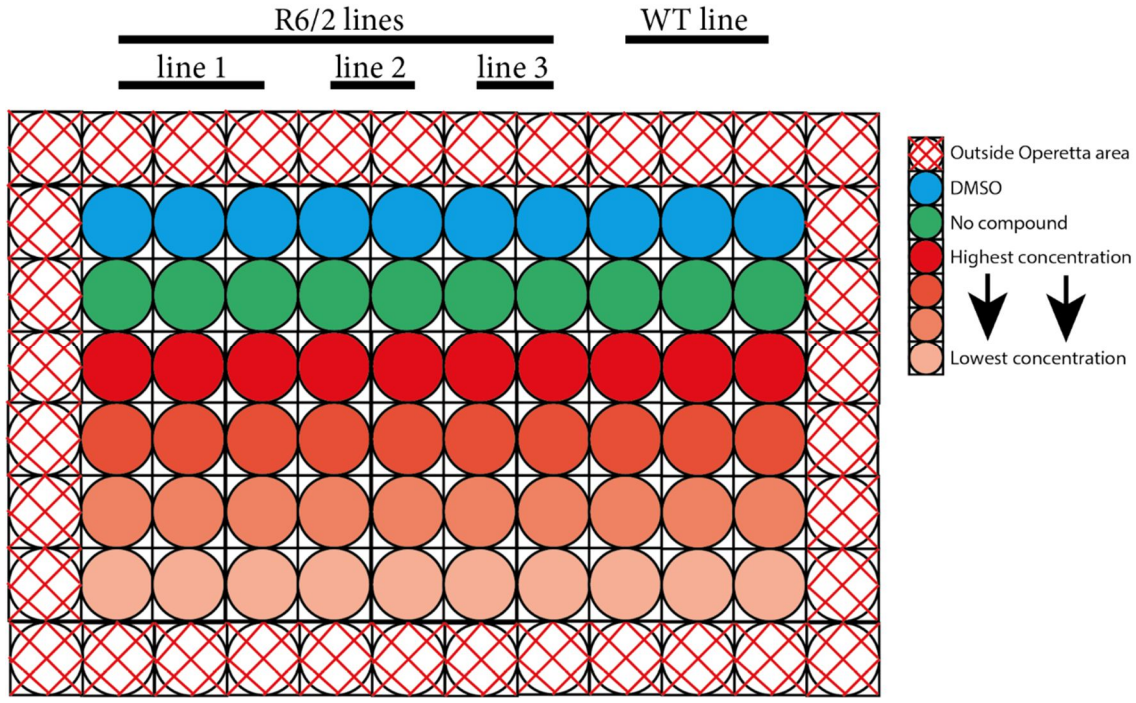

Figure 5-3 Layout of 96-well plates for compound application. R6/2 and WT Dl lines were differentiated in the 96-well plates for analysis with the Operetta. Cells were plated in columns and the compounds were applied in rows as shown. The outermost wells were not used because they were outside the operetta image capture range at higher magnifications. WT=wildtype.

5.6 Assessment of compound affects to nuclear morphology

The compounds were applied to cultures to investigate the effects on nuclear morphology and size in the WT and R6/2 differentiated NPC lines.

The total number of cells in cultures after differentiation for 21 days was affected by all compounds. In the case of O4 (Table 5-6, Figure 5-4), quinidine (Table 5-8, Figure 5-6), and guanabenz (Table 5-11 ,Figure 5-9), this reduction in cells compared with the NC condition was also seen in the DMSO control, suggesting this effect might not be compound related. The hydrazones (Table 5-9, Table 5-10, Figure 5-7, Figure 5-8) also caused a reduction in cell number and to a much larger extent. Both hydrazone compounds, at their highest concentrations, resulted in a considerable degree of cell

death, suggesting their toxicity was more extensive over the longer culture period than in the initial toxicity experiment (Table 5-3). Treatment with β-lapachone (Table 5-7 Summary , Figure 5-5) had the opposite effect and resulted in an increase in cell numbers in the culture, while a reduction in cell number was still seen in the DMSO controls.

The mean area of the WT and R6/2 nuclei was unaffected by treatment with the compounds apart from with the hydrazones, which both slightly reduced the nuclear area at their highest concentrations. This result must be taken in the context of the great reduction in cell number that resulted from hydrazone treatment, as the surviving cells could be adversely affected by the toxic environment. Nuclear roundness was affected by O4, β-lapachone, and guanabenz. O4 and guanabenz resulted in slightly rounder WT nuclei when applied at all concentrations, while DMSO reduced the roundness. Treatment with O4 or guanabenz did not affect the roundness of the R6/2 cells. A similar effect was observed by β-lapachone on the WT cells, with an increase in roundness by application at 2 μM. It is unlikely that this effect observed at only one lower concentration can be used as an important readout. A reduction in roundness was caused by the DMSO control.

The length of WT nuclei, as measured by the thickness through the centre of its longest point, was slightly reduced by O4 and guanabenz. No effect was seen on the thickness of the R6/2 nuclei by the application of these compounds, nor by the other compounds in the WT cells. The width of nuclei, as measured by the thickness through the centre perpendicular to the longest point, was reduced by the highest concentration of both hydrazones. This effect once again might be adversely affected due to the low number of cells surviving in these cultures. The ratio of length:width was affected by treatment with O4, β-lapachone, guanabenz, and the hydrazones. The ratio was increased in the WT cells by the highest concentrations of O4, β-lapachone, and guanabenz, and decreased by the hydrazones. R6/2 nuclei ratios were slightly increased by lower concentrations of β-

lapachone but no effect was observed with treatment with the other compounds. The overall effects are summarised in Table 5-5.

Compound	Effect
O4	⬆ Roundness (WT) ⬆ Length (WT) ⬆ Ratio (WT)
β-lapachone	⬆ Total cells ⬆ Roundness (2 μM) ⬆ Ratio
Quinidine	⬇ Total cells
Hydrazone #6	⬇ Total cells ⬇ Area ⬇ Width ⬇ Ratio
Hydrazone #9	⬇ Total cells ⬇ Area ⬇ Width ⬇ Ratio
Guanabenz	⬇ Total cells ⬆ Roundness (WT) ⬇ Length (WT) ⬆ Ratio (WT)

Table 5-5. Summary of compound effects on nuclear morphology and size in the WT and R6/2 differentiated NPC lines after 21 days. WT=wildtype.

5.6.1 O4

Condition	Gentotype	Total Cells			Nuclear area			Roundness			Length			Width			Ratio		
		Mean	Std.D	Sig.	Mean	Std.D	Sig.	Mean	Std.D	Sig.	Mean	Std.D	Sig.	Mean	Std.D	Sig.	Mean	Std.D	Sig.
NC	WT	581	9		104.39	0.94		0.876	0.001		13.82	0.05		9.01	0.06		0.667	0.002	
	R6/2	650	72		109.60	4.31		0.856	0.009		14.14	0.26		9.32	0.14		0.674	0.007	
DMSO	WT	457	6	###	103.18	3.06		0.858	0.003	##	13.88	0.27		8.84	0.10		0.652	0.001	
	R6/2	318	183		106.96	6.24		0.829	0.031		14.40	0.55		8.76	0.32	§§	0.625	0.032	§§
20 μM	WT	486	4	###	98.56	0.74		0.906	0.004	###	13.01	0.01	#	9.02	0.09		0.705	0.006	##
	R6/2	382	287		105.95	2.41		0.874	0.017		13.72	0.15		9.25	0.21		0.689	0.021	
10 μM	WT	531	1	#	97.36	2.55		0.902	0.000	###	13.08	0.28		8.86	0.07		0.691	0.005	
	R6/2	526	201		104.09	3.05		0.865	0.025		13.91	0.59		9.01	0.18		0.667	0.033	
5 μM	WT	604	21		101.40	0.91		0.906	0.002	###	13.15	0.04		9.25	0.12		0.714	0.010	##
	R6/2	719	91		109.31	9.05		0.872	0.027		13.93	0.77		9.43	0.27		0.692	0.021	
2 μM	WT	566	11		99.70	1.48		0.898	0.002	##	13.28	0.12		8.93	0.01		0.685	0.006	
	R6/2	762	163		108.73	7.19		0.875	0.019		13.84	0.43		9.40	0.32		0.693	0.005	

Table 5-6 Summary of morphological changes induced in 21-day differentiated NPCs by compound O4 measured by the Operetta. Statistical analysis performed as one-way ANOVA with bonferroni post-hoc test. Difference between WT and R6/2 at each condition represented as *p≤0.05 **p≤0.01 ***p≤0.001. Difference from NC denoted as #p≤0.05, ##p≤0.01, ###p≤0.001 for-WT and §p≤0.05, §§p≤0.01, §§§p≤0.001 for R6/2. WT=wildtype, NC=no compound Std.D=standard deviation, Sig=statistical significance of p-value.

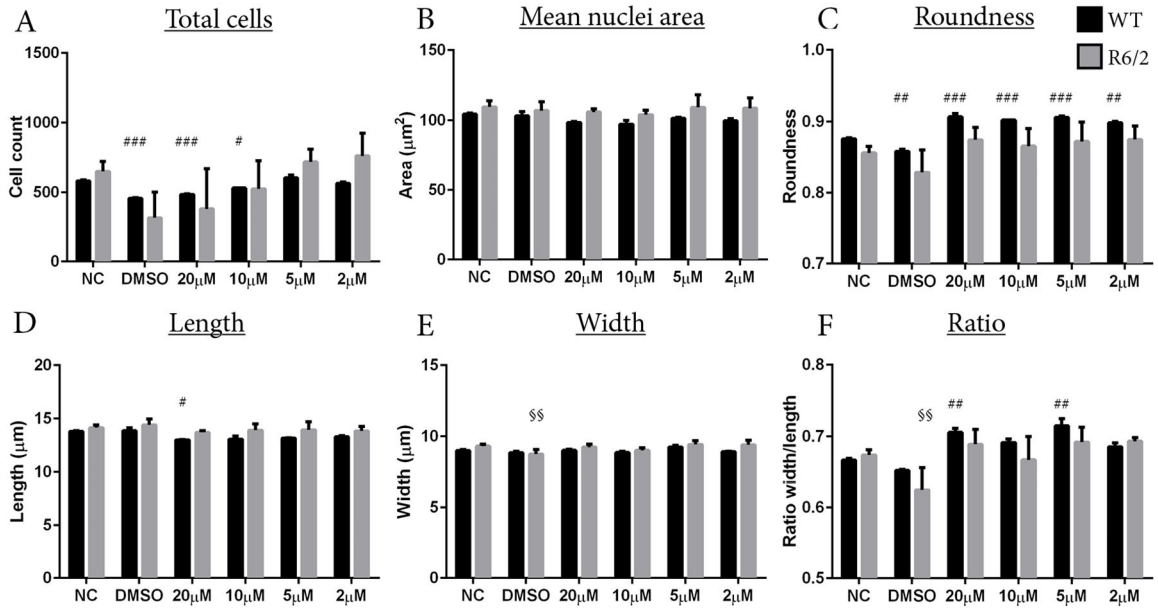

Figure 5-4. Operetta analysis of WT and R6/2 cells after 21 days of O4 application. Automated analysis with the Operetta was used to assess R6/2 and WT cultures differentiated for 21 days in media containing increasing concentrations of the compound O4. (A) Total cells were counted based on DAPI nuclear staining. Analysis of cell morphology for (B) mean size, (C) roundness, (D) length, (E) width, and (F) length:width. Error bars for standard deviation. Statistical analysis carried out using ANOVA with bonferroni post hoc correction. Difference between WT and R6/2 at each condition represented as *p≤0.05 **p≤0.01 ***p≤0.001. Difference from NC denoted as #p≤0.05, ##p≤0.01, ###p≤0.001 for-WT and §p≤0.05, §§p≤0.01, §§§p≤0.001 for R6/2. WT=wildtype, NC=no compound

5.6.2 β-Lapachone

Condition	Gentotype	Total Cells			Nuclear area			Roundness			Length			Width			Ratio		
		Mean	Std.D	Sig.	Mean	Std.D	Sig.	Mean	Std.D	Sig.	Mean	Std.D	Sig.	Mean	Std.D	Sig.	Mean	Std.D	Sig.
NC	WT	613	12		103.02	0.16		0.887	0.001		13.60	0.01		9.08	0.01		0.682	0.001	
	R6/2	582	84		109.30	7.76		0.885	0.009		13.98	0.50		9.39	0.33		0.687	0.011	
DMSO	WT	505	8	###	101.96	0.38		0.877	0.002	#	13.74	0.03		8.89	0.03		0.665	0.003	#
	R6/2	575	105	§§	112.18	11.31		0.877	0.011		14.19	0.67		9.48	0.53		0.683	0.012	
5 μM	WT	796	9	###	104.29	1.77		0.894	0.003		13.52	0.06		9.24	0.08		0.695	0.003	#
	R6/2	903	157	§§	114.47	6.41		0.891	0.006		14.13	0.38		9.76	0.31		0.705	0.008	
2 μM	WT	675	8	##	102.82	0.09		0.900	0.002	##	13.44	0.01		9.13	0.01		0.690	0.002	
	R6/2	920	174	§§	114.51	6.41		0.892	0.006		14.07	0.31		9.81	0.36		0.710	0.014	§
1 μM	WT	713	3	###	106.36	1.54		0.889	0.001		13.68	0.08		9.28	0.08		0.691	0.002	
	R6/2	885	133		117.43	7.87		0.887	0.008		14.24	0.31		9.93	0.45		0.710	0.016	§
0.5 μM	WT	586	2		107.41	1.08		0.887	0.003		13.84	0.05	#	9.29	0.09		0.683	0.005	
	R6/2	793	135		118.63	12.36		0.884	0.014		14.31	0.70		9.96	0.56		0.707	0.007	

Table 5-7 Summary of morphological changes induced in 21-day differentiated NPCs by compound β-Lapachone measured by the Operetta. Statistical analysis performed as one-way ANOVA with bonferroni post-hoc test. Difference between WT and R6/2 at each condition represented as *p≤0.05 **p≤0.01 ***p≤0.001. Difference from NC denoted as #p≤0.05, ##p≤0.01, ###p≤0.001 for-WT and §p≤0.05, §§p≤0.01, §§§p≤0.001 for R6/2. WT=wildtype, NC=no compound Std.D=standard deviation, Sig=statistical significance of p-value.

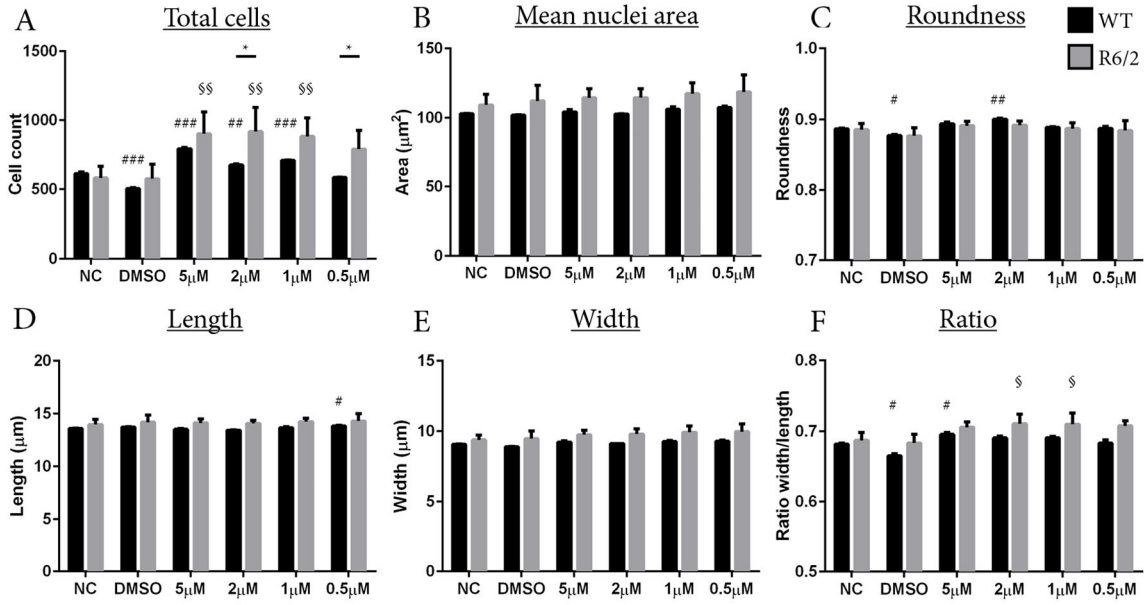

Figure 5-5 Operetta analysis of WT and R6/2 cells after 21 days of β-Lapachone application. Automated analysis with the Operetta was used to assess R6/2 and WT cultures differentiated for 21 days in media containing increasing concentrations of the compound β-Lapachone. (A) Total cells were counted based on DAPI nuclear staining. Analysis of cell morphology for (B) mean size, (C) roundness, (D) length, (E) width, and (F) length:width. Error bars for standard deviation. Statistical analysis carried out using ANOVA with bonferroni post hoc correction. Difference between WT and R6/2 at each condition represented as *p≤0.05 **p≤0.01 ***p≤0.001. Difference from NC denoted as #p≤0.05, ##p≤0.01, ###p≤0.001 for-WT and §p≤0.05, §§p≤0.01, §§§p≤0.001 for R6/2. WT=wildtype, NC=no compound

5.6.3 Quinidine

Condition	Gentotype	Total Cells			Nuclear area			Roundness			Length			Width			Ratio		
		Mean	Std.D	Sig.	Mean	Std.D	Sig.	Mean	Std.D	Sig.	Mean	Std.D	Sig.	Mean	Std.D	Sig.	Mean	Std.D	Sig.
NC	WT	575	2		96.12	1.28		0.899	0.006		13.10	0.16		8.74	0.05		0.683	0.004	
	R6/2	449	101		98.27	4.31		0.899	0.014		13.25	0.23		8.88	0.27		0.686	0.015	
DMSO	WT	662	5		96.01	0.01		0.896	0.003		13.08	0.01		8.75	0.01		0.685	0.001	
	R6/2	335	170		96.89	3.47		0.882	0.020		13.57	0.36		8.53	0.21		0.647	0.022	
20 μM	WT	377	22	#	93.26	1.27		0.892	0.005		13.07	0.22		8.51	0.05		0.670	0.012	
	R6/2	191	119		94.23	7.06		0.884	0.037		13.13	0.58		8.47	0.59		0.663	0.048	
10 μM	WT	576	28		96.14	0.60		0.906	0.001		12.88	0.03		8.93	0.04		0.708	0.003	
	R6/2	345	205		95.35	3.67		0.882	0.019		13.26	0.41		8.53	0.19		0.664	0.026	
5 μM	WT	521	28		97.15	1.05		0.903	0.004		13.10	0.07		8.85	0.11		0.691	0.011	
	R6/2	369	148		97.25	3.62		0.893	0.016		13.25	0.48		8.74	0.11		0.681	0.025	
2 μM	WT	442	50	#	97.20	0.70		0.908	0.005		13.14	0.02		8.82	0.05		0.687	0.003	
	R6/2	458	98		100.59	6.46		0.894	0.013		13.54	0.32		8.87	0.34		0.675	0.012	

Table 5-8. Summary of morphological changes in 21-day differentiated NPCs induced by compound Quinidine measured by the Operetta. Statistical analysis performed as one-way ANOVA with bonferroni post-hoc test. Difference between NC and WT at each condition represented as *p≤0.05 **p≤0.01 ***p≤0.001. Difference from NC denoted as #p≤0.05, ##p≤0.01, ###p≤0.001 for-WT and §p≤0.05, §§p≤0.01, §§§p≤0.001 for R6/2. WT=wildtype, NC=no compound Std.D=standard deviation, Sig=statistical significance of p-value.

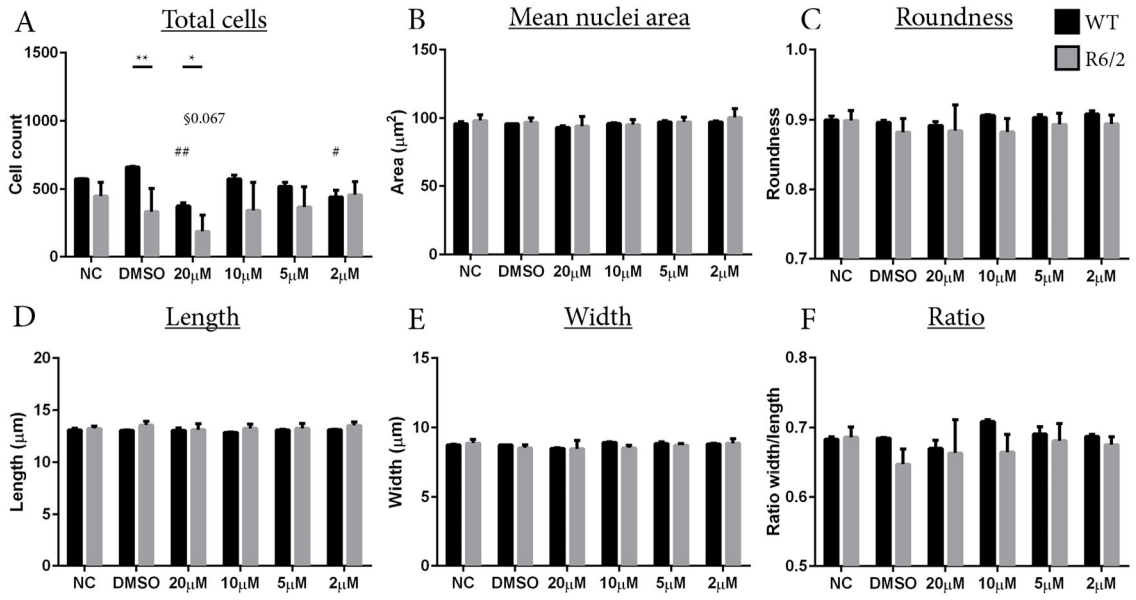

Figure 5-6 Operetta analysis of WT and R6/2 cells after 21 days of Quinidine application. Automated analysis with the Operetta was used to assess R6/2 and WT cultures differentiated for 21 days in media containing increasing concentrations of the compound Quinidine. (A) Total cells were counted based on DAPI nuclear staining. Analysis of cell morphology for (B) mean size, (C) roundness, (D) length, (E) width, and (F) length:width. Error bars for standard deviation. Statistical analysis carried out using ANOVA with bonferroni post hoc correction. Difference between WT and R6/2 at each condition represented as *p≤0.05 **p≤0.01 ***p≤0.001. Difference from NC denoted as #p≤0.05, ##p≤0.01, ###p≤0.001 for-WT and §p≤0.05, §§p≤0.01, §§§p≤0.001 for R6/2. WT=wildtype, NC=no compound.

5.6.4 Hydrazone #6

Condition	Gentotype	Total Cells			Nuclear area			Roundness			Length			Width			Ratio		
		Mean	Std.D	Sig.	Mean	Std.D	Sig.	Mean	Std.D	Sig.	Mean	Std.D	Sig.	Mean	Std.D	Sig.	Mean	Std.D	Sig.
NC	WT	620	5		100.99	0.06		0.866	0.004		13.61	0.06		8.85	0.03		0.665	0.006	
	R6/2	546	204		110.76	13.01		0.853	0.020		14.18	0.70		9.34	0.63		0.674	0.013	
DMSO	WT	456	14	###	103.83	0.19		0.855	0.002		13.99	0.01		8.85	0.00		0.648	0.002	
	R6/2	527	97		111.75	10.93		0.848	0.012		14.47	1.02		9.30	0.33		0.662	0.019	
2 μM	WT	64	7	### §§§	94.61	1.73		0.823	0.059		14.21	0.62		7.86	0.41	#	0.578	0.054	
	R6/2	9	6	§§§	89.01	12.66	§	0.774	0.083	§	13.49	1.52		7.69	0.69	§§§	0.582	0.043	§§§
1 μM	WT	312	4	### §§§	99.92	1.15		0.860	0.002		13.93	0.13		8.54	0.00		0.633	0.007	
	R6/2	70	67	§§§	89.39	12.76	§	0.871	0.037		13.32	1.04		8.32	0.29		0.642	0.031	
0.5 μM	WT	225	3	###	99.56	3.84		0.850	0.006		14.22	0.21		8.26	0.15		0.602	0.000	
	R6/2	166	87	§§§	97.34	7.32		0.844	0.032		14.24	0.44		8.24	0.55	§§§	0.606	0.042	§
0.2 μM	WT	477	21	### §§	102.68	0.27		0.874	0.000		13.88	0.01		8.84	0.06		0.654	0.005	
	R6/2	275	146	§§	101.87	3.64		0.852	0.025		14.17	0.58		8.57	0.38		0.631	0.035	

Table 5-9. Summary of morphological changes in 21-day differentiated NPCs induced by compound Hydrazone #6 measured by the Operetta. Statistical analysis performed as one-way ANOVA with bonferroni post-hoc test. Difference between WT and R6/2 at each condition represented as *p≤0.05 **p≤0.01 ***p≤0.001. Difference from NC denoted as #p≤0.05, ##p≤0.01, ###p≤0.001 for-WT and §p≤0.05, §§p≤0.01, §§§p≤0.001 for R6/2. WT=wildtype, NC=no compound Std.D=standard deviation, Sig=statistical significance of p-value.

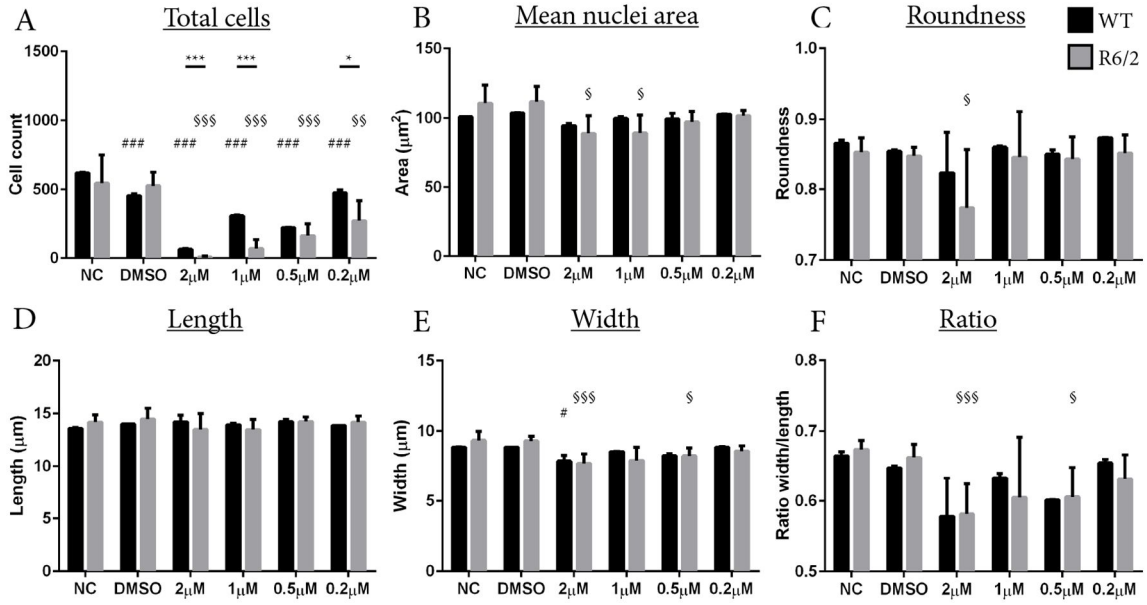

Figure 5-7 Operetta analysis of WT and R6/2 cells after 21 days of Hydrazone #6 application. Automated analysis with the Operetta was used to assess R6/2 and WT cultures differentiated for 21 days in media containing increasing concentrations of the compound Hydrazone #6. (A) Total cells were counted based on DAPI nuclear staining. Analysis of cell morphology for (B) mean size, (C) roundness, (D) length, (E) width, and (F) length:width. Error bars for standard deviation. Statistical analysis carried out using ANOVA with bonferroni post hoc correction. Difference between WT and R6/2 at each condition represented as *p≤0.05 **p≤0.01 ***p≤0.001. Difference from NC denoted as #p≤0.05, ##p≤0.01, ###p≤0.001 for-WT and §p≤0.05, §§p≤0.01, §§§p≤0.001 for R6/2. WT=wildtype, NC=no compound

5.6.5 Hydrazone #9

Condition	Gentotype	Total Cells			Nuclear area			Roundness			Length			Width			Ratio		
		Mean	Std.D	Sig.	Mean	Std.D	Sig.	Mean	Std.D	Sig.	Mean	Std.D	Sig.	Mean	Std.D	Sig.	Mean	Std.D	Sig.
NC	WT	878	26		101.74	0.56		0.900	0.001		13.37	0.03		9.04	0.04		0.689	0.001	
	R6/2	610	47		106.23	7.38		0.899	0.014		13.67	0.58		9.32	0.24		0.699	0.013	
DMSO	WT	878	5		102.37	0.03		0.889	0.000		13.56	0.02		9.05	0.00		0.680	0.001	
	R6/2	514	65		107.72	11.66		0.893	0.005		14.00	0.55		9.24	0.65		0.676	0.022	
5 μM	WT	148	2	###	97.86	8.76		0.880	0.008		13.68	0.81		8.37	0.23	##	0.633	0.019	#
	R6/2	74	57	§§§	87.05	12.45	§	0.831	0.077	§	13.46	1.10		7.73	1.06	§§§	0.614	0.074	§
2 μM	WT	362	13	###	95.41	1.72		0.882	0.014		13.49	0.23		8.37	0.07	##	0.637	0.016	#
	R6/2	203	128	§§§	98.31	7.07		0.880	0.024		13.90	1.30		8.44	0.15		0.631	0.060	
1 μM	WT	527	23	###	100.82	0.67		0.901	0.002		13.43	0.03		8.95	0.08		0.681	0.004	
	R6/2	346	49	§§	100.84	7.08		0.891	0.022		13.62	0.61		8.80	0.34		0.667	0.028	
0.5 μM	WT	827	21		100.10	1.10		0.903	0.002		13.33	0.06		8.94	0.02		0.684	0.000	
	R6/2	529	53		105.89	9.71		0.908	0.009		13.62	0.41		9.25	0.56		0.693	0.018	

Table 5-10. Summary of morphological changes in 21-day differentiaed NPCs induced by compound Hydrazone #9 measured by the Operetta. Statistical analysis performed as one-way ANOVA with bonferroni post-hoc test. Difference between WT and R6/2 at each condition represented as *p≤0.05 **p≤0.01 ***p≤0.001. Difference from NC denoted as #p≤0.05, ##p≤0.01, ###p≤0.001 for-WT and §p≤0.05, §§p≤0.01, §§§p≤0.001 for R6/2. WT=wildtype, NC=no compound Std.D=standard deviation, Sig=statistical significance of p-value.

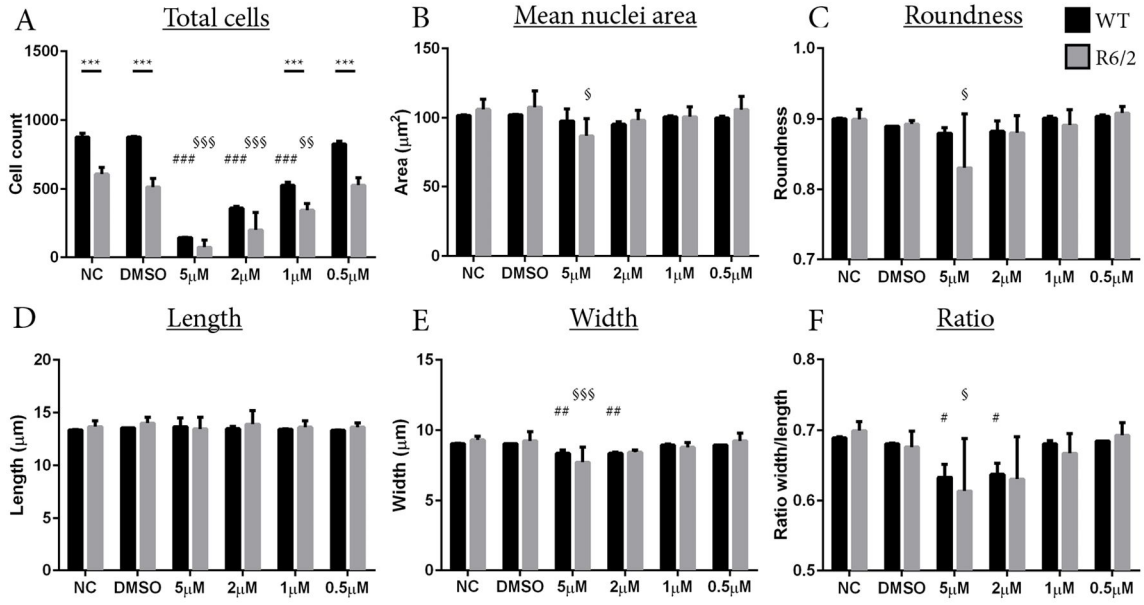

Figure 5-8 Operetta analysis of WT and R6/2 cells after 21 days of Hydrazone #9 application. Automated analysis with the Operetta was used to assess R6/2 and WT cultures differentiated for 21 days in media containing increasing concentrations of the compound Hydrazone #9. (A) Total cells were counted based on DAPI nuclear staining. Analysis of cell morphology for (B) mean size, (C) roundness, (D) length, (E) width, and (F) length:width. Error bars for standard deviation. Statistical analysis carried out using ANOVA with bonferroni post hoc correction. Difference between WT and R6/2 at each condition represented as *p≤0.05 **p≤0.01 ***p≤0.001. Difference from NC denoted as #p≤0.05, ##p≤0.01, ###p≤0.001 for-WT and §p≤0.05, §§p≤0.01, §§§p≤0.001 for R6/2. WT=wildtype, NC=no compound

5.6.6 Guanabenz

Condition	Gentotype	Total Cells			Nuclear area			Roundness			Length			Width			Ratio		
		Mean	Std.D	Sig.	Mean	Std.D	Sig.	Mean	Std.D	Sig.	Mean	Std.D	Sig.	Mean	Std.D	Sig.	Mean	Std.D	Sig.
NC	WT	668	17		102.35	0.78		0.861	0.002		13.75	0.02		8.86	0.05		0.661	0.005	
	R6/2	526	82		105.16	8.53		0.852	0.016		14.06	0.61		9.00	0.35		0.659	0.007	
DMSO	WT	436	8	###	100.39	2.47		0.853	0.001		13.76	0.15		8.68	0.09		0.648	0.000	
	R6/2	275	64	§	103.02	3.55		0.845	0.023		14.16	0.49		8.66	0.20		0.629	0.028	
10 μM	WT	498	10	###	100.23	0.20		0.891	0.002	###	13.34	0.05		9.01	0.06		0.692	0.007	##
	R6/2	216	144	§§	100.56	4.65		0.851	0.060		13.92	1.08		8.69	0.60		0.649	0.068	
5 μM	WT	539	6	###	98.68	0.02		0.895	0.002	###	13.14	0.07	#	8.95	0.01		0.695	0.004	##
	R6/2	389	86		101.15	4.46		0.870	0.008		13.53	0.35		8.90	0.17		0.673	0.012	
2 μM	WT	536	6	###	100.32	0.39		0.885	0.001	###	13.54	0.07		8.88	0.01	*	0.672	0.003	
	R6/2	510	106		106.19	3.27		0.865	0.009		13.86	0.35		9.20	0.12		0.681	0.015	
1 μM	WT	562	5	###	101.71	2.35		0.875	0.005	#	13.76	0.14		8.86	0.12		0.659	0.000	
	R6/2	652	201		110.92	9.20		0.864	0.013		13.99	0.41		9.49	0.53		0.692	0.021	

Table 5-11. Summary of morphological changes in 21-day differentiated NPCs induced by compound Guanabenz measured by the Operetta. Statistical analysis performed as one-way ANOVA with bonferroni post-hoc test. Difference between WT and R6/2 at each condition represented as *p≤0.05 **p≤0.01 ***p≤0.001. Difference from NC denoted as #p≤0.05, ##p≤0.01, ###p≤0.001 for-WT and §p≤0.05, §§p≤0.01, §§§p≤0.001 for R6/2. WT=wildtype, NC=no compound Std.D=standard deviation, Sig=statistical significance of p-value.

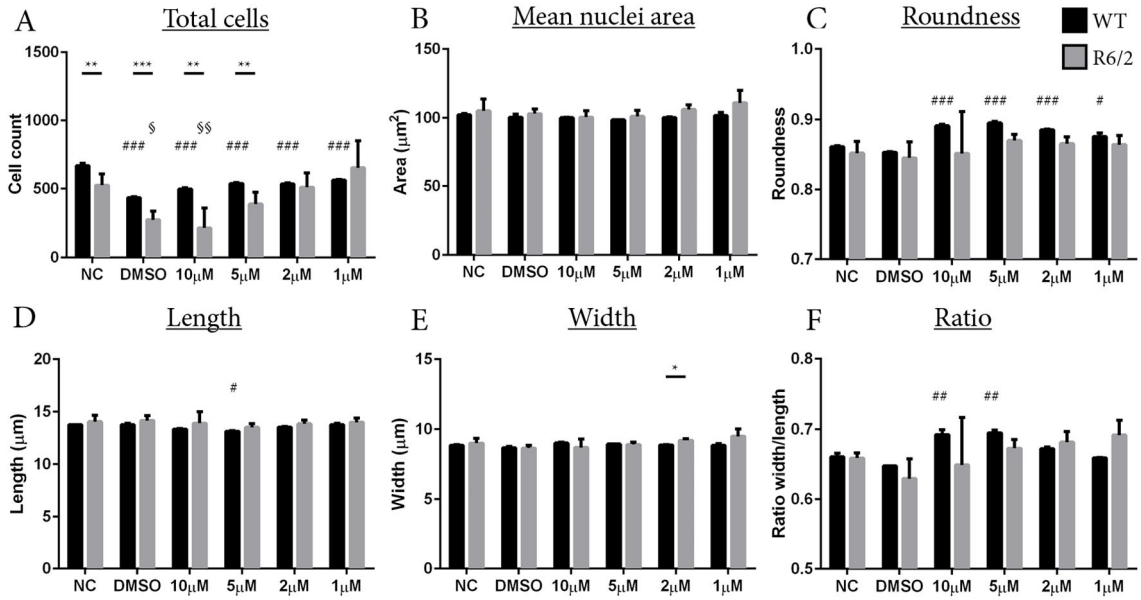

Figure 5-9 Operetta analysis of WT and R6/2 cells after 21 days of Guanabenz application. Automated analysis with the Operetta was used to assess R6/2 and WT cultures differentiated for 21 days in media containing increasing concentrations of the compound Guanabenz. (A) Total cells were counted based on DAPI nuclear staining. Analysis of cell morphology for (B) mean size, (C) roundness, (D) length, (E) width, and (F) length:width. Error bars for standard deviation. Statistical analysis carried out using ANOVA with bonferroni post hoc correction. Difference between WT and R6/2 at each condition represented as *p≤0.05 **p≤0.01 ***p≤0.001. Difference from NC denoted as #p≤0.05, ##p≤0.01, ###p≤0.001 for-WT and §p≤0.05, §§p≤0.01, §§§p≤0.001 for R6/2. WT=wildtype, NC=no compound

5.7 Effects on aggregation.

mHTT aggregation was detected within the nucleus of all cells by S830 ICC, and the R6/2 populations were separated into S830- and S830+ sub-populations based on the S830 threshold, defined in the previous chapter. Within the S830+ population, the number of individual spots per nucleus was calculated. The number of nuclei that reached this S830+ threshold was minimal for the WT cell lines, as expected, and remained so with the application of compounds.

No effect was observed on the number or percentage of S830+ R6/2 cells in the presence O4 (Table 5-13, Figure 5-10) and β-Lapachone (Table 5-15, Figure 5-11). Treatment with both hydrazones (Table 5-19, Figure 5-13, Table 5-21, Figure 5-14) resulted in S830+ R6/2 cell number reduction, to the extent where S830+ R6/2 cells were no longer significantly more abundant than the WT background. However, this was due to the toxicity of the hydrazons rather than any anti-aggregation effect. Quinidine application (Table 5-17, Figure 5-12) also resulted in the number of S830+ R6/2 cells no longer being significantly higher than the WT background. This effect was also observed in the DMSO only control, and so cannot be attributed to the compound alone. Treatment with guanabenz (Table 5-23, Figure 5-15), at its highest concentration, also resulted in the number of S830+ R6/2 cells no longer being significantly higher than the WT background. The percentage of cells this encompassed per culture was not affected, suggesting that an increase in noise in both the WT and R6/2 signal might be behind this alteration. The number of spots of S830 signal within the S830+ nuclei was unaffected by the application of any of the compounds.

Morphological changes to the nuclei between the WT and S830 subgroups were analysed. Nuclear area was only affected by the hydrazons and not the other compounds. The application of the hydrazon compounds also reduced the roundness and width of subgroup

nuclei compared with WT lines, however due to the low number of cells, these data must not be over-interpreted. The roundness of nuclei was unaffected by the other compounds, as was the nuclear length. The width of the S830 subgroup nuclei was significantly increased compared with the WT cells with the application of 2 μM guanabenz. The opposite effect was observed between the S830+ and S830- subgroups with the application of 5 μM quinidine, however the effect was also seen in the DMSO control, albeit at a higher DMSO concentration than the affected quinidine conditions.

The ratio of length:width was affected by the compounds O4, quinidine, and guanabenz. At their lower concentrations these compounds decreased the length:width ratio when comparing the S830 aggregated nuclei with the S830- and WT cells. This suggests a potential elongation of these nuclei. Other differences measured were consistent with either the NC or DMSO controls in those plates and so not considered to be caused by the compounds. The effects of the compounds on aggregation and the morphology of the R6/2 subgroups is summarised in Table 5-12

Compound	Effect
O4	⬆ Ratio (S830+)
β-lapachone	⬆ Length (2 μM)
Quinidine	⬆ Length (2 μM) ⬇ Width (5 μM) ⬇ Ratio
Hydrazone #6	⬇ S830+ number ⬇ Area ⬇ Roundness ⬇ Width
Hydrazone #9	⬇ S830+ number ⬇ Area ⬇ Roundness ⬇ Width
Guanabenz	⬇ S830+ number ⬇ Roundness (2 μM) ⬆ Width (2 μM) ⬇ Ratio(2 μM)

Table 5-12. Summary of compound effects on nuclear morphology and size in the WT and S830+/- subpopulations differentiated NPC lines after 21 days.

5.7.1 O4

Condition	Gentotype	Total S830+ Cells			Percentage S830+ Cells			S830+ Spots		
		Mean	Std.D	Sig.	Mean	Std.D	Sig.	Mean	Std.D	Sig.
NC	WT	4	3	***	0.30	0.24	***			
	R6/2	125	41		18.78	4.71		2.68	0.65	-
DMSO	WT	8	0	*	0.86	0.01	***			
	R6/2	77	42		28.39	11.68		1.69	1.19	-
20 μM	WT	9	4	*	0.87	0.36	*			
	R6/2	66	34		24.15	14.99		1.70	1.19	-
10 μM	WT	3	1	***	0.29	0.09	***			
	R6/2	129	51		25.03	6.34		1.66	1.34	-
5 μM	WT	5	0	***	0.42	0.00	***			
	R6/2	106	41		14.14	3.80		2.34	0.93	-
2 μM	WT	3	1	***	0.23	0.10	***			
	R6/2	140	54		17.65	3.35		2.11	0.65	-

Table 5-13. Summary of nuclear S830 aggregation signal with compound O4 measured by the Operetta. Statistical analysis performed as Students t-test: *p≤0.05, **p≤0.01, ***p≤0.001. WT=wildtype, Std.D=standard deviation, Sig=statistical significance of p-value.

Condition	Gentotype	Nuclear area			Roundness			Length			Width			Ratio		
		Mean	Std.D	Sig.	Mean	Std.D	Sig.	Mean	Std.D	Sig.	Mean	Std.D	Sig.	Mean	Std.D	Sig.
NC	WT	104.39	0.94		0.876	0.001	*	13.82	0.05		9.01	0.06		0.667	0.002	
	S830-	109.86	3.67		0.856	0.012		14.12	0.23		9.36	0.12		0.677	0.009	
	S830+	112.12	8.86		0.849	0.009		14.35	0.44		9.35	0.40		0.667	0.009	
DMSO	WT	103.18	3.06		0.858	0.003		13.88	0.27		8.84	0.10		0.652	0.001	
	S830-	106.82	6.33		0.837	0.033		14.22	0.49		8.82	0.20	##	0.637	0.024	#
	S830+	108.54	3.71		0.808	0.049		14.81	0.88		8.72	0.40		0.608	0.056	
20 μM	WT	98.56	0.74		0.906	0.004		13.01	0.01		9.02	0.09		0.705	0.006	
	S830-	105.26	2.41		0.881	0.011		13.61	0.27		9.28	0.14		0.696	0.022	
	S830+	104.56	6.36		0.870	0.035		13.72	0.66		9.06	0.39		0.676	0.026	
10 μM	WT	97.36	2.55		0.902	0.000		13.08	0.28		8.86	0.07		0.691	0.005	
	S830-	105.58	3.72		0.872	0.025		13.84	0.57		9.17	0.18		0.681	0.030	
	S830+	99.84	3.44		0.855	0.041		13.73	0.53		8.75	0.46		0.654	0.052	
5 μM	WT	101.40	0.91		0.906	0.002		13.15	0.04		9.25	0.12		0.714	0.010	*
	S830-	109.20	9.20		0.876	0.028		13.82	0.75		9.50	0.30		0.702	0.022	
	S830+	110.97	11.19		0.860	0.022		14.34	0.78		9.22	0.45		0.658	0.022	
2 μM	WT	99.70	1.48		0.898	0.002		13.28	0.12		8.93	0.01		0.685	0.006	
	S830-	109.45	7.38		0.878	0.018		13.82	0.42		9.49	0.33		0.700	0.006	**
	S830+	105.46	8.02		0.858	0.024		14.01	0.54		9.00	0.39		0.659	0.012	***

Table 5-14 Summary of morphological changes induced by compound O4 measured by the Operetta between WT and the S830-/+ subgroups. Statistical analysis carried out using ANOVA with bonferroni post hoc correction. Difference between WT and R6/2 subgroups at each condition represented as *p≤0.05 **p≤0.01 ***p≤0.001. Difference from NC denoted as #p≤0.05, ##p≤0.01, ###p≤0.001 for R6/2 S830- and §p≤0.05, §§p≤0.01, §§§p≤0.001 for R6/2 S830+. WT=wildtype, NC=no compound Std.D=standard deviation, Sig=statistical significance of p-value

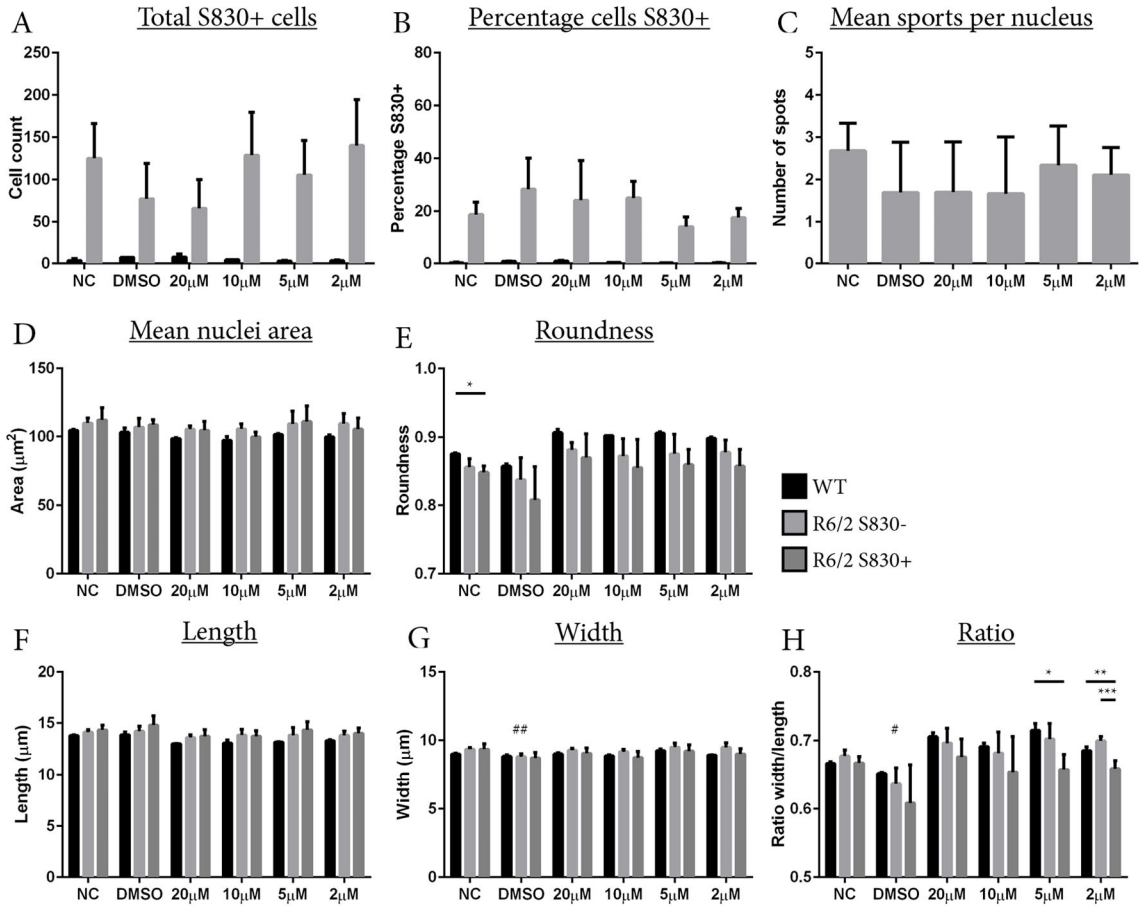

Figure 5-10 Operetta analysis of S830 signal in WT and R6/2 cells after 21 days of O4 application. Automated analysis using the operetta was applied to R6/2 and WT cultures differentiated for 21 days in media containing increasing concentrations of the compound O4 (A) Number of nuclei with a S830 mean intensity above the applied threshold were counted and (B) displayed as a percentage of the total cells analysed. (C) Number of individual intensity spots was calculated and displayed at each time point for three R6/2 lines. The population of S830- and S830+ R6/2 nuclei compared with WT cells for (D) mean size, (E) roundness, (F) length, (G) width, and (H) length:width. Error bars for standard deviation. Statistical analysis carried out using ANOVA with bonferroni post hoc correction. Statistical difference between WT and R6/2 subgroups at each condition represented as *p≤0.05 **p≤0.01 ***p≤0.001. Difference from NC denoted as #p≤0.05, ##p≤0.01, ###p≤0.001 for R6/2 S830- and §p≤0.05, §§p≤0.01, §§§p≤0.001 for R6/2 S830+. WT=wildtype, NC=no compound.

5.7.2 β -Lapachone

Condition	Gentotype	Total S830+ Cells			Percentage S830+ Cells			S830+ Spots		
		Mean	Std.D	Sig.	Mean	Std.D	Sig.	Mean	Std.D	Sig.
NC	WT	15	6	***	1.21	0.51	***			
	R6/2	100	36		16.59	4.48		2.86	0.08	-
DMSO	WT	10	6	**	0.96	0.60	***			
	R6/2	105	43		17.57	4.84		2.72	0.66	-
5 μM	WT	14	11	*	0.85	0.68	***			
	R6/2	154	77		16.18	6.06		2.65	1.13	-
2 μM	WT	7	4	*	0.55	0.30	***			
	R6/2	135	73		13.75	5.20		2.49	0.65	-
1 μM	WT	12	11	*	0.90	0.81	***			
	R6/2	149	80		16.15	6.84		2.92	1.23	-
0.5 μM	WT	18	18	*	1.24	1.27	***			
	R6/2	126	73		15.44	7.72		3.23	1.30	-

Table 5-15. Summary of nuclear S830 aggregation signal with compound β-Lapachone measured by the Operetta. Statistical analysis performed as Students t-test: *p≤0.05, **p≤0.01, ***p≤0.001. WT=wildtype, Std.D=standard deviation, Sig=statistical significance of p-value.

Condition	Gentotype	Nuclear area			Roundness			Length			Width			Ratio		
		Mean	Std.D	Sig.	Mean	Std.D	Sig.	Mean	Std.D	Sig.	Mean	Std.D	Sig.	Mean	Std.D	Sig.
NC	WT	103.02	0.16		0.887	0.001	*	13.60	0.01		9.08	0.01		0.682	0.001	*
	R6/2 S830-	108.81	8.35		0.889	0.009		13.87	0.49		9.43	0.38		0.694	0.010	##§
	R6/2 S830+	112.87	6.76		0.866	0.017		14.55	0.50		9.25	0.30		0.651	0.012	
DMSO	WT	101.96	0.38		0.877	0.002		13.74	0.03		8.89	0.03		0.665	0.003	
	R6/2 S830-	113.21	11.65		0.880	0.011		14.21	0.71		9.58	0.55		0.690	0.017	§§
	R6/2 S830+	109.36	11.24		0.864	0.028		14.35	0.67		9.15	0.68		0.653	0.032	
5 μM	WT	104.29	1.77		0.894	0.003	*	13.52	0.06		9.24	0.08		0.695	0.003	
	R6/2 S830-	114.39	6.42		0.895	0.006		14.04	0.38		9.81	0.30		0.712	0.006	§§
	R6/2 S830+	115.49	7.58		0.873	0.018		14.59	0.57		9.52	0.44		0.672	0.030	
2 μM	WT	102.82	0.09		0.900	0.002	*	13.44	0.01	*	9.13	0.01		0.690	0.002	
	R6/2 S830-	114.62	6.40		0.896	0.005	##§	14.00	0.35		9.88	0.32		0.718	0.011	##§
	R6/2 S830+	113.25	6.69		0.877	0.014		14.32	0.35		9.50	0.44		0.679	0.018	
1 μM	WT	106.36	1.54		0.889	0.001		13.68	0.08		9.28	0.08		0.691	0.002	
	R6/2 S830-	117.82	7.97		0.891	0.007		14.18	0.38		10.01	0.41		0.718	0.010	
	R6/2 S830+	114.54	6.75		0.876	0.018		14.34	0.07		9.58	0.56		0.682	0.034	
0.5 μM	WT	107.41	1.08		0.887	0.003		13.84	0.05		9.29	0.09		0.683	0.005	
	R6/2 S830-	118.52	12.84		0.888	0.014		14.23	0.76		10.02	0.55		0.715	0.007	§§
	R6/2 S830+	118.77	10.96		0.871	0.020		14.56	0.60		9.71	0.56		0.682	0.023	

Table 5-16 Summary of morphological changes induced by compound β-Lapachone measured by the Operetta between WT and the S830-/+ subgroups. Statistical analysis carried out using ANOVA with bonferroni post hoc correction. Difference between WT and R6/2 subgroups at each condition represented as *p≤0.05 **p≤0.01 ***p≤0.001. Difference from NC denoted as #p≤0.05, ##p≤0.01, ###p≤0.001 for R6/2 S830- and §p≤0.05, §§p≤0.01, §§§p≤0.001 for R6/2 S830+. WT=wildtype, NC=no compound Std.D=standard deviation, Sig=statistical significance of p-value

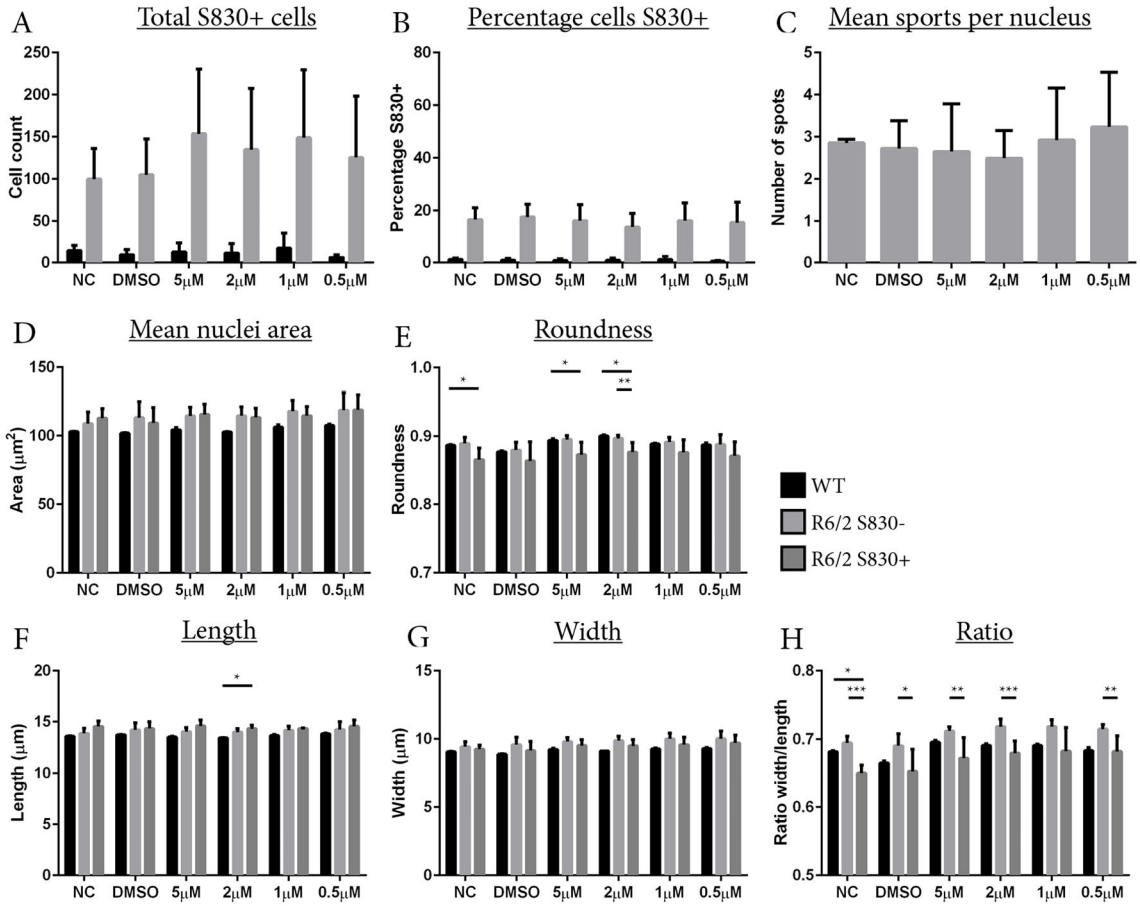

Figure 5-11 Operetta analysis of S830 signal in WT and R6/2 cells after 21days of β-Lapachone application. The automated analysis using the operetta were applied R6/2 and WT cultures differentiated for 21 days in media containing increasing concentrations of the compound β-Lapachone (A) The number of nuclei with a S830 mean intensity above the applied threshold were counted and (B) displayed as a percentage of the total cells analysed. (C) The number of individual intensity spots was calculated and displayed at each time point for 3 three R6/2 lines. The population of S830- and S830+ R6/2 nuclei compared with WT cells for (D) mean size, (E) roundness, (F) length, (G) width, and (H) length:width. Error bars for standard deviation. Statistical analysis carried out using ANOVA with bonferroni post hoc correction. Statistical difference between WT and R6/2 subgroups at each condition represented as *p≤0.05 **p≤0.01 ***p≤0.001. Difference from NC denoted as #p≤0.05, ##p≤0.01, ###p≤0.001 for R6/2 S830- and §p≤0.05, §§p≤0.01, §§§p≤0.001 for R6/2 S830+. WT=wildtype, NC=no compound.

5.7.3 Quinidine

Condition	Gentotype	Total S830+ Cells			Percentage S830+ Cells			S830+ Spots		
		Mean	Std.D	Sig.	Mean	Std.D	Sig.	Mean	Std.D	Sig.
NC	WT	15	6	*	1.30	0.56	***			
	R6/2	129	80		26.69	10.29		2.15	0.86	-
DMSO	WT	21	13	-	1.58	0.95	***			
	R6/2	132	85		37.75	9.01		1.40	0.48	-
20 μM	WT	21	1	-	2.69	0.07	***			
	R6/2	79	61		44.97	18.85		1.44	1.16	-
10 μM	WT	9	8	-	0.97	0.85	***			
	R6/2	131	90		42.40	16.44		1.51	0.99	-
5 μM	WT	19	11	***	1.63	1.07	***			
	R6/2	122	43		34.87	8.43		1.59	0.85	-
2 μM	WT	3	1	**	0.26	0.09	***			
	R6/2	141	62		29.55	7.15		2.08	0.71	-

Table 5-17. Summary of nuclear S830 aggregation signal with compound Quinidine measured by the Operetta. Statistical analysis performed as Students t-test: *p≤0.05, **p≤0.01, ***p≤0.001. WT=wildtype, Std.D=standard deviation, Sig=statistical significance of p-value.

Condition	Gentotype	Nuclear area			Roundness			Length			Width			Ratio		
		Mean	Std.D	Sig.	Mean	Std.D	Sig.	Mean	Std.D	Sig.	Mean	Std.D	Sig.	Mean	Std.D	Sig.
NC	WT	96.12	1.28		0.899	0.006		13.10	0.16		8.74	0.05		0.683	0.004	
	R6/2 S830-	98.45	6.77		0.909	0.007	*	13.13	0.34		8.99	0.33		0.699	0.008	*
	R6/2 S830+	97.70	2.78		0.872	0.029		13.56	0.32		8.56	0.43		0.649	0.037	
DMSO	WT	96.01	0.01		0.896	0.003		13.08	0.01		8.75	0.01		0.685	0.001	
	R6/2 S830-	97.39	3.39		0.901	0.010	*	13.36	0.13	*	8.73	0.24	*	0.671	0.016	*
	R6/2 S830+	95.14	5.47		0.854	0.029		13.77	0.74		8.19	0.34		0.615	0.044	
20 μM	WT	93.26	1.27		0.892	0.005		13.07	0.22		8.51	0.05		0.670	0.012	
	R6/2 S830-	90.70	18.18		0.910	0.025		12.65	1.04		8.48	1.29		0.680	0.073	*
	R6/2 S830+	101.08	17.67		0.863	0.058		13.59	1.28		8.77	0.52		0.669	0.022	
10 μM	WT	96.14	0.60		0.906	0.001		12.88	0.03		8.93	0.04		0.708	0.003	
	R6/2 S830-	93.08	3.03		0.915	0.021	*	12.73	0.41		8.68	0.25		0.698	0.032	*
	R6/2 S830+	94.99	4.17		0.860	0.026		13.56	0.55		8.31	0.32		0.636	0.036	
5 μM	WT	97.15	1.05		0.903	0.004		13.10	0.07		8.85	0.11		0.691	0.011	
	R6/2 S830-	97.37	5.57		0.908	0.008		13.09	0.49		8.90	0.16	*	0.701	0.009	
	R6/2 S830+	96.43	3.31		0.879	0.030		13.37	0.62		8.51	0.30		0.659	0.046	
2 μM	WT	97.20	0.70		0.908	0.005		13.14	0.02	**	8.82	0.05		0.687	0.003	*
	R6/2 S830-	100.27	5.62		0.905	0.013	*	13.33	0.27	*	9.01	0.35		0.693	0.016	*
	R6/2 S830+	103.18	6.95		0.877	0.017		14.08	0.31		8.76	0.39		0.645	0.020	

Table 5-18. Summary of morphological changes induced by compound Quinidine measured by the Operetta between WT and the S830-/+ subgroups. Statistical analysis carried out using ANOVA with bonferroni post hoc correction. Difference between WT and R6/2 subgroups at each condition represented as *p≤0.05 **p≤0.01 ***p≤0.001. Difference from NC denoted as #p≤0.05, ##p≤0.01, ###p≤0.001 for R6/2 S830- and §p≤0.05, §§p≤0.01, §§§p≤0.001 for R6/2 S830+. WT=wildtype, NC=no compound Std.D=standard deviation, Sig=statistical significance of p-value

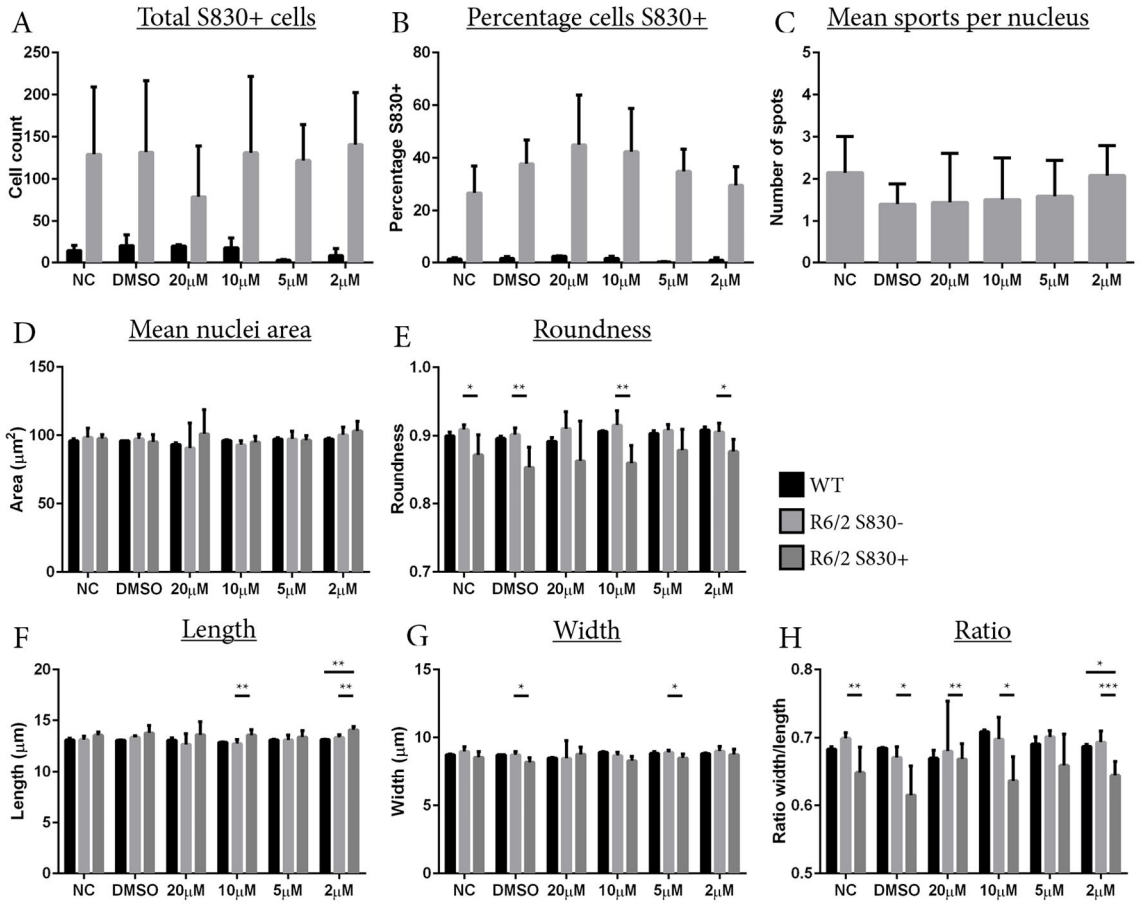

Figure 5-12 Operetta analysis of S830 signal in WT and R6/2 cells after 21days of Quinidine application. The automated analysis using the operetta were applied R6/2 and WT cultures differentiated for 21 days in media containing increasing concentrations of the compound Quinidine (A) The number of nuclei with a S830 mean intensity above the applied threshold were counted and (B) displayed as a percentage of the total cells analysed. (C) The number of individual intensity spots was calculated and displayed at each time point for 3 three R6/2 lines. The population of S830- and S830+ R6/2 nuclei compared with WT cells for (D) mean size, (E) roundness, (F) length, (G) width, and (H) length:width. Error bars for standard deviation. Statistical analysis carried out using ANOVA with bonferroni post hoc correction. Statistical difference between WT and R6/2 subgroups at each condition represented as *p≤0.05 **p≤0.01 ***p≤0.001. Difference from NC denoted as #p≤0.05, ##p≤0.01, ###p≤0.001 for R6/2 S830- and §p≤0.05, §§p≤0.01, §§§p≤0.001 for R6/2 S830+. WT=wildtype, NC=no compound.

5.7.4 Hydrazone #6

Condition	Gentotype	Total S830+ Cells			Percentage S830+ Cells			S830+ Spots		
		Mean	Std.D	Sig.	Mean	Std.D	Sig.	Mean	Std.D	Sig.
NC	WT	18	7	*	1.44	0.58	***			
	R6/2	123	67		22.30	8.87		2.25	1.15	-
DMSO	WT	14	5	***	1.53	0.49	***			
	R6/2	124	34		22.83	4.02		2.34	0.93	-
2 μM	WT	13	10	**	8.98	5.44	-			
	R6/2	3	3	§§	34.34	11.96		1.19	0.44	-
1 μM	WT	12	7		1.18	0.67	*			
	R6/2	37	50	§	41.27	19.89		1.20	0.80	-
0.5 μM	WT	23	0	-	3.64	0.03	**			
	R6/2	64	36		39.89	18.82		0.97	0.79	-
0.2 μM	WT	9	3	*	1.88	0.59	***			
	R6/2	100	46		41.86	16.54		1.06	0.99	-

Table 5-19. Summary of nuclear S830 aggregation signal with compound Hydrazone #6 measured by the Operetta. Statistical analysis performed as Students t-test: *p≤0.05, **p≤0.01, ***p≤0.001. WT=wildtype, Std.D=standard deviation, Sig=statistical significance of p-value.

Condition	Gentotype	Nuclear area			Roundness			Length			Width			Ratio		
		Mean	Std.D	Sig.	Mean	Std.D	Sig.	Mean	Std.D	Sig.	Mean	Std.D	Sig.	Mean	Std.D	Sig.
NC	WT	100.99	0.06		0.866	0.004		13.61	0.06		8.85	0.03		0.665	0.006	
	R6/2 S830-	110.73	14.18		0.859	0.019		14.09	0.79		9.40	0.66		0.681	0.010	
	R6/2 S830+	109.56	7.78		0.850	0.029		14.23	0.60		9.17	0.43		0.663	0.036	
DMSO	WT	103.83	0.19		0.855	0.002		13.99	0.01		8.85	0.00		0.648	0.002	*
	R6/2 S830-	113.24	12.50		0.853	0.009		14.43	0.93		9.44	0.45		0.671	0.019	
	R6/2 S830+	110.19	9.91		0.834	0.018		14.70	1.13		9.00	0.26		0.633	0.026	
2 μM	WT	94.61	1.73		0.823	0.059		14.21	0.62		7.86	0.41		0.578	0.054	
	R6/2 S830-	84.70	10.09	#	0.708	0.036	###	13.71	1.96		7.21	0.65	###	0.551	0.064	#
	R6/2 S830+	101.70	24.98		0.875	0.055	*	14.00	1.40		8.62	1.11		0.619	0.056	
1 μM	WT	99.92	1.15		0.860	0.002		13.93	0.13		8.54	0.00		0.633	0.007	
	R6/2 S830-	83.95	10.72	##	0.901	0.018		12.45	0.52		8.24	0.36		0.672	0.012	*
	R6/2 S830+	90.90	15.42		0.867	0.024		13.40	0.97		8.10	0.73		0.618	0.025	
0.5 μM	WT	99.56	3.84		0.850	0.006		14.22	0.21		8.26	0.15		0.602	0.000	
	R6/2 S830-	95.98	10.14		0.848	0.057		14.34	1.83		8.22	0.75	#	0.612	0.071	
	R6/2 S830+	98.22	3.31		0.847	0.019		14.02	0.43		8.26	0.37		0.608	0.046	
0.2 μM	WT	102.68	0.27		0.874	0.000		13.88	0.01		8.84	0.06		0.654	0.005	
	R6/2 S830-	104.45	10.52		0.867	0.021		14.37	1.23		8.75	0.48		0.635	0.045	
	R6/2 S830+	99.96	4.92		0.837	0.022		13.97	0.69		8.43	0.31		0.626	0.030	

Table 5-20. Summary of morphological changes induced by compound Hydrazone #6 measured by the Operetta between WT and the S830-/+ subgroups. Statistical analysis carried out using ANOVA with bonferroni post hoc correction. Difference between WT and R6/2 subgroups at each condition represented as *p≤0.05 **p≤0.01 ***p≤0.001. Difference from NC denoted as #p≤0.05, ##p≤0.01, ###p≤0.001 for R6/2 S830- and §p≤0.05, §§p≤0.01, §§§p≤0.001 for R6/2 S830+. WT=wildtype, NC=no compound Std.D=standard deviation, Sig=statistical significance of p-value

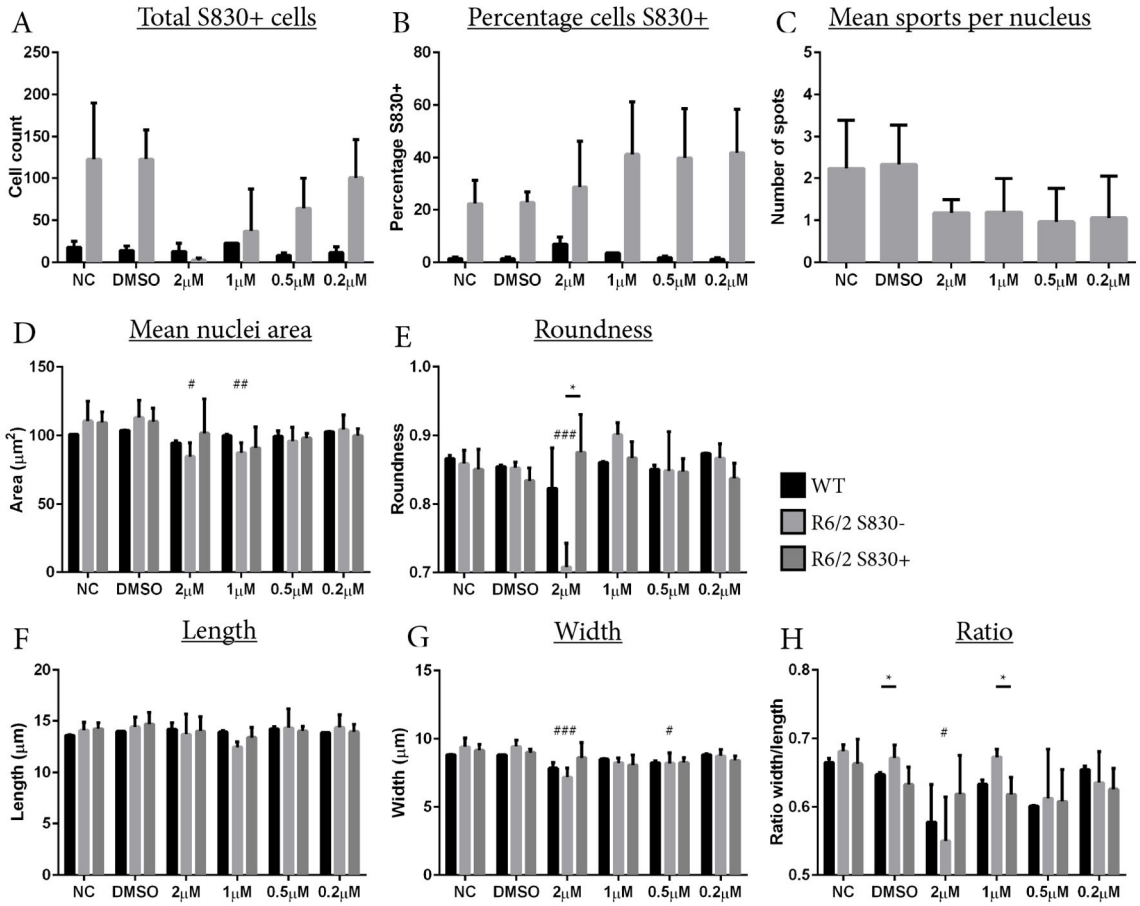

Figure 5-13 Operetta analysis of S830 signal in WT and R6/2 cells after 21days of Hydrazone #6 application. The automated analysis using the operetta were applied R6/2 and WT cultures differentiated for 21 days in media containing increasing concentrations of the compound Hydrazone #6. (A) The number of nuclei with a S830 mean intensity above the applied threshold were counted and (B) displayed as a percentage of the total cells analysed. (C) The number of individual intensity spots was calculated and displayed at each time point for 3 three R6/2 lines. The population of S830- and S830+ R6/2 nuclei compared with WT cells for (D) mean size, (E) roundness, (F) length, (G) width, and (H) length:width. Error bars for standard deviation. Statistical analysis carried out using ANOVA with bonferroni post hoc correction. Statistical difference between WT and R6/2 subgroups at each condition represented as *p≤0.05 **p≤0.01 ***p≤0.001. Difference from NC denoted as #p≤0.05, ##p≤0.01, ###p≤0.001 for R6/2 S830- and §p≤0.05, §§p≤0.01, §§§p≤0.001 for R6/2 S830+. WT=wildtype, NC=no compound.

5.7.5 Hydrazone #9

Condition	Gentotype	Total S830+ Cells			Percentage S830+ Cells			S830+ Spots		
		Mean	Std.D	Sig.	Mean	Std.D	Sig.	Mean	Std.D	Sig.
NC	WT	13	13	***	0.75	0.75	***			
	R6/2	116	14		18.86	2.13		2.56	0.21	-
DMSO	WT	1	0	***	0.04	0.02	***			
	R6/2	102	31		20.09	6.88		2.32	0.50	-
5 μM	WT	24	8	-	7.94	2.68				
	R6/2	27	22		31.05	19.95	§§	0.51	0.63	-
2 μM	WT	7	4	-	0.44	0.25	***			
	R6/2	59	35		32.83	8.36		1.37	0.47	-
1 μM	WT	20	1	**	2.73	0.05	***			
	R6/2	92	34		26.57	9.53		1.83	0.91	-
0.5 μM	WT	14	13	**	1.33	1.30	***			
	R6/2	133	63		25.00	11.06		2.80	1.53	-

Table 5-21. Summary of nuclear S830 aggregation signal with compound Hydrazone #9 measured by the Operetta. Statistical analysis performed as Students t-test: *p≤0.05, **p≤0.01, ***p≤0.001. WT=wildtype, Std.D=standard deviation, Sig=statistical significance of p-value.

Condition	Gentotype	Nuclear area			Roundness			Length			Width			Ratio		
		Mean	Std.D	Sig.	Mean	Std.D	Sig.	Mean	Std.D	Sig.	Mean	Std.D	Sig.	Mean	Std.D	Sig.
NC	WT	101.74	0.56		0.900	0.001		13.37	0.03		9.04	0.04		0.689	0.001	
	R6/2 S830-	105.82	7.67		0.905	0.016		13.59	0.62		9.37	0.25		0.706	0.015	
	R6/2 S830+	106.93	5.80		0.884	0.023		13.92	0.61		9.14	0.21		0.676	0.025	
DMSO	WT	102.37	0.03		0.889	0.000		13.56	0.02		9.05	0.00		0.680	0.001	
	R6/2 S830-	108.24	12.49		0.900	0.005		13.94	0.64		9.34	0.70		0.685	0.028	
	R6/2 S830+	103.99	7.71		0.879	0.014		13.94	0.43		8.89	0.42		0.655	0.011	
5 μM	WT	97.86	8.76		0.880	0.008		13.68	0.81		8.37	0.23		0.633	0.019	
	R6/2 S830-	89.57	14.02		0.852	0.044	##	13.43	0.93		8.29	0.46	##	0.637	0.042	#
	R6/2 S830+	91.15	10.94	§	0.871	0.032		13.05	1.03		8.10	0.30	§§	0.640	0.032	
2 μM	WT	95.41	1.72		0.882	0.014		13.49	0.23		8.37	0.07		0.637	0.016	
	R6/2 S830-	99.45	9.71		0.884	0.023		13.85	1.24		8.51	0.31	#	0.637	0.054	#
	R6/2 S830+	96.31	3.94		0.866	0.030		13.88	1.15		8.34	0.38	§	0.626	0.063	
1 μM	WT	100.82	0.67		0.901	0.002		13.43	0.03		8.95	0.08		0.681	0.004	
	R6/2 S830-	100.89	7.36		0.900	0.010		13.55	0.53		8.86	0.34		0.674	0.019	
	R6/2 S830+	97.92	5.03		0.881	0.032		13.52	0.68		8.58	0.16		0.656	0.035	
0.5 μM	WT	100.10	1.10		0.903	0.002		13.33	0.06		8.94	0.02		0.684	0.000	
	R6/2 S830-	105.10	10.35		0.916	0.008		13.49	0.54		9.29	0.54		0.702	0.015	
	R6/2 S830+	106.86	10.03		0.898	0.019		13.75	0.36		9.22	0.65		0.685	0.026	

Table 5-22. Summary of morphological changes induced by compound Hydrazone #9 measured by the Operetta between WT and the S830-/+ subgroups. Statistical analysis carried out using ANOVA with bonferroni post hoc correction. Difference between WT and R6/2 subgroups at each condition represented as *p≤0.05 **p≤0.01 ***p≤0.001. Difference from NC denoted as #p≤0.05, ##p≤0.01, ###p≤0.001 for R6/2 S830- and §p≤0.05, §§p≤0.01, §§§p≤0.001 for R6/2 S830+. WT=wildtype, NC=no compound Std.D=standard deviation, Sig=statistical significance of p-value

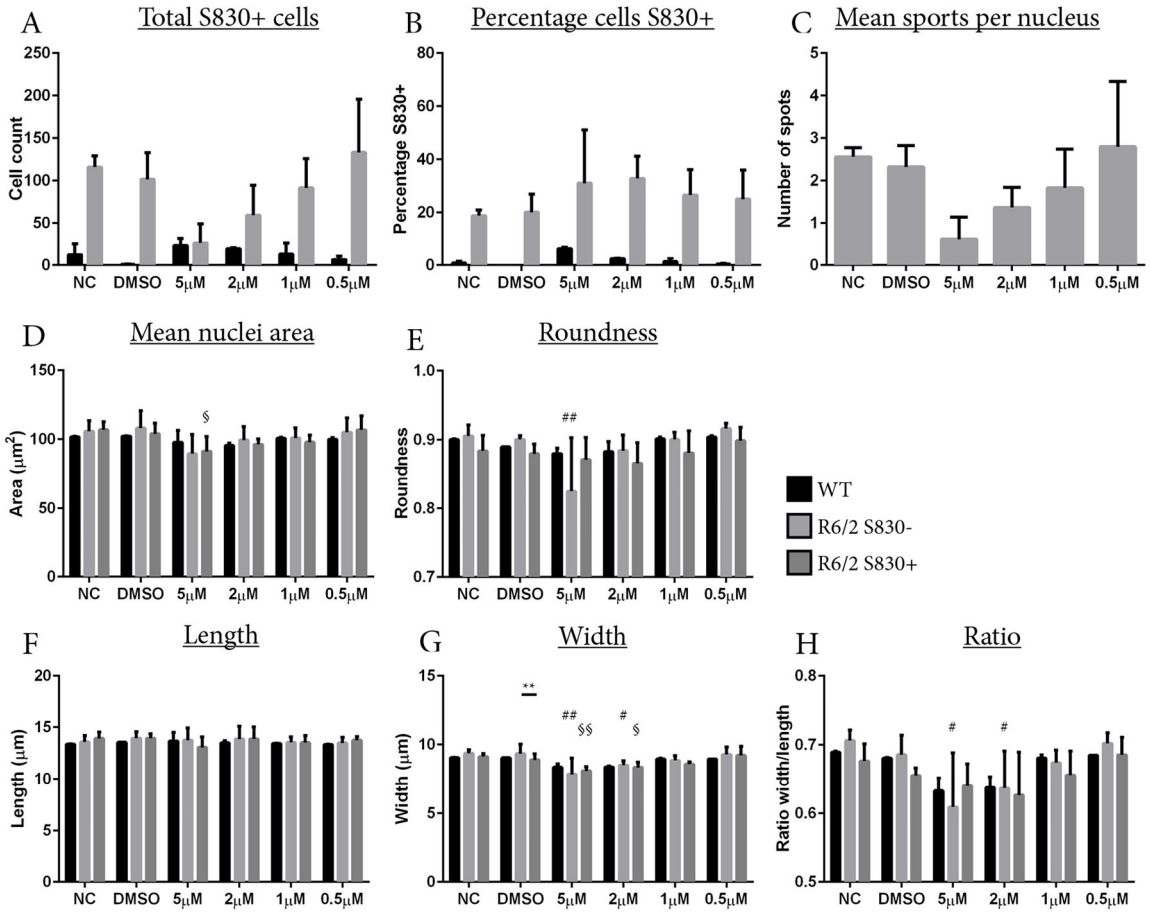

Figure 5-14 Operetta analysis of S830 signal in WT and R6/2 cells after 21days of Hydrazone #9 application. The automated analysis using the operetta were applied R6/2 and WT cultures differentiated for 21 days in media containing increasing concentrations of the compound Hydrazone #9. (A) The number of nuclei with a S830 mean intensity above the applied threshold were counted and (B) displayed as a percentage of the total cells analysed. (C) The number of individual intensity spots was calculated and displayed at each time point for 3 three R6/2 lines. The population of S830- and S830+ R6/2 nuclei compared with WT cells for (D) mean size, (E) roundness, (F) length, (G) width, and (H) length:width. Error bars for standard deviation. Statistical analysis carried out using ANOVA with bonferroni post hoc correction. Statistical difference between WT and R6/2 subgroups at each condition represented as *p≤0.05 **p≤0.01 ***p≤0.001. Difference from NC denoted as #p≤0.05, ##p≤0.01, ###p≤0.001 for R6/2 S830- and §p≤0.05, §§p≤0.01, §§§p≤0.001 for R6/2 S830+. WT=wildtype, NC=no compound.

5.7.6 Guanabenz

Condition	Gentotype	Total S830+ Cells			Percentage S830+ Cells			S830+ Spots		
		Mean	Std.D	Sig.	Mean	Std.D	Sig.	Mean	Std.D	Sig.
NC	WT	27	2	*	1.99	0.16	***			
	R6/2	125	46		22.94	6.07		1.79	0.77	-
DMSO	WT	17	5	**	1.88	0.63	***			
	R6/2	102	33		36.28	7.40		1.25	0.68	-
10 μM	WT	21	14	-	2.08	1.40	***			
	R6/2	68	52		36.79	14.96		1.49	1.93	-
5 μM	WT	16	6	**	1.39	0.56	**			
	R6/2	101	39		27.09	14.56		1.71	1.29	-
2 μM	WT	9	7	***	0.86	0.62	***			
	R6/2	118	9		23.66	5.75		2.25	0.83	-
1 μM	WT	21	10	***	1.97	1.00	***			
	R6/2	118	27		18.43	2.94		2.62	0.18	-

Table 5-23. Summary of nuclear S830 aggregation signal with compound Guanabenz measured by the Operetta. Statistical analysis performed as Students t-test: *p≤0.05, **p≤0.01, ***p≤0.001. WT=wildtype, Std.D=standard deviation, Sig=statistical significance of p-value.

Condition	Gentotype	Nuclear area			Roundness			Length			Width			Ratio		
		Mean	Std.D	Sig.	Mean	Std.D	Sig.	Mean	Std.D	Sig.	Mean	Std.D	Sig.	Mean	Std.D	Sig.
NC	WT	102.35	0.78		0.861	0.002		13.75	0.02		8.86	0.05		0.661	0.005	
	R6/2 S830-	104.62	9.43		0.858	0.017		13.94	0.70		9.05	0.39		0.668	0.017	
	R6/2 S830+	107.24	8.27		0.850	0.021		14.21	0.46		9.03	0.41		0.651	0.022	
DMSO	WT	100.39	2.47		0.853	0.001		13.76	0.15		8.68	0.09		0.648	0.000	
	R6/2 S830-	102.98	4.36		0.859	0.012		14.02	0.41		8.82	0.19		0.646	0.010	
	R6/2 S830+	102.82	5.09		0.823	0.038		14.29	0.74		8.52	0.41		0.618	0.051	
10 μM	WT	100.23	0.20		0.891	0.002		13.34	0.05		9.01	0.06		0.692	0.007	
	R6/2 S830-	97.74	12.27		0.861	0.063		13.64	1.38		8.65	0.86		0.658	0.074	
	R6/2 S830+	103.25	8.08		0.845	0.051		14.13	0.77		8.73	0.67		0.641	0.060	
5 μM	WT	98.68	0.02		0.895	0.002		13.14	0.07		8.95	0.01		0.695	0.004	
	R6/2 S830-	99.59	4.85		0.881	0.012		13.28	0.54		8.94	0.13		0.685	0.024	
	R6/2 S830+	99.03	4.98		0.861	0.025		13.59	0.45		8.68	0.46		0.661	0.042	
2 μM	WT	100.32	0.39		0.885	0.001	*	13.54	0.07		8.88	0.01	*	0.672	0.003	
	R6/2 S830-	106.32	3.16		0.871	0.011	#,§	13.74	0.25		9.30	0.14	#,§	0.694	0.010	§§
	R6/2 S830+	107.33	4.79		0.848	0.018		14.24	0.57		9.04	0.13		0.654	0.028	
1 μM	WT	101.71	2.35		0.875	0.005		13.76	0.14		8.86	0.12		0.659	0.000	
	R6/2 S830-	111.24	9.51		0.866	0.014		13.95	0.44		9.56	0.52		0.698	0.018	
	R6/2 S830+	109.12	9.12		0.865	0.015		14.01	0.36		9.27	0.59		0.676	0.030	

Table 5-24. Summary of morphological changes induced by compound Guanabenz measured by the Operetta between WT and the S830-/+ subgroups. Statistical analysis carried out using ANOVA with bonferroni post hoc correction. Difference between WT and R6/2 subgroups at each condition represented as *p≤0.05 **p≤0.01 ***p≤0.001. Difference from NC denoted as #p≤0.05, ##p≤0.01, ###p≤0.001 for R6/2 S830- and §p≤0.05, §§p≤0.01, §§§p≤0.001 for R6/2 S830+. WT=wildtype, NC=no compound Std.D=standard deviation, Sig=statistical significance of p-value

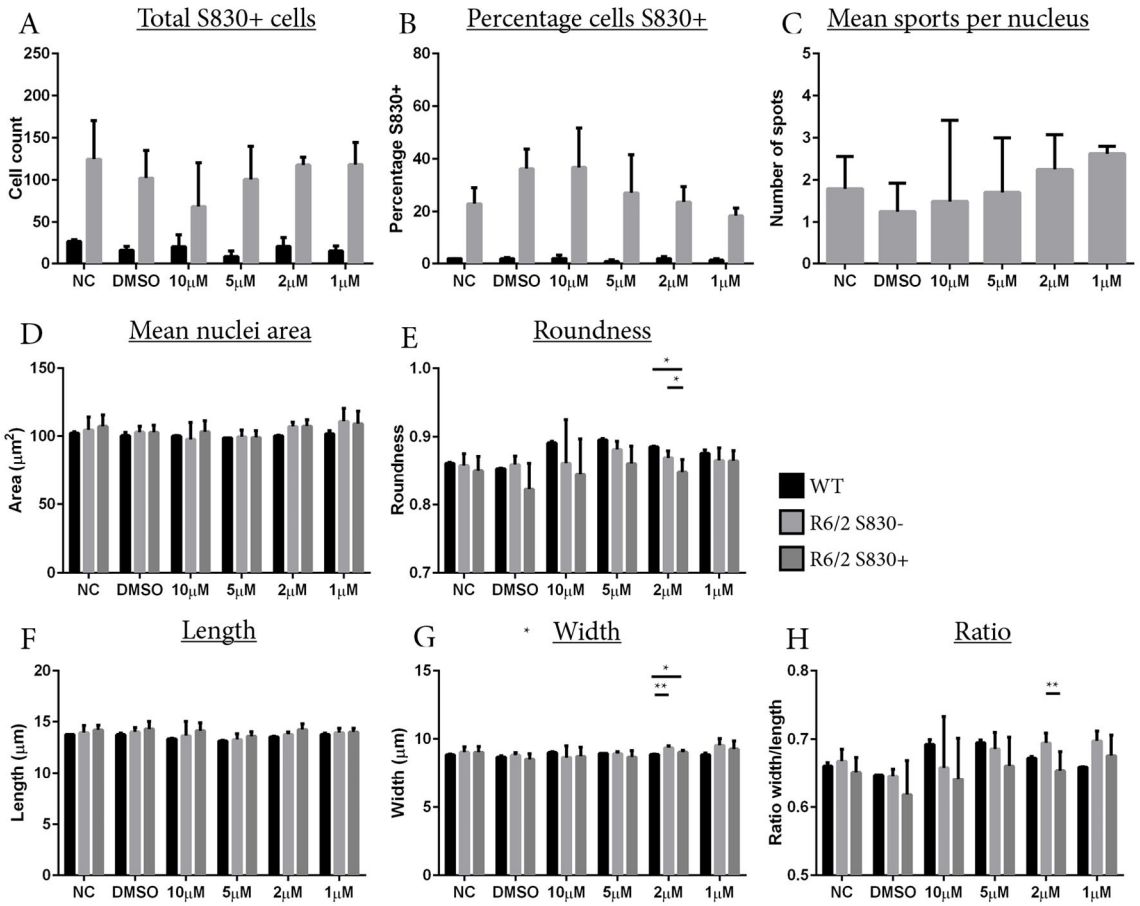

Figure 5-15 Operetta analysis of S830 signal in WT and R6/2 cells after 21days of Guanabenz application. The automated analysis using the operetta were applied R6/2 and WT cultures differentiated for 21 days in media containing increasing concentrations of the compound Guanabenz. (A) The number of nuclei with a S830 mean intensity above the applied threshold were counted and (B) displayed as a percentage of the total cells analysed. (C) The number of individual intensity spots was calculated and displayed at each time point for 3 three R6/2 lines. The population of S830- and S830+ R6/2 nuclei compared with WT cells for (D) mean size, (E) roundness, (F) length, (G) width, and (H) length:width. Error bars for standard deviation. Statistical analysis carried out using ANOVA with bonferroni post hoc correction. Statistical difference between WT and R6/2 subgroups at each condition represented as *p≤0.05 **p≤0.01 ***p≤0.001. Difference from NC denoted as #p≤0.05, ##p≤0.01, ###p≤0.001 for R6/2 S830- and §p≤0.05, §§p≤0.01, §§§p≤0.001 for R6/2 S830+. WT=wildtype, NC=no compound.

5.8 Chapter discussion

5.8.1 Compound effects

The were compounds applied to the NSCs and the effect on the cells screened using the automated operetta machine. The total number of cells in cultures after differentiation was affected by all compounds. O4, quinidine, and guanabenz reduction in cells compared with the NC condition was also seen in the DMSO control, suggesting this effect might not be purely compound related. The hydrazones caused a reduction in cell number to a much larger extent. Both hydrazone compounds, at their highest concentrations, resulted in a considerable degree of cell death, suggesting their toxicity was more extensive over the longer culture period than in the initial toxicity experiment. β-lapachone had the opposite effect and resulted in an increase in cell numbers in the culture, while a reduction in cell number was still seen in the DMSO controls.

The mean area of the WT and R6/2 nuclei was unaffected by treatment with the compounds apart from with the hydrazones, which must be taken in the context of the great reduction in cell number that resulted from hydrazone treatment. Nuclear roundness was affected by O4, β-lapachone, and guanabenz. A similar effect was observed by β-lapachone on the WT cells, with an increase in roundness. The length of WT nuclei, as measured by the thickness through the centre of its longest point, was slightly reduced by O4 and guanabenz. No effect was seen on the thickness of the R6/2 nuclei by the application of these compounds, nor by the other compounds in the WT cells. The width of nuclei, as measured by the thickness through the centre perpendicular to the longest point, was reduced by the highest concentration of both hydrazones. This effect once again might be adversely affected due to the low number of cells surviving in these cultures. The ratio of length:width was affected by treatment with O4, β-lapachone, guanabenz, and the hydrazones.

Nuclear area in the presence of S830 was only affected by the hydrazons and not the other compounds. This was one of the main findings that mHTT had on cell morphology and it was an indication that little therapeutic affect was seen by any compounds. The roundness of nuclei was unaffected by the other compounds, as was the nuclear length. The ratio of length:width was affected by the compounds O4, quinidine, and guanabenz. At their lower concentrations these compounds decreased the length:width ratio when comparing the S830 aggregated nuclei with the S830- and WT cells. This suggests a potential elongation of these nuclei.

5.8.2 Using neural progenitor cells for screening

Analysis of cultured cells from mouse models of HD is an ideal complement to the work done *in vivo* using HD mouse models, for mechanistic studies at the cellular level. NPCs can be maintained in as mitotic progenitors or differentiated in to mature adult neurons and glia making them useful to mimic and study phenotypes found during development and disease onset. Cell culture models with reliable, measurable, phenotypes such as the aggregation found in the R6/2 cultures developed in this thesis would make idea models for drug and compound screens.

The use of *in vitro* cultured cells is a necessary intermediate step between drug discovery of HTT interacting and altering compounds and applying these to whole animal systems. The use of high content analysis can allow multiple conditions to be interrogated at the same time in many wells and plates of cells; and automation of data capture and analysis can be performed in a non-biased way. As a proof of principle of the potential of the NPC cultures developed in this thesis, six novel compound from Erich Wanker's lab in Berlin, which had shown HTT alteration effects in aggregation models, were tested on the R6/2 lines. Most of the data is yet to be published and had been performed using synthetic assays. Unfortunately, the amount of compound supplied was finite and so the

experimental design and application was also limited. In hindsight better planning could have optimised the use of compounds.

The potential toxicity of each compound was unknown so as an initial screen the compounds were applied to cell lines at the recommended concentration rages suggested by the Wanker lab. This screen was carried out over 7 days, which in hindsight was too short a period to properly assess compound toxicity and should have been performed for longer. The subsequent testing of the compounds' effects on nuclear morphology and aggregation profile was carried out over a 21-day period with concentrations adapted to suit the findings of the short toxicity screen. Four of the compounds reduced the number of total cells in culture suggesting their true toxicity had been underestimated in the shorter toxicity experiment. This toxicity hampered the testing of the compounds effects on morphology and aggregation, especially in the experiments using the hydrazones, which had only a few surviving cells at the highest concentration.

Another oversight was that at higher magnifications the operetta cannot capture and analyse the outside wells of a 96 well plate, therefore essentially reducing them to 60 well plates. This limits the number of lines and conditions that can be included in a single plate. Ideally more wells would have been used for a larger number of conditions or more replicates. Three separate R6/2 lines were used which was an ample number of biological repeats, however this left room on the plate for only a single WT line as a control. To design similar experiments in the future, power calculations should be performed to check the number of biological and technical replicates is high enough to obtain meaningful results. Preliminary experiments and longer assessments of toxicity will require larger quantities of compound, the amount of which was limited in this thesis.

The data captured here were not ideal for the reasons stated but the goal of testing whether the high throughput platform could be applied to measure the effects of compounds on

HD-related phenotypes in the cell lines was achieved. With further optimisation and additional resources, greater degree of statistical power could be achieved.

High-content/high-throughput imaging is based on the phenotypic assessment of a variety of physical measures and biological activities. The use of imaging platforms with ability to asses ICC in four fluorescent channels allows for correlation between captured signals of multiple proteins. These data in this chapter have only utilised two or those channels, with Dapi nuclei signal assessed along with S830 mHTT antibody. This leaves scope for two other proteins of interest to be investigated in any follow up use of these cells.

5.9 Summary

The compounds supplied from our collaborators were applied to cultures of WT and R6/2 during differentiation of the cells over a 21-day period. The initial toxicity screen was performed over a 7-day period and showed the need to reduce the concentrations of three of the six compounds. Despite reducing their concentration after the initial toxicity screen, some compounds were still toxic at the lower applied concentrations when the cells were treated for a longer period. The effects of the compounds were marginal on the morphology and aggregation within the cells. As a proof of principle, the use of the cultures created here are ideal for compound screens and will be useful for testing other promising compounds.

Chapter 6 General Discussion

In this thesis novel neural progenitor cell lines were created from the brains of foetal R6/2 and WT mice. This process of harvesting NPCs from foetal brains builds mainly upon the work of the Reynolds and Weiss in the 1990s and the Catteneo lab in the 2000s. This principle was applied to R6/2 mice to establish cell models of HD carrying the human *HTT* gene alongside WT litter mates. These lines were maintained as adherent proliferative monolayer cultures over many passages and banked at regular intervals without affects to karyotype or CAG repeat length. Cultures could be readily differentiated into mixed glia and neuronal populations via modifications to a growth factor free media. Evidence for potential functional neuronal networks was observed with synaptic proteins present at neurite junctions. R6/2 cultures expressed a HTT aggregation phenotype from day 14 of differentiation in a subset of cells. Aggregated detergent insoluble mHTT was detectable by western blot analysis, and observable by ICC as nuclear inclusions, similar to those observed in the R6/2 mouse brain (Davies et al., 1997). The Operetta high throughput analysis system was used to explore morphological difference between WT and R6/2 cultures, as well as within the subset of cells with detectable aggregation. R6/2 nuclei were found to be larger than those of WT cells. This automated analysis system was used as readout to test the effects of aggregation modifying compounds on the R6/2 cell inclusion phenotype after prolonged exposure in differentiation media.

The cell lines created within this thesis advance the HD research field because they form mHTT aggregation without the need for outside influence, such as viral, mechanical or chemical induction. Cell lines with HD-like phenotypes to allow researchers to examine the disease mechanism are greatly needed. To my knowledge, the lines produced in this thesis are the first developed from NPCs dissected from foetal mouse brains that have

successfully been used to model aggregation in neurodegerative disease. Aggregation of mutant or modified protein is observed in a variety of neurodegenerative diseases including Alzheimer's disease, Parkinson's disease, and amyotrophic lateral sclerosis, as well as many others. Based on the approach taken within this thesis, similar methods could be used within these research fields to model disease mechanisms. The usefulness of these lines was demonstrated using a high throughput compound screen. Experiments using the cells produced here with their aggregation phenotype will help researchers to understand how the aggregation of mHTT begins and how it relates to HD symptoms and neuropathology.

6.1 Future Directions

The ability for the cell lines developed here to be used in high content microscopy analysis makes them ideal for the testing of aggregation altering compounds. Further optimisation of the high throughput systems to detect other useful measures of cell morphology and aspects of the aggregation phenotype detected would be useful. The Operetta system and its software (Harmony) have many algorithms that were not used in the analysis performed in this thesis. These further advanced algorithms could potentially allow new novel measures and HD-like phenotypes to be uncovered, such as morphology of the total cell area, beyond the nuclear measures, or neuronal neurite length along with further analysis of the aggregated inclusions.

Primary experiments using the cell lines developed in this thesis have now been carried out using a time-lapse imaging system called PhaseFocus. This technology uses high-fidelity quantitative imaging and microscopy to capture brightfield images and to refocus post-capture if required. Using these images, cells can be tracked over time and information on their number, confluence, proliferation, thickness, volume, and dry mass all obtained. Further work using this system will allow differences between the WT and

R6/2 cultures to be measured while the cells are still mitotic. Cells could then be differentiated and their fates could be traced back to investigate whether single parent cells spawn similar daughter cells with the same fate potential. The PhaseFocus system could also be used to determine whether the sub-population that have detectable aggregation are descended from a single population of parents cells.

Low neurogenic potential limits the study of the molecular effects of HD on neurons, even when detectable aggregation is not present. It would be interesting to use electrophysiology on the neurons in these cultures to both establish their maturity and to probe for rudimental *in vitro* phenotypes recorded *in vivo* with HD mouse models. This would require further development and optimisation of the differentiation protocol and media to attempt to increase the number of neurons or to isolate them using sorting techniques.

In the HD brain and HD mouse models, aggregation is most readily but not exclusively found in neurons (Tong et al., 2014, Shin et al., 2005, Jansen et al., 2016). It cannot be presumed that the population of cells that have limited marker expression are of either a neuronal or glia cell type. Without a method to identify the fates of these cells, experiments to assess the effects of aggregation on mature cell activity such as trafficking in dendrites will be limited. Unless other markers can be found, the isolation of definable populations might be the approach required study these cells.

The R6/2 cell lines developed in this thesis will be fragment models of HD, akin to the R6/2 line, which models the incomplete mRNA splicing that results in an exon 1 HTT protein. The presence of this incomplete splicing event has been found in the human HD brain as well as HD mouse models and could be important in the pathology of the disease. The R6/2 lines developed could be useful in investigating how this splicing contributes to the disease mechanism.

The R6/2 mouse model is a fragment model of HD expressing the first HTT exon to replicate HD. Other mouse models exist using different approaches, such as the knock in lines with endogenous mouse *Htt* expanded to a pathogenic length, exhibit similar HD-like phenotypes but at a slower progression. It would be interesting to develop NSC lines from these other mouse models to examine if aggregation could be detected in vitro. Depending on the CAG length within the knock in line, it can take months before phenotypes can be detected. This may hamper the ability to detect aggregation within a reasonable time frame that cells can be cultured and maintained. If this was to be achieved it would give an excellent insight into how aggregation forms in the cells and if it follows a similar pattern to that observed in this thesis.

The nature of the culture environment appears to limit how long cells can survive once differentiated. To probe the aggregation phenotype further, longer culture conditions would be ideal. In the R6/2 mouse brain the aggregation process is progressive. Not all cells develop inclusions in the same time frame, and indeed, it is not until the later stages of the 16-week lifespan that the majority of neurons in the striatum and cortex display a detectable phenotype. Ageing the differentiated R6/2 cells would allow an investigation into if this was also the case *in vitro*.

6.2 Final conclusions

This thesis presents a series of progressive experiments that have allowed new NPC lines to be established from the R6/2 mouse model of HD. These lines exhibit a measurable progressive aggregation phenotype similar to that seen *in vivo*. There has been a gap in the research field for *in vitro* cellular models that exhibit such a phenotype to complement the work done using the mouse model. The NPC model will allow further investigation into the mechanisms that underlie preferential HTT aggregation in some cells over others.

The expression of the aggregation phenotype was measurable using high-content imaging systems and so is ideal as a model for screening aggregation modifying compounds. The cell lines were probed in a proof of principle experiment with 6 compounds which have shown effects on aggregation in other experimental systems. Although the effects on aggregation were limited on this platform, the potential for further investigation remains. These cell lines will help the HD research community further work towards understanding, and hopefully one-day developing disease-modifying treatments for HD.

Chapter 7 References

AIKEN, C. T., STEFFAN, J. S., GUERRERO, C. M., KHASHWJI, H., LUKACSOVICH, T., SIMMONS, D., PURCELL, J. M., MENHAJI, K., ZHU, Y. Z., GREEN, K., LAFERLA, F., HUANG, L., THOMPSON, L. M. & MARSH, J. L. 2009. Phosphorylation of threonine 3: implications for Huntingtin aggregation and neurotoxicity. *J Biol Chem,* 284**,** 29427-36.

ALBERTS, B. 2012. The breakthroughs of 2012. *Science,* 338**,** 1511.

ALBRECHT, S., BOURDEAU, M., BENNETT, D., MUFSON, E. J., BHATTACHARJEE, M. & LEBLANC, A. C. 2007. Activation of caspase-6 in aging and mild cognitive impairment. *Am J Pathol,* 170**,** 1200-9.

ALEXSON, T. O., HITOSHI, S., COLES, B. L., BERNSTEIN, A. & VAN DER KOOY, D. 2006. Notch signaling is required to maintain all neural stem cell populations--irrespective of spatial or temporal niche. *Dev Neurosci,* 28**,** 34-48.

ALTAR, C. A., CAI, N., BLIVEN, T., JUHASZ, M., CONNER, J. M., ACHESON, A. L., LINDSAY, R. M. & WIEGAND, S. J. 1997. Anterograde transport of brain-derived neurotrophic factor and its role in the brain. *Nature,* 389**,** 856-60.

AN, M. C., ZHANG, N., SCOTT, G., MONTORO, D., WITTKOP, T., MOONEY, S., MELOV, S. & ELLERBY, L. M. 2012. Genetic correction of Huntington's disease phenotypes in induced pluripotent stem cells. *Cell Stem Cell,* 11**,** 253-63.

ANDRADE, M. A. & BORK, P. 1995. HEAT repeats in the Huntington's disease protein. *Nat Genet,* 11**,** 115-6.

ANSALONI, A., WANG, Z. M., JEONG, J. S., RUGGERI, F. S., DIETLER, G. & LASHUEL, H. A. 2014. One-pot semisynthesis of exon 1 of the Huntingtin protein: new tools for elucidating the role of posttranslational modifications in the pathogenesis of Huntington's disease. *Angew Chem Int Ed Engl,* 53**,** 1928-33.

ANTHONY, T. E. & HEINTZ, N. 2008. Genetic lineage tracing defines distinct neurogenic and gliogenic stages of ventral telencephalic radial glial development. *Neural Dev,* 3**,** 30.

APTE, M. V., HABER, P. S., APPLEGATE, T. L., NORTON, I. D., MCCAUGHAN, G. W., KORSTEN, M. A., PIROLA, R. C. & WILSON, J. S. 1998. Periacinar stellate shaped cells in rat pancreas: identification, isolation, and culture. *Gut,* 43**,** 128-33.

ARRASATE, M., MITRA, S., SCHWEITZER, E. S., SEGAL, M. R. & FINKBEINER, S. 2004. Inclusion body formation reduces levels of mutant huntingtin and the risk of neuronal death. *Nature,* 431**,** 805-10.

AZARI, H., SHARIFIFAR, S., RAHMAN, M., ANSARI, S. & REYNOLDS, B. A. 2011. Establishing embryonic mouse neural stem cell culture using the neurosphere assay. *J Vis Exp*.

BABCOCK, D. T. & GANETZKY, B. 2015. Transcellular spreading of huntingtin aggregates in the Drosophila brain. *Proc Natl Acad Sci U S A,* 112**,** E5427-33.

BAKER, M. 2012. Gene-editing nucleases. *Nat Methods,* 9**,** 23-6.

BALLESTERO, J. A., PLAZAS, P. V., KRACUN, S., GOMEZ-CASATI, M. E., TARANDA, J., ROTHLIN, C. V., KATZ, E., MILLAR, N. S. & ELGOYHEN, A. B. 2005. Effects of quinine, quinidine, and chloroquine on alpha9alpha10 nicotinic cholinergic receptors. *Mol Pharmacol,* 68**,** 822-9.

BALLESTEROS-YANEZ, I., BENAVIDES-PICCIONE, R., ELSTON, G. N., YUSTE, R. & DEFELIPE, J. 2006. Density and morphology of dendritic spines in mouse neocortex. *Neuroscience,* 138**,** 403-9.

BARD, J., WALL, M. D., LAZARI, O., ARJOMAND, J. & MUNOZ-SANJUAN, I. 2014. Advances in huntington disease drug discovery: novel approaches to model disease phenotypes. *J Biomol Screen,* 19**,** 191-204.

BARNES, G. T., DUYAO, M. P., AMBROSE, C. M., MCNEIL, S., PERSICHETTI, F., SRINIDHI, J., GUSELLA, J. F. & MACDONALD, M. E. 1994. Mouse Huntington's disease gene homolog (Hdh). *Somat Cell Mol Genet,* 20**,** 87-97.

BASSETT, A. R., TIBBIT, C., PONTING, C. P. & LIU, J. L. 2013. Highly efficient targeted mutagenesis of Drosophila with the CRISPR/Cas9 system. *Cell Rep,* 4**,** 220-8.

BATES, G., TABRIZI, S. & JONES, L. 2014. *Huntington's disease,* Oxford ; New York, Oxford University Press.

BATES, G. P., DORSEY, R., GUSELLA, J. F., HAYDEN, M. R., KAY, C., LEAVITT, B. R., NANCE, M., ROSS, C. A., SCAHILL, R. I., WETZEL, R., WILD, E. J. & TABRIZI, S. J. 2015. Huntington disease. *Nat Rev Dis Primers,* 1**,** 15005.

BAUER, P. O., WONG, H. K., OYAMA, F., GOSWAMI, A., OKUNO, M., KINO, Y., MIYAZAKI, H. & NUKINA, N. 2009. Inhibition of Rho kinases enhances the degradation of mutant huntingtin. *J Biol Chem,* 284**,** 13153-64.

BEAL, M. F. 1994. Huntington's disease, energy, and excitotoxicity. *Neurobiol Aging,* 15**,** 275-6.

BELINSKY, G. S., MOORE, A. R., SHORT, S. M., RICH, M. T. & ANTIC, S. D. 2011. Physiological properties of neurons derived from human embryonic stem cells using a dibutyryl cyclic AMP-based protocol. *Stem Cells Dev,* 20**,** 1733-46.

BENCE, N. F., SAMPAT, R. M. & KOPITO, R. R. 2001. Impairment of the ubiquitin-proteasome system by protein aggregation. *Science,* 292**,** 1552-5.

BENN, C. L., LANDLES, C., LI, H., STRAND, A. D., WOODMAN, B., SATHASIVAM, K., LI, S. H., GHAZI-NOORI, S., HOCKLY, E., FARUQUE, S. M., CHA, J. H., SHARPE, P. T., OLSON, J. M., LI, X. J. & BATES, G. P. 2005. Contribution of nuclear and extranuclear polyQ to neurological phenotypes in mouse models of Huntington's disease. *Hum Mol Genet,* 14**,** 3065-78.

BHATTACHARYYA, A. M., THAKUR, A. K. & WETZEL, R. 2005. polyglutamine aggregation nucleation: thermodynamics of a highly unfavorable protein folding reaction. *Proc Natl Acad Sci U S A,* 102**,** 15400-5.

BIBEL, M., RICHTER, J., LACROIX, E. & BARDE, Y. A. 2007. Generation of a defined and uniform population of CNS progenitors and neurons from mouse embryonic stem cells. *Nat Protoc,* 2**,** 1034-43.

BIELLA, G., DI FEBO, F., GOFFREDO, D., MOIANA, A., TAGLIETTI, V., CONTI, L., CATTANEO, E. & TOSELLI, M. 2007. Differentiating embryonic stem-derived neural stem cells show a maturation-dependent pattern of voltage-gated sodium current expression and graded action potentials. *Neuroscience,* 149**,** 38-52.

BIESCHKE, J., HERBST, M., WIGLENDA, T., FRIEDRICH, R. P., BOEDDRICH, A., SCHIELE, F., KLECKERS, D., LOPEZ DEL AMO, J. M., GRUNING, B. A., WANG, Q., SCHMIDT, M. R., LURZ, R., ANWYL, R., SCHNOEGL, S., FANDRICH, M., FRANK, R. F., REIF, B., GUNTHER, S., WALSH, D. M. & WANKER, E. E. 2012. Small-molecule conversion of toxic oligomers to nontoxic beta-sheet-rich amyloid fibrils. *Nat Chem Biol,* 8**,** 93-101.

BORGHESE, L., DOLEZALOVA, D., OPITZ, T., HAUPT, S., LEINHAAS, A., STEINFARZ, B., KOCH, P., EDENHOFER, F., HAMPL, A. & BRUSTLE, O. 2010. Inhibition of notch signaling in human embryonic stem cell-derived neural stem cells delays G1/S phase transition and accelerates neuronal differentiation in vitro and in vivo. *Stem Cells,* 28**,** 955-64.

BRADLEY, C. K., SCOTT, H. A., CHAMI, O., PEURA, T. T., DUMEVSKA, B., SCHMIDT, U. & STOJANOV, T. 2011. Derivation of Huntington's disease-affected human embryonic stem cell lines. *Stem Cells Dev,* 20**,** 495-502.

BROOKS, B. R., THISTED, R. A., APPEL, S. H., BRADLEY, W. G., OLNEY, R. K., BERG, J. E., POPE, L. E., SMITH, R. A. & GROUP, A.-A. S. 2004. Treatment of pseudobulbar affect in ALS with dextromethorphan/quinidine: a randomized trial. *Neurology,* 63**,** 1364-70.

BROOKS, S., FIELDING, S., DOBROSSY, M., VON HORSTEN, S. & DUNNETT, S. 2009. Subtle but progressive cognitive deficits in the female tgHD hemizygote rat as demonstrated by operant SILT performance. *Brain Res Bull,* 79**,** 310-5.

BROUGHTON, B. R., REUTENS, D. C. & SOBEY, C. G. 2009. Apoptotic mechanisms after cerebral ischemia. *Stroke,* 40**,** e331-9.

BROWN, J. P., COUILLARD-DESPRES, S., COOPER-KUHN, C. M., WINKLER, J., AIGNER, L. & KUHN, H. G. 2003. Transient expression of doublecortin during adult neurogenesis. *J Comp Neurol,* 467**,** 1-10.

CALAKOS, N. & SCHELLER, R. H. 1994. Vesicle-associated membrane protein and synaptophysin are associated on the synaptic vesicle. *J Biol Chem,* 269**,** 24534-7.

CAMNASIO, S., DELLI CARRI, A., LOMBARDO, A., GRAD, I., MARIOTTI, C., CASTUCCI, A., ROZELL, B., LO RISO, P., CASTIGLIONI, V., ZUCCATO, C., ROCHON, C., TAKASHIMA, Y., DIAFERIA, G., BIUNNO, I., GELLERA, C., JACONI, M., SMITH, A., HOVATTA, O., NALDINI, L., DI DONATO, S., FEKI, A. & CATTANEO, E. 2012. The first reported generation of several induced pluripotent stem cell lines from homozygous and heterozygous Huntington's disease patients demonstrates mutation related enhanced lysosomal activity. *Neurobiol Dis,* 46**,** 41-51.

CAMPOS, L. S. 2004. Neurospheres: insights into neural stem cell biology. *J Neurosci Res,* 78**,** 761-9.

CARTER, R. J., LIONE, L. A., HUMBY, T., MANGIARINI, L., MAHAL, A., BATES, G. P., DUNNETT, S. B. & MORTON, A. J. 1999. Characterization of progressive motor deficits in mice transgenic for the human Huntington's disease mutation. *J Neurosci,* 19**,** 3248-57.

CATTANEO, E., RIGAMONTI, D., GOFFREDO, D., ZUCCATO, C., SQUITIERI, F. & SIPIONE, S. 2001. Loss of normal huntingtin function: new developments in Huntington's disease research. *Trends Neurosci,* 24**,** 182-8.

CEPEDA, C., HURST, R. S., CALVERT, C. R., HERNANDEZ-ECHEAGARAY, E., NGUYEN, O. K., JOCOY, E., CHRISTIAN, L. J., ARIANO, M. A. & LEVINE, M. S. 2003. Transient and progressive electrophysiological alterations in the

corticostriatal pathway in a mouse model of Huntington's disease. *J Neurosci,* 23**,** 961-9.

CEPEDA, C., WU, N., ANDRE, V. M., CUMMINGS, D. M. & LEVINE, M. S. 2007. The corticostriatal pathway in Huntington's disease. *Prog Neurobiol,* 81**,** 253-71.

CHAE, J. I., KIM, D. W., LEE, N., JEON, Y. J., JEON, I., KWON, J., KIM, J., SOH, Y., LEE, D. S., SEO, K. S., CHOI, N. J., PARK, B. C., KANG, S. H., RYU, J., OH, S. H., SHIN, D. A., LEE, D. R., DO, J. T., PARK, I. H., DALEY, G. Q. & SONG, J. 2012. Quantitative proteomic analysis of induced pluripotent stem cells derived from a human Huntington's disease patient. *Biochem J,* 446**,** 359-71.

CHENG, P. H., LI, C. L., CHANG, Y. F., TSAI, S. J., LAI, Y. Y., CHAN, A. W., CHEN, C. M. & YANG, S. H. 2013. miR-196a ameliorates phenotypes of Huntington disease in cell, transgenic mouse, and induced pluripotent stem cell models. *Am J Hum Genet,* 93**,** 306-12.

CHIANG, C., JACOBSEN, J. C., ERNST, C., HANSCOM, C., HEILBUT, A., BLUMENTHAL, I., MILLS, R. E., KIRBY, A., LINDGREN, A. M., RUDIGER, S. R., MCLAUGHLAN, C. J., BAWDEN, C. S., REID, S. J., FAULL, R. L., SNELL, R. G., HALL, I. M., SHEN, Y., OHSUMI, T. K., BOROWSKY, M. L., DALY, M. J., LEE, C., MORTON, C. C., MACDONALD, M. E., GUSELLA, J. F. & TALKOWSKI, M. E. 2012. Complex reorganization and predominant non-homologous repair following chromosomal breakage in karyotypically balanced germline rearrangements and transgenic integration. *Nat Genet,* 44**,** 390-7, S1.

CHOJNACKI, A. & WEISS, S. 2008. Production of neurons, astrocytes and oligodendrocytes from mammalian CNS stem cells. *Nat Protoc,* 3**,** 935-40.

CHOU, Y. H., KHUON, S., HERRMANN, H. & GOLDMAN, R. D. 2003. Nestin promotes the phosphorylation-dependent disassembly of vimentin intermediate filaments during mitosis. *Mol Biol Cell,* 14**,** 1468-78.

CHU-LAGRAFF, Q., KANG, X. & MESSER, A. 2001. Expression of the Huntington's disease transgene in neural stem cell cultures from R6/2 transgenic mice. *Brain Res Bull,* 56**,** 307-12.

CICCHETTI, F., LACROIX, S., CISBANI, G., VALLIERES, N., SAINT-PIERRE, M., ST-AMOUR, I., TOLOUEI, R., SKEPPER, J. N., HAUSER, R. A., MANTOVANI, D., BARKER, R. A. & FREEMAN, T. B. 2014. Mutant huntingtin is present in neuronal grafts in Huntington disease patients. *Ann Neurol,* 76**,** 31-42.

CICCHETTI, F. & PARENT, A. 1996. Striatal interneurons in Huntington's disease: selective increase in the density of calretinin-immunoreactive medium-sized neurons. *Mov Disord,* 11**,** 619-26.

CICCHETTI, F., PRENSA, L., WU, Y. & PARENT, A. 2000. Chemical anatomy of striatal interneurons in normal individuals and in patients with Huntington's disease. *Brain Res Brain Res Rev,* 34**,** 80-101.

CIECHANOVER, A. & BRUNDIN, P. 2003. The ubiquitin proteasome system in neurodegenerative diseases: sometimes the chicken, sometimes the egg. *Neuron,* 40**,** 427-46.

CISBANI, G. & CICCHETTI, F. 2012. An in vitro perspective on the molecular mechanisms underlying mutant huntingtin protein toxicity. *Cell Death Dis,* 3**,** e382.

CLAYTON, E., DOUPE, D. P., KLEIN, A. M., WINTON, D. J., SIMONS, B. D. & JONES, P. H. 2007. A single type of progenitor cell maintains normal epidermis. *Nature,* 446**,** 185-9.

CODEGA, P., SILVA-VARGAS, V., PAUL, A., MALDONADO-SOTO, A. R., DELEO, A. M., PASTRANA, E. & DOETSCH, F. 2014. Prospective identification and purification of quiescent adult neural stem cells from their in vivo niche. *Neuron,* 82**,** 545-59.

COLBY, D. W., CASSADY, J. P., LIN, G. C., INGRAM, V. M. & WITTRUP, K. D. 2006. Stochastic kinetics of intracellular huntingtin aggregate formation. *Nat Chem Biol,* 2**,** 319-23.

COLIN, E., ZALA, D., LIOT, G., RANGONE, H., BORRELL-PAGES, M., LI, X. J., SAUDOU, F. & HUMBERT, S. 2008. Huntingtin phosphorylation acts as a molecular switch for anterograde/retrograde transport in neurons. *EMBO J,* 27**,** 2124-34.

CONFORTI, P., CAMNASIO, S., MUTTI, C., VALENZA, M., THOMPSON, M., FOSSALE, E., ZEITLIN, S., MACDONALD, M. E., ZUCCATO, C. & CATTANEO, E. 2013. Lack of huntingtin promotes neural stem cells differentiation into glial cells while neurons expressing huntingtin with expanded polyglutamine tracts undergo cell death. *Neurobiol Dis,* 50**,** 160-70.

CONTI, E., MULLER, C. W. & STEWART, M. 2006. Karyopherin flexibility in nucleocytoplasmic transport. *Curr Opin Struct Biol,* 16**,** 237-44.

CONTI, L. & CATTANEO, E. 2010. Neural stem cell systems: physiological players or in vitro entities? *Nat Rev Neurosci,* 11**,** 176-87.

CONTI, L., POLLARD, S. M., GORBA, T., REITANO, E., TOSELLI, M., BIELLA, G., SUN, Y., SANZONE, S., YING, Q. L., CATTANEO, E. & SMITH, A. 2005. Niche-independent symmetrical self-renewal of a mammalian tissue stem cell. *PLoS Biol,* 3**,** e283.

COOPER, J. K., SCHILLING, G., PETERS, M. F., HERRING, W. J., SHARP, A. H., KAMINSKY, Z., MASONE, J., KHAN, F. A., DELANOY, M., BORCHELT, D. R., DAWSON, V. L., DAWSON, T. M. & ROSS, C. A. 1998. Truncated N-terminal fragments of huntingtin with expanded glutamine repeats form nuclear and cytoplasmic aggregates in cell culture. *Hum Mol Genet,* 7**,** 783-90.

CORNETT, J., CAO, F., WANG, C. E., ROSS, C. A., BATES, G. P., LI, S. H. & LI, X. J. 2005. Polyglutamine expansion of huntingtin impairs its nuclear export. *Nat Genet,* 37**,** 198-204.

CUDKOWICZ, M. & KOWALL, N. W. 1990. Degeneration of pyramidal projection neurons in Huntington's disease cortex. *Ann Neurol,* 27**,** 200-4.

CUMMINGS, C. J., MANCINI, M. A., ANTALFFY, B., DEFRANCO, D. B., ORR, H. T. & ZOGHBI, H. Y. 1998. Chaperone suppression of aggregation and altered subcellular proteasome localization imply protein misfolding in SCA1. *Nat Genet,* 19**,** 148-54.

CUMMINGS, D. M., MILNERWOOD, A. J., DALLERAC, G. M., WAIGHTS, V., BROWN, J. Y., VATSAVAYAI, S. C., HIRST, M. C. & MURPHY, K. P. 2006. Aberrant cortical synaptic plasticity and dopaminergic dysfunction in a mouse model of Huntington's disease. *Hum Mol Genet,* 15**,** 2856-68.

DANOVI, D., FOLARIN, A. A., BARANOWSKI, B. & POLLARD, S. M. 2012. High content screening of defined chemical libraries using normal and glioma-derived neural stem cell lines. *Methods Enzymol,* 506**,** 311-29.

DAVIES, S. W., TURMAINE, M., COZENS, B. A., DIFIGLIA, M., SHARP, A. H., ROSS, C. A., SCHERZINGER, E., WANKER, E. E., MANGIARINI, L. & BATES, G. P. 1997. Formation of neuronal intranuclear inclusions underlies the neurological dysfunction in mice transgenic for the HD mutation. *Cell,* 90**,** 537-48.

DE LA MONTE, S. M., VONSATTEL, J. P. & RICHARDSON, E. P., JR. 1988. Morphometric demonstration of atrophic changes in the cerebral cortex, white matter, and neostriatum in Huntington's disease. *J Neuropathol Exp Neurol,* 47**,** 516-25.

DE LA ROSA, E. J. & DE PABLO, F. 2000. Cell death in early neural development: beyond the neurotrophic theory. *Trends Neurosci,* 23**,** 454-8.

DECKWERTH, T. L. & JOHNSON, E. M., JR. 1993. Temporal analysis of events associated with programmed cell death (apoptosis) of sympathetic neurons deprived of nerve growth factor. *J Cell Biol,* 123**,** 1207-22.

DENG, W., AIMONE, J. B. & GAGE, F. H. 2010. New neurons and new memories: how does adult hippocampal neurogenesis affect learning and memory? *Nat Rev Neurosci,* 11**,** 339-50.

DESMOND, C. R., ATWAL, R. S., XIA, J. & TRUANT, R. 2012. Identification of a karyopherin beta1/beta2 proline-tyrosine nuclear localization signal in huntingtin protein. *J Biol Chem,* 287**,** 39626-33.

DIEZ-ROUX, G., BANFI, S., SULTAN, M., GEFFERS, L., ANAND, S., ROZADO, D., MAGEN, A., CANIDIO, E., PAGANI, M., PELUSO, I., LIN-MARQ, N., KOCH, M., BILIO, M., CANTIELLO, I., VERDE, R., DE MASI, C., BIANCHI, S. A., CICCHINI, J., PERROUD, E., MEHMETI, S., DAGAND, E., SCHRINNER, S., NURNBERGER, A., SCHMIDT, K., METZ, K., ZWINGMANN, C., BRIESKE, N., SPRINGER, C., HERNANDEZ, A. M., HERZOG, S., GRABBE, F., SIEVERDING, C., FISCHER, B., SCHRADER, K., BROCKMEYER, M., DETTMER, S., HELBIG, C., ALUNNI, V., BATTAINI, M. A., MURA, C., HENRICHSEN, C. N., GARCIA-LOPEZ, R., ECHEVARRIA, D., PUELLES, E., GARCIA-CALERO, E., KRUSE, S., UHR, M., KAUCK, C., FENG, G., MILYAEV, N., ONG, C. K., KUMAR, L., LAM, M., SEMPLE, C. A., GYENESEI, A., MUNDLOS, S., RADELOF, U., LEHRACH, H., SARMIENTOS, P., REYMOND, A., DAVIDSON, D. R., DOLLE, P., ANTONARAKIS, S. E., YASPO, M. L., MARTINEZ, S., BALDOCK, R. A., EICHELE, G. & BALLABIO, A. 2011. A high-resolution anatomical atlas of the transcriptome in the mouse embryo. *PLoS Biol,* 9**,** e1000582.

DIFIGLIA, M., SAPP, E., CHASE, K., SCHWARZ, C., MELONI, A., YOUNG, C., MARTIN, E., VONSATTEL, J. P., CARRAWAY, R., REEVES, S. A. & ET AL. 1995. Huntingtin is a cytoplasmic protein associated with vesicles in human and rat brain neurons. *Neuron,* 14**,** 1075-81.

DIFIGLIA, M., SAPP, E., CHASE, K. O., DAVIES, S. W., BATES, G. P., VONSATTEL, J. P. & ARONIN, N. 1997. Aggregation of huntingtin in neuronal intranuclear inclusions and dystrophic neurites in brain. *Science,* 277**,** 1990-3.

DOETSCH, F. & ALVAREZ-BUYLLA, A. 1996. Network of tangential pathways for neuronal migration in adult mammalian brain. *Proc Natl Acad Sci U S A,* 93**,** 14895-900.

DOETSCH, F., PETREANU, L., CAILLE, I., GARCIA-VERDUGO, J. M. & ALVAREZ-BUYLLA, A. 2002. EGF converts transit-amplifying neurogenic precursors in the adult brain into multipotent stem cells. *Neuron,* 36**,** 1021-34.

DRAGATSIS, I., EFSTRATIADIS, A. & ZEITLIN, S. 1998. Mouse mutant embryos lacking huntingtin are rescued from lethality by wild-type extraembryonic tissues. *Development,* 125**,** 1529-39.

DRAGATSIS, I., LEVINE, M. S. & ZEITLIN, S. 2000. Inactivation of Hdh in the brain and testis results in progressive neurodegeneration and sterility in mice. *Nat Genet,* 26**,** 300-6.

DRAGUNOW, M., FAULL, R. L., LAWLOR, P., BEILHARZ, E. J., SINGLETON, K., WALKER, E. B. & MEE, E. 1995. In situ evidence for DNA fragmentation in Huntington's disease striatum and Alzheimer's disease temporal lobes. *Neuroreport,* 6**,** 1053-7.

DUYAO, M. P., AUERBACH, A. B., RYAN, A., PERSICHETTI, F., BARNES, G. T., MCNEIL, S. M., GE, P., VONSATTEL, J. P., GUSELLA, J. F., JOYNER, A. L. & ET AL. 1995. Inactivation of the mouse Huntington's disease gene homolog Hdh. *Science,* 269**,** 407-10.

EDENS, L. J., WHITE, K. H., JEVTIC, P., LI, X. & LEVY, D. L. 2013. Nuclear size regulation: from single cells to development and disease. *Trends Cell Biol,* 23**,** 151-9.

EDWARDS, M. A., YAMAMOTO, M. & CAVINESS, V. S., JR. 1990. Organization of radial glia and related cells in the developing murine CNS. An analysis based upon a new monoclonal antibody marker. *Neuroscience,* 36**,** 121-44.

EHRNHOEFER, D. E., DUENNWALD, M., MARKOVIC, P., WACKER, J. L., ENGEMANN, S., ROARK, M., LEGLEITER, J., MARSH, J. L., THOMPSON, L. M., LINDQUIST, S., MUCHOWSKI, P. J. & WANKER, E. E. 2006. Green tea (-)-epigallocatechin-gallate modulates early events in huntingtin misfolding

and reduces toxicity in Huntington's disease models. *Hum Mol Genet,* 15**,** 2743-51.

ELKABETZ, Y., PANAGIOTAKOS, G., AL SHAMY, G., SOCCI, N. D., TABAR, V. & STUDER, L. 2008. Human ES cell-derived neural rosettes reveal a functionally distinct early neural stem cell stage. *Genes Dev,* 22**,** 152-65.

ENG, L. F. & GHIRNIKAR, R. S. 1994. GFAP and astrogliosis. *Brain Pathol,* 4**,** 229-37.

ERIKSSON, P. S., PERFILIEVA, E., BJORK-ERIKSSON, T., ALBORN, A. M., NORDBORG, C., PETERSON, D. A. & GAGE, F. H. 1998. Neurogenesis in the adult human hippocampus. *Nat Med,* 4**,** 1313-7.

EVANS, S. J., DOUGLAS, I., RAWLINS, M. D., WEXLER, N. S., TABRIZI, S. J. & SMEETH, L. 2013. Prevalence of adult Huntington's disease in the UK based on diagnoses recorded in general practice records. *J Neurol Neurosurg Psychiatry,* 84**,** 1156-60.

FARRER, L. A. & MEANEY, F. J. 1985. An anthropometric assessment of Huntington's disease patients and families. *Am J Phys Anthropol,* 67**,** 185-94.

FELDMANN, M., PATHIPATI, P., SHELDON, R. A., JIANG, X. & FERRIERO, D. M. 2014. Isolating astrocytes and neurons sequentially from postnatal murine brains with a magnetic cell separation technique. *2014*.

FERRANTE, R. J., GUTEKUNST, C. A., PERSICHETTI, F., MCNEIL, S. M., KOWALL, N. W., GUSELLA, J. F., MACDONALD, M. E., BEAL, M. F. & HERSCH, S. M. 1997. Heterogeneous topographic and cellular distribution of huntingtin expression in the normal human neostriatum. *J Neurosci,* 17**,** 3052-63.

FERRANTE, R. J., KOWALL, N. W., BEAL, M. F., MARTIN, J. B., BIRD, E. D. & RICHARDSON, E. P., JR. 1987. Morphologic and histochemical characteristics of a spared subset of striatal neurons in Huntington's disease. *J Neuropathol Exp Neurol,* 46**,** 12-27.

FISHELL, G. 1995. Striatal precursors adopt cortical identities in response to local cues. *Development,* 121**,** 803-12.

FISHER, E. R. & HAYDEN, M. R. 2014. Multisource ascertainment of Huntington disease in Canada: prevalence and population at risk. *Mov Disord,* 29**,** 105-14.

FRANCIS, F., KOULAKOFF, A., BOUCHER, D., CHAFEY, P., SCHAAR, B., VINET, M. C., FRIOCOURT, G., MCDONNELL, N., REINER, O., KAHN, A., MCCONNELL, S. K., BERWALD-NETTER, Y., DENOULET, P. & CHELLY,

J. 1999. Doublecortin is a developmentally regulated, microtubule-associated protein expressed in migrating and differentiating neurons. *Neuron,* 23**,** 247-56.

FRIEDMAN, J. H., TRIESCHMANN, M. E., MYERS, R. H. & FERNANDEZ, H. H. 2005. Monozygotic twins discordant for Huntington disease after 7 years. *Arch Neurol,* 62**,** 995-7.

FROST, B. & DIAMOND, M. I. 2010. Prion-like mechanisms in neurodegenerative diseases. *Nat Rev Neurosci,* 11**,** 155-9.

FUSCO, F. R., CHEN, Q., LAMOREAUX, W. J., FIGUEREDO-CARDENAS, G., JIAO, Y., COFFMAN, J. A., SURMEIER, D. J., HONIG, M. G., CARLOCK, L. R. & REINER, A. 1999. Cellular localization of huntingtin in striatal and cortical neurons in rats: lack of correlation with neuronal vulnerability in Huntington's disease. *J Neurosci,* 19**,** 1189-202.

GABAY, L., LOWELL, S., RUBIN, L. L. & ANDERSON, D. J. 2003. Deregulation of dorsoventral patterning by FGF confers trilineage differentiation capacity on CNS stem cells in vitro. *Neuron,* 40**,** 485-99.

GAGE, F. H., KEMPERMANN, G., PALMER, T. D., PETERSON, D. A. & RAY, J. 1998. Multipotent progenitor cells in the adult dentate gyrus. *J Neurobiol,* 36**,** 249-66.

GALBRAITH, C. G., YAMADA, K. M. & GALBRAITH, J. A. 2007. Polymerizing actin fibers position integrins primed to probe for adhesion sites. *Science,* 315**,** 992-5.

GALBRAITH, C. G. & GALBRAITH, J. A. 2011. Super-resolution microscopy at a glance. *J Cell Sci,* 124**,** 1607-11.

GAUTHIER, L. R., CHARRIN, B. C., BORRELL-PAGES, M., DOMPIERRE, J. P., RANGONE, H., CORDELIERES, F. P., DE MEY, J., MACDONALD, M. E., LESSMANN, V., HUMBERT, S. & SAUDOU, F. 2004. Huntingtin controls neurotrophic support and survival of neurons by enhancing BDNF vesicular transport along microtubules. *Cell,* 118**,** 127-38.

GAVRIELI, Y., SHERMAN, Y. & BEN-SASSON, S. A. 1992. Identification of programmed cell death in situ via specific labeling of nuclear DNA fragmentation. *J Cell Biol,* 119**,** 493-501.

GEORGIOU, N., BRADSHAW, J. L., CHIU, E., TUDOR, A., O'GORMAN, L. & PHILLIPS, J. G. 1999. Differential clinical and motor control function in a pair of monozygotic twins with Huntington's disease. *Mov Disord,* 14**,** 320-5.

GHARAMI, K., XIE, Y., AN, J. J., TONEGAWA, S. & XU, B. 2008. Brain-derived neurotrophic factor over-expression in the forebrain ameliorates Huntington's disease phenotypes in mice. *J Neurochem,* 105**,** 369-79.

GIL, J. M., MOHAPEL, P., ARAUJO, I. M., POPOVIC, N., LI, J. Y., BRUNDIN, P. & PETERSEN, A. 2005. Reduced hippocampal neurogenesis in R6/2 transgenic Huntington's disease mice. *Neurobiol Dis,* 20**,** 744-51.

GIPSON, T. A., NEUEDER, A., WEXLER, N. S., BATES, G. P. & HOUSMAN, D. 2013. Aberrantly spliced HTT, a new player in Huntington's disease pathogenesis. *RNA Biol,* 10**,** 1647-52.

GLUCKSMANN, A. 1951. Cell deaths in normal vertebrate ontogeny. *Biol Rev Camb Philos Soc,* 26**,** 59-86.

GODIN, J. D., COLOMBO, K., MOLINA-CALAVITA, M., KERYER, G., ZALA, D., CHARRIN, B. C., DIETRICH, P., VOLVERT, M. L., GUILLEMOT, F., DRAGATSIS, I., BELLAICHE, Y., SAUDOU, F., NGUYEN, L. & HUMBERT, S. 2010. Huntingtin is required for mitotic spindle orientation and mammalian neurogenesis. *Neuron,* 67**,** 392-406.

GOFFREDO, D., CONTI, L., DI FEBO, F., BIELLA, G., TOSONI, A., VAGO, G., BIUNNO, I., MOIANA, A., BOLOGNINI, D., TOSELLI, M. & CATTANEO, E. 2008. Setting the conditions for efficient, robust and reproducible generation of functionally active neurons from adult subventricular zone-derived neural stem cells. *Cell Death Differ,* 15**,** 1847-56.

GOLDBERG, Y. P., NICHOLSON, D. W., RASPER, D. M., KALCHMAN, M. A., KOIDE, H. B., GRAHAM, R. K., BROMM, M., KAZEMI-ESFARJANI, P., THORNBERRY, N. A., VAILLANCOURT, J. P. & HAYDEN, M. R. 1996. Cleavage of huntingtin by apopain, a proapoptotic cysteine protease, is modulated by the polyglutamine tract. *Nat Genet,* 13**,** 442-9.

GONITEL, R., MOFFITT, H., SATHASIVAM, K., WOODMAN, B., DETLOFF, P. J., FAULL, R. L. & BATES, G. P. 2008. DNA instability in postmitotic neurons. *Proc Natl Acad Sci U S A,* 105**,** 3467-72.

GOODMAN, A. O. & BARKER, R. A. 2011. Body composition in premanifest Huntington's disease reveals lower bone density compared to controls. *PLoS Curr,* 3**,** RRN1214.

GOTZ, M. & HUTTNER, W. B. 2005. The cell biology of neurogenesis. *Nat Rev Mol Cell Biol,* 6**,** 777-88.

GRAHAM, R. K., DENG, Y., SLOW, E. J., HAIGH, B., BISSADA, N., LU, G., PEARSON, J., SHEHADEH, J., BERTRAM, L., MURPHY, Z., WARBY, S. C., DOTY, C. N., ROY, S., WELLINGTON, C. L., LEAVITT, B. R., RAYMOND, L. A., NICHOLSON, D. W. & HAYDEN, M. R. 2006. Cleavage at the caspase-6 site is required for neuronal dysfunction and degeneration due to mutant huntingtin. *Cell,* 125**,** 1179-91.

GRANDBARBE, L., BOUISSAC, J., RAND, M., HRABE DE ANGELIS, M., ARTAVANIS-TSAKONAS, S. & MOHIER, E. 2003. Delta-Notch signaling controls the generation of neurons/glia from neural stem cells in a stepwise process. *Development,* 130**,** 1391-402.

GRAY, E. G. 1959. Electron microscopy of synaptic contacts on dendrite spines of the cerebral cortex. *Nature,* 183**,** 1592-3.

GRAY, M., SHIRASAKI, D. I., CEPEDA, C., ANDRE, V. M., WILBURN, B., LU, X. H., TAO, J., YAMAZAKI, I., LI, S. H., SUN, Y. E., LI, X. J., LEVINE, M. S. & YANG, X. W. 2008. Full-length human mutant huntingtin with a stable polyglutamine repeat can elicit progressive and selective neuropathogenesis in BACHD mice. *J Neurosci,* 28**,** 6182-95.

GREGG, C. & WEISS, S. 2003. Generation of functional radial glial cells by embryonic and adult forebrain neural stem cells. *J Neurosci,* 23**,** 11587-601.

GUSTAFSSON, M. G. 1999. Extended resolution fluorescence microscopy. *Curr Opin Struct Biol,* 9**,** 627-34.

GUSTAFSSON, M. G. 2000. Surpassing the lateral resolution limit by a factor of two using structured illumination microscopy. *J Microsc,* 198**,** 82-7.

HAAS, K. F. & BROADIE, K. 2008. Roles of ubiquitination at the synapse. *Biochim Biophys Acta,* 1779**,** 495-506.

HACK, M. A., SUGIMORI, M., LUNDBERG, C., NAKAFUKU, M. & GOTZ, M. 2004. Regionalization and fate specification in neurospheres: the role of Olig2 and Pax6. *Mol Cell Neurosci,* 25**,** 664-78.

HACKAM, A. S., SINGARAJA, R., WELLINGTON, C. L., METZLER, M., MCCUTCHEON, K., ZHANG, T., KALCHMAN, M. & HAYDEN, M. R. 1998. The influence of huntingtin protein size on nuclear localization and cellular toxicity. *J Cell Biol,* 141**,** 1097-105.

HADZI, T. C., HENDRICKS, A. E., LATOURELLE, J. C., LUNETTA, K. L., CUPPLES, L. A., GILLIS, T., MYSORE, J. S., GUSELLA, J. F., MACDONALD, M. E., MYERS, R. H. & VONSATTEL, J. P. 2012. Assessment

of cortical and striatal involvement in 523 Huntington disease brains. *Neurology,* 79**,** 1708-15.

HALLIDAY, G. M., MCRITCHIE, D. A., MACDONALD, V., DOUBLE, K. L., TRENT, R. J. & MCCUSKER, E. 1998. Regional specificity of brain atrophy in Huntington's disease. *Exp Neurol,* 154**,** 663-72.

HAN, S. S., WILLIAMS, L. A. & EGGAN, K. C. 2011. Constructing and deconstructing stem cell models of neurological disease. *Neuron,* 70**,** 626-44.

HANSEN, D. V., LUI, J. H., PARKER, P. R. & KRIEGSTEIN, A. R. 2010. Neurogenic radial glia in the outer subventricular zone of human neocortex. *Nature,* 464**,** 554-561.

HARTFUSS, E., GALLI, R., HEINS, N. & GOTZ, M. 2001. Characterization of CNS precursor subtypes and radial glia. *Dev Biol,* 229**,** 15-30.

HD IPSC CONSORTIUM 2012. Induced pluripotent stem cells from patients with Huntington's disease show CAG-repeat-expansion-associated phenotypes. *Cell Stem Cell,* 11**,** 264-78.

HDCRG, H. S. D. C. R. G. 1993. A novel gene containing a trinucleotide repeat that is expanded and unstable on Huntington's disease chromosomes. The Huntington's Disease Collaborative Research Group. *Cell,* 72**,** 971-83.

HEDREEN, J. C., PEYSER, C. E., FOLSTEIN, S. E. & ROSS, C. A. 1991. Neuronal loss in layers V and VI of cerebral cortex in Huntington's disease. *Neurosci Lett,* 133**,** 257-61.

HEISER, V., ENGEMANN, S., BROCKER, W., DUNKEL, I., BOEDDRICH, A., WAELTER, S., NORDHOFF, E., LURZ, R., SCHUGARDT, N., RAUTENBERG, S., HERHAUS, C., BARNICKEL, G., BOTTCHER, H., LEHRACH, H. & WANKER, E. E. 2002. Identification of benzothiazoles as potential polyglutamine aggregation inhibitors of Huntington's disease by using an automated filter retardation assay. *Proc Natl Acad Sci U S A,* 99 Suppl 4**,** 16400-6.

HERMEL, E., GAFNI, J., PROPP, S. S., LEAVITT, B. R., WELLINGTON, C. L., YOUNG, J. E., HACKAM, A. S., LOGVINOVA, A. V., PEEL, A. L., CHEN, S. F., HOOK, V., SINGARAJA, R., KRAJEWSKI, S., GOLDSMITH, P. C., ELLERBY, H. M., HAYDEN, M. R., BREDESEN, D. E. & ELLERBY, L. M. 2004. Specific caspase interactions and amplification are involved in selective neuronal vulnerability in Huntington's disease. *Cell Death Differ,* 11**,** 424-38.

HEYTLER, P. G. & PRICHARD, W. W. 1962. A new class of uncoupling agents--carbonyl cyanide phenylhydrazones. *Biochem Biophys Res Commun,* 7**,** 272-5.

HICKEY, M. A., GALLANT, K., GROSS, G. G., LEVINE, M. S. & CHESSELET, M. F. 2005. Early behavioral deficits in R6/2 mice suitable for use in preclinical drug testing. *Neurobiol Dis,* 20**,** 1-11.

HILDITCH-MAGUIRE, P., TRETTEL, F., PASSANI, L. A., AUERBACH, A., PERSICHETTI, F. & MACDONALD, M. E. 2000. Huntingtin: an iron-regulated protein essential for normal nuclear and perinuclear organelles. *Hum Mol Genet,* 9**,** 2789-97.

HITOSHI, S., SEABERG, R. M., KOSCIK, C., ALEXSON, T., KUSUNOKI, S., KANAZAWA, I., TSUJI, S. & VAN DER KOOY, D. 2004. Primitive neural stem cells from the mammalian epiblast differentiate to definitive neural stem cells under the control of Notch signaling. *Genes Dev,* 18**,** 1806-11.

HO, L. W., BROWN, R., MAXWELL, M., WYTTENBACH, A. & RUBINSZTEIN, D. C. 2001. Wild type Huntingtin reduces the cellular toxicity of mutant Huntingtin in mammalian cell models of Huntington's disease. *J Med Genet,* 38**,** 450-2.

HODGES, A., STRAND, A. D., ARAGAKI, A. K., KUHN, A., SENGSTAG, T., HUGHES, G., ELLISTON, L. A., HARTOG, C., GOLDSTEIN, D. R., THU, D., HOLLINGSWORTH, Z. R., COLLIN, F., SYNEK, B., HOLMANS, P. A., YOUNG, A. B., WEXLER, N. S., DELORENZI, M., KOOPERBERG, C., AUGOOD, S. J., FAULL, R. L., OLSON, J. M., JONES, L. & LUTHI-CARTER, R. 2006. Regional and cellular gene expression changes in human Huntington's disease brain. *Hum Mol Genet,* 15**,** 965-77.

HODGSON, J. G., AGOPYAN, N., GUTEKUNST, C. A., LEAVITT, B. R., LEPIANE, F., SINGARAJA, R., SMITH, D. J., BISSADA, N., MCCUTCHEON, K., NASIR, J., JAMOT, L., LI, X. J., STEVENS, M. E., ROSEMOND, E., RODER, J. C., PHILLIPS, A. G., RUBIN, E. M., HERSCH, S. M. & HAYDEN, M. R. 1999. A YAC mouse model for Huntington's disease with full-length mutant huntingtin, cytoplasmic toxicity, and selective striatal neurodegeneration. *Neuron,* 23**,** 181-92.

HOGG, R. C., CHIPPERFIELD, H., WHYTE, K. A., STAFFORD, M. R., HANSEN, M. A., COOL, S. M., NURCOMBE, V. & ADAMS, D. J. 2004. Functional maturation of isolated neural progenitor cells from the adult rat hippocampus. *Eur J Neurosci,* 19**,** 2410-20.

HOLMES, B., BROGDEN, R. N., HEEL, R. C., SPEIGHT, T. M. & AVERY, G. S. 1983. Guanabenz. A review of its pharmacodynamic properties and therapeutic efficacy in hypertension. *Drugs,* 26**,** 212-29.

HOLT, D. J., GRAYBIEL, A. M. & SAPER, C. B. 1997. Neurochemical architecture of the human striatum. *J Comp Neurol,* 384**,** 1-25.

HOOGEVEEN, A. T., WILLEMSEN, R., MEYER, N., DE ROOIJ, K. E., ROOS, R. A., VAN OMMEN, G. J. & GALJAARD, H. 1993. Characterization and localization of the Huntington disease gene product. *Hum Mol Genet,* 2**,** 2069-73.

HUNTINGTON, G. 1872. On chorea. George Huntington, M.D. *J Neuropsychiatry Clin Neurosci,* 15**,** 109-12.

HUNTINGTON STUDY GROUP, C. I. & DORSEY, E. 2012. Characterization of a large group of individuals with huntington disease and their relatives enrolled in the COHORT study. *PLoS One,* 7**,** e29522.

HWANG, J. H., KIM, D. W., JO, E. J., KIM, Y. K., JO, Y. S., PARK, J. H., YOO, S. K., PARK, M. K., KWAK, T. H., KHO, Y. L., HAN, J., CHOI, H. S., LEE, S. H., KIM, J. M., LEE, I., KYUNG, T., JANG, C., CHUNG, J., KWEON, G. R. & SHONG, M. 2009. Pharmacological stimulation of NADH oxidation ameliorates obesity and related phenotypes in mice. *Diabetes,* 58**,** 965-74.

ISHIGURO, H., YAMADA, K., SAWADA, H., NISHII, K., ICHINO, N., SAWADA, M., KUROSAWA, Y., MATSUSHITA, N., KOBAYASHI, K., GOTO, J., HASHIDA, H., MASUDA, N., KANAZAWA, I. & NAGATSU, T. 2001. Age-dependent and tissue-specific CAG repeat instability occurs in mouse knock-in for a mutant Huntington's disease gene. *J Neurosci Res,* 65**,** 289-97.

IWATA, A., RILEY, B. E., JOHNSTON, J. A. & KOPITO, R. R. 2005. HDAC6 and microtubules are required for autophagic degradation of aggregated huntingtin. *J Biol Chem,* 280**,** 40282-92.

JACKSON, S. P. & DUROCHER, D. 2013. Regulation of DNA damage responses by ubiquitin and SUMO. *Mol Cell,* 49**,** 795-807.

JACOBSEN, J. C., BAWDEN, C. S., RUDIGER, S. R., MCLAUGHLAN, C. J., REID, S. J., WALDVOGEL, H. J., MACDONALD, M. E., GUSELLA, J. F., WALKER, S. K., KELLY, J. M., WEBB, G. C., FAULL, R. L., REES, M. I. & SNELL, R. G. 2010. An ovine transgenic Huntington's disease model. *Hum Mol Genet,* 19**,** 1873-82.

JACOBSEN, J. C., GREGORY, G. C., WODA, J. M., THOMPSON, M. N., COSER, K. R., MURTHY, V., KOHANE, I. S., GUSELLA, J. F., SEONG, I. S.,

MACDONALD, M. E., SHIODA, T. & LEE, J. M. 2011. HD CAG-correlated gene expression changes support a simple dominant gain of function. *Hum Mol Genet,* 20**,** 2846-60.

JAIN, M., ARMSTRONG, R. J., TYERS, P., BARKER, R. A. & ROSSER, A. E. 2003. GABAergic immunoreactivity is predominant in neurons derived from expanded human neural precursor cells in vitro. *Exp Neurol,* 182**,** 113-23.

JANSEN, A. H., VAN HAL, M., OP DEN KELDER, I. C., MEIER, R. T., DE RUITER, A. A., SCHUT, M. H., SMITH, D. L., GRIT, C., BROUWER, N., KAMPHUIS, W., BODDEKE, H. W., DEN DUNNEN, W. F., VAN ROON, W. M., BATES, G. P., HOL, E. M. & REITS, E. A. 2016. Frequency of nuclear mutant huntingtin inclusion formation in neurons and glia is cell-type-specific. *Glia*.

JAYARAMAN, M., KODALI, R., SAHOO, B., THAKUR, A. K., MAYASUNDARI, A., MISHRA, R., PETERSON, C. B. & WETZEL, R. 2012. Slow amyloid nucleation via alpha-helix-rich oligomeric intermediates in short polyglutamine-containing huntingtin fragments. *J Mol Biol,* 415**,** 881-99.

JEON, I., LEE, N., LI, J. Y., PARK, I. H., PARK, K. S., MOON, J., SHIM, S. H., CHOI, C., CHANG, D. J., KWON, J., OH, S. H., SHIN, D. A., KIM, H. S., DO, J. T., LEE, D. R., KIM, M., KANG, K. S., DALEY, G. Q., BRUNDIN, P. & SONG, J. 2012. Neuronal properties, in vivo effects, and pathology of a Huntington's disease patient-derived induced pluripotent stem cells. *Stem Cells,* 30**,** 2054-62.

JEONG, H., COHEN, D. E., CUI, L., SUPINSKI, A., SAVAS, J. N., MAZZULLI, J. R., YATES, J. R., 3RD, BORDONE, L., GUARENTE, L. & KRAINC, D. 2012. Sirt1 mediates neuroprotection from mutant huntingtin by activation of the TORC1 and CREB transcriptional pathway. *Nat Med,* 18**,** 159-65.

JIANG, M., WANG, J., FU, J., DU, L., JEONG, H., WEST, T., XIANG, L., PENG, Q., HOU, Z., CAI, H., SEREDENINA, T., ARBEZ, N., ZHU, S., SOMMERS, K., QIAN, J., ZHANG, J., MORI, S., YANG, X. W., TAMASHIRO, K. L., AJA, S., MORAN, T. H., LUTHI-CARTER, R., MARTIN, B., MAUDSLEY, S., MATTSON, M. P., CICHEWICZ, R. H., ROSS, C. A., HOLTZMAN, D. M., KRAINC, D. & DUAN, W. 2012. Neuroprotective role of Sirt1 in mammalian models of Huntington's disease through activation of multiple Sirt1 targets. *Nat Med,* 18**,** 153-8.

JINEK, M., CHYLINSKI, K., FONFARA, I., HAUER, M., DOUDNA, J. A. & CHARPENTIER, E. 2012. A programmable dual-RNA-guided DNA endonuclease in adaptive bacterial immunity. *Science,* 337**,** 816-21.

JOHE, K. K., HAZEL, T. G., MULLER, T., DUGICH-DJORDJEVIC, M. M. & MCKAY, R. D. 1996. Single factors direct the differentiation of stem cells from the fetal and adult central nervous system. *Genes Dev,* 10**,** 3129-40.

KAUSHIK, S., SINGH, R. & CUERVO, A. M. 2010. Autophagic pathways and metabolic stress. *Diabetes Obes Metab,* 12 Suppl 2**,** 4-14.

KEGEL, K. B., MELONI, A. R., YI, Y., KIM, Y. J., DOYLE, E., CUIFFO, B. G., SAPP, E., WANG, Y., QIN, Z. H., CHEN, J. D., NEVINS, J. R., ARONIN, N. & DIFIGLIA, M. 2002. Huntingtin is present in the nucleus, interacts with the transcriptional corepressor C-terminal binding protein, and represses transcription. *J Biol Chem,* 277**,** 7466-76.

KEMP, J. M. & POWELL, T. P. 1971. The structure of the caudate nucleus of the cat: light and electron microscopy. *Philos Trans R Soc Lond B Biol Sci,* 262**,** 383-401.

KENNEDY, L., EVANS, E., CHEN, C. M., CRAVEN, L., DETLOFF, P. J., ENNIS, M. & SHELBOURNE, P. F. 2003. Dramatic tissue-specific mutation length increases are an early molecular event in Huntington disease pathogenesis. *Hum Mol Genet,* 12**,** 3359-67.

KENNEDY, L. & SHELBOURNE, P. F. 2000. Dramatic mutation instability in HD mouse striatum: does polyglutamine load contribute to cell-specific vulnerability in Huntington's disease? *Hum Mol Genet,* 9**,** 2539-44.

KERR, J. F., WYLLIE, A. H. & CURRIE, A. R. 1972. Apoptosis: a basic biological phenomenon with wide-ranging implications in tissue kinetics. *Br J Cancer,* 26**,** 239-57.

KIM, M. W., CHELLIAH, Y., KIM, S. W., OTWINOWSKI, Z. & BEZPROZVANNY, I. 2009. Secondary structure of Huntingtin amino-terminal region. *Structure,* 17**,** 1205-12.

KIM, Y. J., SAPP, E., CUIFFO, B. G., SOBIN, L., YODER, J., KEGEL, K. B., QIN, Z. H., DETLOFF, P., ARONIN, N. & DIFIGLIA, M. 2006. Lysosomal proteases are involved in generation of N-terminal huntingtin fragments. *Neurobiol Dis,* 22**,** 346-56.

KIM, Y. J., YI, Y., SAPP, E., WANG, Y., CUIFFO, B., KEGEL, K. B., QIN, Z. H., ARONIN, N. & DIFIGLIA, M. 2001. Caspase 3-cleaved N-terminal fragments of wild-type and mutant huntingtin are present in normal and Huntington's disease brains, associate with membranes, and undergo calpain-dependent proteolysis. *Proc Natl Acad Sci U S A,* 98**,** 12784-9.

KISS, J. Z., TRONCOSO, E., DJEBBARA, Z., VUTSKITS, L. & MULLER, D. 2001. The role of neural cell adhesion molecules in plasticity and repair. *Brain Res Brain Res Rev,* 36**,** 175-84.

KLAPSTEIN, G. J., FISHER, R. S., ZANJANI, H., CEPEDA, C., JOKEL, E. S., CHESSELET, M. F. & LEVINE, M. S. 2001. Electrophysiological and morphological changes in striatal spiny neurons in R6/2 Huntington's disease transgenic mice. *J Neurophysiol,* 86**,** 2667-77.

KOCH, P., OPITZ, T., STEINBECK, J. A., LADEWIG, J. & BRUSTLE, O. 2009. A rosette-type, self-renewing human ES cell-derived neural stem cell with potential for in vitro instruction and synaptic integration. *Proc Natl Acad Sci U S A,* 106**,** 3225-30.

KOHL, Z., REGENSBURGER, M., AIGNER, R., KANDASAMY, M., WINNER, B., AIGNER, L. & WINKLER, J. 2010. Impaired adult olfactory bulb neurogenesis in the R6/2 mouse model of Huntington's disease. *BMC Neurosci,* 11**,** 114.

KOMATSU, M., WAGURI, S., KOIKE, M., SOU, Y. S., UENO, T., HARA, T., MIZUSHIMA, N., IWATA, J., EZAKI, J., MURATA, S., HAMAZAKI, J., NISHITO, Y., IEMURA, S., NATSUME, T., YANAGAWA, T., UWAYAMA, J., WARABI, E., YOSHIDA, H., ISHII, T., KOBAYASHI, A., YAMAMOTO, M., YUE, Z., UCHIYAMA, Y., KOMINAMI, E. & TANAKA, K. 2007. Homeostatic levels of p62 control cytoplasmic inclusion body formation in autophagy-deficient mice. *Cell,* 131**,** 1149-63.

KUUSISTO, E., SALMINEN, A. & ALAFUZOFF, I. 2001. Ubiquitin-binding protein p62 is present in neuronal and glial inclusions in human tauopathies and synucleinopathies. *Neuroreport,* 12**,** 2085-90.

KWON, S. E. & CHAPMAN, E. R. 2011. Synaptophysin regulates the kinetics of synaptic vesicle endocytosis in central neurons. *Neuron,* 70**,** 847-54.

LAENG, P., PITTS, R. L., LEMIRE, A. L., DRABIK, C. E., WEINER, A., TANG, H., THYAGARAJAN, R., MALLON, B. S. & ALTAR, C. A. 2004. The mood stabilizer valproic acid stimulates GABA neurogenesis from rat forebrain stem cells. *J Neurochem,* 91**,** 238-51.

LANDLES, C., SATHASIVAM, K., WEISS, A., WOODMAN, B., MOFFITT, H., FINKBEINER, S., SUN, B., GAFNI, J., ELLERBY, L. M., TROTTIER, Y., RICHARDS, W. G., OSMAND, A., PAGANETTI, P. & BATES, G. P. 2010. Proteolysis of mutant huntingtin produces an exon 1 fragment that accumulates

as an aggregated protein in neuronal nuclei in Huntington disease. *J Biol Chem,* 285**,** 8808-23.

LANDWEHRMEYER, G. B., MCNEIL, S. M., DURE, L. S. T., GE, P., AIZAWA, H., HUANG, Q., AMBROSE, C. M., DUYAO, M. P., BIRD, E. D., BONILLA, E. & ET AL. 1995. Huntington's disease gene: regional and cellular expression in brain of normal and affected individuals. *Ann Neurol,* 37**,** 218-30.

LANGBEHN, D. R., BRINKMAN, R. R., FALUSH, D., PAULSEN, J. S., HAYDEN, M. R. & INTERNATIONAL HUNTINGTON'S DISEASE COLLABORATIVE, G. 2004. A new model for prediction of the age of onset and penetrance for Huntington's disease based on CAG length. *Clin Genet,* 65**,** 267-77.

LANGBEHN, D. R., HAYDEN, M. R., PAULSEN, J. S. & GROUP, P.-H. I. O. T. H. S. 2010. CAG-repeat length and the age of onset in Huntington disease (HD): a review and validation study of statistical approaches. *Am J Med Genet B Neuropsychiatr Genet,* 153B**,** 397-408.

LANSKA, D. J., LANSKA, M. J., LAVINE, L. & SCHOENBERG, B. S. 1988. Conditions associated with Huntington's disease at death. A case-control study. *Arch Neurol,* 45**,** 878-80.

LAWRENCE, A. D., HODGES, J. R., ROSSER, A. E., KERSHAW, A., FFRENCH-CONSTANT, C., RUBINSZTEIN, D. C., ROBBINS, T. W. & SAHAKIAN, B. J. 1998. Evidence for specific cognitive deficits in preclinical Huntington's disease. *Brain,* 121 (Pt 7)**,** 1329-41.

LAYWELL, E. D., KUKEKOV, V. G. & STEINDLER, D. A. 1999. Multipotent neurospheres can be derived from forebrain subependymal zone and spinal cord of adult mice after protracted postmortem intervals. *Exp Neurol,* 156**,** 430-3.

LEE, J. M., RAMOS, E. M., LEE, J. H., GILLIS, T., MYSORE, J. S., HAYDEN, M. R., WARBY, S. C., MORRISON, P., NANCE, M., ROSS, C. A., MARGOLIS, R. L., SQUITIERI, F., OROBELLO, S., DI DONATO, S., GOMEZ-TORTOSA, E., AYUSO, C., SUCHOWERSKY, O., TRENT, R. J., MCCUSKER, E., NOVELLETTO, A., FRONTALI, M., JONES, R., ASHIZAWA, T., FRANK, S., SAINT-HILAIRE, M. H., HERSCH, S. M., ROSAS, H. D., LUCENTE, D., HARRISON, M. B., ZANKO, A., ABRAMSON, R. K., MARDER, K., SEQUEIROS, J., PAULSEN, J. S., GROUP, P.-H. S. O. T. H. S., LANDWEHRMEYER, G. B., NETWORK, R. S. O. T. E. H. S. D., MYERS, R. H., GROUP, H.-M. S., MACDONALD, M. E., GUSELLA, J. F. & HSG, C. S.

O. T. 2012a. CAG repeat expansion in Huntington disease determines age at onset in a fully dominant fashion. *Neurology,* 78**,** 690-5.

LEE, J. S., PARK, A. H., LEE, S. H., LEE, S. H., KIM, J. H., YANG, S. J., YEOM, Y. I., KWAK, T. H., LEE, D., LEE, S. J., LEE, C. H., KIM, J. M. & KIM, D. 2012b. Beta-lapachone, a modulator of NAD metabolism, prevents health declines in aged mice. *PLoS One,* 7**,** e47122.

LEE, M. K., TUTTLE, J. B., REBHUN, L. I., CLEVELAND, D. W. & FRANKFURTER, A. 1990. The expression and posttranslational modification of a neuron-specific beta-tubulin isotype during chick embryogenesis. *Cell Motil Cytoskeleton,* 17**,** 118-32.

LEVINE, M. S., KLAPSTEIN, G. J., KOPPEL, A., GRUEN, E., CEPEDA, C., VARGAS, M. E., JOKEL, E. S., CARPENTER, E. M., ZANJANI, H., HURST, R. S., EFSTRATIADIS, A., ZEITLIN, S. & CHESSELET, M. F. 1999. Enhanced sensitivity to N-methyl-D-aspartate receptor activation in transgenic and knockin mouse models of Huntington's disease. *J Neurosci Res,* 58**,** 515-32.

LI, H., BABIARZ, J., WOODBURY, J., KANE-GOLDSMITH, N. & GRUMET, M. 2004. Spatiotemporal heterogeneity of CNS radial glial cells and their transition to restricted precursors. *Dev Biol,* 271**,** 225-38.

LI, H., LI, S. H., CHENG, A. L., MANGIARINI, L., BATES, G. P. & LI, X. J. 1999a. Ultrastructural localization and progressive formation of neuropil aggregates in Huntington's disease transgenic mice. *Hum Mol Genet,* 8**,** 1227-36.

LI, S. H., CHENG, A. L., LI, H. & LI, X. J. 1999b. Cellular defects and altered gene expression in PC12 cells stably expressing mutant huntingtin. *J Neurosci,* 19**,** 5159-72.

LI, X., XU, J., BAI, Y., WANG, X., DAI, X., LIU, Y., ZHANG, J., ZOU, J., SHEN, L. & LI, L. 2005. Isolation and characterization of neural stem cells from human fetal striatum. *Biochem Biophys Res Commun,* 326**,** 425-34.

LIEBL, M. P. & HOPPE, T. 2016. It's all about talking: two-way communication between proteasomal and lysosomal degradation pathways via ubiquitin. *Am J Physiol Cell Physiol,* 311**,** C166-78.

LIN, B., NASIR, J., MACDONALD, H., HUTCHINSON, G., GRAHAM, R. K., ROMMENS, J. M. & HAYDEN, M. R. 1994. Sequence of the murine Huntington disease gene: evidence for conservation, alternate splicing and polymorphism in a triplet (CCG) repeat [corrected]. *Hum Mol Genet,* 3**,** 85-92.

LIONE, L. A., CARTER, R. J., HUNT, M. J., BATES, G. P., MORTON, A. J. & DUNNETT, S. B. 1999. Selective discrimination learning impairments in mice expressing the human Huntington's disease mutation. *J Neurosci,* 19**,** 10428-37.

LIU, J., SATO, C., CERLETTI, M. & WAGERS, A. 2010. Notch signaling in the regulation of stem cell self-renewal and differentiation. *Curr Top Dev Biol,* 92**,** 367-409.

LO SARDO, V., ZUCCATO, C., GAUDENZI, G., VITALI, B., RAMOS, C., TARTARI, M., MYRE, M. A., WALKER, J. A., PISTOCCHI, A., CONTI, L., VALENZA, M., DRUNG, B., SCHMIDT, B., GUSELLA, J., ZEITLIN, S., COTELLI, F. & CATTANEO, E. 2012. An evolutionary recent neuroepithelial cell adhesion function of huntingtin implicates ADAM10-Ncadherin. *Nat Neurosci,* 15**,** 713-21.

LOIS, C. & ALVAREZ-BUYLLA, A. 1994. Long-distance neuronal migration in the adult mammalian brain. *Science,* 264**,** 1145-8.

LORINCZ, M. T. & ZAWISTOWSKI, V. A. 2009. Expanded CAG repeats in the murine Huntington's disease gene increases neuronal differentiation of embryonic and neural stem cells. *Mol Cell Neurosci,* 40**,** 1-13.

LOUIS, S. A. & REYNOLDS, B. A. 2005. Generation and differentiation of neurospheres from murine embryonic day 14 central nervous system tissue. *Methods Mol Biol,* 290**,** 265-80.

LU, B. & PALACINO, J. 2013. A novel human embryonic stem cell-derived Huntington's disease neuronal model exhibits mutant huntingtin (mHTT) aggregates and soluble mHTT-dependent neurodegeneration. *FASEB J,* 27**,** 1820-9.

LU, K., PSAKHYE, I. & JENTSCH, S. 2014. Autophagic clearance of polyQ proteins mediated by ubiquitin-Atg8 adaptors of the conserved CUET protein family. *Cell,* 158**,** 549-63.

LUNKES, A., LINDENBERG, K. S., BEN-HAIEM, L., WEBER, C., DEVYS, D., LANDWEHRMEYER, G. B., MANDEL, J. L. & TROTTIER, Y. 2002. Proteases acting on mutant huntingtin generate cleaved products that differentially build up cytoplasmic and nuclear inclusions. *Mol Cell,* 10**,** 259-69.

LUTHI-CARTER, R., STRAND, A., PETERS, N. L., SOLANO, S. M., HOLLINGSWORTH, Z. R., MENON, A. S., FREY, A. S., SPEKTOR, B. S., PENNEY, E. B., SCHILLING, G., ROSS, C. A., BORCHELT, D. R., TAPSCOTT, S. J., YOUNG, A. B., CHA, J. H. & OLSON, J. M. 2000. Decreased

expression of striatal signaling genes in a mouse model of Huntington's disease. *Hum Mol Genet,* 9**,** 1259-71.

MAJUMDER, P., CHATTOPADHYAY, B., MAZUMDER, A., DAS, P. & BHATTACHARYYA, N. P. 2006. Induction of apoptosis in cells expressing exogenous Hippi, a molecular partner of huntingtin-interacting protein Hip1. *Neurobiol Dis,* 22**,** 242-56.

MANGIARINI, L., SATHASIVAM, K., SELLER, M., COZENS, B., HARPER, A., HETHERINGTON, C., LAWTON, M., TROTTIER, Y., LEHRACH, H., DAVIES, S. W. & BATES, G. P. 1996. Exon 1 of the HD gene with an expanded CAG repeat is sufficient to cause a progressive neurological phenotype in transgenic mice. *Cell,* 87**,** 493-506.

MARSDEN, C. D. 1975. A CENTENNIAL BIBLIOGRAPHY OF HUNTINGTON'S CHOREA 1872-1972. *J Neurol Neurosurg Psychiatry,* 38**,** 1038.

MARSHALL, P. E., LANDIS, D. M. & ZALNERAITIS, E. L. 1983. Immunocytochemical studies of substance P and leucine-enkephalin in Huntington's disease. *Brain Res,* 289**,** 11-26.

MARTIN, D. D., LADHA, S., EHRNHOEFER, D. E. & HAYDEN, M. R. 2015. Autophagy in Huntington disease and huntingtin in autophagy. *Trends Neurosci,* 38**,** 26-35.

MARTINDALE, D., HACKAM, A., WIECZOREK, A., ELLERBY, L., WELLINGTON, C., MCCUTCHEON, K., SINGARAJA, R., KAZEMI-ESFARJANI, P., DEVON, R., KIM, S. U., BREDESEN, D. E., TUFARO, F. & HAYDEN, M. R. 1998. Length of huntingtin and its polyglutamine tract influences localization and frequency of intracellular aggregates. *Nat Genet,* 18**,** 150-4.

MASLOV, A. Y., BARONE, T. A., PLUNKETT, R. J. & PRUITT, S. C. 2004. Neural stem cell detection, characterization, and age-related changes in the subventricular zone of mice. *J Neurosci,* 24**,** 1726-33.

MAYNARD, C. J., BOTTCHER, C., ORTEGA, Z., SMITH, R., FLOREA, B. I., DIAZ-HERNANDEZ, M., BRUNDIN, P., OVERKLEEFT, H. S., LI, J. Y., LUCAS, J. J. & DANTUMA, N. P. 2009. Accumulation of ubiquitin conjugates in a polyglutamine disease model occurs without global ubiquitin/proteasome system impairment. *Proc Natl Acad Sci U S A,* 106**,** 13986-91.

MCMURRAY, C. T. 2008. Hijacking of the mismatch repair system to cause CAG expansion and cell death in neurodegenerative disease. *DNA Repair (Amst),* 7**,** 1121-34.

MCMURRAY, C. T. 2010. Mechanisms of trinucleotide repeat instability during human development. *Nat Rev Genet,* 11**,** 786-99.

MEADE, C. A., DENG, Y. P., FUSCO, F. R., DEL MAR, N., HERSCH, S., GOLDOWITZ, D. & REINER, A. 2002. Cellular localization and development of neuronal intranuclear inclusions in striatal and cortical neurons in R6/2 transgenic mice. *J Comp Neurol,* 449**,** 241-69.

MEIER, P., FINCH, A. & EVAN, G. 2000. Apoptosis in development. *Nature,* 407**,** 796-801.

MENALLED, L., EL-KHODOR, B. F., PATRY, M., SUAREZ-FARINAS, M., ORENSTEIN, S. J., ZAHASKY, B., LEAHY, C., WHEELER, V., YANG, X. W., MACDONALD, M., MORTON, A. J., BATES, G., LEEDS, J., PARK, L., HOWLAND, D., SIGNER, E., TOBIN, A. & BRUNNER, D. 2009. Systematic behavioral evaluation of Huntington's disease transgenic and knock-in mouse models. *Neurobiol Dis,* 35**,** 319-36.

MENEZES, J. R. & LUSKIN, M. B. 1994. Expression of neuron-specific tubulin defines a novel population in the proliferative layers of the developing telencephalon. *J Neurosci,* 14**,** 5399-416.

MERKLE, F. T., TRAMONTIN, A. D., GARCIA-VERDUGO, J. M. & ALVAREZ-BUYLLA, A. 2004. Radial glia give rise to adult neural stem cells in the subventricular zone. *Proc Natl Acad Sci U S A,* 101**,** 17528-32.

MIYATA, T., KAWAGUCHI, A., OKANO, H. & OGAWA, M. 2001. Asymmetric inheritance of radial glial fibers by cortical neurons. *Neuron,* 31**,** 727-41.

MOCHIZUKI, H., GOTO, K., MORI, H. & MIZUNO, Y. 1996. Histochemical detection of apoptosis in Parkinson's disease. *J Neurol Sci,* 137**,** 120-3.

MOELLER, M. L. & DIMITRIJEVICH, S. D. 2004. A new strategy for analysis of phenotype marker antigens in hollow neurospheres. *J Neurosci Methods,* 139**,** 43-50.

MORRISON, P. J., HARDING-LESTER, S. & BRADLEY, A. 2011. Uptake of Huntington disease predictive testing in a complete population. *Clin Genet,* 80**,** 281-6.

MORTON, A. J. 2013. Circadian and sleep disorder in Huntington's disease. *Exp Neurol,* 243**,** 34-44.

MORTON, A. J., FAULL, R. L. & EDWARDSON, J. M. 2001. Abnormalities in the synaptic vesicle fusion machinery in Huntington's disease. *Brain Res Bull,* 56**,** 111-7.

MORTON, A. J., GLYNN, D., LEAVENS, W., ZHENG, Z., FAULL, R. L., SKEPPER, J. N. & WIGHT, J. M. 2009. Paradoxical delay in the onset of disease caused by super-long CAG repeat expansions in R6/2 mice. *Neurobiol Dis,* 33**,** 331-41.

MORTON, A. J., LAGAN, M. A., SKEPPER, J. N. & DUNNETT, S. B. 2000. Progressive formation of inclusions in the striatum and hippocampus of mice transgenic for the human Huntington's disease mutation. *J Neurocytol,* 29**,** 679-702.

MURPHY, K. P., CARTER, R. J., LIONE, L. A., MANGIARINI, L., MAHAL, A., BATES, G. P., DUNNETT, S. B. & MORTON, A. J. 2000. Abnormal synaptic plasticity and impaired spatial cognition in mice transgenic for exon 1 of the human Huntington's disease mutation. *J Neurosci,* 20**,** 5115-23.

NAGAOKA, U., KIM, K., JANA, N. R., DOI, H., MARUYAMA, M., MITSUI, K., OYAMA, F. & NUKINA, N. 2004. Increased expression of p62 in expanded polyglutamine-expressing cells and its association with polyglutamine inclusions. *J Neurochem,* 91**,** 57-68.

NAKAGAWA, M., TANIGUCHI, Y., SENDA, S., TAKIZAWA, N., ICHISAKA, T., ASANO, K., MORIZANE, A., DOI, D., TAKAHASHI, J., NISHIZAWA, M., YOSHIDA, Y., TOYODA, T., OSAFUNE, K., SEKIGUCHI, K. & YAMANAKA, S. 2014. A novel efficient feeder-free culture system for the derivation of human induced pluripotent stem cells. *Sci Rep,* 4**,** 3594.

NASIR, J., FLORESCO, S. B., O'KUSKY, J. R., DIEWERT, V. M., RICHMAN, J. M., ZEISLER, J., BOROWSKI, A., MARTH, J. D., PHILLIPS, A. G. & HAYDEN, M. R. 1995. Targeted disruption of the Huntington's disease gene results in embryonic lethality and behavioral and morphological changes in heterozygotes. *Cell,* 81**,** 811-23.

NAT, R. & DECHANT, G. 2011. Milestones of directed differentiation of mouse and human embryonic stem cells into telencephalic neurons based on neural development in vivo. *Stem Cells Dev,* 20**,** 947-58.

NEICE, A. 2010. Chapter 3 - Methods and Limitations of Subwavelength Imaging. *In:* PETER, W. H. (ed.) *Advances in Imaging and Electron Physics.* Elsevier.

NELSON, A. D., SUZUKI, M. & SVENDSEN, C. N. 2008. A high concentration of epidermal growth factor increases the growth and survival of neurogenic radial glial cells within human neurosphere cultures. *Stem Cells,* 26**,** 348-55.

NICLIS, J., TROUNSON, A. O., DOTTORI, M., ELLISDON, A., BOTTOMLEY, S. P., VERLINSKY, Y. & CRAM, D. 2009. Human embryonic stem cell models of Huntington disease. *Reprod Biomed Online,* 19**,** 106-13.

NOCTOR, S. C., MARTINEZ-CERDENO, V. & KRIEGSTEIN, A. R. 2008. Distinct behaviors of neural stem and progenitor cells underlie cortical neurogenesis. *J Comp Neurol,* 508**,** 28-44.

NOUJAIM, S. F., STUCKEY, J. A., PONCE-BALBUENA, D., FERRER-VILLADA, T., LOPEZ-IZQUIERDO, A., PANDIT, S. V., SANCHEZ-CHAPULA, J. A. & JALIFE, J. 2011. Structural bases for the different anti-fibrillatory effects of chloroquine and quinidine. *Cardiovasc Res,* 89**,** 862-9.

NUCIFORA, L. G., BURKE, K. A., FENG, X., ARBEZ, N., ZHU, S., MILLER, J., YANG, G., RATOVITSKI, T., DELANNOY, M., MUCHOWSKI, P. J., FINKBEINER, S., LEGLEITER, J., ROSS, C. A. & POIRIER, M. A. 2012. Identification of novel potentially toxic oligomers formed in vitro from mammalian-derived expanded huntingtin exon-1 protein. *J Biol Chem,* 287**,** 16017-28.

ONORATI, M., BINETTI, M., CONTI, L., CAMNASIO, S., CALABRESE, G., ALBIERI, I., DI FEBO, F., TOSELLI, M., BIELLA, G., MARTYNOGA, B., GUILLEMOT, F., CONSALEZ, G. G. & CATTANEO, E. 2011. Preservation of positional identity in fetus-derived neural stem (NS) cells from different mouse central nervous system compartments. *Cell Mol Life Sci,* 68**,** 1769-83.

OSSATO, G., DIGMAN, M. A., AIKEN, C., LUKACSOVICH, T., MARSH, J. L. & GRATTON, E. 2010. A two-step path to inclusion formation of huntingtin peptides revealed by number and brightness analysis. *Biophys J,* 98**,** 3078-85.

PALMER, T. D., TAKAHASHI, J. & GAGE, F. H. 1997. The adult rat hippocampus contains primordial neural stem cells. *Mol Cell Neurosci,* 8**,** 389-404.

PANKIV, S., LAMARK, T., BRUUN, J. A., OVERVATN, A., BJORKOY, G. & JOHANSEN, T. 2010. Nucleocytoplasmic shuttling of p62/SQSTM1 and its role in recruitment of nuclear polyubiquitinated proteins to promyelocytic leukemia bodies. *J Biol Chem,* 285**,** 5941-53.

PARK, D., XIANG, A. P., MAO, F. F., ZHANG, L., DI, C. G., LIU, X. M., SHAO, Y., MA, B. F., LEE, J. H., HA, K. S., WALTON, N. & LAHN, B. T. 2010. Nestin is required for the proper self-renewal of neural stem cells. *Stem Cells,* 28**,** 2162-71.

PARK, I. H., ARORA, N., HUO, H., MAHERALI, N., AHFELDT, T., SHIMAMURA, A., LENSCH, M. W., COWAN, C., HOCHEDLINGER, K. & DALEY, G. Q. 2008. Disease-specific induced pluripotent stem cells. *Cell,* 134**,** 877-86.

PECHO-VRIESELING, E., RIEKER, C., FUCHS, S., BLECKMANN, D., ESPOSITO, M. S., BOTTA, P., GOLDSTEIN, C., BERNHARD, M., GALIMBERTI, I., MULLER, M., LUTHI, A., ARBER, S., BOUWMEESTER, T., VAN DER PUTTEN, H. & DI GIORGIO, F. P. 2014. Transneuronal propagation of mutant huntingtin contributes to non-cell autonomous pathology in neurons. *Nat Neurosci,* 17**,** 1064-72.

PERUTZ, M. F. 1996. Glutamine repeats and inherited neurodegenerative diseases: molecular aspects. *Curr Opin Struct Biol,* 6**,** 848-58.

PERUTZ, M. F., JOHNSON, T., SUZUKI, M. & FINCH, J. T. 1994. Glutamine repeats as polar zippers: their possible role in inherited neurodegenerative diseases. *Proc Natl Acad Sci U S A,* 91**,** 5355-8.

PILLAI, J. A., HANSEN, L. A., MASLIAH, E., GOLDSTEIN, J. L., EDLAND, S. D. & COREY-BLOOM, J. 2012. Clinical severity of Huntington's disease does not always correlate with neuropathologic stage. *Mov Disord,* 27**,** 1099-103.

PINTO, L., MADER, M. T., IRMLER, M., GENTILINI, M., SANTONI, F., DRECHSEL, D., BLUM, R., STAHL, R., BULFONE, A., MALATESTA, P., BECKERS, J. & GOTZ, M. 2008. Prospective isolation of functionally distinct radial glial subtypes--lineage and transcriptome analysis. *Mol Cell Neurosci,* 38**,** 15-42.

POLLARD, S. M., CONTI, L., SUN, Y., GOFFREDO, D. & SMITH, A. 2006. Adherent neural stem (NS) cells from fetal and adult forebrain. *Cereb Cortex,* 16 Suppl 1**,** i112-20.

POLLARD, S. M., WALLBANK, R., TOMLINSON, S., GROTEWOLD, L. & SMITH, A. 2008. Fibroblast growth factor induces a neural stem cell phenotype in foetal forebrain progenitors and during embryonic stem cell differentiation. *Mol Cell Neurosci,* 38**,** 393-403.

QUARRELL, O. 2009. *Juvenile Huntington's disease : (and other trinucleotide repeat disorders),* Oxford ; New York, Oxford University Press.

RAJKOWSKA, G., SELEMON, L. D. & GOLDMAN-RAKIC, P. S. 1998. Neuronal and glial somal size in the prefrontal cortex: a postmortem morphometric study of schizophrenia and Huntington disease. *Arch Gen Psychiatry,* 55**,** 215-24.

RAMALHO-SANTOS, M. & WILLENBRING, H. 2007. On the origin of the term "stem cell". *Cell Stem Cell,* 1**,** 35-8.

RATOVITSKI, T., NAKAMURA, M., D'AMBOLA, J., CHIGHLADZE, E., LIANG, Y., WANG, W., GRAHAM, R., HAYDEN, M. R., BORCHELT, D. R., HIRSCHHORN, R. R. & ROSS, C. A. 2007. N-terminal proteolysis of full-length mutant huntingtin in an inducible PC12 cell model of Huntington's disease. *Cell Cycle,* 6**,** 2970-81.

RATTRAY, I., SMITH, E., GALE, R., MATSUMOTO, K., BATES, G. P. & MODO, M. 2013. Correlations of behavioral deficits with brain pathology assessed through longitudinal MRI and histopathology in the R6/2 mouse model of HD. *PLoS One,* 8**,** e60012.

RAVIKUMAR, B., DUDEN, R. & RUBINSZTEIN, D. C. 2002. Aggregate-prone proteins with polyglutamine and polyalanine expansions are degraded by autophagy. *Hum Mol Genet,* 11**,** 1107-17.

RAYCHAUDHURI, S., SINHA, M., MUKHOPADHYAY, D. & BHATTACHARYYA, N. P. 2008. HYPK, a Huntingtin interacting protein, reduces aggregates and apoptosis induced by N-terminal Huntingtin with 40 glutamines in Neuro2a cells and exhibits chaperone-like activity. *Hum Mol Genet,* 17**,** 240-55.

REDDY, U. R., VENKATAKRISHNAN, G., ROY, A. K., CHEN, J., HARDY, M., MAVILIO, F., ROVERA, G., PLEASURE, D. & ROSS, A. H. 1991. Characterization of two neuroblastoma cell lines expressing recombinant nerve growth factor receptors. *J Neurochem,* 56**,** 67-74.

REINER, A., DEL MAR, N., MEADE, C. A., YANG, H., DRAGATSIS, I., ZEITLIN, S. & GOLDOWITZ, D. 2001. Neurons lacking huntingtin differentially colonize brain and survive in chimeric mice. *J Neurosci,* 21**,** 7608-19.

REIS, S. A., THOMPSON, M. N., LEE, J. M., FOSSALE, E., KIM, H. H., LIAO, J. K., MOSKOWITZ, M. A., SHAW, S. Y., DONG, L., HAGGARTY, S. J., MACDONALD, M. E. & SEONG, I. S. 2011. Striatal neurons expressing full-length mutant huntingtin exhibit decreased N-cadherin and altered neuritogenesis. *Hum Mol Genet,* 20**,** 2344-55.

REN, P. H., LAUCKNER, J. E., KACHIRSKAIA, I., HEUSER, J. E., MELKI, R. & KOPITO, R. R. 2009. Cytoplasmic penetration and persistent infection of mammalian cells by polyglutamine aggregates. *Nat Cell Biol,* 11**,** 219-25.

REUBINOFF, B. E., PERA, M. F., FONG, C. Y., TROUNSON, A. & BONGSO, A. 2000. Embryonic stem cell lines from human blastocysts: somatic differentiation in vitro. *Nat Biotechnol,* 18**,** 399-404.

REYNOLDS, B. A. & RIETZE, R. L. 2005. Neural stem cells and neurospheres--re-evaluating the relationship. *Nat Methods,* 2**,** 333-6.

REYNOLDS, B. A., TETZLAFF, W. & WEISS, S. 1992. A multipotent EGF-responsive striatal embryonic progenitor cell produces neurons and astrocytes. *J Neurosci,* 12**,** 4565-74.

REYNOLDS, B. A. & WEISS, S. 1992. Generation of neurons and astrocytes from isolated cells of the adult mammalian central nervous system. *Science,* 255**,** 1707-10.

RICHARD, J. P. & MARAGAKIS, N. J. 2015. Induced pluripotent stem cells from ALS patients for disease modeling. *Brain Res,* 1607**,** 15-25.

RIGAMONTI, D., BAUER, J. H., DE-FRAJA, C., CONTI, L., SIPIONE, S., SCIORATI, C., CLEMENTI, E., HACKAM, A., HAYDEN, M. R., LI, Y., COOPER, J. K., ROSS, C. A., GOVONI, S., VINCENZ, C. & CATTANEO, E. 2000. Wild-type huntingtin protects from apoptosis upstream of caspase-3. *J Neurosci,* 20**,** 3705-13.

RIGAMONTI, D., SIPIONE, S., GOFFREDO, D., ZUCCATO, C., FOSSALE, E. & CATTANEO, E. 2001. Huntingtin's neuroprotective activity occurs via inhibition of procaspase-9 processing. *J Biol Chem,* 276**,** 14545-8.

RITCH, J. J., VALENCIA, A., ALEXANDER, J., SAPP, E., GATUNE, L., SANGREY, G. R., SINHA, S., SCHERBER, C. M., ZEITLIN, S., SADRI-VAKILI, G., IRIMIA, D., DIFIGLIA, M. & KEGEL, K. B. 2012. Multiple phenotypes in Huntington disease mouse neural stem cells. *Mol Cell Neurosci,* 50**,** 70-81.

ROSAS, H. D., LIU, A. K., HERSCH, S., GLESSNER, M., FERRANTE, R. J., SALAT, D. H., VAN DER KOUWE, A., JENKINS, B. G., DALE, A. M. & FISCHL, B. 2002. Regional and progressive thinning of the cortical ribbon in Huntington's disease. *Neurology,* 58**,** 695-701.

ROSAS, H. D., SALAT, D. H., LEE, S. Y., ZALETA, A. K., PAPPU, V., FISCHL, B., GREVE, D., HEVELONE, N. & HERSCH, S. M. 2008. Cerebral cortex and the

clinical expression of Huntington's disease: complexity and heterogeneity. *Brain,* 131**,** 1057-68.

RUBENSTEIN, J. L., MARTINEZ, S., SHIMAMURA, K. & PUELLES, L. 1994. The embryonic vertebrate forebrain: the prosomeric model. *Science,* 266**,** 578-80.

RUE, L., LOPEZ-SOOP, G., GELPI, E., MARTINEZ-VICENTE, M., ALBERCH, J. & PEREZ-NAVARRO, E. 2013. Brain region- and age-dependent dysregulation of p62 and NBR1 in a mouse model of Huntington's disease. *Neurobiol Dis,* 52**,** 219-28.

RUGGERI, F. S., VIEWEG, S., CENDROWSKA, U., LONGO, G., CHIKI, A., LASHUEL, H. A. & DIETLER, G. 2016. Nanoscale studies link amyloid maturity with polyglutamine diseases onset. Sci Rep, 6, 31155.

RUTISHAUSER, U., ACHESON, A., HALL, A. K., MANN, D. M. & SUNSHINE, J. 1988. The neural cell adhesion molecule (NCAM) as a regulator of cell-cell interactions. *Science,* 240**,** 53-7.

SAH, D. W., RAY, J. & GAGE, F. H. 1997. Regulation of voltage- and ligand-gated currents in rat hippocampal progenitor cells in vitro. *J Neurobiol,* 32**,** 95-110.

SAHL, S. J., WEISS, L. E., DUIM, W. C., FRYDMAN, J. & MOERNER, W. E. 2012. Cellular inclusion bodies of mutant huntingtin exon 1 obscure small fibrillar aggregate species. *Sci Rep,* 2**,** 895.

SANCES, S., BRUIJN, L. I., CHANDRAN, S., EGGAN, K., HO, R., KLIM, J. R., LIVESEY, M. R., LOWRY, E., MACKLIS, J. D., RUSHTON, D., SADEGH, C., SAREEN, D., WICHTERLE, H., ZHANG, S. C. & SVENDSEN, C. N. 2016. Modeling ALS with motor neurons derived from human induced pluripotent stem cells. *Nat Neurosci,* 19**,** 542-53.

SANCHEZ, C., DIAZ-NIDO, J. & AVILA, J. 2000. Phosphorylation of microtubule-associated protein 2 (MAP2) and its relevance for the regulation of the neuronal cytoskeleton function. *Prog Neurobiol,* 61**,** 133-68.

SANCHEZ, P., DE CARCER, G., SANDOVAL, I. V., MOSCAT, J. & DIAZ-MECO, M. T. 1998. Localization of atypical protein kinase C isoforms into lysosome-targeted endosomes through interaction with p62. *Mol Cell Biol,* 18**,** 3069-80.

SANCHO, M., HERRERA, A. E., GORTAT, A., CARBAJO, R. J., PINEDA-LUCENA, A., ORZAEZ, M. & PEREZ-PAYA, E. 2011. Minocycline inhibits cell death and decreases mutant Huntingtin aggregation by targeting Apaf-1. *Hum Mol Genet,* 20**,** 3545-53.

SATHASIVAM, K., NEUEDER, A., GIPSON, T. A., LANDLES, C., BENJAMIN, A. C., BONDULICH, M. K., SMITH, D. L., FAULL, R. L., ROOS, R. A., HOWLAND, D., DETLOFF, P. J., HOUSMAN, D. E. & BATES, G. P. 2013. Aberrant splicing of HTT generates the pathogenic exon 1 protein in Huntington disease. *Proc Natl Acad Sci U S A,* 110**,** 2366-70.

SATHASIVAM, K., WOODMAN, B., MAHAL, A., BERTAUX, F., WANKER, E. E., SHIMA, D. T. & BATES, G. P. 2001. Centrosome disorganization in fibroblast cultures derived from R6/2 Huntington's disease (HD) transgenic mice and HD patients. *Hum Mol Genet,* 10**,** 2425-35.

SAUDOU, F., FINKBEINER, S., DEVYS, D. & GREENBERG, M. E. 1998. Huntingtin acts in the nucleus to induce apoptosis but death does not correlate with the formation of intranuclear inclusions. *Cell,* 95**,** 55-66.

SCHERZINGER, E., SITTLER, A., SCHWEIGER, K., HEISER, V., LURZ, R., HASENBANK, R., BATES, G. P., LEHRACH, H. & WANKER, E. E. 1999. Self-assembly of polyglutamine-containing huntingtin fragments into amyloid-like fibrils: implications for Huntington's disease pathology. *Proc Natl Acad Sci U S A,* 96**,** 4604-9.

SCHILLING, G., KLEVYTSKA, A., TEBBENKAMP, A. T., JUENEMANN, K., COOPER, J., GONZALES, V., SLUNT, H., POIRER, M., ROSS, C. A. & BORCHELT, D. R. 2007. Characterization of huntingtin pathologic fragments in human Huntington disease, transgenic mice, and cell models. *J Neuropathol Exp Neurol,* 66**,** 313-20.

SCHINDELIN, J., ARGANDA-CARRERAS, I., FRISE, E., KAYNIG, V., LONGAIR, M., PIETZSCH, T., PREIBISCH, S., RUEDEN, C., SAALFELD, S., SCHMID, B., TINEVEZ, J. Y., WHITE, D. J., HARTENSTEIN, V., ELICEIRI, K., TOMANCAK, P. & CARDONA, A. 2012. Fiji: an open-source platform for biological-image analysis. *Nat Methods,* 9**,** 676-82.

SCHOLZEN, T. & GERDES, J. 2000. The Ki-67 protein: from the known and the unknown. *J Cell Physiol,* 182**,** 311-22.

SCOTTER, E. L., GOODFELLOW, C. E., GRAHAM, E. S., DRAGUNOW, M. & GLASS, M. 2010. Neuroprotective potential of CB1 receptor agonists in an in vitro model of Huntington's disease. *Br J Pharmacol,* 160**,** 747-61.

SEABERG, R. M. & VAN DER KOOY, D. 2003. Stem and progenitor cells: the premature desertion of rigorous definitions. *Trends Neurosci,* 26**,** 125-31.

SEGAL, D. J. & MECKLER, J. F. 2013. Genome engineering at the dawn of the golden age. *Annu Rev Genomics Hum Genet,* 14**,** 135-58.

SHAO, J., WELCH, W. J. & DIAMOND, M. I. 2008. ROCK and PRK-2 mediate the inhibitory effect of Y-27632 on polyglutamine aggregation. *FEBS Lett,* 582**,** 1637-42.

SHARP, A. H., LOEV, S. J., SCHILLING, G., LI, S. H., LI, X. J., BAO, J., WAGSTER, M. V., KOTZUK, J. A., STEINER, J. P., LO, A. & ET AL. 1995. Widespread expression of Huntington's disease gene (IT15) protein product. *Neuron,* 14**,** 1065-74.

SHELBOURNE, P. F., KELLER-MCGANDY, C., BI, W. L., YOON, S. R., DUBEAU, L., VEITCH, N. J., VONSATTEL, J. P., WEXLER, N. S., GROUP, U. S.-V. C. R., ARNHEIM, N. & AUGOOD, S. J. 2007. Triplet repeat mutation length gains correlate with cell-type specific vulnerability in Huntington disease brain. *Hum Mol Genet,* 16**,** 1133-42.

SHELBOURNE, P. F., KILLEEN, N., HEVNER, R. F., JOHNSTON, H. M., TECOTT, L., LEWANDOSKI, M., ENNIS, M., RAMIREZ, L., LI, Z., IANNICOLA, C., LITTMAN, D. R. & MYERS, R. M. 1999. A Huntington's disease CAG expansion at the murine Hdh locus is unstable and associated with behavioural abnormalities in mice. *Hum Mol Genet,* 8**,** 763-74.

SHEN, Q., WANG, Y., DIMOS, J. T., FASANO, C. A., PHOENIX, T. N., LEMISCHKA, I. R., IVANOVA, N. B., STIFANI, S., MORRISEY, E. E. & TEMPLE, S. 2006. The timing of cortical neurogenesis is encoded within lineages of individual progenitor cells. *Nat Neurosci,* 9**,** 743-51.

SHIN, B. H., LIM, Y., OH, H. J., PARK, S. M., LEE, S. K., AHNN, J., KIM, D. H., SONG, W. K., KWAK, T. H. & PARK, W. J. 2013. Pharmacological activation of Sirt1 ameliorates polyglutamine-induced toxicity through the regulation of autophagy. *PLoS One,* 8**,** e64953.

SHIN, J. Y., FANG, Z. H., YU, Z. X., WANG, C. E., LI, S. H. & LI, X. J. 2005. Expression of mutant huntingtin in glial cells contributes to neuronal excitotoxicity. *J Cell Biol,* 171**,** 1001-12.

SINGEC, I., KNOTH, R., MEYER, R. P., MACIACZYK, J., VOLK, B., NIKKHAH, G., FROTSCHER, M. & SNYDER, E. Y. 2006. Defining the actual sensitivity and specificity of the neurosphere assay in stem cell biology. *Nat Methods,* 3**,** 801-6.

SIVANANDAM, V. N., JAYARAMAN, M., HOOP, C. L., KODALI, R., WETZEL, R. & VAN DER WEL, P. C. 2011. The aggregation-enhancing huntingtin N-terminus is helical in amyloid fibrils. *J Am Chem Soc,* 133**,** 4558-66.

SLOW, E. J., VAN RAAMSDONK, J., ROGERS, D., COLEMAN, S. H., GRAHAM, R. K., DENG, Y., OH, R., BISSADA, N., HOSSAIN, S. M., YANG, Y. Z., LI, X. J., SIMPSON, E. M., GUTEKUNST, C. A., LEAVITT, B. R. & HAYDEN, M. R. 2003. Selective striatal neuronal loss in a YAC128 mouse model of Huntington disease. *Hum Mol Genet,* 12**,** 1555-67.

SMITH, E. J., STROEMER, R. P., GORENKOVA, N., NAKAJIMA, M., CRUM, W. R., TANG, E., STEVANATO, L., SINDEN, J. D. & MODO, M. 2012. Implantation site and lesion topology determine efficacy of a human neural stem cell line in a rat model of chronic stroke. *Stem Cells,* 30**,** 785-96.

SMITH, R., BRUNDIN, P. & LI, J. Y. 2005. Synaptic dysfunction in Huntington's disease: a new perspective. *Cell Mol Life Sci,* 62**,** 1901-12.

SNIDER, B. J., MOSS, J. L., REVILLA, F. J., LEE, C. S., WHEELER, V. C., MACDONALD, M. E. & CHOI, D. W. 2003. Neocortical neurons cultured from mice with expanded CAG repeats in the huntingtin gene: unaltered vulnerability to excitotoxins and other insults. *Neuroscience,* 120**,** 617-25.

SOFRONIEW, M. V. & VINTERS, H. V. 2010. Astrocytes: biology and pathology. *Acta Neuropathol,* 119**,** 7-35.

SONG, H. J., STEVENS, C. F. & GAGE, F. H. 2002. Neural stem cells from adult hippocampus develop essential properties of functional CNS neurons. *Nat Neurosci,* 5**,** 438-45.

SPILIOTOPOULOS, D., GOFFREDO, D., CONTI, L., DI FEBO, F., BIELLA, G., TOSELLI, M. & CATTANEO, E. 2009. An optimized experimental strategy for efficient conversion of embryonic stem (ES)-derived mouse neural stem (NS) cells into a nearly homogeneous mature neuronal population. *Neurobiol Dis,* 34**,** 320-31.

SPIRES, T. L., GROTE, H. E., GARRY, S., CORDERY, P. M., VAN DELLEN, A., BLAKEMORE, C. & HANNAN, A. J. 2004. Dendritic spine pathology and deficits in experience-dependent dendritic plasticity in R6/1 Huntington's disease transgenic mice. *Eur J Neurosci,* 19**,** 2799-807.

STACK, E. C., KUBILUS, J. K., SMITH, K., CORMIER, K., DEL SIGNORE, S. J., GUELIN, E., RYU, H., HERSCH, S. M. & FERRANTE, R. J. 2005. Chronology

of behavioral symptoms and neuropathological sequela in R6/2 Huntington's disease transgenic mice. *J Comp Neurol,* 490**,** 354-70.

STEFFAN, J. S., AGRAWAL, N., PALLOS, J., ROCKABRAND, E., TROTMAN, L. C., SLEPKO, N., ILLES, K., LUKACSOVICH, T., ZHU, Y. Z., CATTANEO, E., PANDOLFI, P. P., THOMPSON, L. M. & MARSH, J. L. 2004. SUMO modification of Huntingtin and Huntington's disease pathology. *Science,* 304**,** 100-4.

STENMAN, J. M., WANG, B. & CAMPBELL, K. 2003. Tlx controls proliferation and patterning of lateral telencephalic progenitor domains. *J Neurosci,* 23**,** 10568-76.

STERNECKERT, J. L., REINHARDT, P. & SCHOLER, H. R. 2014. Investigating human disease using stem cell models. *Nat Rev Genet,* 15**,** 625-39.

STRONG, T. V., TAGLE, D. A., VALDES, J. M., ELMER, L. W., BOEHM, K., SWAROOP, M., KAATZ, K. W., COLLINS, F. S. & ALBIN, R. L. 1993. Widespread expression of the human and rat Huntington's disease gene in brain and nonneural tissues. *Nat Genet,* 5**,** 259-65.

SUN, Y., POLLARD, S., CONTI, L., TOSELLI, M., BIELLA, G., PARKIN, G., WILLATT, L., FALK, A., CATTANEO, E. & SMITH, A. 2008. Long-term tripotent differentiation capacity of human neural stem (NS) cells in adherent culture. *Mol Cell Neurosci,* 38**,** 245-58.

TAKAHASHI, K., TANABE, K., OHNUKI, M., NARITA, M., ICHISAKA, T., TOMODA, K. & YAMANAKA, S. 2007. Induction of pluripotent stem cells from adult human fibroblasts by defined factors. *Cell,* 131**,** 861-72.

TAKAHASHI, K. & YAMANAKA, S. 2006. Induction of pluripotent stem cells from mouse embryonic and adult fibroblast cultures by defined factors. *Cell,* 126**,** 663-76.

TAKAHASHI, T., KIKUCHI, S., KATADA, S., NAGAI, Y., NISHIZAWA, M. & ONODERA, O. 2008. Soluble polyglutamine oligomers formed prior to inclusion body formation are cytotoxic. *Hum Mol Genet,* 17**,** 345-56.

TARTARI, M., GISSI, C., LO SARDO, V., ZUCCATO, C., PICARDI, E., PESOLE, G. & CATTANEO, E. 2008. Phylogenetic comparison of huntingtin homologues reveals the appearance of a primitive polyQ in sea urchin. *Mol Biol Evol,* 25**,** 330-8.

TELENIUS, H., KREMER, B., GOLDBERG, Y. P., THEILMANN, J., ANDREW, S. E., ZEISLER, J., ADAM, S., GREENBERG, C., IVES, E. J., CLARKE, L. A. &

ET AL. 1994. Somatic and gonadal mosaicism of the Huntington disease gene CAG repeat in brain and sperm. *Nat Genet,* 6**,** 409-14.

TEMPLE, S. 1989. Division and differentiation of isolated CNS blast cells in microculture. *Nature,* 340**,** 471-3.

TEMPLE, S. 2001. The development of neural stem cells. *Nature,* 414**,** 112-7.

THAKUR, A. K., JAYARAMAN, M., MISHRA, R., THAKUR, M., CHELLGREN, V. M., BYEON, I. J., ANJUM, D. H., KODALI, R., CREAMER, T. P., CONWAY, J. F., GRONENBORN, A. M. & WETZEL, R. 2009. Polyglutamine disruption of the huntingtin exon 1 N terminus triggers a complex aggregation mechanism. *Nat Struct Mol Biol,* 16**,** 380-9.

THOMPSON, L. M., AIKEN, C. T., KALTENBACH, L. S., AGRAWAL, N., ILLES, K., KHOSHNAN, A., MARTINEZ-VINCENTE, M., ARRASATE, M., O'ROURKE, J. G., KHASHWJI, H., LUKACSOVICH, T., ZHU, Y. Z., LAU, A. L., MASSEY, A., HAYDEN, M. R., ZEITLIN, S. O., FINKBEINER, S., GREEN, K. N., LAFERLA, F. M., BATES, G., HUANG, L., PATTERSON, P. H., LO, D. C., CUERVO, A. M., MARSH, J. L. & STEFFAN, J. S. 2009. IKK phosphorylates Huntingtin and targets it for degradation by the proteasome and lysosome. *J Cell Biol,* 187**,** 1083-99.

THOMSON, J. A., ITSKOVITZ-ELDOR, J., SHAPIRO, S. S., WAKNITZ, M. A., SWIERGIEL, J. J., MARSHALL, V. S. & JONES, J. M. 1998. Embryonic stem cell lines derived from human blastocysts. *Science,* 282**,** 1145-7.

TONG, X., AO, Y., FAAS, G. C., NWAOBI, S. E., XU, J., HAUSTEIN, M. D., ANDERSON, M. A., MODY, I., OLSEN, M. L., SOFRONIEW, M. V. & KHAKH, B. S. 2014. Astrocyte Kir4.1 ion channel deficits contribute to neuronal dysfunction in Huntington's disease model mice. *Nat Neurosci,* 17**,** 694-703.

TOURETTE, C., LI, B., BELL, R., O'HARE, S., KALTENBACH, L. S., MOONEY, S. D. & HUGHES, R. E. 2014. A large scale Huntingtin protein interaction network implicates Rho GTPase signaling pathways in Huntington disease. *J Biol Chem,* 289**,** 6709-26.

TRETTEL, F., RIGAMONTI, D., HILDITCH-MAGUIRE, P., WHEELER, V. C., SHARP, A. H., PERSICHETTI, F., CATTANEO, E. & MACDONALD, M. E. 2000. Dominant phenotypes produced by the HD mutation in STHdh(Q111) striatal cells. *Hum Mol Genet,* 9**,** 2799-809.

TRIBOUILLARD-TANVIER, D., BERINGUE, V., DESBAN, N., GUG, F., BACH, S., VOISSET, C., GALONS, H., LAUDE, H., VILETTE, D. & BLONDEL, M. 2008.

Antihypertensive drug guanabenz is active in vivo against both yeast and mammalian prions. *PLoS One,* 3**,** e1981.

TROTTIER, Y., LUTZ, Y., STEVANIN, G., IMBERT, G., DEVYS, D., CANCEL, G., SAUDOU, F., WEBER, C., DAVID, G., TORA, L. & ET AL. 1995. Polyglutamine expansion as a pathological epitope in Huntington's disease and four dominant cerebellar ataxias. *Nature,* 378**,** 403-6.

TRUANT, R., ATWAL, R. & BURTNIK, A. 2006. Hypothesis: Huntingtin may function in membrane association and vesicular trafficking. *Biochem Cell Biol,* 84**,** 912-7.

TRUANT, R., ATWAL, R. S. & BURTNIK, A. 2007. Nucleocytoplasmic trafficking and transcription effects of huntingtin in Huntington's disease. *Prog Neurobiol,* 83**,** 211-27.

TRUSHINA, E., DYER, R. B., BADGER, J. D., 2ND, URE, D., EIDE, L., TRAN, D. D., VRIEZE, B. T., LEGENDRE-GUILLEMIN, V., MCPHERSON, P. S., MANDAVILLI, B. S., VAN HOUTEN, B., ZEITLIN, S., MCNIVEN, M., AEBERSOLD, R., HAYDEN, M., PARISI, J. E., SEEBERG, E., DRAGATSIS, I., DOYLE, K., BENDER, A., CHACKO, C. & MCMURRAY, C. T. 2004. Mutant huntingtin impairs axonal trafficking in mammalian neurons in vivo and in vitro. *Mol Cell Biol,* 24**,** 8195-209.

TSAYTLER, P., HARDING, H. P., RON, D. & BERTOLOTTI, A. 2011. Selective inhibition of a regulatory subunit of protein phosphatase 1 restores proteostasis. *Science,* 332**,** 91-4.

TULINO, R., BENJAMIN, A. C., JOLINON, N., SMITH, D. L., CHINI, E. N., CARNEMOLLA, A. & BATES, G. P. 2016. SIRT1 Activity Is Linked to Its Brain Region-Specific Phosphorylation and Is Impaired in Huntington's Disease Mice. *PLoS One,* 11**,** e0145425.

TURMAINE, M., RAZA, A., MAHAL, A., MANGIARINI, L., BATES, G. P. & DAVIES, S. W. 2000. Nonapoptotic neurodegeneration in a transgenic mouse model of Huntington's disease. *Proc Natl Acad Sci U S A,* 97**,** 8093-7.

USDIN, M. T., SHELBOURNE, P. F., MYERS, R. M. & MADISON, D. V. 1999. Impaired synaptic plasticity in mice carrying the Huntington's disease mutation. *Hum Mol Genet,* 8**,** 839-46.

UYTTENHOVE, C., PILOTTE, L., THEATE, I., STROOBANT, V., COLAU, D., PARMENTIER, N., BOON, T. & VAN DEN EYNDE, B. J. 2003. Evidence for a tumoral immune resistance mechanism based on tryptophan degradation by indoleamine 2,3-dioxygenase. *Nat Med,* 9**,** 1269-74.

VAGO, T., MERONI, R., DAGANI, R., BALDI, G., PAGANI, M., BEVILACQUA, M. & NORBIATO, G. 1985. Characterization of alpha 2-adrenoceptor binding properties of imidazoline-like drugs, azoloazepine derivatives and beta-phenethylamine-like drugs in human platelet membranes. *J Pharm Pharmacol,* 37**,** 593-6.

VAN DER BORGHT, K. & BRUNDIN, P. 2007. Reduced expression of PSA-NCAM in the hippocampus and piriform cortex of the R6/1 and R6/2 mouse models of Huntington's disease. *Exp Neurol,* 204**,** 473-8.

VASIOUKHIN, V., BAUER, C., YIN, M. & FUCHS, E. 2000. Directed actin polymerization is the driving force for epithelial cell-cell adhesion. *Cell,* 100**,** 209-19.

VELIER, J., KIM, M., SCHWARZ, C., KIM, T. W., SAPP, E., CHASE, K., ARONIN, N. & DIFIGLIA, M. 1998. Wild-type and mutant huntingtins function in vesicle trafficking in the secretory and endocytic pathways. *Exp Neurol,* 152**,** 34-40.

VERLINSKY, Y., STRELCHENKO, N., KUKHARENKO, V., RECHITSKY, S., VERLINSKY, O., GALAT, V. & KULIEV, A. 2005. Human embryonic stem cell lines with genetic disorders. *Reprod Biomed Online,* 10**,** 105-10.

VON HORSTEN, S., SCHMITT, I., NGUYEN, H. P., HOLZMANN, C., SCHMIDT, T., WALTHER, T., BADER, M., PABST, R., KOBBE, P., KROTOVA, J., STILLER, D., KASK, A., VAARMANN, A., RATHKE-HARTLIEB, S., SCHULZ, J. B., GRASSHOFF, U., BAUER, I., VIEIRA-SAECKER, A. M., PAUL, M., JONES, L., LINDENBERG, K. S., LANDWEHRMEYER, B., BAUER, A., LI, X. J. & RIESS, O. 2003. Transgenic rat model of Huntington's disease. *Hum Mol Genet,* 12**,** 617-24.

VONSATTEL, J. P., KELLER, C. & CORTES RAMIREZ, E. P. 2011. Huntington's disease - neuropathology. *Handb Clin Neurol,* 100**,** 83-100.

WALDVOGEL, H. J., KIM, E. H., THU, D. C., TIPPETT, L. J. & FAULL, R. L. 2012. New Perspectives on the Neuropathology in Huntington's Disease in the Human Brain and its Relation to Symptom Variation. *J Huntingtons Dis,* 1**,** 143-53.

WARBY, S. C., CHAN, E. Y., METZLER, M., GAN, L., SINGARAJA, R. R., CROCKER, S. F., ROBERTSON, H. A. & HAYDEN, M. R. 2005. Huntingtin phosphorylation on serine 421 is significantly reduced in the striatum and by polyglutamine expansion in vivo. *Hum Mol Genet,* 14**,** 1569-77.

WARBY, S. C., DOTY, C. N., GRAHAM, R. K., CARROLL, J. B., YANG, Y. Z., SINGARAJA, R. R., OVERALL, C. M. & HAYDEN, M. R. 2008. Activated caspase-6 and caspase-6-cleaved fragments of huntingtin specifically colocalize in the nucleus. *Hum Mol Genet,* 17**,** 2390-404.

WEBSTER, M., WITKIN, K. L. & COHEN-FIX, O. 2009. Sizing up the nucleus: nuclear shape, size and nuclear-envelope assembly. *J Cell Sci,* 122**,** 1477-86.

WEISS, S., DUNNE, C., HEWSON, J., WOHL, C., WHEATLEY, M., PETERSON, A. C. & REYNOLDS, B. A. 1996. Multipotent CNS stem cells are present in the adult mammalian spinal cord and ventricular neuroaxis. *J Neurosci,* 16**,** 7599-609.

WELLINGTON, C. L., ELLERBY, L. M., HACKAM, A. S., MARGOLIS, R. L., TRIFIRO, M. A., SINGARAJA, R., MCCUTCHEON, K., SALVESEN, G. S., PROPP, S. S., BROMM, M., ROWLAND, K. J., ZHANG, T., RASPER, D., ROY, S., THORNBERRY, N., PINSKY, L., KAKIZUKA, A., ROSS, C. A., NICHOLSON, D. W., BREDESEN, D. E. & HAYDEN, M. R. 1998. Caspase cleavage of gene products associated with triplet expansion disorders generates truncated fragments containing the polyglutamine tract. *J Biol Chem,* 273**,** 9158-67.

WELLINGTON, C. L. & HAYDEN, M. R. 2000. Caspases and neurodegeneration: on the cutting edge of new therapeutic approaches. *Clin Genet,* 57**,** 1-10.

WEXLER, N. S., LORIMER, J., PORTER, J., GOMEZ, F., MOSKOWITZ, C., SHACKELL, E., MARDER, K., PENCHASZADEH, G., ROBERTS, S. A., GAYAN, J., BROCKLEBANK, D., CHERNY, S. S., CARDON, L. R., GRAY, J., DLOUHY, S. R., WIKTORSKI, S., HODES, M. E., CONNEALLY, P. M., PENNEY, J. B., GUSELLA, J., CHA, J. H., IRIZARRY, M., ROSAS, D., HERSCH, S., HOLLINGSWORTH, Z., MACDONALD, M., YOUNG, A. B., ANDRESEN, J. M., HOUSMAN, D. E., DE YOUNG, M. M., BONILLA, E., STILLINGS, T., NEGRETTE, A., SNODGRASS, S. R., MARTINEZ-JAURRIETA, M. D., RAMOS-ARROYO, M. A., BICKHAM, J., RAMOS, J. S., MARSHALL, F., SHOULSON, I., REY, G. J., FEIGIN, A., ARNHEIM, N., ACEVEDO-CRUZ, A., ACOSTA, L., ALVIR, J., FISCHBECK, K., THOMPSON, L. M., YOUNG, A., DURE, L., O'BRIEN, C. J., PAULSEN, J., BRICKMAN, A., KRCH, D., PEERY, S., HOGARTH, P., HIGGINS, D. S., JR., LANDWEHRMEYER, B. & PROJECT, U. S.-V. C. R. 2004. Venezuelan

kindreds reveal that genetic and environmental factors modulate Huntington's disease age of onset. *Proc Natl Acad Sci U S A,* 101**,** 3498-503.

WHEELER, V. C., AUERBACH, W., WHITE, J. K., SRINIDHI, J., AUERBACH, A., RYAN, A., DUYAO, M. P., VRBANAC, V., WEAVER, M., GUSELLA, J. F., JOYNER, A. L. & MACDONALD, M. E. 1999. Length-dependent gametic CAG repeat instability in the Huntington's disease knock-in mouse. *Hum Mol Genet,* 8**,** 115-22.

WIEDENMANN, B., FRANKE, W. W., KUHN, C., MOLL, R. & GOULD, V. E. 1986. Synaptophysin: a marker protein for neuroendocrine cells and neoplasms. *Proc Natl Acad Sci U S A,* 83**,** 3500-4.

XIA, J., LEE, D. H., TAYLOR, J., VANDELFT, M. & TRUANT, R. 2003. Huntingtin contains a highly conserved nuclear export signal. *Hum Mol Genet,* 12**,** 1393-403.

XIONG, F., GAO, H., ZHEN, Y., CHEN, X., LIN, W., SHEN, J., YAN, Y., WANG, X., LIU, M. & GAO, Y. 2011. Optimal time for passaging neurospheres based on primary neural stem cell cultures. *Cytotechnology,* 63**,** 621-31.

XU, C., INOKUMA, M. S., DENHAM, J., GOLDS, K., KUNDU, P., GOLD, J. D. & CARPENTER, M. K. 2001. Feeder-free growth of undifferentiated human embryonic stem cells. *Nat Biotechnol,* 19**,** 971-4.

YANG, D., WANG, C. E., ZHAO, B., LI, W., OUYANG, Z., LIU, Z., YANG, H., FAN, P., O'NEILL, A., GU, W., YI, H., LI, S., LAI, L. & LI, X. J. 2010. Expression of Huntington's disease protein results in apoptotic neurons in the brains of cloned transgenic pigs. *Hum Mol Genet,* 19**,** 3983-94.

YANG, S. H., CHENG, P. H., BANTA, H., PIOTROWSKA-NITSCHE, K., YANG, J. J., CHENG, E. C., SNYDER, B., LARKIN, K., LIU, J., ORKIN, J., FANG, Z. H., SMITH, Y., BACHEVALIER, J., ZOLA, S. M., LI, S. H., LI, X. J. & CHAN, A. W. 2008. Towards a transgenic model of Huntington's disease in a non-human primate. *Nature,* 453**,** 921-4.

YANG, W., DUNLAP, J. R., ANDREWS, R. B. & WETZEL, R. 2002. Aggregated polyglutamine peptides delivered to nuclei are toxic to mammalian cells. *Hum Mol Genet,* 11**,** 2905-17.

YEO, W. & GAUTIER, J. 2004. Early neural cell death: dying to become neurons. *Dev Biol,* 274**,** 233-44.

ZALA, D., COLIN, E., RANGONE, H., LIOT, G., HUMBERT, S. & SAUDOU, F. 2008. Phosphorylation of mutant huntingtin at S421 restores anterograde and retrograde transport in neurons. *Hum Mol Genet,* 17**,** 3837-46.

ZAPPONE, M. V., GALLI, R., CATENA, R., MEANI, N., DE BIASI, S., MATTEI, E., TIVERON, C., VESCOVI, A. L., LOVELL-BADGE, R., OTTOLENGHI, S. & NICOLIS, S. K. 2000. Sox2 regulatory sequences direct expression of a (beta)-geo transgene to telencephalic neural stem cells and precursors of the mouse embryo, revealing regionalization of gene expression in CNS stem cells. *Development,* 127**,** 2367-82.

ZEITLIN, S., LIU, J. P., CHAPMAN, D. L., PAPAIOANNOU, V. E. & EFSTRATIADIS, A. 1995. Increased apoptosis and early embryonic lethality in mice nullizygous for the Huntington's disease gene homologue. *Nat Genet,* 11**,** 155-63.

ZEMSKOV, E. A., JANA, N. R., KUROSAWA, M., MIYAZAKI, H., SAKAMOTO, N., NEKOOKI, M. & NUKINA, N. 2003. Pro-apoptotic protein kinase C delta is associated with intranuclear inclusions in a transgenic model of Huntington's disease. *J Neurochem,* 87**,** 395-406.

ZHANG, J., PENG, Q., LI, Q., JAHANSHAD, N., HOU, Z., JIANG, M., MASUDA, N., LANGBEHN, D. R., MILLER, M. I., MORI, S., ROSS, C. A. & DUAN, W. 2010a. Longitudinal characterization of brain atrophy of a Huntington's disease mouse model by automated morphological analyses of magnetic resonance images. *Neuroimage,* 49**,** 2340-51.

ZHANG, J., YANG, Z. & DONG, J. 2016. P62: An emerging oncotarget for osteolytic metastasis. *J Bone Oncol,* 5**,** 30-7.

ZHANG, N., AN, M. C., MONTORO, D. & ELLERBY, L. M. 2010b. Characterization of Human Huntington's Disease Cell Model from Induced Pluripotent Stem Cells. *PLoS Curr,* 2**,** RRN1193.

ZHANG, Y., LEAVITT, B. R., VAN RAAMSDONK, J. M., DRAGATSIS, I., GOLDOWITZ, D., MACDONALD, M. E., HAYDEN, M. R. & FRIEDLANDER, R. M. 2006. Huntingtin inhibits caspase-3 activation. *EMBO J,* 25**,** 5896-906.

ZHENG, Z., LI, A., HOLMES, B. B., MARASA, J. C. & DIAMOND, M. I. 2013. An N-terminal nuclear export signal regulates trafficking and aggregation of Huntingtin (Htt) protein exon 1. *J Biol Chem,* 288**,** 6063-71.

ZHOU, T., BENDA, C., DUNZINGER, S., HUANG, Y., HO, J. C., YANG, J., WANG, Y., ZHANG, Y., ZHUANG, Q., LI, Y., BAO, X., TSE, H. F., GRILLARI, J., GRILLARI-VOGLAUER, R., PEI, D. & ESTEBAN, M. A. 2012. Generation of human induced pluripotent stem cells from urine samples. *Nat Protoc,* 7**,** 2080-9.

ZINK, D., FISCHER, A. H. & NICKERSON, J. A. 2004. Nuclear structure in cancer cells. *Nat Rev Cancer,* 4**,** 677-87.

ZUCCATO, C. & CATTANEO, E. 2007. Role of brain-derived neurotrophic factor in Huntington's disease. *Prog Neurobiol,* 81**,** 294-330.

ZUCCATO, C., CIAMMOLA, A., RIGAMONTI, D., LEAVITT, B. R., GOFFREDO, D., CONTI, L., MACDONALD, M. E., FRIEDLANDER, R. M., SILANI, V., HAYDEN, M. R., TIMMUSK, T., SIPIONE, S. & CATTANEO, E. 2001. Loss of huntingtin-mediated BDNF gene transcription in Huntington's disease. *Science,* 293**,** 493-8.

ZUCCATO, C., TARTARI, M., CROTTI, A., GOFFREDO, D., VALENZA, M., CONTI, L., CATAUDELLA, T., LEAVITT, B. R., HAYDEN, M. R., TIMMUSK, T., RIGAMONTI, D. & CATTANEO, E. 2003. Huntingtin interacts with REST/NRSF to modulate the transcription of NRSE-controlled neuronal genes. *Nat Genet,* 35**,** 76-83.